Travelling Wave Control of Stringed Musical Instruments

Submitted in partial fulfilment of the requirements of the Degree of Doctor of Philosophy

Liam Donovan

November 13, 2018

Statement of Originality

I, Liam Donovan, confirm that the research included within this thesis is my own work or that where it has been carried out in collaboration with, or supported by others, that this is duly acknowledged below and my contribution indicated. Previously published material is also acknowledged below.

I attest that I have exercised reasonable care to ensure that the work is original, and does not to the best of my knowledge break any UK law, infringe any third party's copyright or other Intellectual Property Right, or contain any confidential material.

I accept that the College has the right to use plagiarism detection software to check the electronic version of the thesis.

I confirm that this thesis has not been previously submitted for the award of a degree by this or any other university.

Signature: 

Date: November 13, 2018

Acknowledgements

I would like to thank my supervisor, Andrew McPherson, for giving me the chance to research such an interesting topic and for putting such a huge amount of effort into this work over the years; my mum, Jenny Donovan, for a lifetime of inspiration and for keeping me on track the whole way through; everyone at the Augmented Instruments Laboratory and on the Bela team for providing such a stimulating working environment; everyone studying on or involved with the MAT program for some incredible experiences; and last but not least my flatmate Jay Pancholi for putting up with me writing this thing in his living room one long winter.

Abstract

Despite the increasing sophistication of digital musical instruments, many performers, composer and listeners remain captivated by traditional acoustic instruments. Interest has grown in the past 2 decades in augmenting acoustic instruments with sensor and actuator technology and integrated digital signal processing, expanding the instrument's capabilities while retaining its essential acoustic character. In this thesis we present a technique, travelling wave control, which allows active control of the vibrations of musical strings and yet has been little explored in the musical instrument literature to date. The thesis seeks to demonstrate that travelling wave control is capable of active damping and of modifying the timbre of a musical string in ways that go beyond those available through the more conventional modal control paradigm. However, we show that travelling wave control is highly sensitive to nonlinearity, which in practical settings can lead to harmonic distortion and even instability in the string response. To avoid these problems, we design and build a highly linear optical string displacement sensor, and investigate the use of piezoelectric stacks to actuate the termination point of a string. With these components we design and build a functioning travelling wave control system which is capable of damping the vibrations of a plucked string without adversely affecting its timbre. We go on to show that by deliberately adding nonlinearity into the control system, we are able to modify the timbre of the string in a natural way by affecting the evolution of the modal amplitudes. The results demonstrate the feasibility of the concept and lay the groundwork for future integration of travelling wave control into future actuated musical instruments.

Contents

List of Figures

Chapter 1

Introduction

When talking about musical instruments the word *acoustic* is generally taken to mean "not having electrical amplification"[1], and is therefore an example of an interesting linguistic quirk: a retronym, or a word used to differentiate the original form of something from a newer version. Before the invention of the electric guitar all instruments were acoustic, it was only once the technology of electrical amplification had developed to the point that the design of guitars was being reimagined to accommodate it that the need to differentiate acoustic instruments arose.

The advent of synthesisers and computer music brought about another even larger paradigm shift in musical instrument technology. Traditional musical instruments with their fragile wooden bodies and delicate construction, their constant propensity to go out of tune and their dependance on the skills of enigmatic luthiers are no longer the only way for musicians to practice their craft. Instead the sound of every traditional instrument in existence can be replicated by a far more robust and reliable digital system using techniques such as physical modelling [98] and sampling synthesis [61], and included along with a host of new and previously impossible synthesised sounds.

But despite the practical advantages and sonic freedom offered by digital instruments, acoustic instruments are still found captivating by audiences and performers alike and are ubiquitous in mainstream musical practice. While there is an element of cultural nostalgia and a yearning for the traditional musical experience to be found in their continuing popularity, the physical nature of the sound-creating mechanisms in acoustic instruments gives them certain qualities which digital instruments have been unable to reproduce or exceed.

[1] Oxford English Dictionary

This could be because of the difficulty in reproducing some of the more subtle nuances of acoustic instruments digitally; nonlinearities and higher-order effects for example contribute significantly to the sound produced by a plucked string but they can be extremely difficult to model and reproduce accurately [108]. The absence of some sounds which are produced by acoustic instruments but which may be naively considered as undesirable, such as the sliding of fingers along a string or the buzzing of a string hitting a fretboard, will generally be absent from digital models giving them a sanitised feel which can be perceived as less aesthetically pleasing. The three-dimensional radiation of sound from an acoustic instrument is often significantly different from that produced by a speaker [34, 116] which can impact an audience's impression of a live performance.

For musicians, reasons for preferring acoustic over digital instruments go beyond the quality of the sound produced. The process of interacting with an acoustic instrument is a tangible, multimodal experience which often allows a high degree of control over the behaviour of the acoustic system. The subtlety and power of the control offered to a musician by being able to directly manipulate a vibrating string, along with the haptic, visual and audible feedback a musician receives when doing so is not something digital interfaces have yet been able to replicate [8]. The physical nature and *embodiment* of an acoustic instrument is cited by musicians as a reason for a preference toward the acoustic [60].

Cultural factors are also important to understand the continued prevalence of acoustic instruments. Learning any instrument to a virtuosic level of skill requires an enormous time investment [84], while true mastery requires a lifetime of work. There are strong cultural and practical incentives for students to begin learning to play with traditional acoustic instruments and once such an investment has been made there is little incentive for an expert musician to switch to using a digital reproduction.

At the intersection of electronic synthesis and acoustic instruments lie actuated musical instruments, defined as instruments *which produce sound via vibrating element(s) that are co-manipulated by humans and electromechanical systems* [81]. The aim is to use electronic control and actuation methods to vibrate physical, acoustic resonators found in traditional instruments such as strings and air cavities and create new ways of interacting with them without losing the qualities which make acoustic instruments attractive. Novel and previously impossible techniques such as infinite sustain and volume swells can be applied alongside traditional techniques such as plucking and bowing to extend the expressive capabilities of an instrument, allowing a musician to explore new musical terrain while retaining the subtlety, physicality and familiarity of an acoustic instrument.

Examples of actuated stringed instruments include the magnetic resonator piano [67] and the

feedback resonator guitar [9]. Generally they augment the functionality of the instrument by using electromagnetic actuators to induce strings into resonance, either in an open-loop fashion or paired with sensors in a feedback loop, while still allowing the instrument to be played with traditional techniques. Despite using electronic actuation and control, the sound produced by these instruments is generated acoustically through the physical vibrations of strings, allowing them to retain many of the positive qualities of traditional acoustic instruments.

While these instruments are capable of creating aesthetically pleasing new timbres, they are somewhat limited in scope by their actuation and control methods. Direct electromagnetic actuation of strings is far less capable of generating fast attacks than manual actuation for example, and control over and variation in the timbre produced tends to be limited.

In this thesis we explore a new technique for controlling the vibration of a musical string: *travelling wave control*. Based on a technique developed in the domain of industrial vibration suppression, travelling wave control directly affects the energy propagating along a string in the form of travelling waves. When applied in a musical context it has the potential to afford deliberate control over the timbre of a vibrating string, laying the foundations for the creation of new actuated musical instruments which retain many of the advantages of traditional acoustic instruments while also offering the possibility to explore a new timbral space rooted in the natural acoustic sound of a vibrating string.

1.1 Introduction to Travelling Wave Control

A high-level description of how travelling wave control works is given in Appendix A, while a detailed mathematical model of its application is presented in Chapter 3. To summarise, a pair of string displacement sensors along the continuous portion of the string are used to detect the wave travelling along the string towards one of the terminations. This signal is fed forward to an actuator located under the termination which is then displaced by an amount proportional to the wave incident upon it, absorbing some of the energy of the wave and preventing it from being reflected back into the string.

The technique was developed for the suppression of vibrations in structural beams [114] as a response to the deficiency of classical modal control methods [73]. Beams and strings are both commonly modelled as one-dimensional elements whose motion is governed by the wave equation, and so techniques developed for one can often be applied to the other. They both feature the property that their vibration consists of an infinite number of modal frequencies which sum to constitute the overall motion of the structure. The harmonic modal frequencies

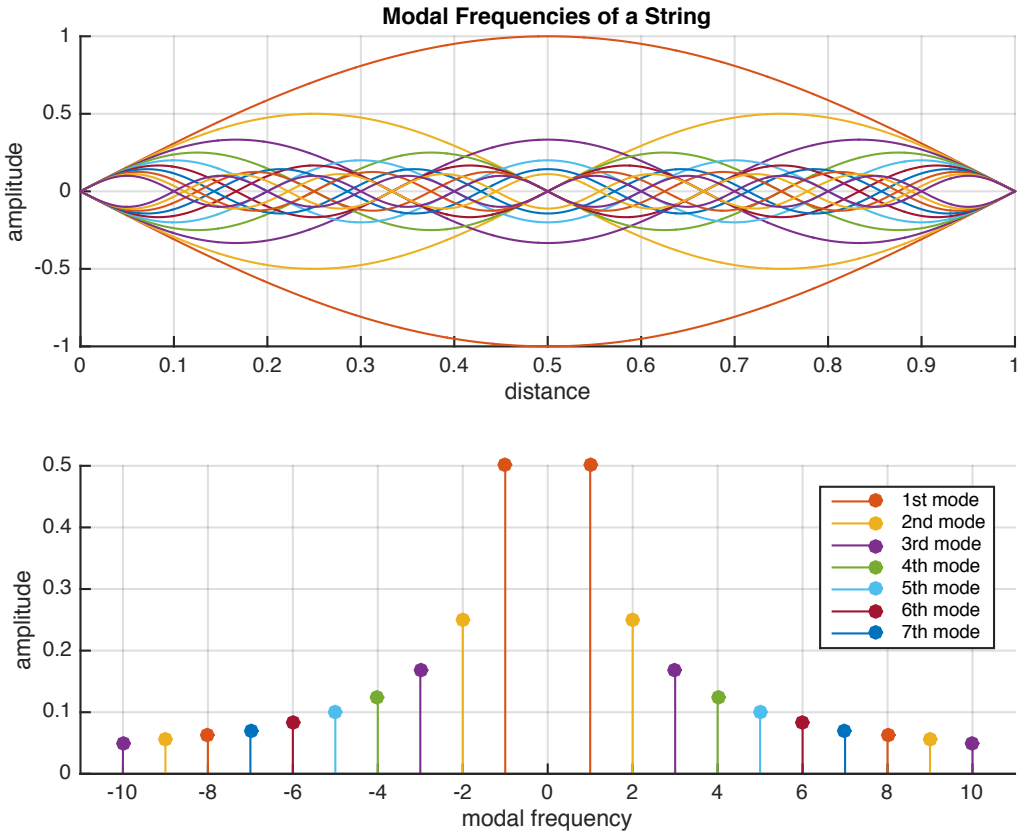

Figure 1.1: A visualisation of the first ten harmonic modal frequencies of an ideal string in the spatial domain (top) and the frequency domain (bottom)

of an ideal string are visualised in Figure 1.1.

In the classical modal control paradigm the properties of these modes, i.e. their amplitude, frequency and quality factor, are controlled directly through feedback. In general, the control of a structure requires a separate sensor-actuator pair and feedback loop for each mode which is to be controlled [74], which presents a problem when attempting to control musical strings with infinite modes. The control techniques used in most actuated stringed instruments including those advocated by Berdahl [6] and used in products such as the E-Bow [40] can be classified as modal control.

In travelling wave control the boundary or termination of the string is actuated in order to exert control over all of the modes of the string simultaneously [101], bypassing the fundamental limitations of modal control. In its ideal form it is capable of removing all of the

energy from the string within a single period and completely preventing the string's modes from being activated, though as we will show in this thesis ideal travelling wave control is not possible with currently existing technology.

The technique is conceptually similar to digital waveguide synthesis, in which the sound created by acoustically resonating one-dimensional structures such as strings is synthesised in the digital domain through the explicit modelling of waves travelling around the structure [96, 48, 97, 109]. In order to reduce complexity and computational cost, waves are generally modelled as travelling in an ideal, lossless fashion with simple delay lines, while processes which affect the waves are consolidated at the terminations of the waveguide. This draws an interesting parallel with the termination-based actuation of a travelling wave control system.

1.2 Nonlinearity and Timbre

Understanding the effect of nonlinearity on a travelling wave control system is crucial to being able to successfully apply the control to a real vibrating string. As we show in Chapter 3, nonlinearity in the sensor or actuator systems can significantly degrade the ability of the system to remove energy from the string, increasing the damping time and in extreme cases causing instability.

A more subtle effect of nonlinearity is to shift energy from the lower modes of the string up into the higher harmonics, inducing harmonic distortion in the string's motion and modifying its timbre. It is very similar in principle to the *javari* effect which is responsible for the unique and distinctive timbre of many Indian stringed instruments including the sitar and tanbura [88]. The bridge of those instruments, commonly called a javari bridge, is rounded and gently sloped in such a way that it causes part of the string to wrap around it on every vibration. This nonlinear constraint at the termination point of the string has a similar effect to that of nonlinear travelling wave control, shifting energy between the modal frequencies of the string and causing the distinctive buzzing timbre and falling formants associated with those instruments [17, 95].

The primary goal of this thesis is to demonstrate that nonlinear travelling wave control can be used to modify the timbre of a string in a deliberate, natural and controllable way. In order to do that it is first necessary to demonstrate the feasibility of a sufficiently linear control system which is capable of damping the vibrations of a string without significantly modifying its timbre in the process, so that nonlinearity can then be added to the system in a controlled way. This is a significant challenge, as most commercially available string sensors and those described in the actuated instrument literature are inherently nonlinear,

as are many of the typical actuators used in actuated instruments.

Timbre itself is a fairly nebulous concept, generally defined as the qualities of a musical sound which differentiate it from another with the same pitch, loudness and duration. Timbres are usually classified by their location in an abstract *timbre space* constructed from perceptual dimensions [35]. A meta-analysis of a large number of studies of musical instrument timbre found that it is best mapped into a three-dimensional space with dimensions falling into the generalised categories of spectral, temporal, and spectro-temporal qualities [63]. The last of these, the spectro-temporal quality of a sound, is the least well-defined but refers in general to how the spectrum of a sound evolves over time, and is the quality which a nonlinear travelling wave control system may most be able to affect.

The perceptual elements of timbre and the classification of sounds within timbre space fall outside of the scope of this thesis. Instead of directly considering the effect of nonlinearity in the control system on the abstract concept of timbre, we instead use the evolution of the amplitudes of the modal frequencies of the string and the total harmonic distortion of the string's motion as clearly defined mathematical proxies for the spectro-temporal elements of the string's timbre. These measures can be viewed as a starting point for an investigation into the effect of the control system on the timbre of the string.

1.3 Inharmonicity

The motion of ideal strings such as that presented in 1.1 consists of the superimposition of perfectly harmonically related modes, that is modes with frequencies that are exact integer multiples of the fundamental. In real strings a number of phenomena contribute to subtly shifting the modal frequencies away from perfect integer multiples, an effect which is called inharmonicity.

The main sources of inharmonicity are the stiffness of the string [30] and the coupling of the string to the surrounding system through terminations with non-zero admittance [117]. The latter effect is complicated by the fact that the admittance of a termination in the vertical direction may be different to its admittance the horizontal direction, causing the modal frequencies of the string to be different depending on the polarisation of its motion. The characteristics of the termination can even cause the effective length of the string to be different between the two polarisations, further compounding the effect [121].

As we will show in Chapter 3, nonlinearities in a travelling wave control system do generate perfect harmonics, and while the differences in frequency between the inharmonic modes of a real string and the products of nonlinearities in the control system are small they may still

be significant. While we do not consider the effects of string inharmonicity explicitly in this thesis, it is an area which is worthy of further investigation.

1.4 Research Questions

In this thesis we develop the theory of travelling wave control, originally presented in the literature for vibration suppression in structural beams, in the context of idealised musical strings. We particularly consider the effect of nonlinearity in the control system on the behaviour of the string, focussing on the evolution of the modal amplitudes as a proxy for the spectro-temporal elements of the string's timbre. We go on to detail the design and construction of a practical travelling wave control system, featuring custom optical string displacement sensors, a signal processing algorithm to decompose the travelling wave components from string measurements, and a piezoelectric actuation system. Particular care is taken to identify and minimise sources of nonlinearity in the sensor system in order to build a control system capable of damping a plucked string without inducing excessive harmonic distortion in the string's motion and modifying its timbre. The ability of the system to damp the vibrations of the string and the effect of adding nonlinearity to the system are both evaluated and compared to theory.

The purpose of the thesis is to demonstrate that a highly linear travelling wave control system can be developed and used in practice to damp the vibrations of a string without significantly modifying its timbre. It lays the foundations for using such a system to explore a new timbre space for acoustic stringed instruments by adding nonlinearity into the control system. The thesis limits its scope to the effect of the control system on the physical behaviour of the string alone, and is not concerned with the perceptual effects of the control system, or with building a complete musical instrument.

In the thesis we attempt to answer the following research questions:

1.4.1 How can travelling wave control be used to damp the vibrations of a musical string in the presence of realistic non-ideal conditions?

The theory of travelling wave control (Chapter 3) shows that in an ideal situation it is capable of completely damping the vibrations of a string within a single period of vibration. In reality, a number of non-idealities prevent this from being possible. Perhaps the most

important of these is nonlinearity which is discussed in more detail in subsequent questions, but other important factors include sensor noise and limited actuator amplitude.

In Section 4.1 we discuss one of the fundamental challenges of travelling wave control: how to decompose the travelling wave components of the string's motion from measurements of its displacement. A number of algorithms for doing this in a musical context have been proposed, but many of them are unstable in the presence of sensor noise. We take an algorithm from the domain of industrial vibration suppression which takes a stochastic approach to estimating the travelling wave components in the presence of sensor noise and apply it to a musical string. Analysis shows that the accuracy of the algorithm is sensitive to the signal-to-noise ratio of the sensor readings, so in Section 4.4 we take particular care to design circuitry for our custom sensors which minimises any sources of noise.

In Chapter 5 we discuss the relative advantages of different actuator technologies for use in the control system. The linearity, stiffness and bandwidth of piezoelectric stack actuators make them the ideal choice, however their limited maximum displacement in relation to the amplitude of the travelling wave components of the string has consequences for the rate at which the control system is capable of removing energy from the string. In Section 3.3.1 we develop the theory of travelling wave control in the presence of limited actuator amplitude, and in Section 5.3 we investigate nonlinear techniques for improving the speed of damping with limited actuator amplitude, including clipping the output and an adaptive gain algorithm.

1.4.2 How does nonlinearity affect the response of the travelling wave control system and the resulting behaviour of the string?

Travelling wave control is highly sensitive to nonlinearity, which in a musical context has both positive and negative consequences.

The potential negative consequences of nonlinearity include increased damping time, harmonic distortion and in extreme cases instability. We analyse the theoretical consequences of nonlinearity on the string's motion in Section 3.4.3, and we draw up a generalised stability criterion in Section 3.3 which we then apply to third-order polynomial nonlinearity in Section 3.3.1. Different forms of nonlinearity result in different kinds of behaviour; positive cubic nonlinearity helps to stabilise the string and reduce damping time in some situations while sufficient amounts of quadratic nonlinearity can cause instability independent of the control gain. The negative effects of nonlinearity mean that it is essential to reduce the structural

nonlinearities in the control system to maximise its performance.

The positive effect of nonlinearity is that it causes energy to flow between the harmonic frequencies of the string, modifying the spectro-temporal elements of the string's timbre in a similar way to the javari effect found in traditional Indian instruments such as the sitar and tanbura. Simulations of the effect of nonlinearity on the modal amplitudes of the string are presented in Section 3.5, and its effect on an actual travelling wave control system is examined in Section 6.5.

1.4.3 What are the main sources of structural nonlinearity in a travelling wave control system, and how can they be minimised?

The manufacturers of commercial string sensors for musical instruments have little incentive to optimise their products for linearity because they are rather more concerned with their subjective sound quality. The most common form of electromagnetic guitar pickup for example consists of a coil of wire wrapped around a permanent magnet placed close to a ferro-magnetic string. As the string vibrates it modifies the direction of the magnetic field lines which cut through the coiled wire, inducing a current approximately proportional to the velocity of the string. This design is inherently highly nonlinear because of the non-uniformity of the magnetic field generated by permanent magnets through which the string travels [83].

The sensors are by far the largest source of nonlinearity in the control system, so in Chapter 4 we design our own highly linear custom sensors. We choose a form of optical transmission-based sensor which has been used before in the musical string control literature because of its high potential for linearity, and mathematically model its behaviour to identify major sources of nonlinearity. We discover and model two serious sources of nonlinearity with the potential to induce significant harmonic distortion in the string and even cause instability: out-of-plane motion of the string (Section 4.3.1) and non-uniform light distribution (Section 4.3.2). We eliminate the former by collimating the light in the sensor with lenses, and we minimise the second by using wide-angled LEDs located a significant distance from the string.

1.5 Thesis Structure

In **Chapter 2** (Literature Review) we review relevant literature in the fields of actuated and augmented instruments, active control of musical strings, musical acoustics, string sensing

technologies and vibration suppression in one-dimensional structures.

In **Chapter 3** (Travelling Wave Control) we construct a mathematical model of the travelling wave control system and examine its theoretical behaviour. We investigate the stability properties of the system, and the effect of non-ideal conditions such as nonlinearity and limited actuator amplitude on the response of the string, using analytical techniques and simulations.

In **Chapter 4** (Sensing Travelling Waves) we review the advantages of available string sensor technologies and configurations in the context of travelling wave control. We go on to design and build a pair of custom optical string sensors, identifying and minimising major sources of nonlinearity. We also investigate algorithms for decomposing the travelling wave components from measurements of the string's displacement.

In **Chapter 5** (Termination-Based Actuation) we describe the advantages of using termination-based actuation in the context of a travelling wave control system, and review the various actuation technologies available. We investigate the consequences of limited actuator amplitude on the system, and propose an adaptive gain algorithm to reduce its effect.

In **Chapter 6** (Experimental Results) we present a functioning travelling wave control system capable of damping the vibrations of a plucked string, and analyse its sensitivity to key parameters. We then investigate the effect of deliberately adding nonlinearity into the control system to modify the behaviour of the string.

In **Appendix A** (Termination-Point Impedance) we present an analysis of the travelling wave control system from the perspective of the impedance of the actuated termination. We find this perspective can be useful to gain an intuitive understanding of how the system works, but of less use in mathematical modelling its behaviour.

In **Appendix B** (Active Control of a String Instrument Bridge using the Posicast Technique) we reproduce a paper submitted to the 138th Convention of the AES concerning electromagnetic termination-based actuation of strings. It helps motivate the context of the work presented in this thesis, but does not contribute to it directly.

In **Appendix C** (Photographs) we display photographs of the travelling wave control system built during the thesis.

Chapter 2

Literature Review

2.1 Actuated Instruments

The context of this work is in creating digital musical instruments [77]. The canonical approach to digital musical instruments is to include sensor inputs, sound outputs, and a mapping layer between them. A full review of DMI design is beyond the scope of this thesis but reviews can be found in [87, 120, 115, 45]. Within the DMI design community, considerable attention has focused on sensor types [72] and mapping [43, 59, 110], however sound output is an area with much left to explore. While physical modelling of acoustic musical instruments remains an active area of research [49, 93, 96, 98, 108] and new digital sound synthesis techniques are still introduced including physically-inspired modelling [24], scanned synthesis [62] and concatenative synthesis [92], sound production based on acoustic vibrating elements still holds interest for composers and performers.

The following sections will review recent work in combining acoustic and electronic elements in musical instruments. The review will be divided into two sections: focused acoustic studies of active control of acoustic instruments, and augmented instruments which include an element of sound production through acoustic means other than loudspeakers. In practice there is considerable overlap between these categories.

2.1.1 Active Feedback Control

In studies of musical instrument acoustics it is common to model the sound-creating elements of an instrument as a passive, linear vibrating structure such as a string or air cavity, coupled

to a nonlinear excitation element such as a bow or a reed [64, 29]. The vibrating structures are generally modelled as having an infinite number of modal frequencies [31] which are activated by the nonlinear excitation element as the structure is brought into resonance. The precise properties of the excitation element and how it influences the evolution of the amplitudes of the modal frequencies of the resonating element partly defines the timbre of the instrument [103].

In traditional instruments the excitation mechanism is physical and performed manually by the instrumentalist, e.g. by blowing over a reed or dragging a bow across a string. There is growing interest in replacing these manual excitation mechanisms with electronically-controllable transducers that have the potential to elicit new and previously impossible behaviour from the resonating element, and new timbres from the instrument. Maganza placed a loudspeaker at the entrance of an acoustical air cavity, inducing it into self-sustaining resonance with bifurcating behaviour [58]. This technique was further explored by Buys to produce a hybrid wind instrument capable of inducing self-sustained oscillations in a clarinet bore excited by a loudspeaker driven by physical models of reeds, bow-string interactions, and abstract nonlinear mathematical functions [18, 19]. Meurisse et al. have applied active control to the air column of a clarinet to influence its modal properties [75] and to induce self-sustaining oscillations [76], and Boutin et al. have applied active control to a xylophone bar [14, 13] and to a violin bridge [15] to modify their modal properties.

Other experiments focus on actuating string instruments. Berdahl [5] applied collocated optical sensing and electromagnetic actuation to actively damp resonances in a musical string. Benacchio et al. [3, 2] applied full state feedback control to the soundboard of a stringed instrument in order to modify the radiated sound.

2.1.2 Unusual Behaviours and Chaos

McIntyre et al. [64] showed in an appendix that the vibration of the air column of a clarinet can be approximated by a nonlinear difference equation or iterated map, which under certain conditions can exhibit chaotic behaviour. The consequences of this iterated model, in which the nonlinearity arises as a natural consequence of the effect of the blown reed at one boundary of the air column, has been studied by a number of authors, demonstrating the emergence of period doubling, bifurcations and chaos [58, 100].

Control of the one-dimensional wave equation through velocity feedback at the boundaries was investigated in theory by Chen [21, 22]. He also noted that due to the travelling wave solution to the wave equation a string's motion could be modelled as a first-order recurrence relation in which the boundary conditions mapped the state of the string back into itself

after each period of vibration. When the boundary conditions are nonlinear, Chen discovered the system could exhibit exotic behaviours such as bifurcations and quasi-periodic motion. Under very specific conditions, in which energy is added linearly at one boundary, and either a cubic nonlinearity or a self-regulating Van der Pol nonlinearity is present at the other boundary, Chen discovered the system could exhibit chaotic behaviour [23]. Xu et al. found that the form of boundary-based velocity feedback used by Chen is unstable in the presence of any non-zero time delay in the feedback law [122].

Collectively, these findings suggest that termination-based actuation in the right conditions might be able to introduce unusual vibration regimes into a musical string, producing results that would not be obtained by other acoustic means.

2.1.3 Augmented Instruments

The references in the preceding sections covered experiments in altering the properties of an acoustic system through active feedback control, mainly under experimental laboratory conditions. Actuation of acoustic instruments is frequently applied to create *augmented* instruments, traditional instruments whose capabilities have been extended with the addition of new modes of interaction or sound production.

Many, even most, augmented instruments do not include acoustic actuation. More common is to add external speaker-based sound reproduction or even to construct entirely new synthetic instruments in the form of familiar acoustic instruments (what Wanderley and Depalle call "instrument-like controllers") [115]. In this section we provide a review of the instruments which manipulate traditional acoustic structures, with a particular focus on strings. We leave aside robotic instruments [47], a separate domain of hybrid acoustic-electronic instruments in which the human player is replaced by electromechanical actuators.

Berdahl, separately from his experiments in active damping [5], applied active feedback between an electromagnetic pickup and an electromagnetic actuator to induce self-sustaining vibrations in his Feedback Resonance Guitar [81]. Other approaches to actuating the guitar including the E-Bow [40], a handheld device which induces vibrations in a string through feedback between sensor and actuator coils, and the more sophisticated Vo-96 [112] by Paul Vo, which uses a pair of actuators per string to control the first 16 modes of each string. At the time of this writing, a handheld version of a similar concept, the Wond II [111], was in development. Lahdeoja [53] and Benacchio et al. [4] approach active control through actuation of the soundboard rather than the strings, a concept developed commercially as the HyVibe guitar [44]. Similar to Lahdeoja, Harriman [39] uses vibration transducers in

his Feedback Lap Steel, but he applies them directly under the bridge rather than to the soundboard.

Electromagnetic actuation has been applied to the creation of augmented pianos. Berdahl and Bloland created the Electromagnetically Prepared Piano (EMPP) [7, 11] which uses 12 electromagnetic actuators on selected strings to create infinite sustain in an acoustic piano. The EMPP actuators are used in an open-loop configuration, with signals generated externally by a human performer or an automated process. The Magnetic Resonator Piano (MRP) by McPherson [70, 67] used a piezoelectric sensor on the soundboard of an acoustic grand piano and as many as 88 individual electromagnetic actuators create infinite sustain, harmonics and new timbres in the piano strings. The MRP, like the EMPP, is not a strict feedback control system, in that the amplitude and spectrum of the actuator signals are controlled externally by the pianist. However, the piezo sensor in the MRP drives a series of phase-locked loops which keep the actuator signals aligned in frequency and phase with the motion of the string.

Britt et al. [16] used electromagnetic actuators to create new timbres with the EMvibe, an actuated vibraphone. Since aluminium vibraphone bars cannot be directly actuated with electromagnets, small neodymium magnets were affixed to the bottom of each bar. Actuation has also been applied to drum membranes, such as the EMdrum [89] which is driven by a loudspeaker, to cymbals [86], and to the metal tines of a Fender Rhodes electric piano [94]. Eldridge added electromagnetic pickups, a speaker and a number of transducers to the body of an acoustic cello to induce new forms of resonance [27]. Halldor Ulfarsson has created cello-like instruments with similar feedback principles in his Halldorophone project [107]. The Overtone Fiddle [82] uses an electromagnetic pickup and a magnetic soundboard transducer in a custom-built fiddle. The instrument uses an onboard iPod touch to process the sound and apply effects controlled by several sensors mounted on the instrument.

2.1.4 String Sensors

The most common form of sensor for detecting the motion of a string in a musical context is the electromagnetic guitar pickup. Many different pickup designs and configurations exist, but the general principle is that the motion of a ferromagnetic string disturbs an applied magnetic field, inducing current in a nearby conductor approximately proportional to the string's velocity. They exhibit an uneven frequency response and high levels of nonlinearity [83], which make them less than ideal for use in a control system.

Piezoelectric pickups are also commonly used in musical instruments. They require mechanical coupling to the string as they generate a voltage linearly related to the force applied to them,

and so are usually located under a termination point. Multi-axis piezoelectric sensors which can separately detect vertical and horizontal motion of a string have been developed [32]. Distributed piezoelectric sensors are often deployed outside of a musical context for sensing vibrations in one-dimensional structural beams [55].

Optical pickups are used in the LightWave bass guitar sensor system [57], but they are generally less common than electromagnetic and piezoelectric sensors in commercial musical instruments. Reflectance-based sensors which work by shining light onto the string and measuring the intensity of the light reflected back, have been used with violins [56]. In the Overtone Violin, Overholt [80] used transmission-based optical sensors in which light was shone onto the string projecting its shadow onto two adjacent discrete photodiodes. The amplitude of the sensor was limited and can only be applied adjacent to the termination of the string.

Weinreich [118] proposed another form of transmission-based optical sensors in which the shadow of a string is projected onto a large planar photodiode masked into a triangular shape. This form of sensor was also used by Berdahl due to its high potential for linearity and large amplitude [6]. In this thesis, we further develop the transmission-based optical approach to string sensing, showing that several sources of nonlinearity nonetheless persist in these designs, and mitigating them through improved optical design.

Beyond the musical domain, optical sensors are also used outside of a musical context to sense vibrations in one-dimensional structures such as suspension bridge cables [1].

2.2 Active String Control

The instruments mentioned in the previous section use a wide variety of different actuation and control methods. Many of the augmented instruments are essentially open-loop in their actuation strategy, synthesising signals in response to external human or automated control, but not adapting these signals to the measured vibrations of the instrument. In this thesis, we seek to introduce new means of controlling the vibration of strings to achieve sonic effects that would not be easily produced by existing means. This section therefore discusses the existing approaches to controlling the vibrations of strings. The preponderance of work in this area uses a strategy called *modal control*.

2.2.1 Modal Control

When a structure is excited by an external force and then allowed to vibrate freely, the resulting motion consists of a superposition of that structure's modes. Continuous one-dimensional structures such as strings have an infinite number of modes which contribute to their motion. Many musically relevant properties are directly related to modal properties: pitch is strongly influenced by the frequency of the fundamental mode, dynamics are influenced by the quality factors of the dominant modes, and timbre depends on the temporal evolution of the relationships between the dominant modes, amongst other factors. It therefore seems sensible to control the musical properties of a resonator through control over its modes.

The application of modal control to musical strings has been thoroughly explored by Berdahl [6], who typically placed a single sensor and actuator pair at some point along the continuous length of the string, co-locating them where possible, and used a variety of linear and positive-real feedback laws to control the response of the string. He demonstrated that this strategy is successful at quickly damping string vibrations [5], but he also showed that it requires a factor of Q^2 more power to shift the resonant frequency of a mode than to damp a mode; Q is the quality factor of the mode and tends to be very large in the context of musical strings, making frequency shifting difficult to achieve. As an additional complication, altering the pitch of a string requires more than just shifting the frequency of the fundamental mode, all the dominant modal frequencies must be shifted proportionally to maintain harmonicity otherwise the resulting sound will be distorted. This is difficult to achieve using traditional modal control and requires either very complex controllers with many precisely located poles and zeros, or an independent sensor and actuator pair per dominant mode.

Modal control has also been applied to the suppression of vibration in one-dimensional structural beams [73]. The infinite number of modes which contribute to the motion of such structures and the need for multiple actuators to independently control multiple modes is identified as a weakness of the modal control paradigm [74], and a fundamental limitation of modal control [114].

2.2.2 Travelling Wave Control

An alternative approach to the problem involving controlling the propagation of energy around the structure has also been developed, motivated at first by the suppression of bending waves in flexible spacecraft structures [113]. In this approach, referred to here as *travelling wave control*, the energy propagating around the structure in the form of travelling waves is absorbed using some form of actuator. In theory it is possible to construct

perfect wave absorbers which swallow all of the energy incident upon them [114], damping the vibration of the structure far more efficiently than modal control and bypassing many of its fundamental limitations. Tanaka et al. describe [101] and implement [102] such a wave absorber calling it an *active sink*. By placing an active sink at the boundary of a one-dimensional structure, they show how the travelling waves reflecting from the boundaries can be completely suppressed, preventing standing waves from occurring and completely inactivating the structure's modes.

Feedforward control systems using the principles of travelling wave control and the active sink have been developed to suppress flexural waves propagating in structural beams [28, 51] and torsional waves propagating in oil rig drill strings [50]. In these systems travelling waves moving in one direction in the structure are detected using an array of sensors, and this information is fed forward to an actuator downstream of the sensor which absorbs the wave.

Berdahl considered a form of travelling wave control in his thesis [6], but it was of a different structure to that suggested by the active sink method, involving actuators located along the continuous portion of the string rather than at the terminations, and it was not implemented. One of the justifications presented for not implementing it was that it would be extremely sensitive to and possibly unstable in the presence of nonlinearity, though this was not rigorously demonstrated mathematically.

Several different methods have been proposed in the literature for detecting a travelling wave moving in one direction in a one-dimensional structure using an array of sensors; some are summarised for the case of a musical string by Berdahl [10]. Naucler [79] derived a robust generalised estimator of travelling waves using stochastic modelling to explicitly account for and optimise the estimate in the presence of measurement noise. This thesis builds on Naucler's estimator to develop a practical travelling wave control system for musical strings.

2.3 Timbre

Timbre is generally defined as the quality of a musical note which differentiates it from another with the same pitch, loudness and duration. It essentially encompasses all perceptually-relevant qualities of a sound which can't be described as pitch or dynamics. With such a loose definition it is difficult to quantify. Grey proposed the concept of a timbre space [35] through which an individual sound can be represented by its position in an abstract multi-dimensional euclidean space defined by orthogonal axes representing low-level sound characteristics.

Many attempts have been made in the literature to construct a timbre space for acoustic

musical instruments [35, 36, 37, 119, 52, 63, 54]. These papers consistently conclude that timbre is best mapped into a three-dimensional space, and a meta-analysis conducted by McAdams [63] found that although each study used subtly different perceptual dimensions to map the space, they generally fell into three distinct categories: temporal, spectral, and spectro-temporal. More specifically, the dimensions were generally subsets of the following three categories: attack characteristics, spectral shape and spectral flux. The meta-analysis actually found a total of 72 individual mathematical descriptors for timbre and attempted to correlate each with the perceptual dimensions described above, but concluded there was too much overlap and that more work was needed.

The complexity, subtlety and multi-dimensionality of timbre make it a difficult concept to quantify, but a promising lens through which to view the creation of new sounds. Wessel [119] looked into the possibility of synthesising sound based on position within a timbre space. He noted that Grey [35] had produced hybrid timbres by combining two sounds with differing timbres into one, and that the resulting timbre lay in the timbre space as if the new sound had been linearly interpolated from the two originals. He then constructed a system by which he could control the attack rate and spectral energy distribution (i.e the first two dimensions of a timbre space) of a synthesised tone. He found he was able to smoothly control timbre in this way, though he did not attempt to use the third timbre-space dimension i.e. the spectro-temporal elements of the sound, which has been found to be extremely important in achieving realistic sounds for re-synthesis of acoustic instruments [90].

In this thesis we will examine the effect of travelling wave control on the evolution of the modal amplitudes of the string, using that as a mathematical proxy for the spectro-temporal elements of the string's timbre. By demonstrating that we can affect how the spectrum of the sound created by the string evolves, we aim to demonstrate the potential of the travelling wave control paradigm to elicit new timbres from an acoustically vibrating musical string.

2.4 Summary

The work presented in this chapter shows the significant interest in electronic actuation of acoustic musical instruments, either for acoustics research or for the creation of augmented instruments for musical performance. Of those augmented instruments that feature acoustic actuation, most use simplified open-loop approaches to generating signals for the actuators, and for those instruments that do use feedback, modal control is by far the most common approach. This situation leaves an opening for a new approach to acoustic instrument

actuation based on travelling-wave control, whose behaviours and constraints differ from those of modal control. The following chapters, in developing a practical control system, will also contribute to less-explored technology in the musical instrument domain, including travelling-wave decomposition, transmission-based optical pickups and termination-point actuation.

Chapter 3

Travelling Wave Control

In this chapter we present a model of a system for active control of a vibrating string through direct control over the energy propagating along the string in the form of travelling waves. The system consists of a sensor for measuring travelling waves which is presented in Chapter 4, and an actuator for manipulating travelling waves which is presented in Chapter 5. This chapter will focus on the theory behind travelling wave control with a view towards the practical implementation of such a system in a laboratory setting, the results of which will be presented in Chapter 6.

The proposed strategy is to terminate a plain steel guitar string over an actuator, and to displace that actuator by an amount related to the displacement of the travelling wave incident upon it, according to information fed forward from the travelling wave sensor. In theory, we will show that if the displacement of the actuator is equal to that of the wave, the wave can be completely absorbed at the termination point without any reflection, causing the string to be damped within a single period of oscillation. In reality such a result is not possible as the practical capabilities of both the sensor and actuator deviate from the ideal; the range of displacement of the actuator is very small in comparison to the typical amplitude of a plucked guitar string, and the output of the travelling wave sensor can never be perfectly linear. Therefore, this chapter introduces theoretical models for commonly-encountered non-ideal behaviours, including limited actuator excursion and sensor non-linearity, paying particular attention to how that theory can be applied to the design of the sensor and actuator systems in the following chapters.

In order to demonstrate that a travelling wave control system is capable of precise and deliberate control over the musical properties of a string, we aim first to demonstrate that

the system has the ability to simply dampen a string's vibrations in a reasonable time and without inducing excessive spectral distortion.

3.1 The Wave Equation

The small-amplitude transverse displacement $u(x,t)$ of a string held under constant tension is described by the wave equation, a famous second-order hyperbolic partial differential equation in space x and time t:

$$\frac{\partial^2 u}{\partial x^2} = \frac{1}{c^2}\frac{\partial^2 u}{\partial t^2} \tag{3.1}$$

The travelling wave solution to this equation, originally proposed by French mathematician D'Alembert, states that the displacement can be modelled as the sum of a pair of waves $\overleftarrow{u}(x,t)$ and $\overrightarrow{u}(x,t)$ propagating along the string in opposite directions at constant speed:

$$u(x,t) = \overleftarrow{u}(x,t) + \overrightarrow{u}(x,t) \tag{3.2}$$

Rearranging Equation 3.2 and looking specifically at the termination point at $x = L$, the leftward-travelling wave emerging from the termination $\overleftarrow{u}(L,t)$ is equal to an inverted version of the incident rightward-travelling wave $\overrightarrow{u}(L,t)$ superimposed with the displacement of the termination $u(L,t)$:

$$\overleftarrow{u}(L,t) = u(L,t) - \overrightarrow{u}(L,t) \tag{3.3}$$

A similar expression can be derived for the rightward-travelling wave emerging from the termination at $x = 0$:

$$\overrightarrow{u}(0,t) = u(0,t) - \overleftarrow{u}(0,t) \tag{3.4}$$

In the travelling wave control system proposed here actuators are located at the terminations of the string so that the termination displacements $u(0,t)$ and $u(L,t)$ are under direct control, and can be thought of as inputs to the system. We choose to displace each termination by an amount which is a function of the travelling wave incident upon it:

$$\begin{aligned} u(0,t) &= f(\overleftarrow{u}(0,t)) \\ u(L,t) &= g(\overrightarrow{u}(L,t)) \end{aligned} \tag{3.5}$$

The form of the termination displacement functions f and g, which can also be considered the boundary conditions of the system described by the wave equation Equation 3.1, is crucial in determining the behaviour of the string. If f is set to zero (i.e $f(\overleftarrow{u}) = 0$) then Equation 3.4 becomes:

$$\overrightarrow{u}(0,t) = -\overleftarrow{u}(0,t) \tag{3.6}$$

This is the well-studied case of the rigidly terminated string, where the incident wave is inverted and perfectly reflected without modification. Conversely if the termination function f is equal to the incident wave, i.e $f(\overleftarrow{u}) = \overleftarrow{u}$, Equation 3.4 becomes:

$$\begin{aligned} \overrightarrow{u}(0,t) &= \overleftarrow{u}(0,t) - \overleftarrow{u}(0,t) \\ &= 0 \end{aligned} \tag{3.7}$$

In this case there is no reflected wave, the incident wave is completely absorbed by the active termination point. This illustrates the potential power of travelling wave control - if total absorption of a wave at the termination is possible, then any vibration of the string can be damped within a single period.

3.2 Non-ideal Termination Displacement Functions

In reality there are a number of practical constraints which prevent perfect absorption of the incident travelling wave.

3.2.1 Amplitude Constraints

As shall be explored in more detail in Chapter 5 the actuators we will be using have a limited maximum amplitude, A_{max}. As such the amplitude of the termination displacement functions f and g must always be below this limit:

$$|f(\overleftarrow{u})|_{max} \leq A_{max} \tag{3.8}$$

If the amplitude of the incident travelling wave is greater than this limit the amplitude of the termination displacement can be limited by introducing a frequency-independant control gain K:

$$f(\overleftarrow{u}) = K\overleftarrow{u} \tag{3.9}$$

To ensure the actuator remains within its linear region the value of K must be chosen to scale the maximum amplitude of the travelling wave to A_{max}. If the system is stable and damping the string, its maximum amplitude is the peak value of the initial travelling wave $\overleftarrow{u}(x,0)_{max}$:

$$K \leq \frac{A_{max}}{\overleftarrow{u}(x,0)_{max}} \tag{3.10}$$

This is the linear form of travelling wave control, and the effect of K on the string's vibration will be investigated in 3.3.1.

For simplicity and in order to remain as close as possible to the ideal form of travelling wave control we only consider the case of a control gain K which is independent of frequency. While a frequency-dependant gain could have the potential to improve the damping performance of the system, by for example increasing the gain at high frequencies to damp higher modes more quickly while decreasing the gain at low frequencies to prevent clipping, it would explicitly change the evolution of the spectral content of the string and thus its timbre, complicating the process of creating new timbres through nonlinearity. Care would also need to be taken in treating the way the frequency-dependant controller would affect the phase of the modal frequencies, particularly if a non-linear phase controller is used, which could cause instability in the system.

3.2.2 Nonlinearity

In reality the termination displacement f is actually a function of an estimate of the incident wave $\overleftarrow{u}_e$. Memoryless nonlinearities such as those caused by non-uniform light distribution in the sensor (Section 4.3.2), clipping of the actuator (Section 5.3.1) and those which we can add to the system to modify its timbre mean that $\overleftarrow{u}_e$ can be modelled as a polynomial function of the travelling wave $\overleftarrow{u}$. For simplicity we chose to model it as a third-order polynomial, consisting of an even-order quadratic nonlinearity with magnitude b', and an odd-order cubic nonlinearity with magnitude c':

$$\overleftarrow{u}_e = a'\overleftarrow{u} + b'\overleftarrow{u}^2 + c'\overleftarrow{u}^3 \tag{3.11}$$

With the addition of the control gain K the nonlinear termination displacement function becomes:

$$f(\overleftarrow{u}) = K(\overleftarrow{u} + b\overleftarrow{u}^2 + c\overleftarrow{u}^3) \tag{3.12}$$

Note that for simplicity the polynomial has been normalised such that the coefficient $a^{'}$ and the applied gain $K^{'}$ are absorbed into the gain K, leading to the following relationships:

$$\begin{aligned} K &= K^{'}a^{'} \\ b &= \frac{b^{'}}{K} \\ c &= \frac{c^{'}}{K} \end{aligned} \tag{3.13}$$

The effect of the nonlinearity on the behaviour of the string can be significant and complicated; we investigate its effect on the stability of the system in 3.3 and its effect on the behaviour of the string in 3.4.

3.2.3 Time Delay

The travelling wave control system proposed here is a feedforward system - the travelling wave is detected with a sensor at a particular location along the continuous portion of the string and then delayed by the amount of time it takes for the wave to travel to the termination. Errors in this time delay, perhaps caused by the finite sample rate of the digital system used to implement the control, cause the termination displacement to be described as:

$$u(0,t) = f(\overleftarrow{u}(0, t-\tau)) \tag{3.14}$$

We will examine the effect of this form of non-ideality experimentally in Chapter 6.

3.3 Stability Analysis

In many control systems stability is of prime importance, as the consequences of instability, defined as a system having unbounded outputs to bounded inputs, can be catastrophic. In the context of a musical string instability results in energy consistently being added to the string over time, causing the amplitude of vibration to increase, and pushing the string

into vibration regimes where its motion is no longer governed by the linear wave equation (Equation 3.1).

As unstable vibrations can be musically interesting it is not right to say that instability must be avoided at all costs, however its unpredictability and uncontrollability mean that for a system to exert meaningful control over the string it must at least be possible to avoid instability when desired. Analysis of the stability of any proposed control system can therefore give good insights into the feasibility of the system and where the boundaries of acceptable response lie.

3.3.1 Lyapunov's Stability Criterion

Aleksandr Lyapunov was a Russian mathematician who proposed a number of tests for the stability of a system. His second (or direct) method broadly states that if a positive-definite function of the system state (often called a lyapunov function) can be found to have a negative-definite derivative along the system trajectories, then the system is stable [46]. For purely physical systems such as a vibrating string it is often convenient to use the total physical energy stored in the system as a lyapunov function, and in this case the stability criterion reduces to establishing that the time derivative of the energy is always less than or equal to zero. This is conceptually easy to grasp, as if the rate of change of energy in the system is negative for all t, it must eventually decay to 0, meaning the string is at rest.

Note that during the rest of this section for brevity the partial derivatives of u with respect to x and t will be written using a subscript notation so that:

$$\begin{aligned} \frac{\partial u}{\partial x} &= u_x(x,t) \\ \frac{\partial u}{\partial t} &= u_t(x,t) \\ \frac{\partial^2 u}{\partial t^2} &= u_{tt}(x,t) \end{aligned} \tag{3.15}$$

Except where their explicit inclusion is useful, we will also assume we are working in a dimensionless context. As such the wave equation (Equation 3.1) can be expressed as:

$$u_{xx}(x,t) = u_{tt}(x,t) \tag{3.16}$$

The energy in a vibrating string is the sum of its kinetic and potential energies and can be expressed in dimensionless form as:

$$E(t) = \frac{1}{2}\int_0^L \left(u_x^2(x,t) + u_t^2(x,t)\right) dx \tag{3.17}$$

The stability criterion for the travelling wave control system can then be summarised as:

$$\frac{d}{dt}E(t) \leq 0 \tag{3.18}$$

Stability analysis of a string under travelling wave control

To express the stability criterion in terms of the boundary conditions of the string (and therefore ultimately the termination displacement functions $f(\overleftarrow{u})$ and $g(\overrightarrow{u})$) we begin by following the analysis of Chen [21].

To differentiate the energy of a string (Equation 3.17) with respect to time we can ignore the integral, take the two terms inside separately and use the chain rule:

$$\begin{aligned}\frac{\partial}{\partial t}(u_x^2) &= \frac{\partial(u_x^2)}{\partial u_x} \cdot \frac{\partial u_x}{\partial t} \\ &= 2u_x u_{xt}\end{aligned} \tag{3.19}$$

$$\begin{aligned}\frac{\partial}{\partial t}(u_t^2) &= \frac{\partial(u_t^2)}{\partial u_t} \cdot \frac{\partial u_t}{\partial t} \\ &= 2u_t u_{tt}\end{aligned} \tag{3.20}$$

The derivative of the energy can then be expressed as follows:

$$\frac{d}{dt}E(t) = \int_0^L u_x u_{xt} dx + \int_0^L u_t u_{tt} dx \tag{3.21}$$

Integrating the first term by parts gives:

$$\int_0^L u_x u_{xt} dx = [u_x u_t]_{x=0}^{x=L} - \int_0^L u_t u_{xx} dx \tag{3.22}$$

Then substituting this back into Equation 3.21 gives:

$$\frac{d}{dt}E(t) = [u_x u_t]_{x=0}^{x=L} - \int_0^L u_t u_{xx} dx + \int_0^L u_t u_{tt} dx \tag{3.23}$$

From the wave equation Equation 3.16 we know that $u_{tt} = u_{xx}$ and after making that substitution the final two terms in the equation above cancel, allowing the integral to be solved:

$$\frac{d}{dt}E(t) = u_x(L,t)u_t(L,t) - u_x(0,t)u_t(0,t) \tag{3.24}$$

Departing from Chen's analysis we now express the displacement u as the sum of the two travelling waves $\overleftarrow{u}(x,t) = u_l(x+t)$ and $\overrightarrow{u}(x,t) = u_r(x-t)$. Here we choose to represent those functions as complex exponentials, reflecting their periodicity in both space and time:

$$\begin{aligned} u(x,t) &= \overleftarrow{u}(x,t) + \overrightarrow{u}(x,t) \\ &= e^{j(x+t)} + e^{j(x-t)} \end{aligned} \tag{3.25}$$

We can then differentiate with respect to x:

$$\begin{aligned} u_x(x,t) &= je^{j(x+t)} + je^{j(x-t)} \\ &= j(\overleftarrow{u}(x,t) + \overrightarrow{u}(x,t)) \end{aligned} \tag{3.26}$$

and with respect to t:

$$\begin{aligned} u_t(x,t) &= je^{j(x+t)} - je^{j(x-t)} \\ &= j(\overleftarrow{u}(x,t) - \overrightarrow{u}(x,t)) \end{aligned} \tag{3.27}$$

Substituting these back into Equation 3.24 gives:

$$\frac{d}{dt}E(t) = (\overleftarrow{u}^2(0,t) + \overleftarrow{u}^2(L,t)) - (\overrightarrow{u}^2(0,t) + \overrightarrow{u}^2(L,t)) \tag{3.28}$$

Recalling the travelling wave control boundary conditions Equation 3.5 and the travelling wave solution to the wave equation at the termination points described by Equation 3.3 and Equation 3.4, we have the following expressions:

$$\begin{aligned} \overrightarrow{u}(0,t) &= f(\overleftarrow{u}(0,t)) - \overleftarrow{u}(0,t) \\ \overleftarrow{u}(L,t) &= g(\overrightarrow{u}(L,t)) - \overrightarrow{u}(L,t) \end{aligned} \tag{3.29}$$

Squaring these and substituting back into Equation 3.28 the energy flow into the system can be expressed in terms of the termination displacement functions f and g:

$$\frac{d}{dt}E(t) = f^2(\overleftarrow{u}\,(0,t)) - 2f(\overleftarrow{u}\,(0,t))\overleftarrow{u}\,(0,t) - (g^2(\overrightarrow{u}\,(L,t)) - 2g(\overrightarrow{u}\,(L,t))\overrightarrow{u}\,(L,t)) \quad (3.30)$$

Assuming that the right-hand termination is held rigid, $u(L,t) = g(\overrightarrow{u}\,(L,t)) = 0$, the stability criterion for the system becomes:

$$f^2(\overleftarrow{u}\,) - 2f(\overleftarrow{u}\,)\overleftarrow{u} \leq 0 \quad (3.31)$$

We will now explore the effect of various different forms of the termination displacement function f on the stability of the system.

The linear case

In the case of a perfectly linear constant-gain travelling wave control system, the termination displacement function is given by

$$f(\overleftarrow{u}\,) = K\overleftarrow{u} \quad (3.32)$$

where K is a constant scaling factor or gain. Applying the stability criterion Equation 3.31 results in a quadratic inequality in K:

$$K(K-2) \leq 0 \quad (3.33)$$

It is fairly straightforward to see that this can be solved by values of K within the range:

$$0 \leq K \leq 2 \quad (3.34)$$

So in the case of a perfectly linear travelling wave control function, where the displacement of the termination is a scaled but otherwise identical copy of the wave travelling towards it, the system is stable if the gain K is between zero and two.

It is interesting to consider what happens when the gain is at the limits of the inequality above, i.e. when $K = 0$ or $K = 2$. In this case the rate of change of energy in the system is 0

and the system is marginally stable, meaning that its state will neither become unbounded nor converge. For $K = 0$ the actuated termination point is rigid and the string appears as it would without control, with the wave coming towards the termination inverted and reflected back into the string.

When $K = 2$, the termination is displaced to double the height of the incoming wave, fully absorbing its energy and then creating a new wave travelling away from the termination with identical characteristics to the incoming one. In contrast to when $K = 0$ the wave is reflected but not inverted, flipping around the x axis but not the u axis. This is the conceptual equivalent of a free boundary which does not occur often in the case of vibrating strings but is encountered in the motion of cantilever beams and axially vibrating rods.

Quadratic non-linearity

Now we see what happens when we add a purely quadratic non-linearity into the termination displacement function:

$$f(\overleftarrow{u}) = K(\overleftarrow{u} + b\overleftarrow{u}^2) \tag{3.35}$$

Plugging the above function into the stability criterion (Equation 3.31) results in a quartic inequality in $\overleftarrow{u}$:

$$K^2\overleftarrow{u}^2(b\overleftarrow{u} + 1)(b\overleftarrow{u} + 1 - \frac{2}{K}) \leq 0 \tag{3.36}$$

For the system to be stable the above inequality must be true for all values of $\overleftarrow{u}$ in the interval $-1 \leq \overleftarrow{u} \leq 1$. The factor of $K^2\overleftarrow{u}^2$ which appears outside of the brackets is positive for all values of K and $\overleftarrow{u}$ so it can safely be ignored and we can focus on the quadratic polynomial inside the brackets, $h(\overleftarrow{u})$:

$$h(\overleftarrow{u}) = b^2\overleftarrow{u}^2 + b(2 - \frac{2}{K})\overleftarrow{u} + (1 - \frac{2}{K}) \tag{3.37}$$

At the centre of the interval at $\overleftarrow{u} = 0$, we have

$$h(0) = 1 - \frac{2}{K} \tag{3.38}$$

If we can show that $h(0)$ is itself less than or equal to 0, and that $h(\overleftarrow{u})$ does not cross the $\overleftarrow{u}$ axis in the interval $-1 \leq \overleftarrow{u} \leq 1$, then the system must be stable. Applying the condition $h(0) \leq 0$ results in the same constraints on K as in the linear case:

$$0 \leq K \leq 2 \tag{3.39}$$

The roots of $h(\overleftarrow{u})$, i.e the locations where it crosses the $\overleftarrow{u}$ axis are given by:

$$\begin{aligned} \overleftarrow{u}_1 &= -\frac{1}{b} \\ \overleftarrow{u}_2 &= \frac{\frac{2}{K} - 1}{b} \end{aligned} \tag{3.40}$$

Both of the roots exist for all values of b and K, but for the first root $\overleftarrow{u}_1$ to lie outside the relevant interval, the quadratic coefficient b must satisfy

$$-1 \leq b \leq 1 \tag{3.41}$$

Interestingly this inequality is independent of the gain K which means that it is not possible to reduce the control gain to prevent the system going unstable if the amount of quadratic nonlinearity present in the system exceeds the limits the inequality imposes. For the second root $\overleftarrow{u}_2$ to lie outside the interval, b and K must satisfy

$$1 - \frac{2}{K} \leq b \leq \frac{2}{K} - 1 \tag{3.42}$$

While this inequality is dependant on K, for $0 \leq K \leq 1$ the previous inequality imposes stricter limits on b, and this inequality is only relevant for $1 \leq K \leq 2$. It is also interesting to note that each of the inequalities in b are symmetrical and so the sign of the quadratic coefficient b is irrelevant, it is only its magnitude which determines the stability of the system. The complete stability criterion for the system with purely quadratic nonlinearity can be expressed with the following three compound inequalities, which are plotted on a b - K plane in Figure 3.1:

$$\begin{aligned} 0 \leq K \leq 2 \\ -1 \leq b \leq 1 \\ 1 - \frac{2}{K} \leq b \leq \frac{2}{K} - 1 \end{aligned} \tag{3.43}$$

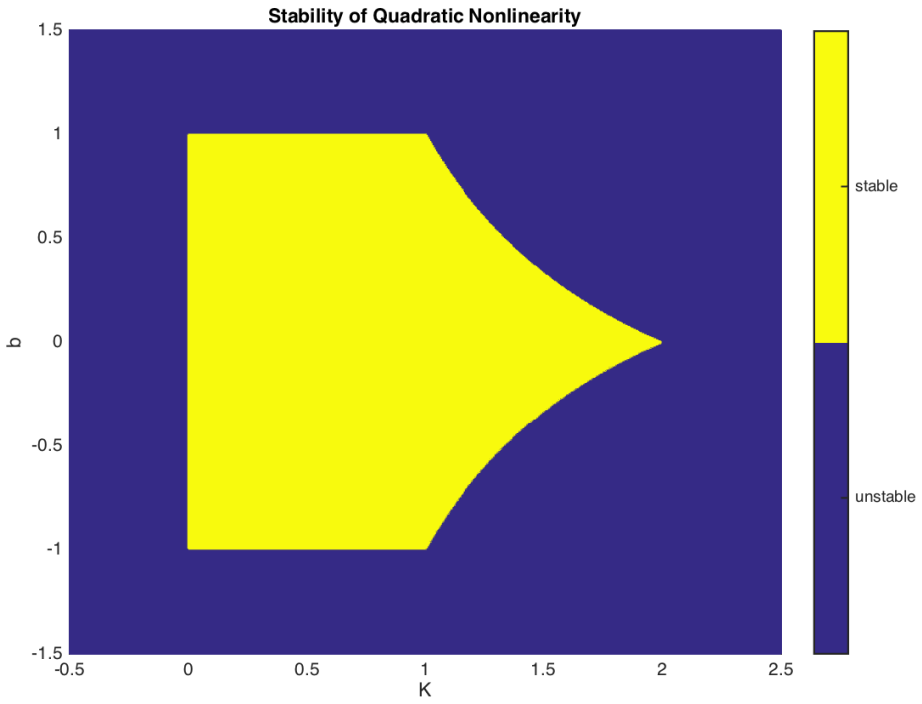

Figure 3.1: The stable regions of a system with a purely quadratic nonlinearity in the termination displacement function $f(\overleftarrow{u}) = K(\overleftarrow{u} + b\overleftarrow{u}^2)$.

Cubic non-linearity

Now we look at a different form of non-linearity with a cubic term in the termination displacement function:

$$f(\overleftarrow{u}) = K(\overleftarrow{u} + c\overleftarrow{u}^3) \tag{3.44}$$

Applying the stability criterion results in a sixth-order inequality in $\overleftarrow{u}$:

$$K^2\overleftarrow{u}^2(c\overleftarrow{u}^2 + 1)(c\overleftarrow{u}^2 + 1 - \frac{2}{K}) \leq 0 \tag{3.45}$$

We can again ignore the always-positive factor of $K^2\overleftarrow{u}^2$ outside the brackets and focus on the remaining quartic polynomial:

$$h(\overleftarrow{u}) = c^2\overleftarrow{u}^4 + c(2 - \frac{2}{K})\overleftarrow{u}^2 + (1 - \frac{2}{K}) \tag{3.46}$$

We apply the same logic as in the quadratic case, that if $h(0) \leq 0$ and the roots of the polynomial $h(\overleftarrow{u})$ do not exist in the interval $-1 \leq \overleftarrow{u} \leq 1$, then the system is stable. As before we have

$$h(0) = 1 - \frac{2}{K} \tag{3.47}$$

leading to the familiar constraint on K:

$$0 \leq K \leq 2 \tag{3.48}$$

The quartic polynomial $h(\overleftarrow{u})$ has four roots given by:

$$\begin{aligned} \overleftarrow{u}_1 &= \pm\sqrt{-\frac{1}{c}} \\ \overleftarrow{u}_2 &= \pm\sqrt{\frac{\frac{2}{K} - 1}{c}} \end{aligned} \tag{3.49}$$

The first pair of roots $\overleftarrow{u}_1$ don't exist for real values if c is positive. If c is negative, $\overleftarrow{u}_1$ lie inside the relevant interval for $c \leq -1$ leading to a one-sided stability constraint on c:

$$c \geq -1 \tag{3.50}$$

The numerator of the second pair of roots $\overleftarrow{u}_2$ can take any positive value for stable values of K but cannot go negative, so if c is negative the roots do not exist. If c is positive then the roots exist in the interval if c is smaller than the numerator, leading to another one-sided stability constraint:

$$c \leq \frac{2}{K} - 1 \tag{3.51}$$

The complete stability criterion for the system with a purely cubic nonlinearity can therefore be expressed with the following two inequalities, which are plotted on the c - K plane in Figure 3.2:

$$\begin{aligned} 0 \leq K \leq 2 \\ -1 \leq c \leq \frac{2}{K} - 1 \end{aligned} \tag{3.52}$$

The behaviour of the cubic nonlinearity is clearly quite different to the quadratic case. The constraint on the cubic coefficient c is asymmetrical; when c is negative there is a hard limit at $c = -1$ which is independent of the gain K, whereas when it is positive the constraint is dependant on K, meaning that systems which are pushed into instability by a positive cubic coefficient can be stabilised by reducing the gain.

Third-order polynomial nonlinearity

Finally we take a look at what happens when f takes the form of a general third-order polynomial nonlinearity.

$$f(\overleftarrow{u}) = K(\overleftarrow{u} + b\overleftarrow{u}^2 + c\overleftarrow{u}^3) \tag{3.53}$$

After applying the stability criterion we are left with the following sixth-order inequality:

$$K^2\overleftarrow{u}^2(c\overleftarrow{u}^2 + b\overleftarrow{u} + 1)(c\overleftarrow{u}^2 + b\overleftarrow{u} + 1 - \frac{2}{K}) \leq 0 \tag{3.54}$$

As before we can ignore the always-positive factor of $K^2\overleftarrow{u}^2$ outside the brackets and focus on the remaining quartic polynomial:

$$h(\overleftarrow{u}) = c^2\overleftarrow{u}^4 + 2bc\overleftarrow{u}^3 + c(2 - \frac{2}{K})\overleftarrow{u}^2 + b(2 - \frac{2}{K})\overleftarrow{u} + 1 - \frac{2}{K} \tag{3.55}$$

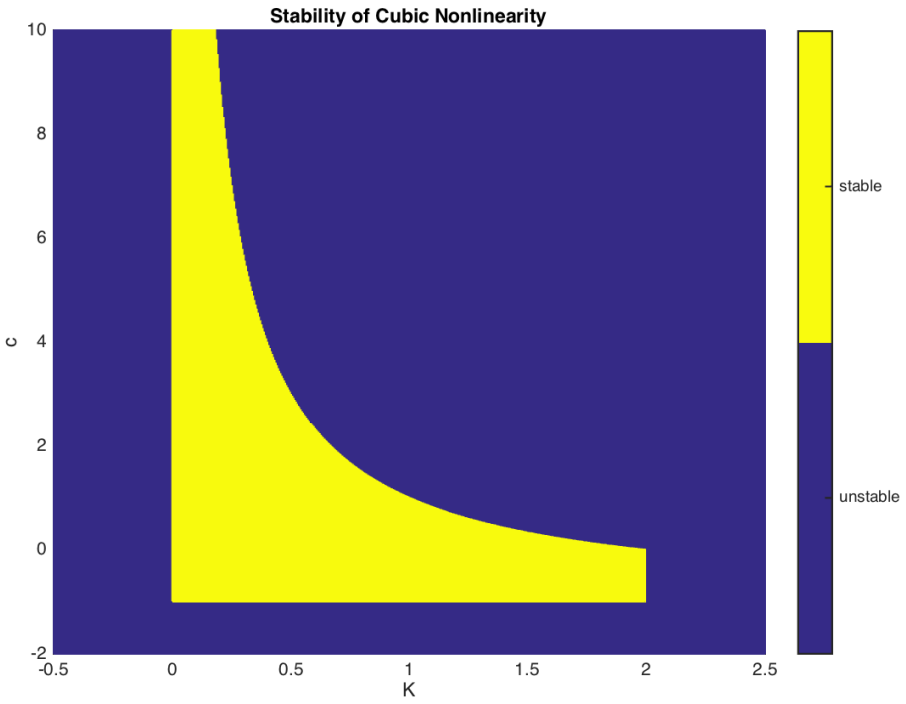

Figure 3.2: The stable regions of a system with a purely cubic nonlinearity in the termination displacement function $f(\overleftarrow{u}) = K(\overleftarrow{u} + c\overleftarrow{u}^3)$

As before applying the condition $h(0) \leq 0$ gives us the same stable range of K as the linear case:

$$0 \leq K \leq 2 \tag{3.56}$$

The roots of $h(\overleftarrow{u})$ are given by:

$$\begin{aligned} \overleftarrow{u}_1 &= \frac{-b \pm \sqrt{b^2 - 4c}}{2c} \\ \overleftarrow{u}_2 &= \frac{-b \pm \sqrt{b^2 - 4c(1 - \frac{2}{K})}}{2c} \end{aligned} \tag{3.57}$$

The first pair of roots $\overleftarrow{u}_1$ does not exist for

$$b^2 \leq 4c \tag{3.58}$$

This inequality defines a parabola on the b - c plane which is independent of the gain K, and is the dominant constraint on the quadratic coefficient b for $c > 1$.

For $-1 \leq c \leq 1$ the dominant constraint on b is found by ensuring that when the first pair of roots $\overleftarrow{u}_1$ exist, they exist outside the interval $-1 \leq \overleftarrow{u} \leq 1$. Applying this condition yields a pair of linear inequalities in b and c which are again independent of the gain K:

$$-(1 + c) \leq b \leq (1 + c) \tag{3.59}$$

Finally, for large values of c the dominant constraints on b are found by ensuring that when the second pair of roots $\overleftarrow{u}_2$ exist, they exist outside the interval $-1 \leq \overleftarrow{u} \leq 1$. This yields another linear pair of inequalities in b and c, which are on this occasion dependant on K:

$$-(1 - \frac{2}{K} + c) \leq b \leq (1 - \frac{2}{K} + c) \tag{3.60}$$

The complete stability criterion for a system with a third-order polynomial nonlinearity is plotted on b - c plane for various values of K in Figure 3.3. Several results from the analysis of purely quadratic and cubic nonlinearities carry over into the general case, including the fact that the constraints on b are symmetrical and so its sign is irrelevant, whereas the constraints on c are asymmetrical and its sign matters. We still have a hard constraint $c \geq -1$ which is independent of K. In fact, the gain K only affects the constraints on positive

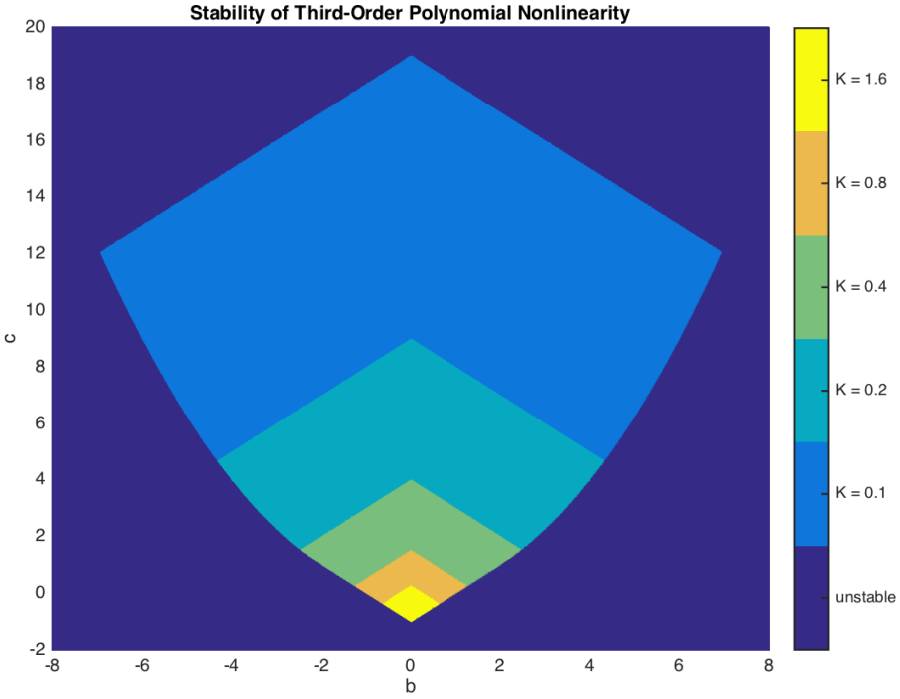

Figure 3.3: The stable regions of a system with a third-order polynomial nonlinearity in the termination displacement function $f(\overleftarrow{u}) = K(\overleftarrow{u} + b\overleftarrow{u}^2 + c\overleftarrow{u}^3)$, plotted on a b-c plane for different values of K

c and the constraints on b when c is positive and large, and for many forms of nonlinearity stability is essentially independent of K.

This demonstrates just how sensitive the travelling wave control system is to nonlinearity in the termination displacement function $f(\overleftarrow{u})$. If nonlinearities in the travelling wave sensor exceed any of the constraints which we have shown here to be independent of the gain K then the system cannot be easily stabilised. Even when constraining the amplitude of the actuator by applying a gain which is infinitesimally close to 0, the system will be unstable and will induce uncontrollable vibrations of the string with unbounded amplitude.

3.4 String Behaviour

Stability analysis is useful to understand if a travelling wave control system is feasible in the presence of limited actuator amplitude or sensor non-linearities, however it gives no insight into the effects of these imperfections on the behaviour of a string and the resulting timbre.

3.4.1 Iterative Solution

So far, we have only considered the termination displacement functions f and g as operating on the single part of the wave which is incident upon their respective terminations at the instantaneous time t:

$$\begin{aligned} \overrightarrow{u}(0,t) &= f(\overleftarrow{u}(0,t)) - \overleftarrow{u}(0,t) \\ \overleftarrow{u}(L,t) &= g(\overrightarrow{u}(L,t)) - \overrightarrow{u}(L,t) \end{aligned} \tag{3.61}$$

Now consider what happens to the element of the leftward travelling wave which at time t is located one quarter of the way along the string, $\overleftarrow{u}(\frac{L}{4},t)$. As time goes by the wave travels to the left until after one eighth of the period of the string has elapsed, at time $t+\frac{T}{8}$, our element reaches the termination at $x=0$:

$$\overleftarrow{u}(0,t+\frac{T}{8}) = \overleftarrow{u}(\frac{L}{4},t) \tag{3.62}$$

It is then operated on by f and reflected, becoming part of the rightward travelling wave:

$$\begin{aligned}\overrightarrow{u}(0, t + \frac{T}{8}) &= f(\overleftarrow{u}(0, t + \frac{T}{8})) - \overleftarrow{u}(0, t + \frac{T}{8}) \\ &= f(\overleftarrow{u}(\frac{L}{4}, t)) - \overleftarrow{u}(\frac{L}{4}, t)\end{aligned} \tag{3.63}$$

Our element now begins travelling to the right, until after a further three-eighths of a period, i.e at $t = \frac{T}{2}$, it has reached three-quarters of the way along the string:

$$\begin{aligned}\overrightarrow{u}(\frac{3L}{4}, t + \frac{T}{2}) &= \overrightarrow{u}(0, t + \frac{T}{8}) \\ &= f(\overleftarrow{u}(\frac{L}{4}, t)) - \overleftarrow{u}(\frac{L}{4}, t)\end{aligned} \tag{3.64}$$

Performing this same calculation for every element of the leftward travelling wave from $x = 0$ to $x = L$, we find it is possible to define a mapping function F which maps the entire leftward travelling wave at time t into the rightward travelling wave half a period later at time $t + \frac{T}{2}$ in terms of the termination displacement function f:

$$\begin{aligned}\overrightarrow{u}(x, t + \frac{T}{2}) &= F(\overleftarrow{u}(L - x, t)) \\ &= f(\overleftarrow{u}(L - x, t)) - \overleftarrow{u}(L - x, t)\end{aligned} \tag{3.65}$$

Note the appearance of $L - x$ in the equation above which means the wave is flipped in the x dimension by the mapping function F. We can define a similar mapping function G in terms of the termination displacement function g which maps the rightward travelling wave into the leftward travelling wave half a period later:

$$\begin{aligned}\overleftarrow{u}(x, t + \frac{T}{2}) &= G(\overrightarrow{u}(L - x, t)) \\ &= g(\overrightarrow{u}(L - x, t)) - \overrightarrow{u}(L - x, t)\end{aligned} \tag{3.66}$$

These functions can be combined, allowing both travelling waves at time t to be mapped into themselves one period later at time $t + T$:

$$\begin{aligned}\overleftarrow{u}(x, t + T) &= G \cdot F(\overleftarrow{u}(x, t)) \\ \overrightarrow{u}(x, t + T) &= F \cdot G(\overrightarrow{u}(x, t))\end{aligned} \tag{3.67}$$

Here the dot notation is used to express that the output of the first function is used as the input to the second:

$$F \cdot G(y) = F(G(y)) \tag{3.68}$$

Note that because both F and G flip the wave in the x-dimension after one period each wave has been flipped back to its original orientation. If we again assume that the right-hand termination at $x = L$ is held rigid, $g(\overrightarrow{u}) = 0$ and $G(\overrightarrow{u}) = -\overrightarrow{u}$ we can simplify Equation 3.67 to

$$\begin{aligned} \overleftarrow{u}_{m+1} &= -F(\overleftarrow{u}_m) \\ \overrightarrow{u}_{m+1} &= F(-\overrightarrow{u}_m) \end{aligned} \tag{3.69}$$

where the subscript m is used to indicate the number of periods which have passed, such that $\overleftarrow{u}_m = \overleftarrow{u}(x, mT)$. Equations of this form, where the next state of the system at time $m+1$ is a function of the current state at time m, are known as first-order difference equations or recurrence relations. They imply that with knowledge of the initial state of the travelling waves $\overleftarrow{u}_0$ and $\overrightarrow{u}_0$ and the mapping function F, the state of the string at any number m periods in the future can be determined through iteration of the function F m times:

$$\begin{aligned} u_m &= \overleftarrow{u}_m + \overrightarrow{u}_m \\ &= -F_m(\overleftarrow{u}_0) + F_m(-\overrightarrow{u}_0) \end{aligned} \tag{3.70}$$

We can therefore use the equations to analyse how different forms of F influence the behaviour of the string over time.

3.4.2 The Linear Case

In the linear case the termination displacement function, mapping function and recurrence relation are given as follows:

$$\begin{aligned} f(\overleftarrow{u}) &= K\overleftarrow{u} \\ F(\overleftarrow{u}) &= (K-1)\overleftarrow{u} \\ u_{m+1} &= (1-K)u_m \end{aligned} \tag{3.71}$$

It is simple to identify a closed-form solution for the displacement after m periods:

$$u_m = (1 - K)^m u_0 \tag{3.72}$$

For stable values of the gain $0 \leq K \leq 2$ linear travelling wave control acts like linear damping and the amplitude of the vibration decays at an exponential rate with a half life $t_{\frac{1}{2}}$ measured in units of the period of the string:

$$t_{\frac{1}{2}} = \frac{\ln(\frac{1}{2})}{\ln(1 - K)} \tag{3.73}$$

Figure 3.4 shows the relationship between the half-life and the constant frequency-independent gain K, highlighting that when $K = 1$ the half life is 0 as the string is fully damped within one period. The dependance of the half-life on the string's period is interesting, as it implies that a string tuned to a higher pitch will be damped more quickly.

As is to be expected linear control does not alter the frequency content of the vibration, and therefore has no effect on the spectro-temporal elements of the timbre.

3.4.3 Non-Linearity

With a quadratic non-linearity in the control system the displacement and mapping functions become:

$$\begin{aligned} f(\overleftarrow{u}) &= K(\overleftarrow{u} + b\overleftarrow{u}^2) \\ F(\overleftarrow{u}) &= (K - 1)\overleftarrow{u} + Kb\overleftarrow{u}^2 \end{aligned} \tag{3.74}$$

Because F is now non-linear, $F(-\overleftarrow{u})$ is not equal to $-F(\overleftarrow{u})$ and the recurrence relations for the waves travelling in opposite directions are different:

$$\begin{aligned} \overrightarrow{u}_{m+1} &= F(-\overrightarrow{u}_m) \\ &= (1 - K)\overrightarrow{u}_m + Kb\overrightarrow{u}_m^2 \\ \overleftarrow{u}_{m+1} &= -F(\overleftarrow{u}_m) \\ &= (1 - K)\overleftarrow{u}_m - Kb\overleftarrow{u}_m^2 \end{aligned} \tag{3.75}$$

Unlike in the linear case there is no straightforward closed-form solution for $\overleftarrow{u}_m$ or $\overrightarrow{u}_m$.

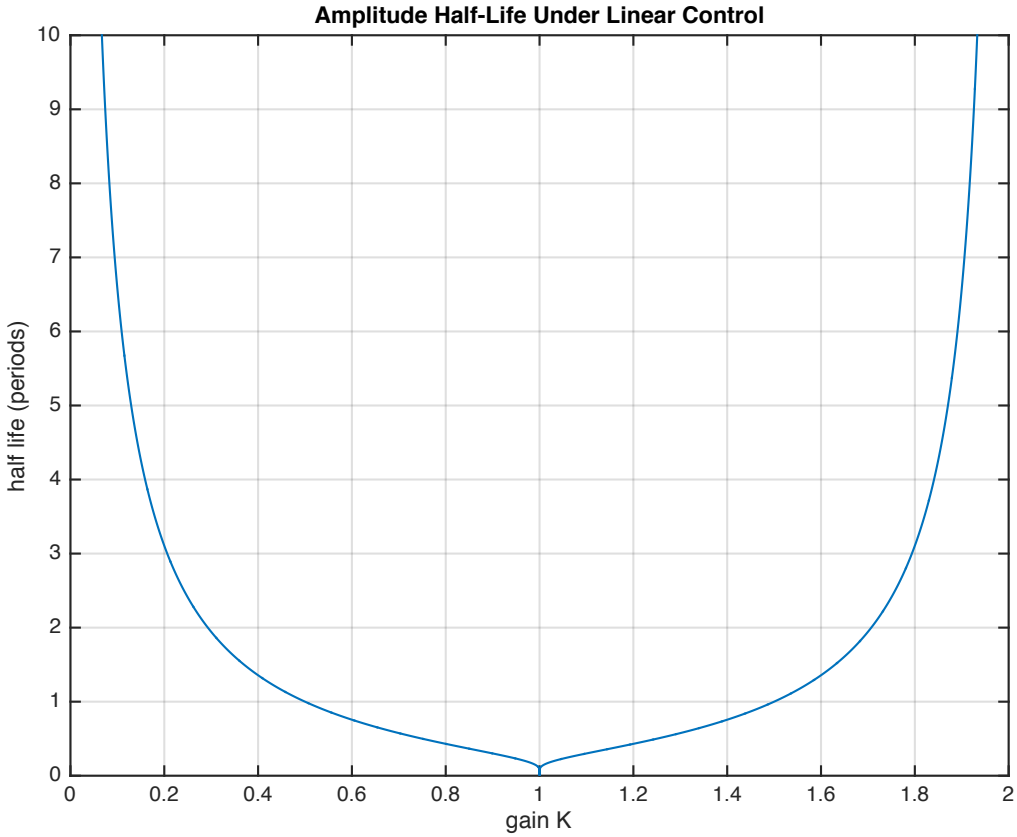

Figure 3.4: The half-life of the string's amplitude $t_{\frac{1}{2}}$ plotted against the gain K of a linear travelling wave control system

Initial Conditions

To simplify the following analysis we choose the initial displacement of the string u_0 to be a simple sinusoid at the fundamental frequency of the string in the spatial domain:

$$\begin{aligned} u_0 &= 2sin(k_0 x) \\ k_0 &= \frac{\pi}{L} \end{aligned} \tag{3.76}$$

We also specify that the initial velocity of the string is zero, $\frac{du_0}{dt} = 0$ so the initial travelling waves are equal and have an amplitude of 1:

$$\overleftarrow{u}_0 = \overrightarrow{u}_0 = sin(k_0 x) \tag{3.77}$$

Time Domain Analysis

Defining the constants $\alpha = (1 - K)$ and $\beta = Kb$, we can examine the first two iterations of the rightward travelling wave in the time domain:

$$\begin{aligned} \overrightarrow{u}_0 &= \overrightarrow{u}_0 \\ \overrightarrow{u}_1 &= \alpha \overrightarrow{u}_0 + \beta \overrightarrow{u}_0^2 \\ \overrightarrow{u}_2 &= \alpha \overrightarrow{u}_1 + \beta \overrightarrow{u}_1^2 \\ &= \alpha^2 \overrightarrow{u}_0 + \alpha\beta(1+\alpha) \overrightarrow{u}_0^2 + 2\alpha\beta^2 \overrightarrow{u}_0^3 + \beta^3 \overrightarrow{u}_0^4 \end{aligned} \tag{3.78}$$

Applying the initial conditions $\overleftarrow{u}_0 = \overrightarrow{u}_0 = \sin(k_0 x)$ and variations on the trigonometric identity $\sin^2(k_0 x) = \frac{1}{2}(1 - \cos(2k_0 x))$, the iterations can be expressed in terms of the modal frequencies of the string:

$$
\begin{aligned}
\overrightarrow{u}_0 &= \sin(k_0 x) \\
\overrightarrow{u}_1 &= \frac{1}{2}\beta + \alpha \sin(k_0 x) - \frac{1}{2}\beta \cos(2k_0 x) \\
\overrightarrow{u}_2 &= \frac{1}{2}\beta(\alpha(1+\alpha) + \frac{3}{4}\beta^2) \\
&\quad + \alpha(\alpha + \frac{3}{2}\beta^2)\sin(k_0 x) \\
&\quad - \frac{1}{2}\beta(\alpha(1+\alpha) + \beta^2)\cos(2k_0 x) \\
&\quad - \frac{1}{2}\alpha\beta^2 \sin(3k_0 x) \\
&\quad + \frac{1}{8}\beta^3 \cos(4k_0 x)
\end{aligned}
\tag{3.79}
$$

The dramatic effect of the non-linearity now becomes clear; it shifts energy up into higher frequencies, activating modes that were not present in the initial condition $\overrightarrow{u}_0$. After only two periods of vibration components of all the modes up to the fourth are already present in the response and the highest mode present doubles after each iteration such that after m iterations the highest frequency present is $2^m k_0$. As only modal frequencies are present in the response the mth iteration can be described by a fourier series:

$$
\overrightarrow{u}_m = \sum_{n=-2^m}^{2^m} C_n e^{jnk_0 x} \tag{3.80}
$$

Unfortunately there is no closed-form expression for the modal coefficients C_n and the only way to determine them is to perform the iteration, though doing this analytically is difficult as the algebra rapidly becomes impractical.

Performing a similar analysis for the leftward-travelling wave yields an answer identical to the rightward but with the sign of the coefficients of the even modes (i.e $n = 2$, $n = 4$ etc) inverted. It is tempting to say that when the iterated travelling waves are summed to get the actual displacement of the string, these even modes will cancel and not appear in the response. This is only true for the precise instants in time which are multiples of the string's period, i.e $t = mT$, for the rest of the time between these moments the phase of these components will not align, so the even modes do appear in the resulting sound produced by the string.

For the case of a pure cubic non-linearity in the control system we have:

$$
\begin{aligned}
f(\overleftarrow{u}) &= K(\overleftarrow{u} + c\overleftarrow{u}^3) \\
F(\overleftarrow{u}) &= (K-1)\overleftarrow{u} + c\overleftarrow{u}^3
\end{aligned}
\tag{3.81}
$$

In this case, despite the nonlinearity, we have $F(-\overleftarrow{u}) = -F(\overleftarrow{u})$ so the two travelling waves are identical. Performing the iterations on $\overleftarrow{u}_0$ results in a similar outcome as in the quadratic case, with a few notable differences. Firstly, even modes (i.e $n = 2$, $n = 4$ etc) are not present in either travelling wave, and are therefore not present in the resulting sound. Secondly, the highest mode present after m periods is greater than in the case of pure quadratic non-linearity, and is equal to 3^m. It is actually possible to say that in the case of a generalised non-linear termination displacement function f of order p, the response after m periods can be expressed as the fourier series:

$$
u(x, mT) = \sum_{n=-p^m}^{p^m} C_n e^{jnk_0 x} \tag{3.82}
$$

3.5 Simulations

As the equations which describe the behaviour of the nonlinear travelling wave control system do not have closed-form solutions and are too complicated to explore analytically, it is necessary to resort to numerical simulations to understand the effect of nonlinearities on the timbre of the sound produced by the system. The simulations presented here start with the initial conditions

$$
\begin{aligned}
\overleftarrow{u}_0 &= sin(k_0 x) \\
\overrightarrow{u}_0 &= sin(k_0 x) \\
k_0 &= \frac{\pi}{L}
\end{aligned}
\tag{3.83}
$$

i.e both travelling waves are a simple sinusoid at the fundamental frequency of the string. The iterative equations (Equation 3.69) are then used to advance time forward by one period for each iteration. After each period a fourier transform of the travelling waves is taken, allowing the amplitude of the modal frequencies (and properties which are derived from them such as total harmonic distortion) to be plotted against time.

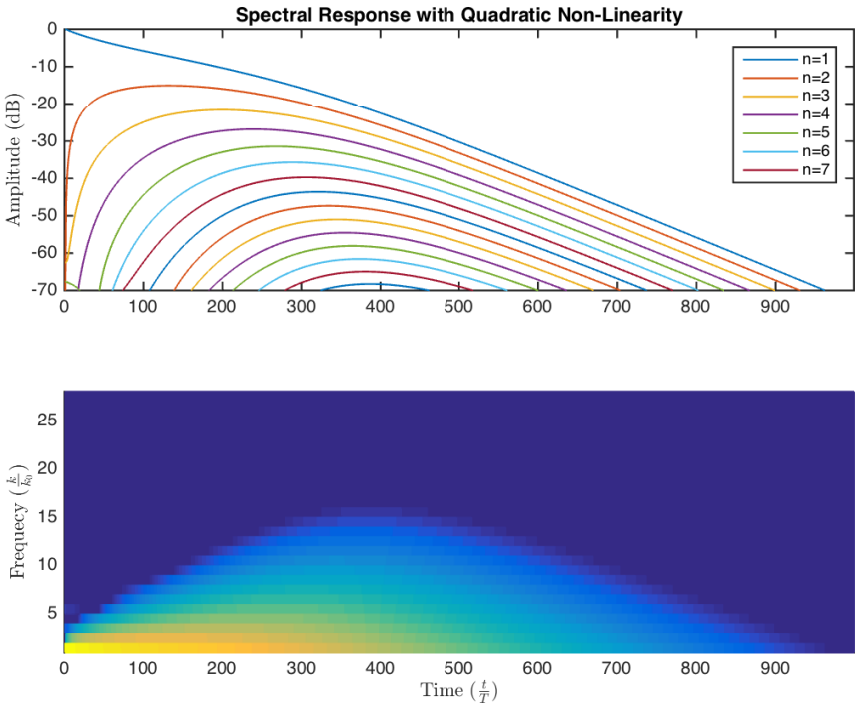

Figure 3.5: The evolution of the modal frequencies of the string with a purely quadratic nonlinearity in the termination displacement function $f(\overleftarrow{u}) = K(\overleftarrow{u} + b\overleftarrow{u}^2 + c\overleftarrow{u}^3)$ with $K = 0.01$, $b = 0.95$ and $c = 0$ and initial conditions $\overleftarrow{u}_0 = \overrightarrow{u}_0 = sin(k_0 x)$

3.5.1 Modal Frequency Plots

In Figure 3.5 to Figure 3.7 the evolution of the modal amplitudes is plotted as both a line graph and a spectrogram for a purely quadratic nonlinearity, a purely cubic nonlinearity, and a general third-order polynomial nonlinearity. The plots show the dramatic effect of nonlinearities in the control system on the spectro-temporal timbre of the string.

3.5.2 Total Harmonic Distortion

We define the total harmonic distortion of the string's response to be the ratio of the RMS amplitude of the higher modes to that of the fundamental as follows:

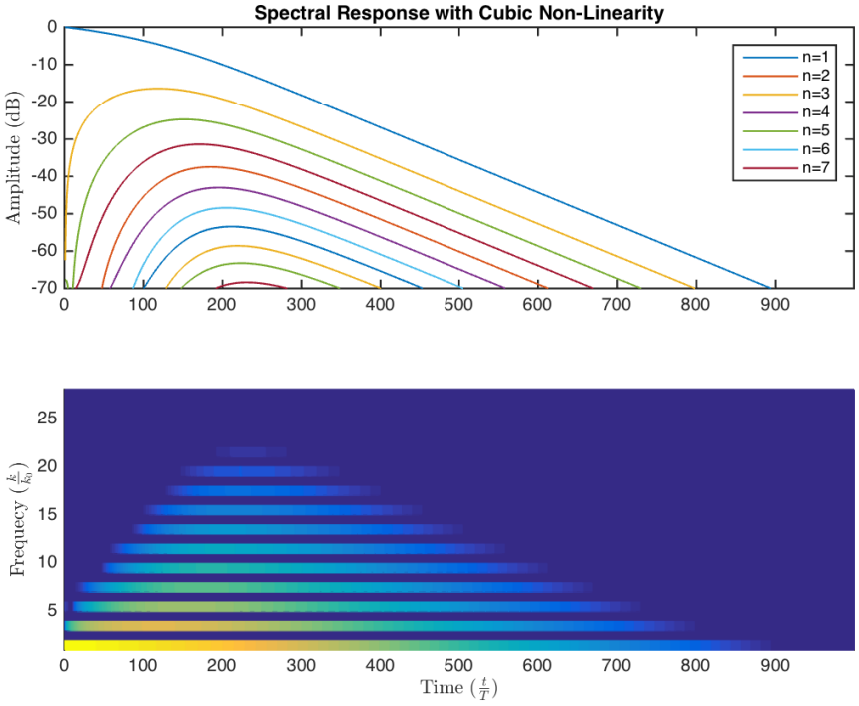

Figure 3.6: The evolution of the modal frequencies of the string with a purely cubic nonlinearity in the termination displacement function $f(\overleftarrow{u}) = K(\overleftarrow{u} + b\overleftarrow{u}^2 + c\overleftarrow{u}^3)$ with $K = 0.01$, $b = 0$ and $c = -0.95$ and initial conditions $\overleftarrow{u}_0 = \overrightarrow{u}_0 = sin(k_0 x)$

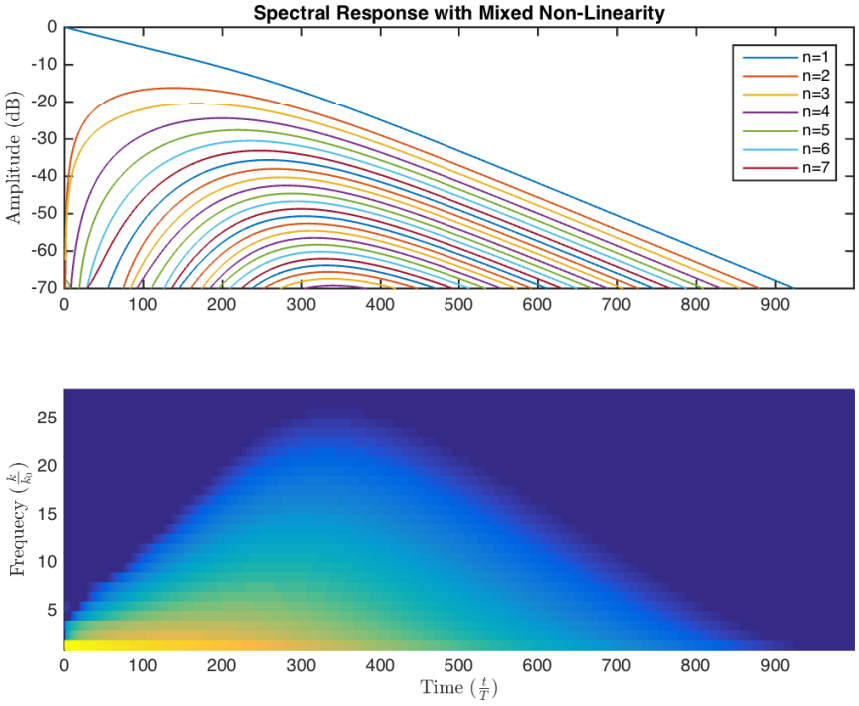

Figure 3.7: The evolution of the modal frequencies of the string with a third-order polynomial nonlinearity in the termination displacement function $f(\overleftarrow{u}) = K(\overleftarrow{u} + b\overleftarrow{u}^2 + c\overleftarrow{u}^3)$ with $K = 0.01$, $b = 0.49$ and $c = -0.49$ and initial conditions $\overleftarrow{u}_0 = \overrightarrow{u}_0 = sin(k_0 x)$

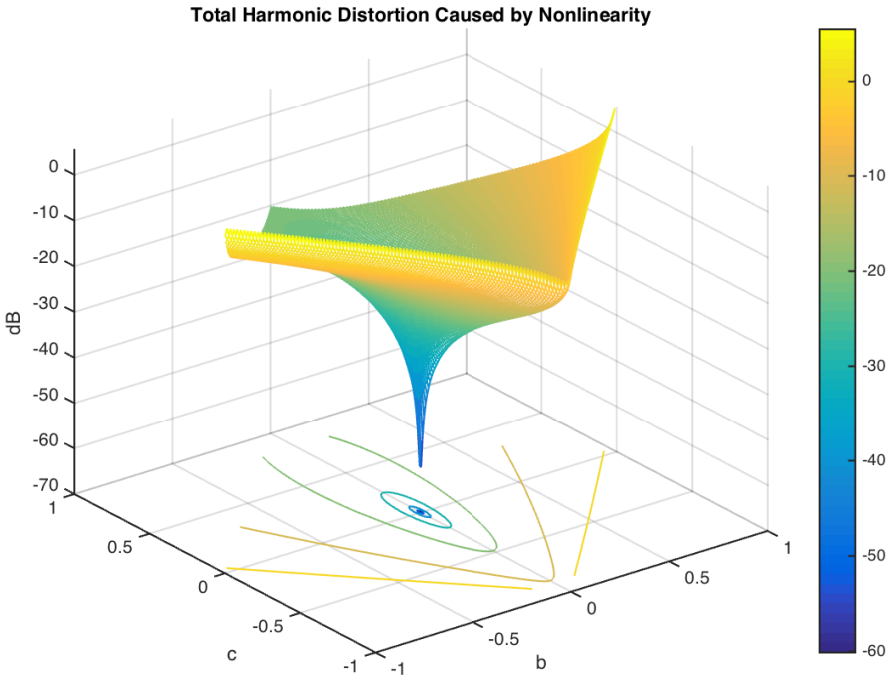

Figure 3.8: The peak total harmonic distortion of the string's response plotted on a b-c plane where b and c are nonlinear coefficients in the termination displacement function $f(\overleftarrow{u}) = K(\overleftarrow{u} + b\overleftarrow{u}^2 + c\overleftarrow{u}^3)$, with $K = 0.1$. Initial conditions are $\overleftarrow{u}_0 = \overrightarrow{u}_0 = sin(k_0 x)$

$$thd = \frac{\sqrt{\sum_{n=2}^{\infty} C_n^2}}{|C_1|} \tag{3.84}$$

It is a useful measure of the audible distortion induced in the string by nonlinearity, and can be treated as a value to be minimised in order to reduce the uncontrollable effect of the nonlinearity on timbre. Figure 3.8 shows a plot of the peak total harmonic distortion as the string is damped for stable values of the nonlinear coefficients in the termination displacement function f. The plot only displays values for which the peak amplitude of the termination displacement is limited to less than twice the gain K.

The initial conditions for this plot are again chosen to be a single sinusoid at the fundamental frequency, where $thd = -\infty$dB. All non-zero values of the thd are therefore caused by the

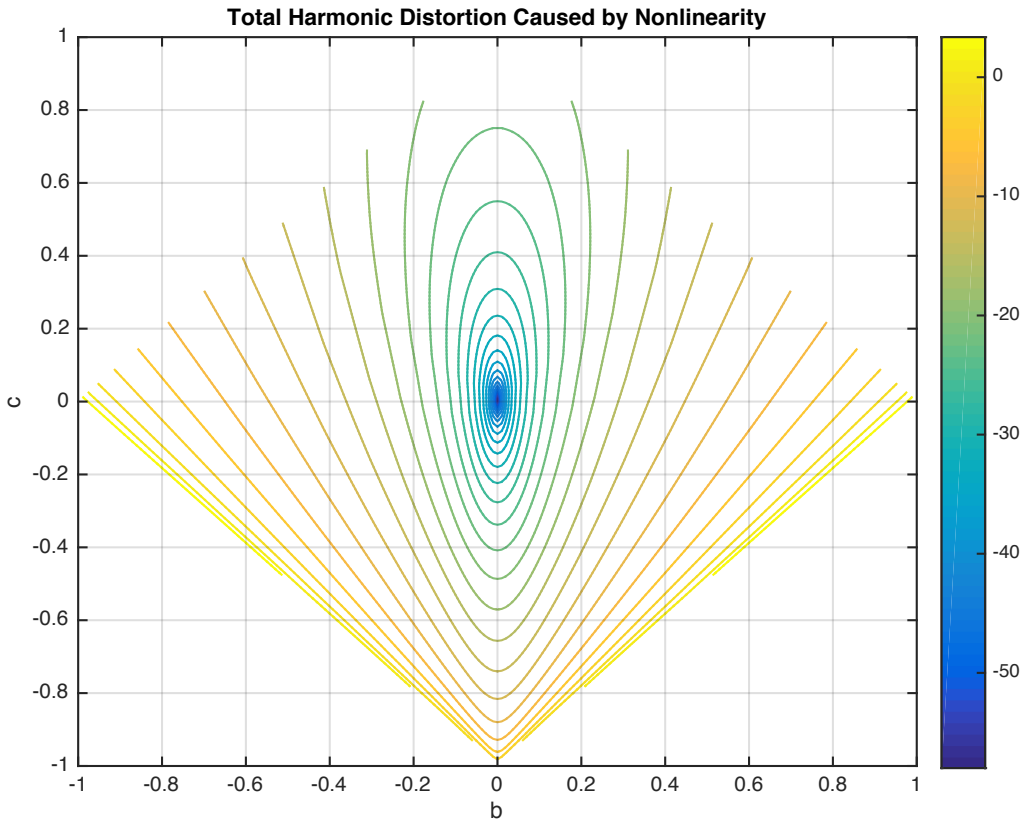

Figure 3.9: A more detailed contour plot of the data presented in Figure 3.8

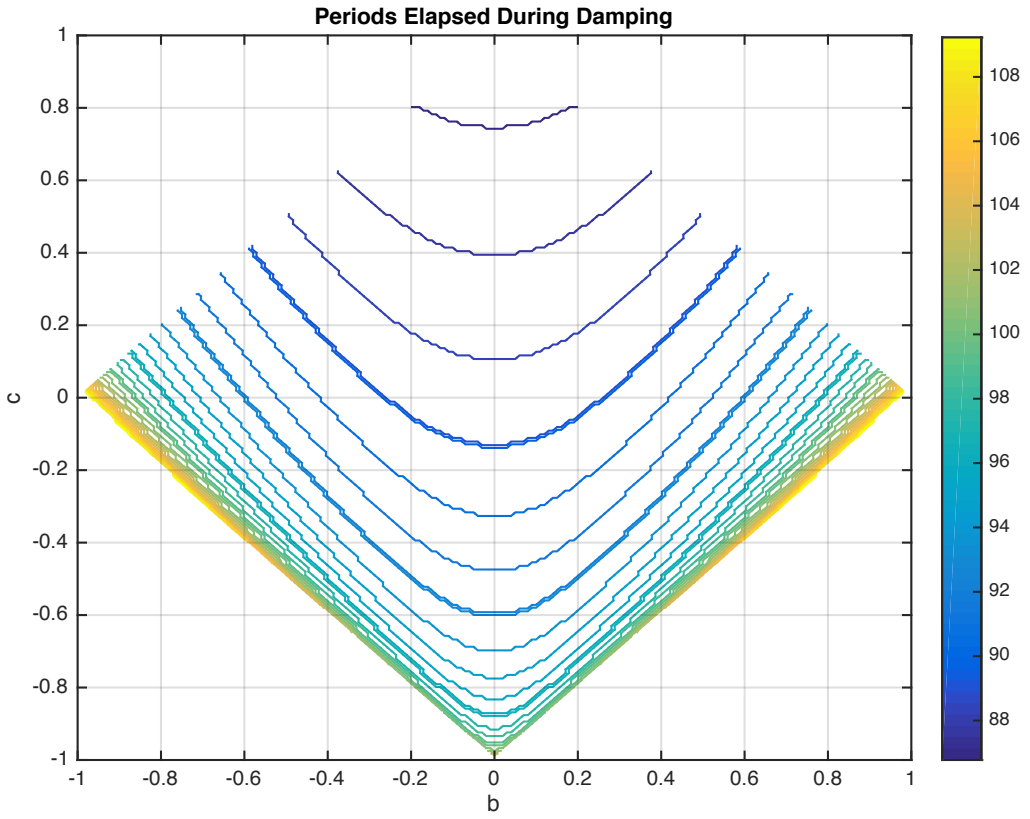

Figure 3.10: A contour plot of the number of periods elapsed before the string is damped below −80dB plotted on a b-c plane where b and c are nonlinear coefficients in the termination displacement function $f(\overleftarrow{u}) = K(\overleftarrow{u} + b\overleftarrow{u}^2 + c\overleftarrow{u}^3)$, with $K = 0.1$. Initial conditions are $\overleftarrow{u}_0 = \overrightarrow{u}_0 = sin(k_0 x)$

nonlinearity. It is clear from the plots that only a small amount of nonlinearity causes a significant amount of distortion in the string's sound. It can also be seen that cubic nonlinearity has a smaller effect than quadratic nonlinearity and is again asymmetrical, with positive values of the cubic coefficient c causing less distortion than negative values.

Figure 3.10 is a contour plot showing the effect of nonlinearity on the damping time of the string. It shows that positive cubic nonlinearity improves the speed of the damping, while all other forms of nonlinearity degrade it.

3.6 Summary

In this chapter we have presented a mathematical model of travelling wave control applied to a vibrating string. We showed that in an ideal form of the control system where the termination point of the string is displaced by an amount perfectly equal to the incident wave, the vibrations of the string are damped within a single period of vibration. We then highlighted a number of realistic non-idealities, and modelled their effects.

We showed that if the control system is linear the vibrations in the string can be damped without inducing harmonic distortion in the string's motion. The speed with which the string is damped is dependant upon the gain K.

We showed that the behaviour of the system can be modelled iteratively, with the termination displacement function $f(\overleftarrow{u})$ mapping the current state of the string into the next one period at a time. Nonlinearities in the system cause energy to be shifted between the harmonic frequencies during each period, inducing harmonic distortion in the string's motion and modifying its timbre.

We derived a generalised stability criterion for the system and applied it to the linear and nonlinear forms of travelling wave control. We identified that stable values of the control gain K vary from 0 to 2, while different forms of nonlinearity cause different stability behaviours. For $K < 1$ values of the nonlinear quadratic coefficient b with magnitudes greater than 1 will cause instability regardless of the gain, as will negative values of the cubic coefficient c which are less than -1. In contrast positive values of the cubic coefficient have the potential to stabilise the system when the gain is low.

We demonstrated that any amount of nonlinearity in the system can cause harmonic distortion in the string's motion and affect its timbre, though positive cubic nonlinearity has a lesser effect than other forms. Most forms of nonlinearity also degrade the speed with which the system can remove energy from the string and damp vibrations, except for positive cubic nonlinearity which can actually improve the damping time.

The most important conclusion to draw from this chapter is that nonlinearity can be both a curse and a blessing in a musical travelling wave control system. Structural nonlinearities in the system are a curse because they degrade its performance by increasing the damping time, inducing harmonic distortion and modifying timbre in an uncontrollable way, and potentially causing instability. For this reason in the next two chapters we focus on designing highly linear sensor and actuator systems for a practical control system.

If the control system itself is linear, than deliberately adding nonlinearity has the effect of modifying the evolution of the modal amplitudes of the string (and through that the

spectro-temporal elements of it timbre) in a novel and natural way.

Chapter 4

Sensing Travelling Waves

Travelling wave control places unusual demands upon sensors from both a hardware and a signal processing perspective. The physical quantity which must be measured, i.e. the displacement of the wave travelling along the string towards the termination point, is not measurable directly, instead it must be estimated with an algorithm from an array of measurements of the string's overall displacement. This estimation must be done quickly; the typical speed of transverse waves on a tensioned steel musical instrument string exceeds hundreds of meters per second. The estimation must also be done accurately; errors resulting from noise and nonlinearities lead to degraded performance, harmonic distortion and instability.

This chapter details the design and build of a system for sensing travelling waves consisting of a pair of optical displacement sensors. It first investigates an algorithm for decomposing the travelling wave components from the measurements collected by the sensors.

Major sources of nonlinearity in the sensors and mitigations to lessen effects on the full travelling wave control system are then investigated and modelled. Two important sources are identified: out-of-plane or elliptical motion of the string, and non-uniform light distribution on the surface of the sensor. Both of these effects are shown to be capable of destabilising a travelling wave control system if the sensor is designed without considering their effects. The design of the sensor is optimised to reduce the amount of harmonic distortion in the motion of the string caused by both effects.

Finally a low-noise preamplifier circuit is presented which electrically biases the photodiodes used in the sensor correctly, and converts their output to a voltage of the correct range. The contribution of various elements in the circuit is analysed, and the signal-to-noise ratio of

the circuit is optimised.

4.1 Travelling Wave Decomposition

The travelling wave solution to the wave equation states that the displacement of any point along the string is composed of the sum of a pair of waves travelling in opposite directions:

$$u(x,t) = \overleftarrow{u}(x,t) + \overrightarrow{u}(x,t) \tag{4.1}$$

The waves translate in the negative and positive x-directions (or more informally to the left and to the right respectively) at speed c, and are constant along the characteristics $x + ct$ and $x - ct$

$$\begin{aligned} \overleftarrow{u}(x,t) &= \overleftarrow{u}(x+ct) \\ \overrightarrow{u}(x,t) &= \overrightarrow{u}(x-ct) \end{aligned} \tag{4.2}$$

The travelling waves can not be measured directly as under typical conditions components of both travelling waves are present in any measurement of the string's displacement $u(x,t)$ and must be decomposed from multiple measurements using an algorithm. The most simple algorithm uses a pair of sensors separated by a distance Δx. The left-hand sensor at position x_0 is sampled first at time t_0 giving the output u_1, while the second sensor at $x_0 + \Delta x$ is sampled slightly later at $t_0 + \Delta t$ to give the output u_2:

$$\begin{aligned} u_1 &= \overleftarrow{u}(x_0 + ct_0) + \overrightarrow{u}(x_0 - ct_0) \\ u_2 &= \overleftarrow{u}(x_0 + \Delta x + c(t_0 + \Delta t)) + \overrightarrow{u}(x_0 + \Delta x - c(t_0 + \Delta t)) \end{aligned} \tag{4.3}$$

The intervals Δx and Δt are chosen such that they are directly related to the speed of the waves travelling along the string c:

$$\frac{\Delta x}{\Delta t} = c \tag{4.4}$$

Substituting this into the expression above, the second sensor reading u_2 becomes:

$$u_2 = \overleftarrow{u}(x_0 + c(t_0 + 2\Delta t)) + \overrightarrow{u}(x_0 - ct_0) \tag{4.5}$$

By subtracting the first sensor reading from the second, the rightward-travelling wave is cancelled:

$$u_2 - u_1 = \overleftarrow{u}(x_0 + c(t_0 + 2\Delta t)) - \overleftarrow{u}(x_0 + ct_0) \tag{4.6}$$

The leftward travelling wave at time $t_0 + 2\Delta t$ can then be recovered from the sensor readings and the previous estimate from $2\Delta t$ in the past:

$$\overleftarrow{u}(x_0 + c(t_0 + 2\Delta t)) = u_2 - u_1 + \overleftarrow{u}(x_0 + ct_0) \tag{4.7}$$

The way that the next estimate is made by adding sensor readings to the previous estimate means that errors accumulate, making the algorithm sensitive to drift and unstable in the presence of sensor noise.

Naucler et al [79] examined this algorithm in some detail and presented the following generalised formula for estimating the leftward-travelling wave using a digital system with a sampling period of T:

$$\overleftarrow{\hat{u}} = \frac{u_1 z^{-\tau} - u_2 z^{-3\tau}}{1 - \theta z^{-4\tau}} \tag{4.8}$$

Here θ is a variable parameter, u_1 and u_2 are the sensor readings, z is the delay operator and τ is an integer related to the distance between the sensors Δx, the sampling period T and the wave speed c as:

$$\tau = \frac{\Delta x}{cT} \tag{4.9}$$

Because τ must be an integer it places a constraint on the distance between the sensors with respect to the wave speed of the string. The rightward-travelling wave estimate $\overrightarrow{\hat{u}}$ can also be obtained from Equation 4.8 by swapping the sensor readings u_1 and u_2.

Naucler identified that the estimator error ϵ, i.e the difference between the estimated wave $\overleftarrow{\hat{u}}$ and the actual wave $\overleftarrow{u}$, is a function of both the actual wave $\overleftarrow{u}$ and the sensor noise $\hat{e}$ which is assumed to be identical for both sensors:

$$\begin{aligned} \epsilon &= \overleftarrow{u} - \overleftarrow{\hat{u}} \\ &= H(z)\overleftarrow{u} - E(z)\hat{e} \end{aligned} \tag{4.10}$$

The transfer functions $H(z)$ and $E(z)$ are given by:

$$\begin{aligned} H(z) &= 1 - \frac{1 - z^{-4\tau}}{1 - \theta z^{-4\tau}} \\ E(z) &= \frac{1}{1 - \theta z^{-4\tau}} \end{aligned} \tag{4.11}$$

The frequency response of these transfer functions is plotted for various different values of θ in Figure 4.1, and the time-domain output of the estimator is plotted in Figure 4.2.

When $\theta = 1$ the transfer function between the estimator error and the wave $H(z)$ is equal to 0 and in the absence of sensor noise the estimator perfectly decomposes the travelling wave, with a slight phase lag. In this form the estimator is similar to the algorithm given in Equation 4.7 and suffers from the same problems, including sensitivity to drift and instability in the presence of sensor noise. This can be seen by examining the transfer function between the estimator error and the sensor noise $E(z)$ which has its poles located on the unit circle when $\theta = 1$ and is therefore unstable, with spikes of infinite gain in its frequency response. The sensitivity of the estimator to low-frequency noise and its inability to reject DC offsets in the sensor readings can be seen clearly in the time-domain plot Figure 4.2 which exhibits a significant DC offset and spurious high-frequency noise originating from approximations used in the simulations despite being produced by a model which does not model sensor noise.

By decreasing θ the poles of $E(z)$ are moved inside the unit circle, reducing the height of the spikes in its frequency response and stabilising the estimator error in the presence of sensor noise. This comes at the cost of introducing a non-zero frequency dependance into $H(z)$, meaning that the estimator is no longer perfectly decomposing the travelling wave but is introducing errors which are a function of the travelling wave.

As θ gets close to 1, the errors in amplitude and phase of the estimator due to $H(z)$ become smaller, but the sensitivity to sensor noise due to $E(z)$ becomes larger. It is therefore imperative that the signal-to-noise ratio of the sensors used to generate the estimate is as low as possible, allowing the value of θ to approach 1 without causing instability in the estimate due to noise. This will result in the peaks in $E(z)$ being finite though still very large, causing any noise present in those frequency ranges to be amplified. Because the peaks are toward the top of the frequency range it is possible when using a sample rate very much higher than the dominant modal frequencies of the string to filter the noise amplified by those peaks out of the estimate using a combination of notch and low-pass filters without affecting the dominant modal frequencies of the string. This is considered further in 6.3.

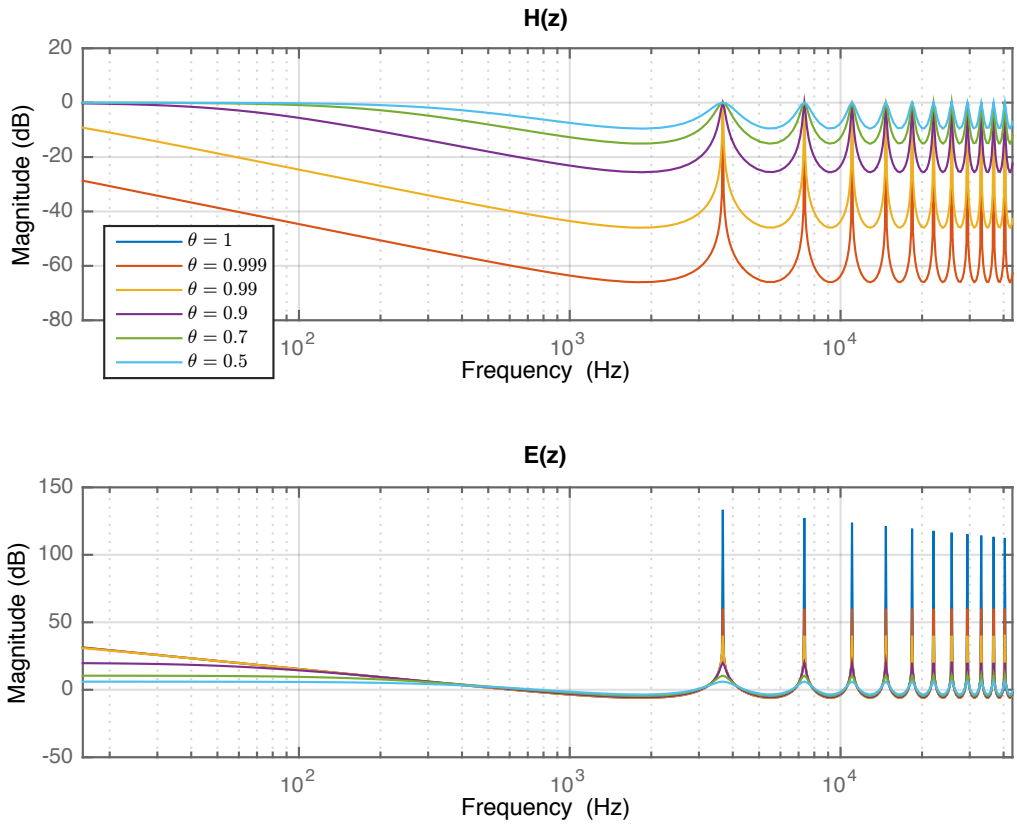

Figure 4.1: Bode plots of the transfer function between the estimator error ϵ and the travelling wave $\overleftarrow{u}$ $(H(z))$ and the sensor noise $\hat{e}$ $(E(z))$ with $\tau = 6$ and $\frac{1}{T} = 88.2kHz$ for various values of the estimation parameter θ. In both plots lower values result in lower error and therefore better estimation of the travelling wave.

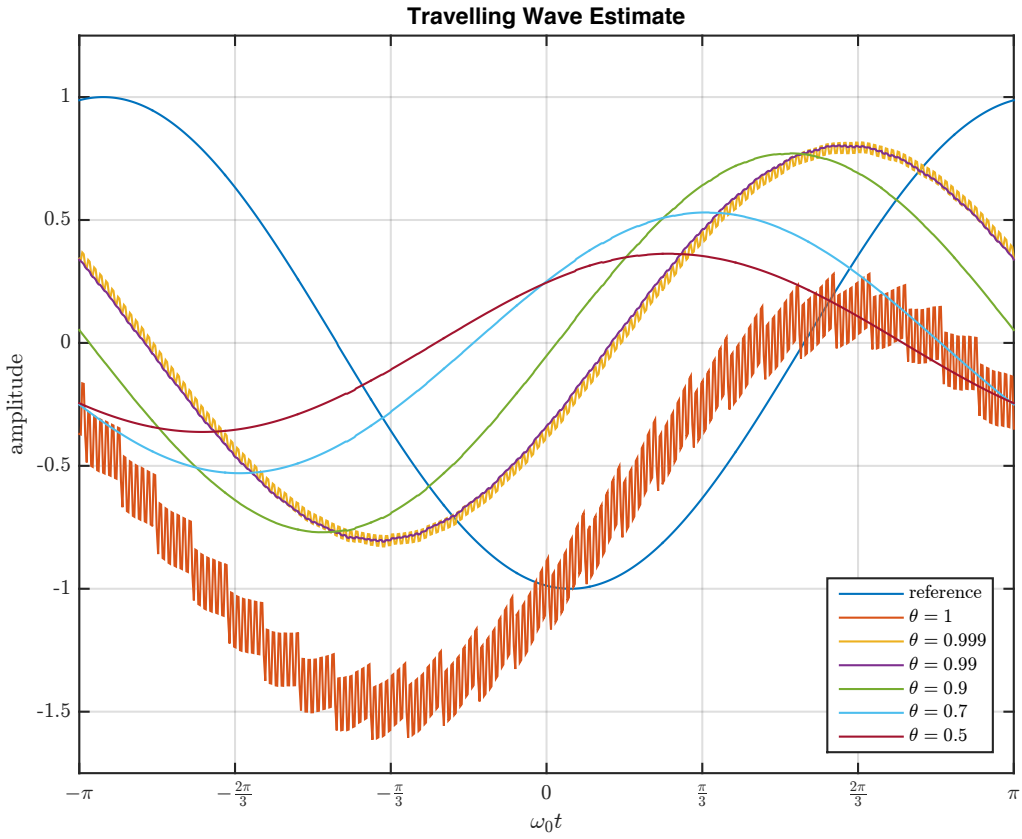

Figure 4.2: Time domain plots of the estimator output for various values of θ. The plot labeled *reference* is the true value of the travelling wave, while the other plots are outputs of the estimator. All estimates suffer from phase errors, but these are not a concern as they are equivalent to small delays in the control system. Values of θ close to 1 suffer least from phase and amplitude errors, but are sensitive to high-frequency noise and drift

4.2 Sensor Hardware

4.2.1 Electromagnetic Sensors

The most common solution to the problem of sensing string vibrations in a musical context is the electromagnetic pickup, found on most electric guitars and other steel stringed instruments. While cheap and robust, electromagnetic pickups exhibit a tonal quality indicative of an uneven frequency response, and output a signal proportional to the velocity of the string rather than its displacement. Neither of these properties is a problem for typical musical uses of an electric guitar, but both are undesirable when trying to measure string displacement as accurately as possible. Typical electromagnetic pickups are also inherently nonlinear due to the difficulty of creating a perfectly uniformly distributed magnetic field in the volume of space through which the string vibrates [83].

4.2.2 Optical Sensors

Optical sensors present a higher-performance alternative and although they are seldom used in commercially available instruments (with the notable exception of the Lightwave pickup system[1]), they have been explored in a variety of configurations in an academic context. Reflection-based optical sensors which have been developed for the violin [56, 85] and used in other musical contexts [65], work by shining light onto the string and measuring the intensity of the light reflected back, which varies with the distance of the string from the sensor. The intensity of light falls with the inverse-square of the distance it travels which introduces an inherent nonlinearity into this sensing method; the intensity of light reflecting back from the string is also very low due to the small size and round shape of the string introducing limitations in the potential achievable signal-to-noise ratio.

Transmission-based optical sensors work by shining light across the string and measuring the intensity and distribution of the light which is transmitted. In the Overtone Violin, Overholt [80] uses two adjacent discrete photodiodes in a differential configuration with the shadow of the string masking an area of each photodiode depending on its displacement. This configuration has the advantage of relatively low sensitivity to ambient light (since the two photodiode signals are subtracted, much like a humbucker pickup), but crossover point distortion is a potential problem, and the linear amplitude range of the sensor is severely restricted.

In a different transmission-based configuration described by Weinreich et al [118], used by

[1] https://www.willcoxguitars.com/lightwave-optical-pickup-system

Berdahl [9] and detailed in Figure 4.3, a square planar photodiode is masked to give its light-sensitive surface a triangular shape; light is shone directly through the string projecting its shadow onto the diode. As the string vibrates the triangular mask causes the amount of light hitting the diode to change in relation to the string's displacement. The potential linear range of sensors in this configuration is relatively high as planar photodiodes with a dimension of $1cm$ are readily available.

The following section explores the geometry of this form of sensor in detail, demonstrating its potential to produce a perfectly linear representation of string displacement in an idealised setting. Subsequent sections explore potential sources of and mitigations against nonlinearities which arise in realistic implementations of the sensor.

4.2.3 Sensor Geometry

With the photodiode operated in photoconductive mode its output is a current I_{pd} which is directly proportional to the light power incident upon its surface. Assuming the surface is uniformly lit by the LED, the current can be said to be directly proportional to the illuminated area of the diode.

Figure 4.3 shows how the shadow of the string is projected onto the masked photodiode. The illuminated area of the diode A_I is equal to the total exposed area $\frac{L^2}{2}$ (where L is the length of one side) subtracted by the area occluded by the string. Assuming the string remains approximately horizontal (which is reasonable given how much longer the string is than the diode is wide) the shadow forms a trapezium with area equal to its thickness s multiplied by its mean width, which because the diode is square is equal to the distance from the top of the diode to the midpoint of the shadow $h(t)$. The illuminated area $A_I(t)$ of the photodiode can then be expressed as a function of the string height $h(t)$:

$$A_I(t) = \frac{L^2}{2} - sh(t) \tag{4.12}$$

To obtain the greatest range of movement the sensor is calibrated so that with the string at rest the shadow is centred at the midpoint of the sensor, $\frac{L}{2}$ from the top, allowing the distance $h(t)$ to be expressed in terms of the displacement of the string's shadow from rest $y(t)$:

$$h(t) = \frac{L}{2} - y(t) \tag{4.13}$$

The illuminated area then becomes:

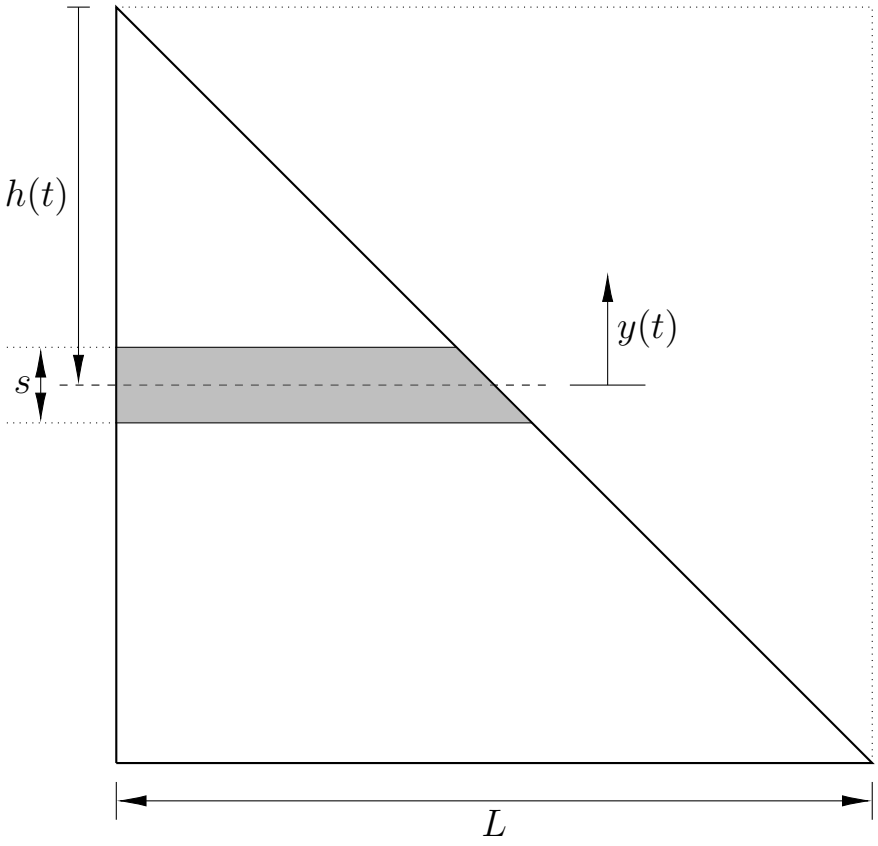

Figure 4.3: Schematic diagram of the shadow projected by the string (indicated by the shaded area) onto the masked surface of the photodiode

$$A_I(t) = \frac{L}{2}(L - s) + sy(t) \tag{4.14}$$

The term $\frac{L}{2}(L - s)$ which corresponds to the illuminated area of the diode when the string is at rest is approximately constant and dominates the expression, meaning that the output current of the photodiode is made up of a large DC component I_0 with the smaller signal superimposed on top:

$$I_{pd}(t) = I_0 + ky(t) \tag{4.15}$$

Point Source Illumination

Figure 4.4 shows a side-on view of the sensor when illuminated with a simple LED approximated as a perfect point source. The string is located a distance v_0 from the photodiode, while the LED is at distance D. The string is shown at rest and also displaced vertically by a variable quantity $u(x_0, t)$, which is the quantity the sensor is ultimately attempting to measure. When the string's motion is confined to the vertical plane the relationship between the string's displacement $u(x_0, t)$ and that of its shadow $y(t)$ is linear:

$$y(t) = u(x_0, t)\frac{1}{1 - \frac{v_0}{D}} \tag{4.16}$$

The quantity $\frac{1}{1-\frac{v_0}{D}}$, referred to from here on as the geometric gain K_g of the sensor, is an important quantity which varies non-linearly with v_0 from a minimum of 1 when v_0 is zero, tending to infinity when v_0 approaches D. It also relates the radius of the string r to the height of the shadow projected onto the photodiode s:

$$s = 2rK_g \tag{4.17}$$

The illuminated area of the photodiode can then be expressed in terms of the geometric gain:

$$A_I(t) = \frac{L - 2rK_g}{2} + 2rK_g^2 u(x_0, t) \tag{4.18}$$

In this idealised situation the illuminated area and therefore the output of the sensor is related linearly to the string's displacement $u(x_0, t)$.

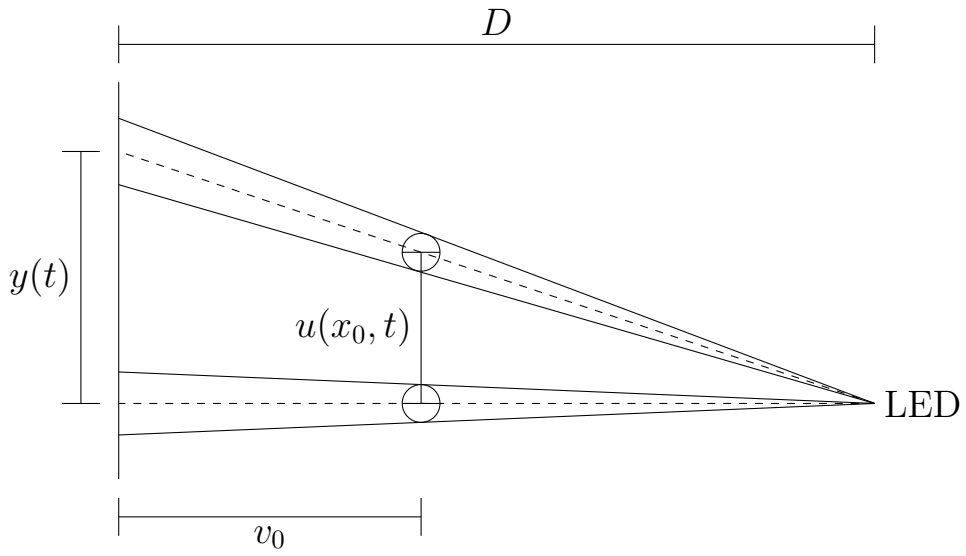

Figure 4.4: Side-on view of the sensor geometry showing how the shadow of the string is projected onto the photodiode's surface (left edge of figure)

4.3 Sensor Nonlinearities

There are two main sources of nonlinearity in the sensor design described above. The first arises from the fact that the string's motion is not confined to the vertical plane, instead tracing out an ellipse in the plane perpendicular to the string. The second arises from the fact that the intensity of the light is not necessarily uniform across the full surface of the photodiode. In the following section the mechanisms behind these phenomena and their impact on the travelling wave control system is explored, and the design of the sensor is refined to minimise or eliminate their effects.

4.3.1 Elliptical String Motion

Due to certain linear and nonlinear effects which are not modelled by the linear wave equation (Equation 3.1), a real string vibrating in a vertical plane will spontaneously develop motion in the horizontal plane causing it to whirl in an elliptical fashion [91]. Additional nonlinearities caused by differences in typical rigid termination conditions for vertical and horizontal string motion cause the ellipse traced out by the string to precess [33], exaggerating the effect. The equations which govern this elliptical motion and in particular the precession of the ellipse

are complicated and dependant on the particular geometry of the string and its terminations, so are beyond the scope of this thesis. Here we will examine the effect of a simple and static form of elliptical motion on the output of the sensor described above in which the vertical motion of the string forms the major axis of an ellipse and is a simple sinusoid at the fundamental frequency of the string with a constant amplitude of 1:

$$u(x_0, t) = \cos(\omega_0 t) \tag{4.19}$$

While the horizontal motion of the string forms the minor axis of the ellipse, lagging the vertical motion in phase by 90°, with amplitude d:

$$v(t) = d \sin(\omega_0 t) \tag{4.20}$$

Assuming that the string is located halfway between the LED and the sensor when at rest we have $v_0 = \frac{D}{2}$ and the static geometric gain K_g is 2. The equation relating the output of the sensor $\hat{u}(t)$ to the vertical motion of the string $u(x_0, t)$ is:

$$\begin{aligned} \hat{u}(t) &= \frac{1}{\frac{1}{2} - \frac{v(t)}{D}} u(t) \\ &= \frac{1}{\frac{1}{2} - \frac{d}{D} \sin(\omega_0 t)} \cos(\omega_0 t) \end{aligned} \tag{4.21}$$

The amplitude of the horizontal motion d is physically constrained to vary from a minimum of 0, in which case the string's motion is entirely vertical and the sensor's output is linear with a static gain of 2; to a maximum of $\frac{D}{2}$, in which case the string's horizontal motion occupies the entire space between the LED and the sensor, and the sensor's output is highly nonlinear.

An example of the effect of this form of elliptical motion for $\frac{d}{D} = \frac{1}{4}$ is plotted in Figure 4.5. For the first half of the period the horizontal motion of the string brings it closer to the sensor than the LED, reducing the geometric gain of the sensor and leading to the magnitude of the sensor's output being lower than the string's displacement, while during the second half of the period the opposite is true. The maximum and minimum points of the sensor output are larger in magnitude and shifted in time relative to the actual displacement, and the induced error is significant.

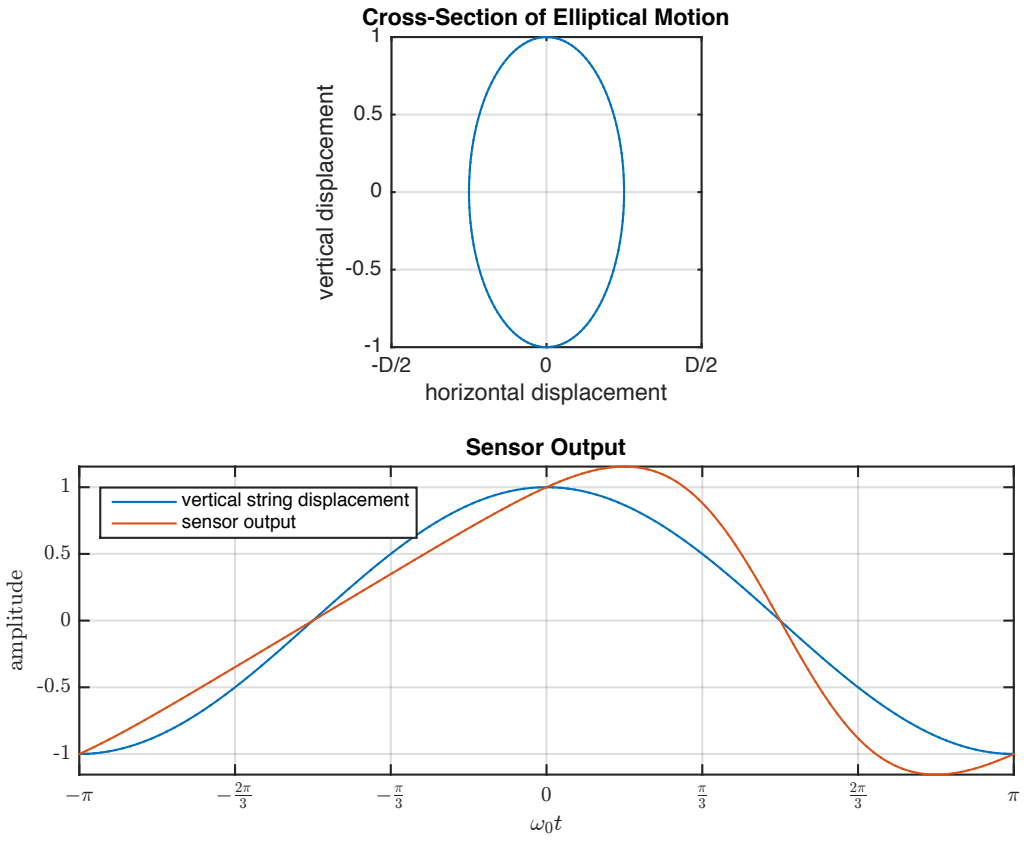

Figure 4.5: The effect of elliptical string motion on sensor output with horizontal amplitude $\frac{d}{D} = \frac{1}{4}$. The plotted sensor output is halved to eliminate the sensor's geometric gain of 2 when the string is at rest.

Effect of Elliptical Motion on Stability

The errors induced in the sensor reading due to elliptical string motion have consequences for the stability of the travelling wave control system. From Equation 3.31 the stability criterion is

$$f(\overleftarrow{u})^2 - 2f(\overleftarrow{u})\overleftarrow{u} \leq 0 \tag{4.22}$$

where $\overleftarrow{u}$ is the wave travelling toward the actuated termination at $x = 0$ and $f(\overleftarrow{u})$ is the termination displacement function. Assuming as above that the travelling wave is a simple sinusoid at the fundamental frequency of the string, i.e $\overleftarrow{u} = \cos(\omega_0 t)$, that we have a perfect travelling wave decomposition algorithm, and that no other nonlinearities are present in the system, under elliptical string motion the termination displacement function becomes:

$$f(t) = K\frac{1}{\frac{1}{2} - \frac{d}{D}\sin(\omega_0 t)}\cos(\omega_0 t) \tag{4.23}$$

Here K is the control gain. The stability function becomes:

$$\begin{aligned} h(t) &= f(t)^2 - 2f(t)\cos(\omega_0 t) \\ &= \frac{K}{\frac{1}{2} - \frac{d}{D}\sin(\omega_0 t)}\left(\frac{K}{\frac{1}{2} - \frac{d}{D}\sin(\omega_0 t)} - 2\right)\cos^2(\omega_0 t) \end{aligned} \tag{4.24}$$

For stability we must have $h(t) \leq 0$ for $-\pi \leq \omega_0 t \leq \pi$, which as $h(t)$ has no poles because the maximum value of $\frac{d}{D}$ is 0.5 must be true if we can show that $h(0) \leq 0$ and and that $h(t)$ does not cross the t-axis in the relevant interval. At $t = 0$ we have:

$$h(0) = 4K(K-1) \tag{4.25}$$

The condition $h(0) \leq 0$ is therefore solved by:

$$0 \leq K \leq 1 \tag{4.26}$$

This seems to differ from the stability constraint on K in the case of linear f (given by $0 \leq K \leq 2$), though accounting for the geometric gain of the sensor when the string is at rest which is 2 it is actually equivalent.

To complete the stability criterion we must find the roots of $h(t)$, i.e values of t at which $h(t)$ crosses the t-axis and the solutions to the equation $h(t) = 0$, and ensure that they do not exist within the interval $-\pi \leq \omega_0 t \leq \pi$.

Due to the $\cos^2(\omega_0 t)$ term, $h(t)$ always has a pair of repeated roots at $\omega_0 t = \pm\frac{\pi}{2}$, however because the roots are repeated $h(t)$ only touches the t-axis at these points without crossing, and they do not cause instability. The other factor of $h(t)$ outside the brackets

$$\frac{K}{\frac{1}{2} - \frac{d}{D}\sin(\omega_0 t)} \tag{4.27}$$

is always positive for stable values of K and physically feasible values of $\frac{d}{D}$, so it contributes no roots to the function and does not cause instability. We can therefore say that for stability the remaining factor of $h(t)$ within the brackets must not equal zero within the relevant interval of $\omega_0 t$, leading to the following stability criterion:

$$\frac{d}{D} \leq \frac{1 - K}{2} \tag{4.28}$$

Figure 4.6 shows plots of the stability function $h(t)$ for a stable and an unstable elliptical motion, showing the pair of repeated roots in both cases, and in the unstable case the additional pair of roots which cause the instability.

The elliptical stability criterion Equation 4.28 provides two possible ways to stabilise a system in the presence of elliptical motion; either the gain K can be reduced, or the distance between the LED and the photodiode D can be increased. Both of these have undesirable side-effects, as reducing the gain K reduces the overall power of the control system, while increasing the distance D reduces the intensity of the light hitting the sensor and therefore the signal-to-noise ratio, while also increasing the amount of space the sensor assembly takes up. So while it is always possible to stabilise the system by reducing the gain, it is clear that a naively designed sensor can cause instability in the travelling wave control system in the presence of a relatively small amount of out-of-plane motion.

Effect of Elliptical Motion on Harmonic Distortion

The output of the sensor under elliptical motion can be described by a Fourier series:

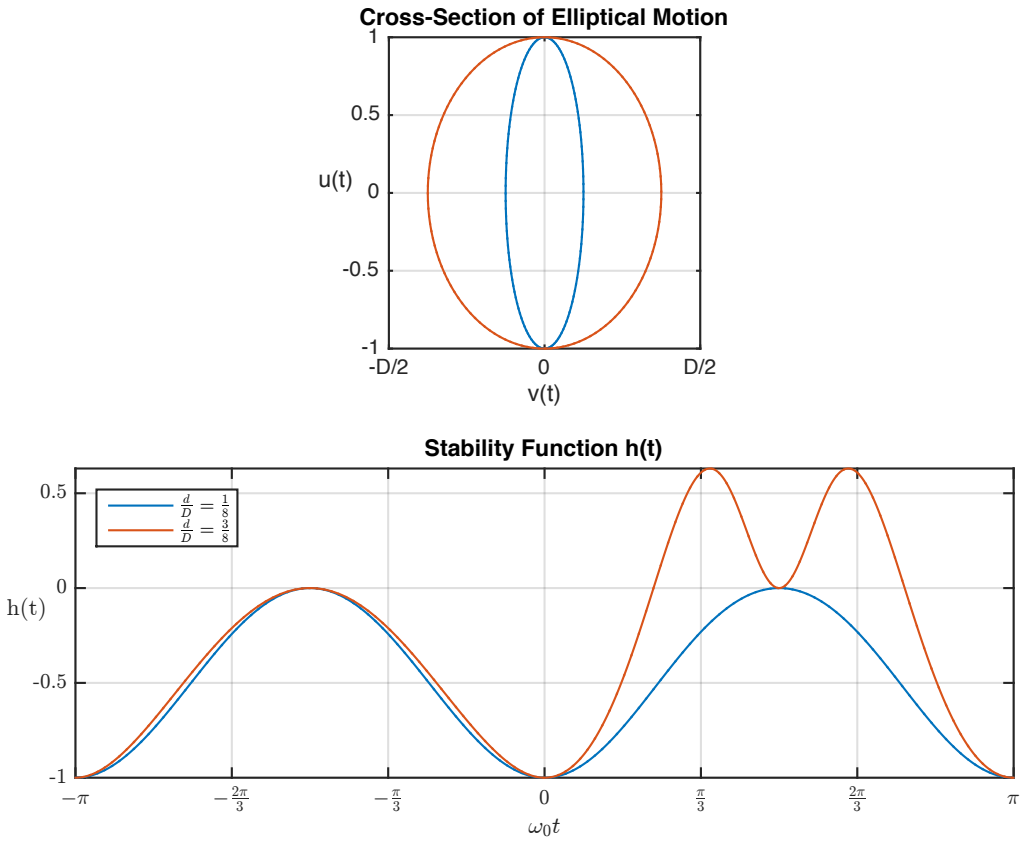

Figure 4.6: The stability function h(t) for a stable amount of elliptical motion with $\frac{d}{D} = \frac{1}{8}$ and an unstable amount with $\frac{d}{D} = \frac{3}{8}$. The gain $K = 0.5$ in both cases.

$$\begin{aligned}\hat{u}(t) &= \frac{1}{\frac{1}{2} - \frac{d}{D}\sin(\omega_0 t)}\cos(\omega_0 t) \\ &= \frac{1}{2}a_0 + \sum_{n=1}^{\infty} a_n \cos(n\omega_0 t) + \sum_{n=1}^{\infty} b_n \sin(n\omega_0 t)\end{aligned} \tag{4.29}$$

Exploiting orthogonality, the coefficients a_n and b_n can be expressed as integrals:

$$\begin{aligned}a_n &= \frac{1}{\pi}\int_{-\pi}^{\pi} \hat{u}(t)\cos(n\omega_0 t)dt \\ b_n &= \frac{1}{\pi}\int_{-\pi}^{\pi} \hat{u}(t)\sin(n\omega_0 t)dt\end{aligned} \tag{4.30}$$

Expanding the series up to $n = 3$ many of the coefficients are zero and the sensor output can be expressed as:

$$\hat{u}(t) \approx a_1 \cos(\omega_0 t) + b_2 \sin(2\omega_0 t) + a_3 \cos(3\omega_0 t) \tag{4.31}$$

After performing the integrals, the coefficients of the series can be expressed in terms of the horizontal amplitude of elliptical motion d:

$$\begin{aligned}a_1 &= \frac{1 - 2\sqrt{\frac{1}{4} - \left(\frac{d}{D}\right)^2}}{\left(\frac{d}{D}\right)^2} \\ b_2 &= \frac{1 - 2\left(\frac{d}{D}\right)^2 - 2\sqrt{\frac{1}{4} - \left(\frac{d}{D}\right)^2}}{\left(\frac{d}{D}\right)^3} \\ a_3 &= \frac{4\left(\frac{d}{D}\right)^4 - 5\left(\frac{d}{D}\right)^2 + 1 + (3\left(\frac{d}{D}\right)^2 - 1)\sqrt{1 - 4\left(\frac{d}{D}\right)^2}}{\left(\frac{d}{D}\right)^4\sqrt{1 - 4\left(\frac{d}{D}\right)^2}}\end{aligned} \tag{4.32}$$

The total harmonic distortion present at the output of the sensor is then given by:

$$thd_{sensor} = \frac{\sqrt{b_2^2 + a_3^2}}{a_1} \tag{4.33}$$

This quantity is plotted against $\frac{d}{D}$ in Figure 4.7. It can be seen that the distortion increases dramatically with only a small amount of out-of-plane motion, reaching -20dB when $\frac{d}{D}$ is only 0.1. This will have a severe effect on the audible distortion created by the travelling wave control system and it is essential to minimise it in order to achieve meaningful and precise control of the spectro-temporal elements of the timbre of the string.

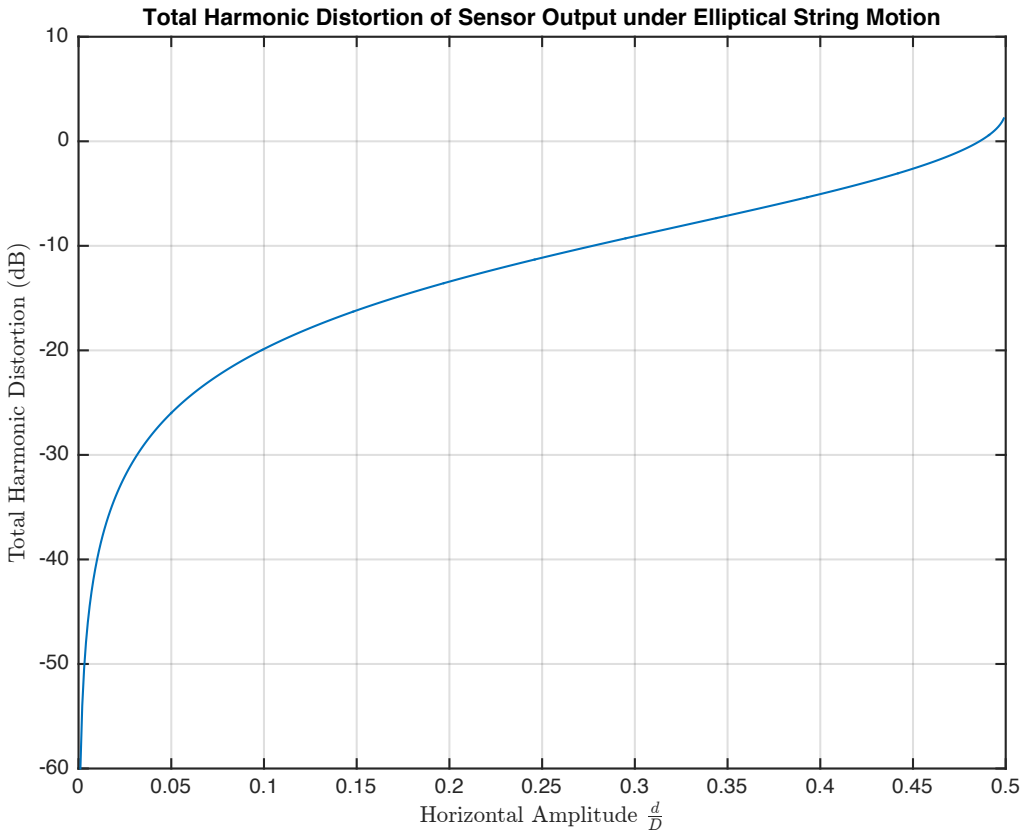

Figure 4.7: The total harmonic distortion at the output of the sensor due to elliptical motion of the string.

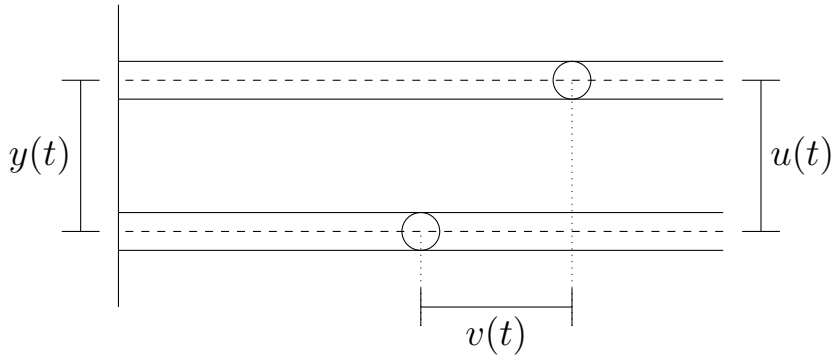

Figure 4.8: Side-on view of the sensor geometry with collimated light showing how horizontal motion $v(t)$ does not effect the vertical displacement of the string's shadow $y(t) = u(x_0, t)$

Collimating Lenses

One way to reduce the amount of distortion created by the elliptical motion and ensure the stability of the control system is to increase D, the distance between the LED and the photodiode. If D is increased to infinity, the effect is completely eliminated; the harmonic distortion disappears and stability is guaranteed for any amount of motion in the horizontal plane. This happens because when a light source is infinitely distant, the rays it emits are parallel to each other rather than diverging as when emitted from a finitely distant point source, fixing the geometric gain K_g at 1 and causing the output of the sensor to equal the vertical displacement of the string even in the presence of horizontal displacement $v(t)$ (see Figure 4.8).

Light which exhibits this property is said to be collimated, and while locating a light source infinitely far from the string is clearly impractical, there are other ways of achieving the same effect. Some varieties of lasers produce collimated light, though laser diodes which are really the only kind of laser which could practically be used in this application do not. The solution is to locate the LED at the focal point of a plano-convex spherical lens [104], i.e a lens with one planar surface and one convex spherical surface, which transforms the divergent light emitted by the LED into collimated light suitable for use in the sensor. This eliminates the effect of horizontal out-of-plane motion of the string on the output of the sensor and the travelling wave control system. For a diagram of the assembled sensor including the lens, see Section 6.1, and for photos of the assembled sensor see Appendix C.

4.3.2 Light Intensity Distribution

If the light hitting the surface of the sensor has a perfectly even distribution then the output of the sensor $\hat{u}$ is related linearly to the vertical displacement of the string's shadow projected onto the surface $y(t)$ as in Equation 4.14. In reality the intensity of the light emitted by an LED varies in relation to the viewing angle, and its projection onto the surface of the sensor has a variable distribution $G(x, y)$, causing the relationship to become nonlinear.

Surface Integral

The output of the sensor $\hat{u}(t)$ is equal to the distribution $G(x, y)$ integrated over the full surface of the masked photodiode subtracted by the amount of light occluded by the string, which is given by the distribution integrated over the area occupied by the string's shadow projected onto the surface:

$$\hat{u}(t) = \int\limits_{A_{total}} G(x, y)dA - \int\limits_{A_{string}} G(x, y)dA \tag{4.34}$$

The first of these integrals is constant with string displacement and so for the purposes of this analysis it can be ignored. The second can be expressed as a double integral in the x-y plane:

$$\int\limits_{A_{string}} G(x, y)dA = \int\limits_{y_1}^{y_2}\int\limits_{x_1}^{x_2} G(x, y)dxdy \tag{4.35}$$

If the LED is pointed directly at the centre of the square photodiode which we define as the origin of our x-y coordinate system, then the line which separates the masked and unmasked areas of the sensor has equation:

$$x = -y \tag{4.36}$$

This defines the upper limit of integration for the inner integral x_2, while the lower limit x_1 is defined by the boundary of the sensor at $x = -\frac{L}{2}$. The limits of the outer integral are equal to the boundaries of the shadow projected onto the sensor by the string. Assuming we are using collimated light and do not have to be concerned with the geometric gain of the sensor, these limits are equal to the vertical displacement of the string $u(t)$ added to and subtracted by the radius of the string r:

$$\int_{A_{string}} G(x,y)dA = \int_{(u(t)-r)}^{(u(t)+r)} \int_{-\frac{L}{2}}^{-y} G(x,y)dxdy \tag{4.37}$$

Gaussian Distribution

The intensity distribution of the light emitted by the LED and projected onto the sensor is well-modelled by a two-dimensional gaussian function [78]:

$$G(x,y) = e^{-\frac{x^2+y^2}{2\sigma^2}} \tag{4.38}$$

The amplitude of the distribution is at a maximum of 1 at the origin (i.e the centre of the square sensor at which the LED is pointing) and falls off uniformly in all directions (see Figure 4.9).

The spread of an LED is characterised by its manufacturer with a property called the "half angle" $\theta_{\frac{1}{2}}$, which is the viewing angle at which the LED's intensity has dropped to half of its maximum. This quantity can be related to the spread of the projected gaussian distribution σ:

$$\sigma = \frac{D\tan\theta_{\frac{1}{2}}}{\sqrt{2ln(2)}} \tag{4.39}$$

When using a simple point-source LED the distance D in Equation 4.39 is equal to the distance from the LED to the sensor surface. When using a collimating lens, D is actually the distance from the LED to the lens (which must be equal to the focal length of the lens for successful collimation) as the effect of the lens is to prevent further divergence of the light and project the distribution incident upon itself onto the sensor.

Through separation of variables the two-dimensional gaussian function $G(x,y)$ can be split into the product of two one-dimensional gaussians:

$$\begin{aligned} G(x,y) &= G(x)G(y) \\ G(x) &= e^{-\left(\frac{x}{\sqrt{2}\sigma}\right)^2} \\ G(y) &= e^{-\left(\frac{y}{\sqrt{2}\sigma}\right)^2} \end{aligned} \tag{4.40}$$

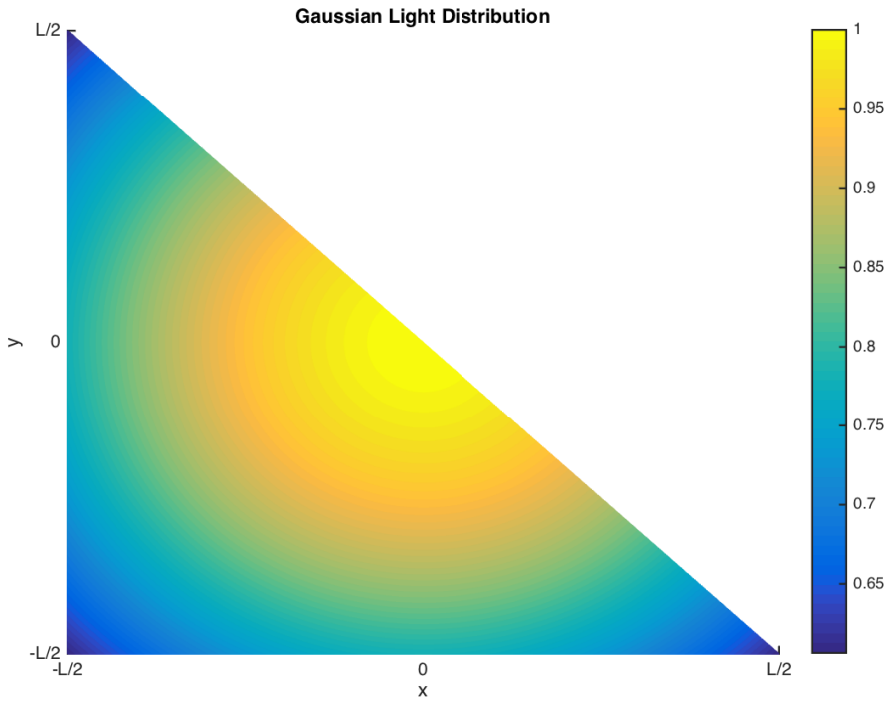

Figure 4.9: A two-dimensional gaussian light distribution with spread $\sigma = \frac{\sqrt{2}}{2}$ projected onto a triangular sensor with dimension $L = 1$

The integral of the distribution over the string's shadow Equation 4.37 can then also be separated with the inner integration in terms of x being performed first:

$$\int_{(u(t)-r)}^{(u(t)+r)} \int_{-\frac{L}{2}}^{-y} G(x,y)dxdy = \int_{(u(t)-r)}^{(u(t)+r)} G(y) \left(\int_{-\frac{L}{2}}^{-y} G(x)dx \right) dy \tag{4.41}$$

Series Approximation and Integration

It is not possible to directly integrate a gaussian with finite limits, but the function can be approximated using a Taylor series:

$$\begin{aligned} G(x) &= \sum_{n=0}^{N} a_n x^{2n} \\ a_n &= \frac{(-1)^n}{n!(\sigma\sqrt{2})^{2n}} \end{aligned} \tag{4.42}$$

Substituting Equation 4.42 into Equation 4.41 we can perform the inner integral in terms of x:

$$\begin{aligned} \int_{-\frac{L}{2}}^{-y} G(x)dx &= \int_{-\frac{L}{2}}^{-y} \sum_{n=0}^{N} a_n x^{2n} dx \\ &= \left[\sum_{n=0}^{N} \frac{a_n}{2n+1} x^{2n+1} \right]_{-\frac{L}{2}}^{-y} \\ &= \sum_{n=0}^{N} \frac{a_n}{2n+1} \left(\left(\frac{L}{2} \right)^{2n+1} - y^{2n+1} \right) \end{aligned} \tag{4.43}$$

This expression must be multiplied by $G(y)$ before integrating a second time. $G(y)$ can be expressed as a finite series as in Equation 4.42 and its multiplication with the result of Equation 4.43 can be expressed as a convolution:

$$\begin{aligned} G(y) \int_{-\frac{L}{2}}^{-y} G(x)dx &= \sum_{n=0}^{N} a_n y^{2n} \left[\sum_{n=0}^{N} \frac{a_n}{2n+1} \left(\left(\frac{L}{2} \right)^{2n+1} - y^{2n+1} \right) \right] \\ &= \sum_{n=0}^{2N} \sum_{m=0}^{n} \frac{a_m a_{n-m}}{2(n-m)+1} \left(\left(\frac{L}{2} \right)^{2n+1} y^{2m} - y^{2n+1} \right) \end{aligned} \tag{4.44}$$

This complicated expression can be simplified to a power series in y with the highest power equal to $4N+1$:

$$G(y)\int_{-\frac{L}{2}}^{-y} G(x)dx = \sum_{n=0}^{4N+1} b_n y^n \tag{4.45}$$

The coefficients b_n, which can be found by expanding the sum in Equation 4.44 and comparing coefficients, are functions of the size of the sensor L and the spread of the light intensity distribution σ, and are constant in y. The outer integral from Equation 4.41 can now be completed:

$$\begin{aligned}\int_{(u(t)-r)}^{(u(t)+r)} G(y)\int_{-\frac{L}{2}}^{-y} G(x)dxdy &= \int_{(u(t)-r)}^{(u(t)+r)} \sum_{n=0}^{4N+1} b_n y^n \\ &= \left[\sum_{n=0}^{4N+1} \frac{b_n}{n+1} y^{n+1}\right]_{u(t)-r}^{u(t)+r} \\ &= \sum_{n=0}^{4N+1} \frac{b_n}{n+1}\left((u(t)+r)^{n+1} - (u(t)-r)^{n+1}\right)\end{aligned} \tag{4.46}$$

The bracketed expressions in Equation 4.46 can be expanded using the binomial theorem, allowing the result of the integration to be expressed as a power series in $u(t)$:

$$\begin{aligned}\sum_{n=0}^{4N+1} \frac{b_n}{n+1}\left((u+r)^{n+1} - (u-r)^{n+1}\right) &= \sum_{n=0}^{4N+1} \frac{b_n}{n+1} \sum_{k=0}^{n+1} \binom{n+1}{k} r^k (1-(-1)^k) u^{n-k+1} \\ &= \sum_{n=0}^{4N+1} c_n u^n(t)\end{aligned} \tag{4.47}$$

Substituting this back into Equation 4.34 allows the output of the sensor to be expressed in terms of the string displacement:

$$\hat{u}(t) = u_0 - \sum_{n=0}^{4N+1} c_n u^n(t) \tag{4.48}$$

Here u_0 is the constant term representing the integration of the light distribution over the whole area of the sensor, and the coefficients c_n which can be found by expanding the sum

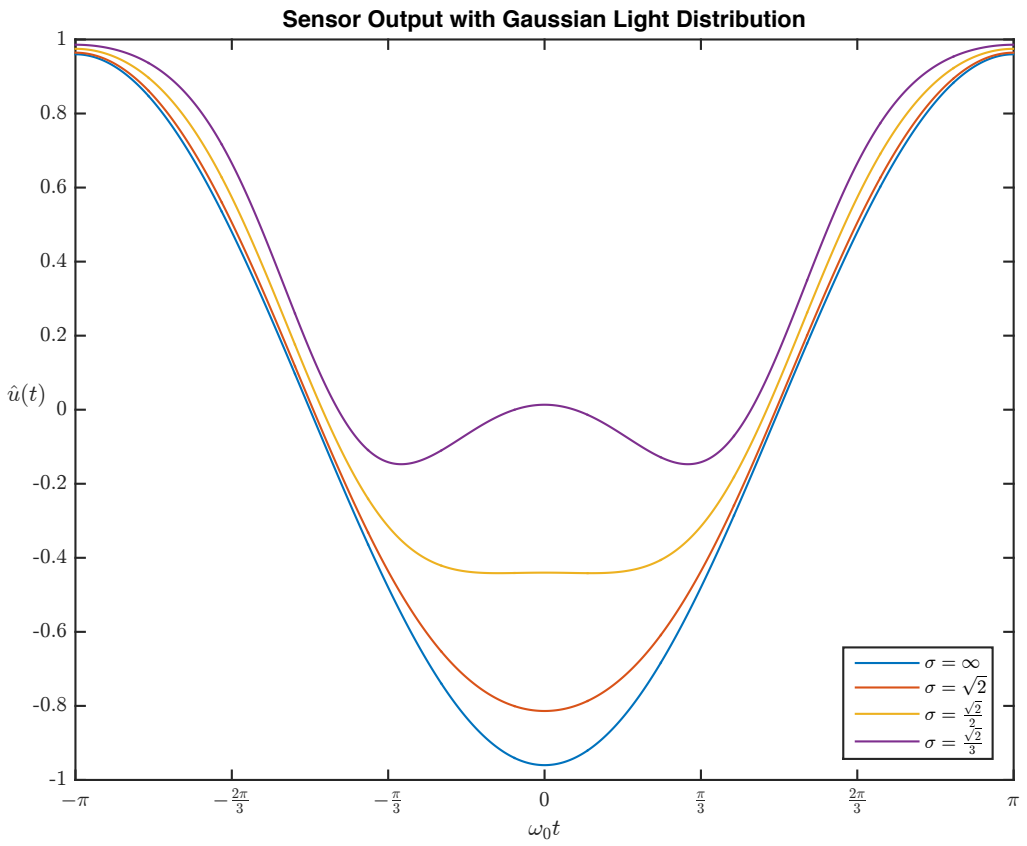

Figure 4.10: The output of the sensor with dimension $L = 1$ in response to a sinusoid at the fundamental frequency of the string under a gaussian light distribution with spread σ.

in Equation 4.47 are functions of the size of the sensor L, the spread of the light distribution σ and the radius of the string r.

The effect of a gaussian light distribution on the output of the sensor is plotted in Figure 4.10. With $\sigma = \infty$ the distribution is uniform and the sensor's response is linear, perfectly representing the sinusoidal motion of the string. As σ decreases, the string's motion in the positive u direction when the shadow is located over the thin top-half of the sensor is still well-represented by the sensor, however significant errors are introduced in the negative u direction when the shadow is traversing the wider bottom-half of the sensor and is exposed to more variation in the light distribution $G(x, y)$. As σ is reduced to more extreme levels the trough at the bottom of the output continues to flatten until eventually it becomes non-monotonic.

Effect on Harmonic Distortion

When the input to the sensor system is a perfect sinusoid at the fundamental frequency of the string, i.e $u(t) = \cos(\omega_0 t)$, ignoring the constant term u_0 the output of the sensor becomes:

$$\hat{u}(t) = \sum_{n=0}^{4N+1} c_n \cos^n(\omega_0 t) \tag{4.49}$$

By using a combination of Euler's theorem and the binomial theorem, this can be expressed in terms of the harmonic coefficients d_n:

$$\begin{aligned}
\sum_{n=0}^{4N+1} c_n \cos^n(\omega_0 t) &= \sum_{n=0}^{4N+1} \frac{c_n}{2^n} \left(e^{j\omega_0 t} + e^{-j\omega_0 t}\right)^n \\
&= \sum_{n=0}^{4N+1} \frac{c_n}{2^n} \sum_{k=0}^{n} \binom{n}{k} e^{j(2k-n)\omega_0 t} \\
&= \sum_{n=0}^{4N+1} \frac{c_n}{2^n} \sum_{k=0}^{n} \binom{n}{k} \cos((2k-n)\omega_0 t) \\
&= \sum_{n=0}^{4N+1} d_n \cos(n\omega_0 t)
\end{aligned} \tag{4.50}$$

The total harmonic distortion of the sensor can then be expressed in terms of the harmonic coefficients d_n:

$$thd = \frac{\sqrt{\sum_{n=2}^{4N+1} d_n^2}}{|d_1|} \tag{4.51}$$

The total harmonic distortion is plotted in Figure 4.11 against the normalised distance $\frac{D}{L}$, i.e the ratio between the distance from the LED and the photodiode (or the focal length of the collimating lens if one is being used) and the size of the sensor, for different values of the LED half-angle $\theta_{\frac{1}{2}}$.

It is clear that a naively designed sensor using an LED with a narrow beam angle can exhibit a significant amount of distortion. In order to achieve a low total harmonic distortion of less than 60dB it is necessary to use a very wide-angled LED with a half-angle of over 67.5° and a collimating lens with a focal length greater than 4 times the size of the sensor - 4cm

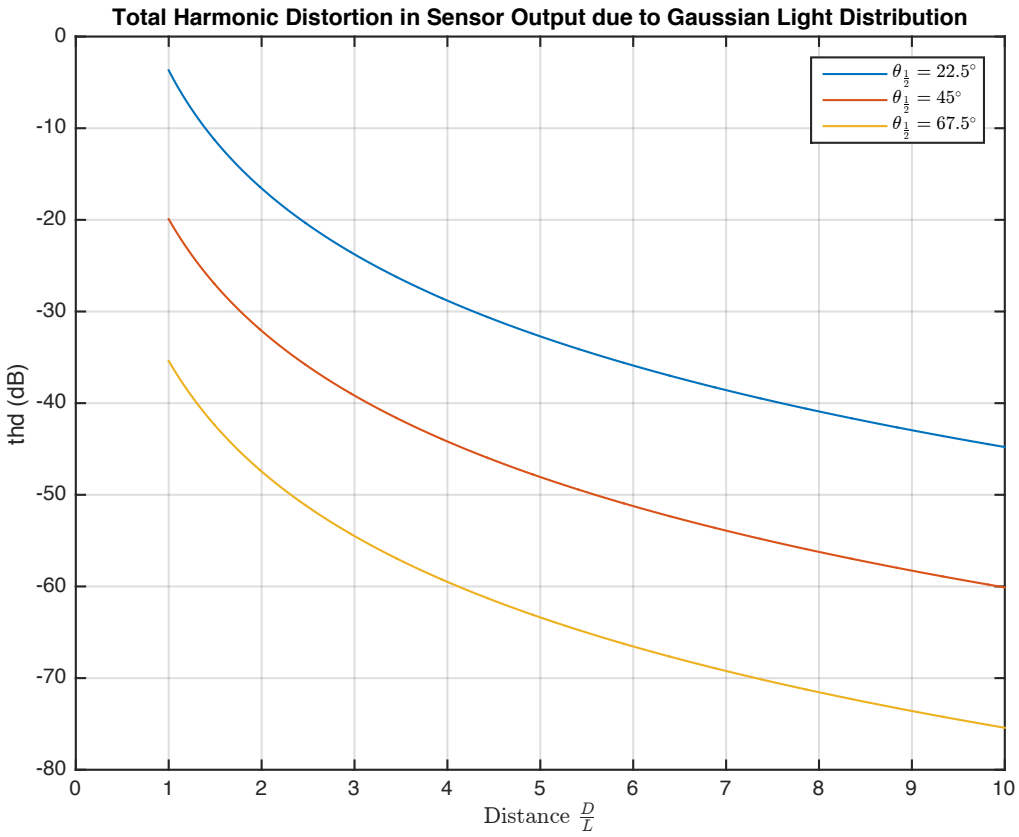

Figure 4.11: The total harmonic distortion at the output of the sensor plotted against the distance from the LED to the photodiode D normalised against the dimension of the sensor L for various values of the LED half-angle $\theta_{\frac{1}{2}}$. The intensity distribution is modelled as a gaussian with $N = 5$.

for the sensor used in our experiments. Both of these mitigations have the side-effect of reducing the absolute intensity of the light hitting the photodiode, requiring higher gains in the pre-amplifier stage to maintain the level of the output, and degrading the signal-to-noise ratio of the sensor.

Impact on Travelling Wave Control

We will now examine the impact of the nonlinearity caused by uneven light distribution on the ability of the travelling wave control system to damp the string. We will look at the stability of the system, the harmonic distortion induced in the motion of the string, and the time taken for the string to be fully damped.

Stability

Assuming a perfect travelling wave decomposition algorithm and no other nonlinearities present in the system, the presence of an uneven light distribution in the sensor will cause the termination displacement function of the control system $f(\overleftarrow{u})$ to become a nonlinear polynomial in $\overleftarrow{u}$:

$$f(\overleftarrow{u}) = K^{'} c_1 \sum_{n=1}^{4N+1} \frac{c_n}{c_1} \overleftarrow{u}^n \tag{4.52}$$

The coefficients of $\overleftarrow{u}^n$ are the c_n defined in Equation 4.47 normalised against the linear coefficient c_1, and $K^{'}$ is the applied gain. The values of the first four coefficients are plotted in Figure 4.12 against the normalised distance from the LED to the photodiode $\frac{D}{L}$ for a relatively narrow-angled LED with $\theta_{\frac{1}{2}} = 22.5°$

At short distances the response is dominated by a negative cubic nonlinearity and also features a significant amount of quadratic nonlinearity. Ignoring powers of $\overleftarrow{u}$ higher than 3, the relevant stability criterion for this form of nonlinearity, derived in Equation 3.59 is:

$$\begin{aligned} b &\leq 1 + c \\ \frac{c_2}{c_1} &\leq 1 + \frac{c_3}{c_1} \end{aligned} \tag{4.53}$$

This stability criterion is independent of the gain $K^{'}$, meaning that there is no easy way of preventing a badly designed sensor from causing instability in the system. The minimum distance at which a stable response can be obtained when using an LED with a half-angle of

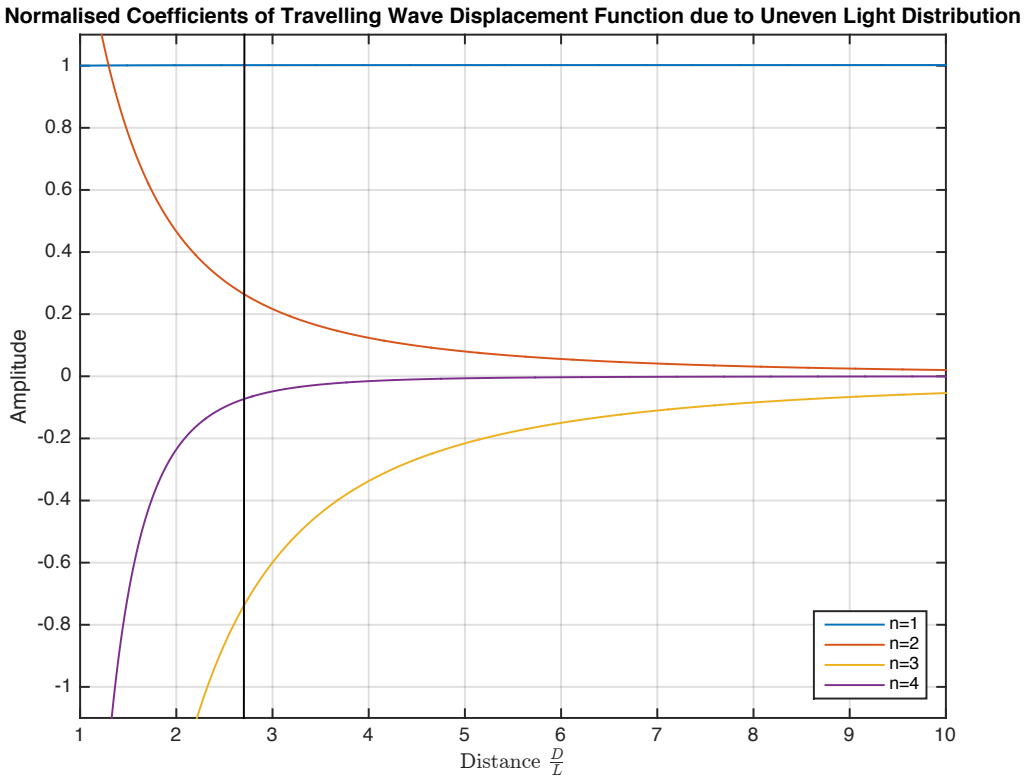

Figure 4.12: The normalised coefficients of the nonlinear polynomial termination displacement function $f(\overleftarrow{u})$ caused by the uneven light distribution from a narrow-angled LED with $\theta_{\frac{1}{2}} = 22.5°$, plotted against the normalised distance between the LED and the photodiode. The black vertical bar shows the boundary of stable motion.

$\theta_{\frac{1}{2}} = 22.5°$ is $\frac{D}{L} = 2.71$, i.e just under 3cm when using a sensor with dimension 1cm, which is well within realistic limits. For $\theta_{\frac{1}{2}} = 45°$ it drops to $\frac{D}{L} = 1.13$, while for $\theta_{\frac{1}{2}} = 67.5°$ it drops below 1, signifying that using a wide-angled LED will guarantee stability at any sensible distance $\frac{D}{L}$.

Harmonic Distortion of String's Motion

The peak total harmonic distortion exhibited by the string's motion during damping as a result of the uneven light distribution, obtained using the simulations described in Section 3.5, is plotted in Figure 4.13. There is more harmonic distortion in the string's response than in the sensor's output and it increases dramatically when approaching instability, reinforcing the need to use a wide-angled LED at a distance of $\frac{D}{L} > 4$ to minimise the effect of this form of nonlinearity on the system, and bring the harmonic distortion below 50dB.

Damping Time

The effect of the light distribution on damping time, obtained using the same simulation as with the harmonic distortion above, is plotted in Figure 4.14. The effect is significant at low gains, particularly at distances close to causing instability, and can be explained by Figure 4.15 which shows that the nonlinearity reduces the peak amplitude of the actuator. This reduces the affect of the travelling wave control system on the behaviour of the string, and again reinforces the need to use a wide-angled LED at a distance of $\frac{D}{L} > 4$ to minimise the effect of this form of nonlinearity on the system.

4.4 Sensor Electronics

As the accuracy of the algorithm used to decompose the travelling waves from the sensor readings is sensitive to noise it is important to maximise the signal-to-noise ratio (SNR) of the sensor system through careful design of the electronics.

Photodiodes can be operated in two modes; photovoltaic mode, where the voltage across the junction is held at zero, and photoconductive mode, where the junction is reverse-biased. The effect of reverse-biasing the diode is to shrink the size of the depletion region [105], reducing the junction capacitance and thereby the noise gain. It also reduces the amount of energy required for an electron to move across the junction, increasing the linearity of the photodiode's response at the cost of a small leakage current, often called the dark current. As discussed in Section 4.1 the way that the sensor is configured in this application means that

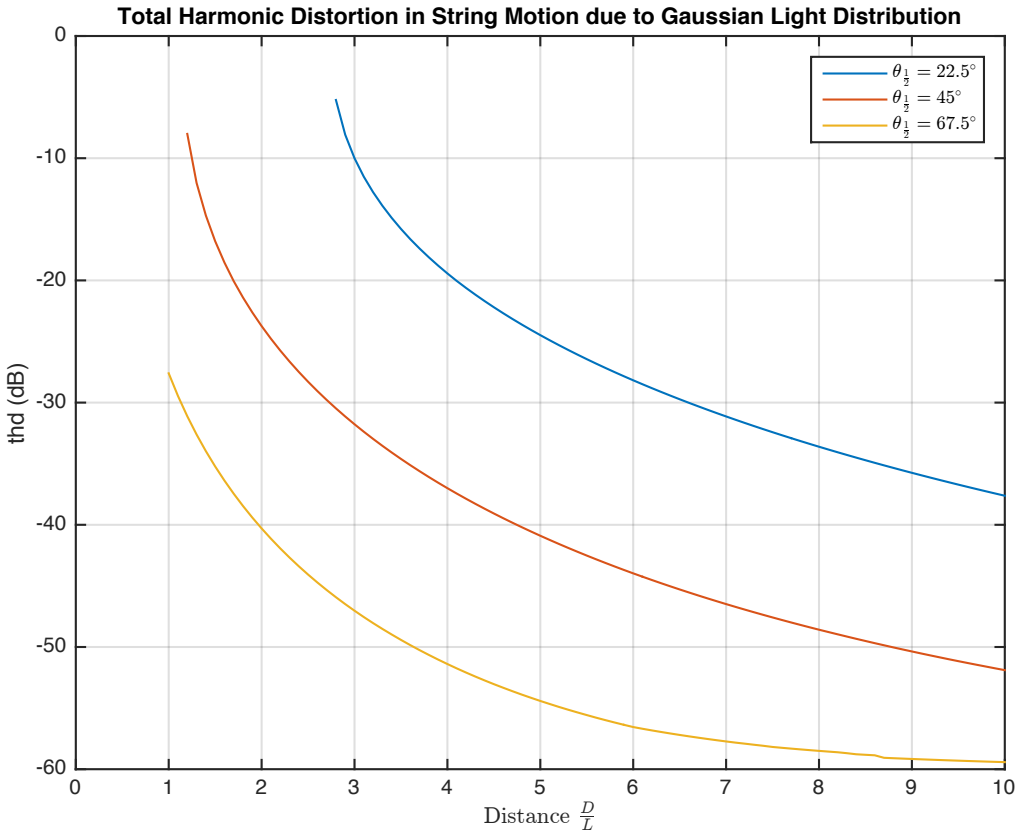

Figure 4.13: The peak total harmonic distortion present in the motion of the string during damping as a result of a gaussian light distribution on the sensor's surface.

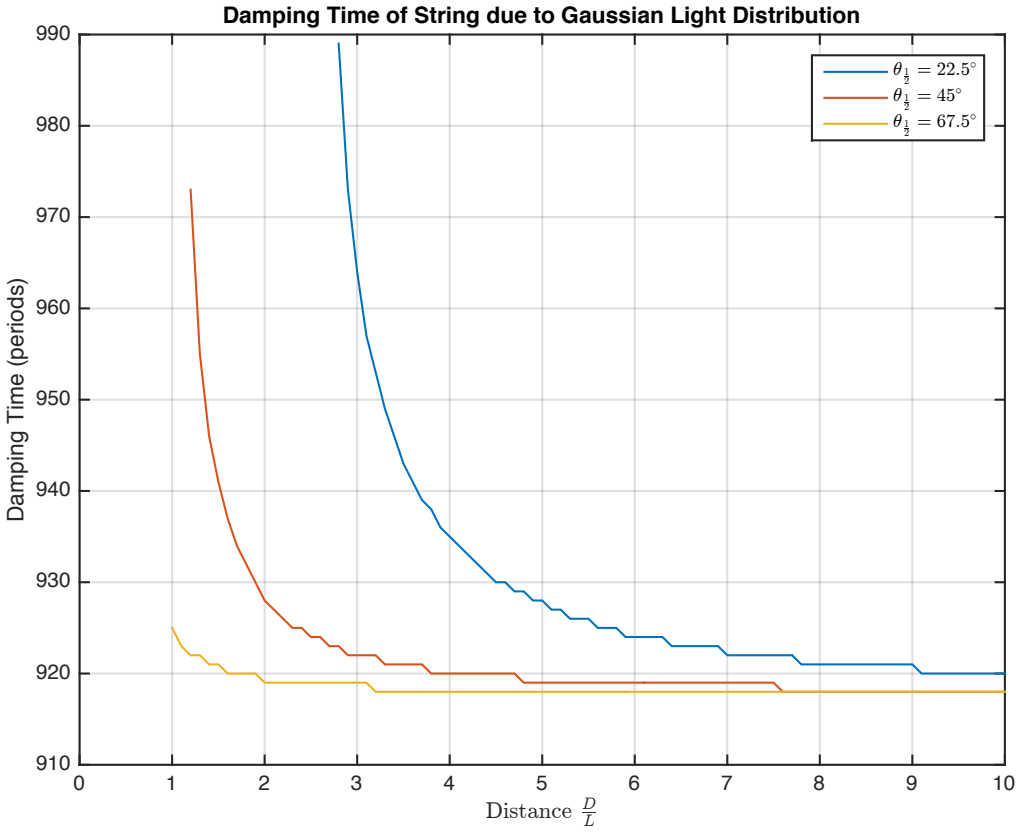

Figure 4.14: The number of periods required to damp the string, i.e bring the amplitude of all harmonics to below $-80dB$, with gain $K = 0.01$.

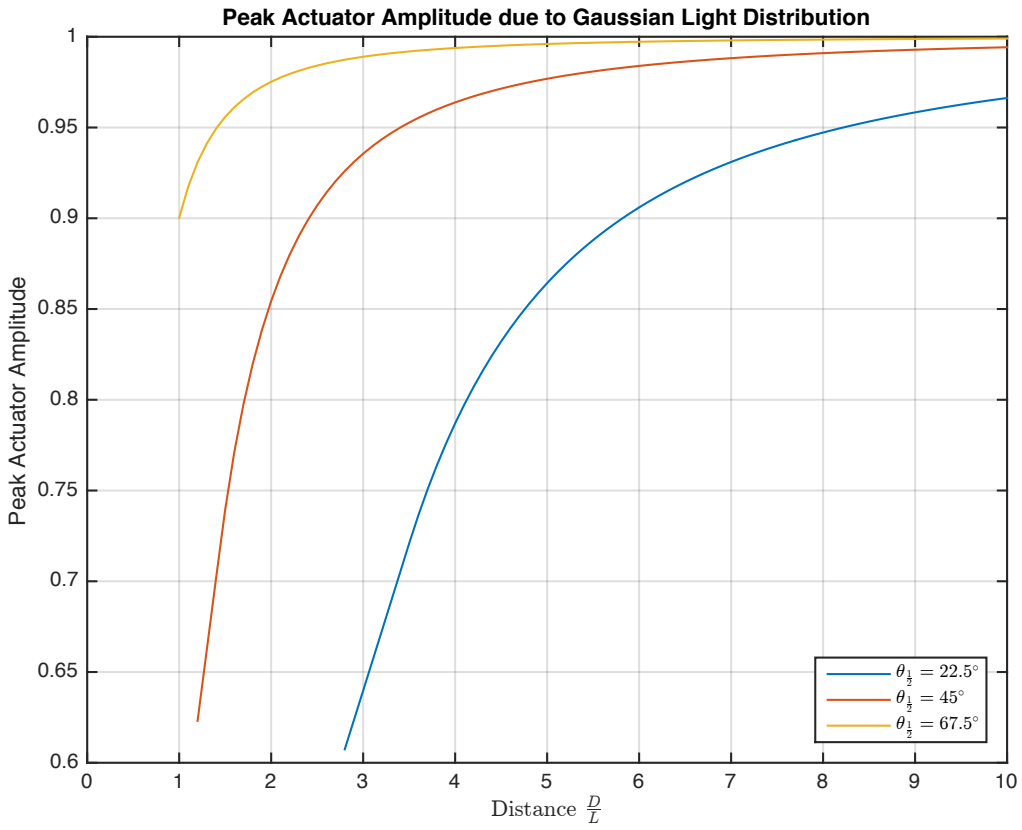

Figure 4.15: The peak actuator amplitude normalised against the gain K when damping the string in the presence of a gaussian light distribution on the sensor's surface.

there is already a sizeable DC current flowing through the photodiode due to the constant illumination, so the very small dark current produced has a negligible effect. The diode is therefore operated in photoconductive mode.

The output of the photodiode in photoconductive mode is a current $I_{pd}(t)$ which consists of a large constant term I_0 resulting from the constant illumination of the diode, a smaller variable term $I_s(t)$ which is proportional to the vertical displacement of the string, and a final variable term I_N representing noise originating from sources such as the illuminating LED and ambient light:

$$I_{pd}(t) = I_0 + I_s(t) + I_n \tag{4.54}$$

The purpose of the first stage of the sensor electronics, the preamplifier, is to correctly reverse-bias the photodiode in order to keep it in photoconductive mode, and to convert the output current I_{pd} into a voltage V_{pd}. This voltage is then fed into the second stage, the amplifier, the purpose of which is to reject the DC component resulting from the I_0 term and to amplify and bias the variable component proportional to the string displacement to the specifications of the third stage, the analog-to-digital converter. Both of the first two stages must be carefully designed to minimise the affect of all sources of noise, and maximise the SNR of the output.

4.4.1 Circuit Description

First Stage Preamplifier

The preamplifier is a transconductance amplifier which converts the photodiode current I_{pd} into a voltage V_{pd} (see Figure 4.16). The anode of the photodiode is connected to $0V$ and the cathode is connected directly to the inverting input of an operational amplifier, the non-inverting input of which is connected to a virtual ground at half of the supply voltage, $\frac{V_{cc}}{2}$. This has the effect of reverse-biasing the diode and holding it in photoconductive mode.

The feedback impedance Z_f connecting the output of the op-amp to its inverting input consists of a resistor R_f in parallel with a capacitor c_f. Assuming that the input impedance of the op-amp is significantly larger than Z_f the photodiode current I_{pd} flows entirely through the feedback impedance, and by Ohm's Law the voltage at the output of the preamplifier is given by:

$$\begin{aligned} V_{pd} &= Z_f I_{pd} \\ &= \frac{R_f}{1 + j\omega R_f c_f} I_{pd} \end{aligned} \tag{4.55}$$

At low frequencies the relationship approaches $V_{pd} = R_f I_{pd}$ and the gain of the preamplifier is determined by the value of the feedback resistor. The presence of the feedback capacitor c_f introduces a first order roll-off in the frequency response of the circuit at $\omega_f = \frac{1}{c_f R_f}$.

Second Stage Band-Pass Amplifier

The second stage of the circuit is a first-order bandpass filter and amplifier which rejects the DC components of the signal from the photodiode V_{pd}, amplifies the frequencies within its pass-band and attenuates higher frequencies. The transfer function of the second stage is given by:

$$\frac{V_{out}}{V_{pd}} = -\frac{j\omega c_1 R_2}{(1 + j\omega c_1 R_1)(1 + j\omega c_2 R_2)} \tag{4.56}$$

The corner frequencies which define the upper and lower bounds of the pass-band (or more specifically the -3db points) are:

$$\begin{aligned} \omega_l &= \frac{1}{c_1 R_1} \\ \omega_h &= \frac{1}{c_2 R_2} \end{aligned} \tag{4.57}$$

The gain in the pass band is given by the ratio of the two resistors:

$$G_{pb} = \frac{R_2}{R_1} \tag{4.58}$$

4.4.2 Noise Analysis

The primary source of noise in the system is I_n, the component of the photodiode current which results from external factors e.g ambient light hitting the sensor, broadband noise in the light emitted by the sensor's light source, or capacitative coupling from external sources of electromagnetic radiation. These factors are best tackled using external measures, such as

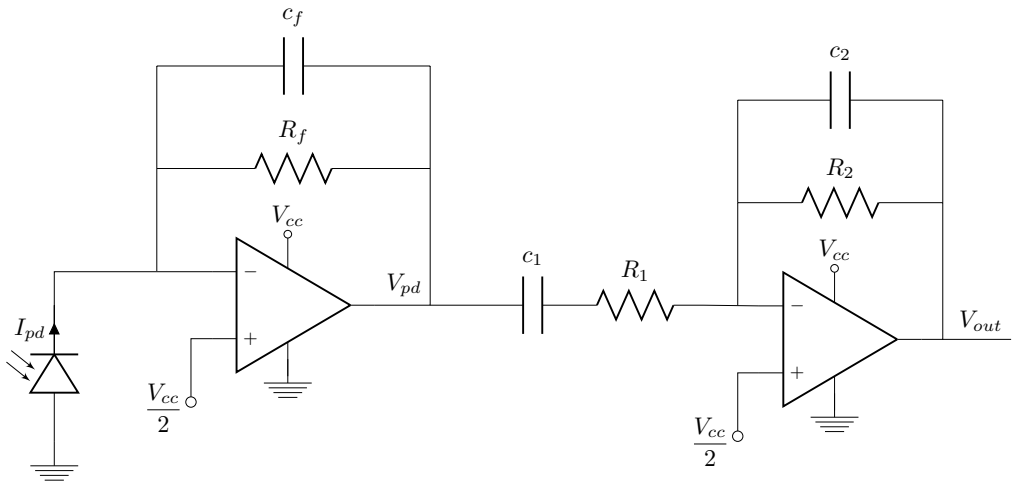

Figure 4.16: Schematic of the sensor circuit featuring the first-stage preamplifier and the second-stage band-pass amplifier

enclosing the sensor in a light-proof box or regulating and filtering the current powering the sensor's LEDs. Because the current produced by the photodiode I_{pd} is very low, on the order of tens of microamps, the cable which carries that current from the photodiode to the first op-amp is particularly sensitive to electromagnetic interference. It is therefore imperative to keep that cable as short as possible and to ensure that it forms no loops which can function as unintended antennae, picking up noise from nearby sources of radiation.

Some of the external noise sources will have frequency ranges which overlap with the frequency range of the signal $I_s(t)$ and there is nothing that the sensor circuit can do to attenuate them without also adversely affecting the signal. Some sources however, particularly those which produce broadband noise, can be at least partially rejected by strictly limiting the bandwidth of the circuit to the useful frequencies present in the signal, filtering out noise at higher frequencies and boosting the SNR. This can be done by choosing components such that the corner frequencies at which high frequencies begin to be attenuated, i.e ω_f for the first stage and ω_2 for the second stage, are equal to approximately 16kHz, limiting the bandwidth to the audio range with a second-order roll-off.

As well as attenuating external sources of noise, the sensor circuit must limit the effect of noise sources which it introduces itself. The most prominent of these sources is Johnson noise, which originates from the resistors in the circuit, and op-amp voltage noise.

Johnson Noise

Johnson noise is present in all passive components and is caused by the thermal agitation of electrons. The density of the Johnson noise produced by the resistors in the circuit, measured in units of volts-per-root-hertz ($\frac{V}{\sqrt{Hz}}$), is given by:

$$\bar{e}_R = \sqrt{4kTR} \tag{4.59}$$

Here k is Boltzmann's constant (approximately $1.38e^{-23}$), T is the ambient temperature in Kelvin (assumed to be approximately 295K) and R is the resistance.

As the noise is proportional to the square root of resistance, the effect of Johnson noise can be minimised by using smaller resistors. Reducing the magnitude of the resistors in the second stage R_1 and R_2 reduces their contribution to the total noise present at the output, and therefore boosts the SNR of the circuit.

While reducing the magnitude of the feedback resistor in the first stage R_f similarly reduces the level of Johnson noise it produces by the square root of its resistance, the first stage is a transconductance amplifier and the magnitude of the signal V_{pd} is directly proportional to the resistance R_f. The SNR of the circuit is therefore improved by maximising the value of R_f despite the fact that this increases the Johnson noise. The magnitude of R_f is limited by the constant term in the photodiode current I_0 and by the supply voltage of the first stage op-amp V_{cc}:

$$R_f < \frac{V_{cc}}{I_0} \tag{4.60}$$

If R_f exceeds this limit it will saturate the op-amp and cause the signal to be lost.

Op-amp Voltage Noise

The voltage noise produced by an op-amp has two distinct flavours; flicker noise, also called $\frac{1}{f}$ noise because of its frequency dependance, which dominates at frequencies below the corner frequency f_c, and shot noise which dominates above the corner frequency and which is approximately white, i.e constant with frequency. Op-amps also produce current noise, however when using CMOS-technology op-amps this effect is so small as to be negligible. The noise density of an op-amp is usually specified in its datasheet as referred to the input.

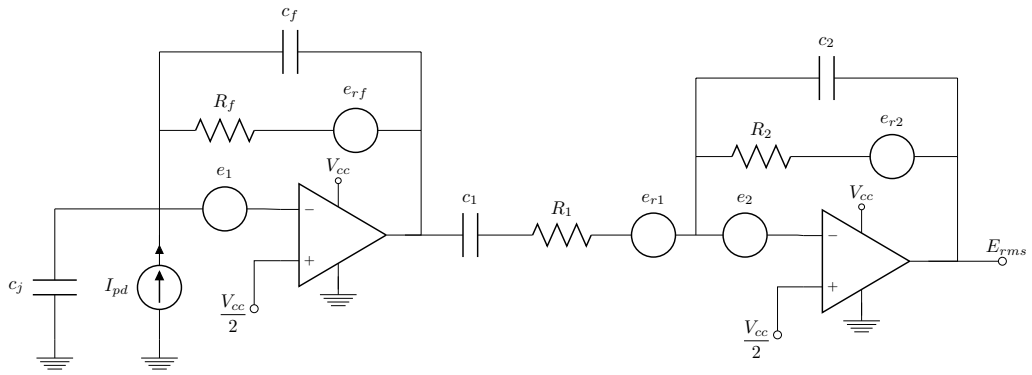

Figure 4.17: Circuit diagram showing all noise sources and with the photodiode replaced by an equivalent circuit featuring a current source and a capacitor representing the junction capacitance c_j

Noise Calculations

Figure 4.17 shows the circuit with all noise sources added, and with the photodiode replaced by an equivalent circuit featuring a current source and the junction capacitance of the diode. As all the noise sources are uncorrelated the RMS noise voltage at the output E_{rms} is equal to the square root of the sum of the squares of the RMS voltages of each of the individual noise sources transformed to the output:

$$E_{rms} = \sqrt{E_{rf}^2 + E_{r1}^2 + E_{r2}^2 + E_1^2 + E_2^2} \tag{4.61}$$

To transform the noise densities displayed in Figure 4.17 to RMS voltages at the output they must be multiplied by the relevant frequency-dependant gain and integrated over the bandwidth of the circuit, which for simplicity we take to be equal to the pass-band of the second stage, from $f_l = 1.6$Hz to $f_h = 16$kHz.

The Johnson noise from R_2 appears directly at the output:

$$\begin{aligned} E_{r2} &= \int_{f_l}^{f_h} \bar{e}_{r2} df \\ &= \sqrt{4kTR_2}(f_h - f_l) \end{aligned} \tag{4.62}$$

The Johnson noise from R_1 must be multiplied by the noise gain of the second stage to

transform it to the output. The noise gain is equal to the signal gain specified in Equation 4.56 plus 1, which like the signal gain is approximately constant over the pass-band and equal to G_{pb}:

$$\begin{aligned} E_{r1} &= \int_{f_l}^{f_h} G_{pb}\bar{e}_{r1}df \\ &= G_{pb}\sqrt{4kTR_1}(f_h - f_l) \end{aligned} \tag{4.63}$$

The Johnson noise from the feedback resistor in the first stage R_f must be multiplied by the signal gain of the second stage, which is also approximately constant over the pass-band and equal to G_{pb}:

$$\begin{aligned} E_{rf} &= \int_{f_l}^{f_h} G_{pb}\bar{e}_{rf}df \\ &= G_{pb}\sqrt{4kTR_f}(f_h - f_l) \end{aligned} \tag{4.64}$$

The second stage op-amp voltage noise density which consists of both $\frac{1}{f}$ noise and white noise with a density of $\bar{e}_{op}$ must be multiplied by the second stage noise gain and is integrated as follows:

$$\begin{aligned} E_2 &= \int_{f_l}^{f_h} G_{pb}\bar{e}_{op}\left(\frac{f_c}{f} + 1\right)df \\ &= G_{pb}\bar{e}_{op}\left(f_c ln\left(\frac{f_h}{f_l}\right) + f_h - f_l\right) \end{aligned} \tag{4.65}$$

The first stage op-amp voltage noise must be multiplied by the noise gain of the first stage followed by the signal gain of the second stage. The first stage noise gain is given by:

$$NG_1 = \frac{1 + j\omega(c_f R_f + c_j R_f)}{1 + j\omega c_f R_f} \tag{4.66}$$

It is a high-pass shelving filter with its top corner frequency at $\omega_2 = \frac{1}{c_f R_f}$, the boundary of the pass-band, and its lower corner frequency at $\omega = \frac{1}{c_f R_f + c_j R_f}$ (see Figure 4.18). Typical large planar photodiodes have junction capacitance $c_j \approx 2$nF which is reduced when the

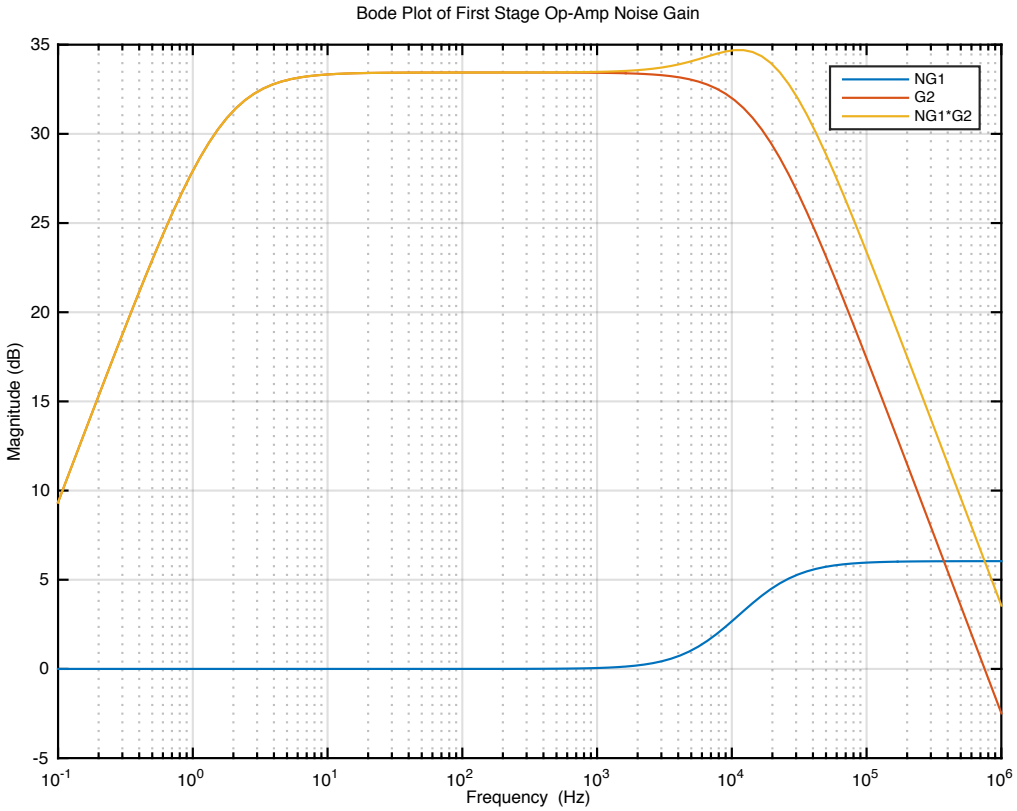

Figure 4.18: A bode plot of the transfer function between the first stage op-amp input voltage noise density and the output of the circuit. NG1 is the noise gain of the first stage, G2 is the gain of the second stage, and the third line is the product of the two. The plot assumes $c_j = 1\text{nF}$

diode is biased with a negative voltage and so the lower corner of the noise gain tends to be close in frequency to the top corner. This means that the noise gain is unity for most of the pass-band, and it is reasonable to approximate the gain experienced by the first stage op-amp voltage noise to the signal gain of the second stage:

$$\begin{aligned} E_1 &= \int_{f_l}^{f_h} G_{pb}\bar{e}_{op}\left(\frac{f_c}{f}+1\right)df \\ &= G_{pb}\bar{e}_{op}\left(f_c ln\left(\frac{f_h}{f_l}\right)+f_h-f_l\right) \end{aligned} \tag{4.67}$$

Signal-To-Noise Ratio

At the output of the circuit the signal is equal to the variable component of the photodiode current $I_s(t)$ multiplied by the signal gains of both stages. Assuming the frequency content of the signal lies within the pass band, it is given by:

$$V_{out}(t) = R_f G_{pb} I_s(t) \tag{4.68}$$

The signal-to-noise ratio in decibels is then given by:

$$SNR = 20log_{10}\left(\frac{E_{rms}}{V_{out}}\right) \tag{4.69}$$

4.4.3 Choosing Components

The critical passive component in the circuit is the first stage feedback resistor, R_f. From the noise analysis we know that larger values of R_f give better SNR, but we also have an upper limit defined by the supply voltage V_{cc} and the constant term of the photodiode current I_0 (see Equation 4.60). In our experimental setup the supply voltage is 5V and the constant current I_0 is approximately 0.4mA so the optimal value of R_f is approximately $10k\Omega$, though this is highly dependant upon the exact configuration of the sensor assembly, including the photodiode, LEDs and lenses. From Equation 4.57 we can then choose the feedback capacitor c_f to be 1nF.

The optimal gain of the second stage G_{pd} is chosen to match the output voltage amplitude to the supply voltage of the op-amp as follows:

$$G_{pd} \approx \frac{V_{cc}}{2R_f I_s(t)} \tag{4.70}$$

The amplitude of the signal current $I_s(t)$ with the string vibrating at its maximum amplitude in our experimental setup is approximately 5µA (though again this is highly dependant on the sensor configuration) and so the optimal gain is approximately 50 resulting in a constraint on the value of the resistors in the second stage R_1 and R_2:

$$\frac{R_2}{R_1} \approx 50 \tag{4.71}$$

We know from the noise analysis that the value of these resistors should be minimised to reduce the effect of Johnson noise, however there is another constraint originating from the values of the corner frequencies (Equation 4.57) which must be achievable using unpolarised surface-mount ceramic capacitors. As such the values for the second stage passive components were chosen to be:

$$\begin{aligned} R_1 &= 1k\Omega \\ c_1 &= 100\mu F \\ R_2 &= 47k\Omega \\ c_2 &= 220pF \end{aligned} \tag{4.72}$$

The remaining components left to choose are the op-amps. The SNR of the whole circuit is plotted against the input voltage noise density of the op-amps in Figure 4.19, assuming that both are identical and that the corner frequency f_c is 1kHz. It is clearly important to choose an op-amp with a low voltage noise rating. If e.g LM358s are used, with a poor noise density of approximately $40\frac{\text{nV}}{\sqrt{\text{Hz}}}$, the SNR is approximately -32dB, while with a low-noise op-amp such as the TLC2272 with a noise density of $9\frac{\text{nV}}{\sqrt{\text{Hz}}}$, the SNR is reduced to -42.5dB.

The contributions of each of the components to the RMS noise voltage at the output are plotted in Figure 4.20 for a TLC2272 op-amp and with the component values described above. The largest contributors of noise are the op-amps, with the white noise E_{1w} and E_{2w} being a larger contributor than the flicker noise E_{1f} and E_{2f}. The next-largest contributor is the Johnson noise of the feedback resistor E_{rf}, while the Johnson noise of the second stage resistors is much smaller and practically negligible.

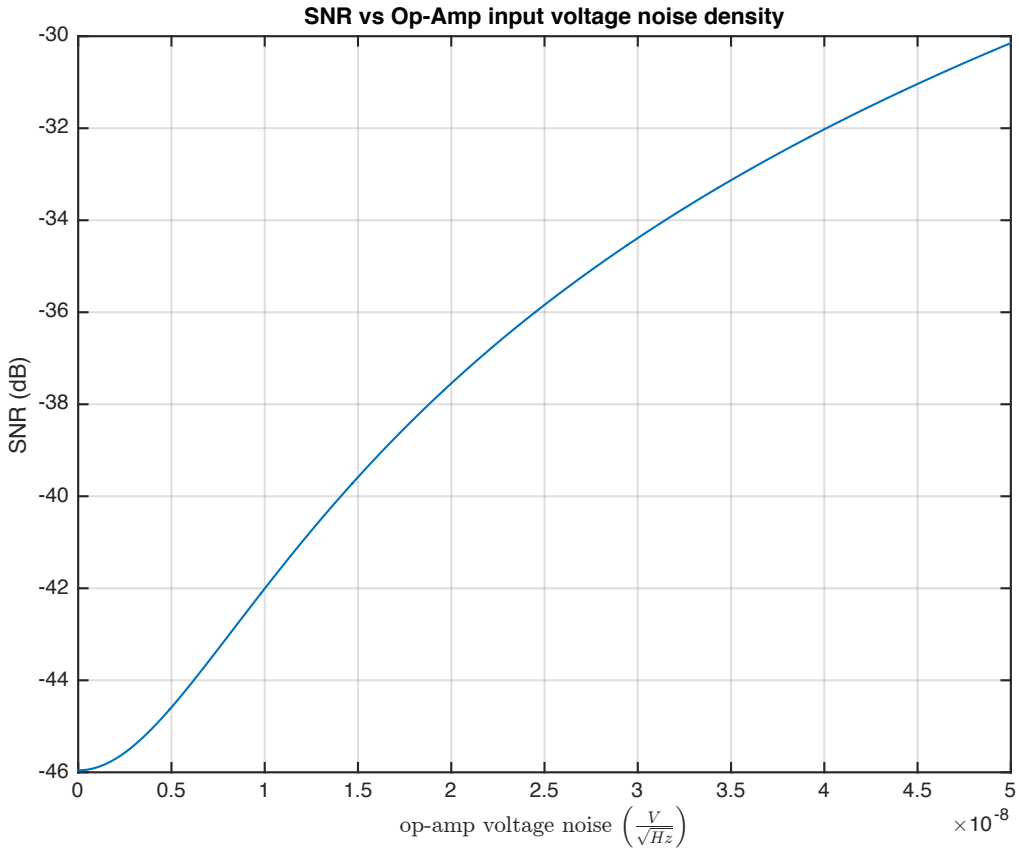

Figure 4.19: The signal-to-noise ratio of the circuit plotted against the op-amp input voltage noise density, assuming both op-amps are identical and the corner frequency $f_0 = 1\text{kHz}$

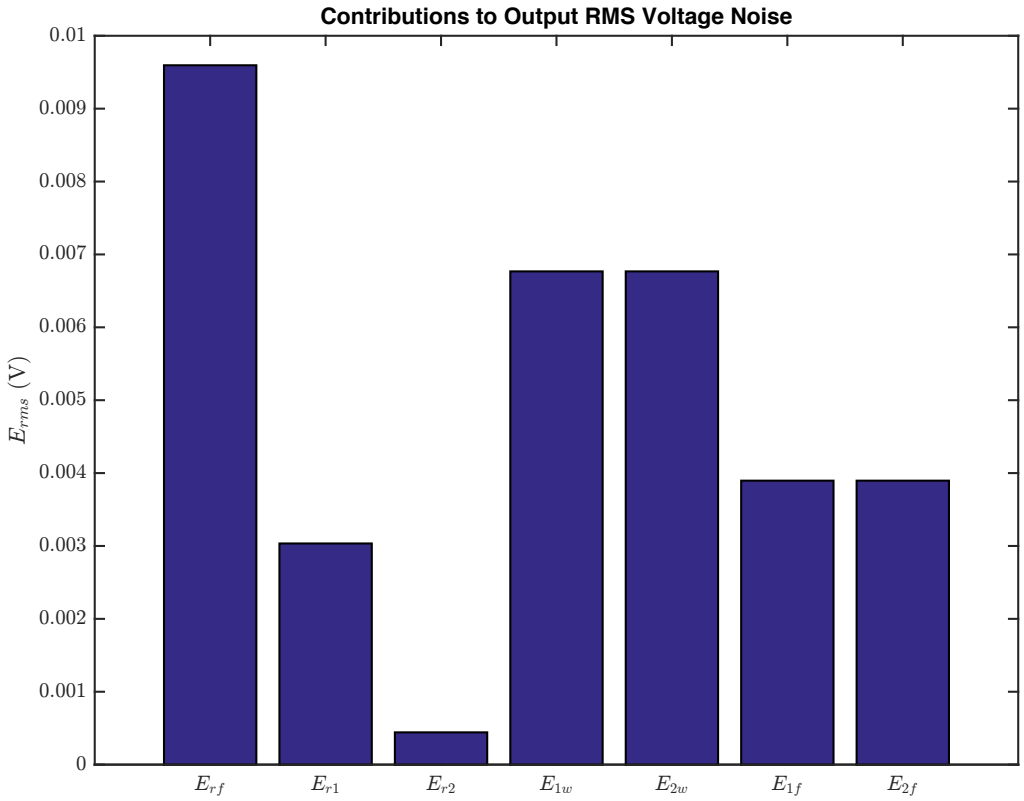

Figure 4.20: The contributions of each noise source in the circuit to the RMS noise voltage at the output.

4.5 Summary

In this chapter we have presented the design of a highly linear low-noise travelling wave sensor.

We presented an algorithm originating from the industrial vibration suppression literature and applied it to the problem of sensing the waves travelling along a musical string. The algorithm features a tunable parameter θ which can be used to reduce its sensitivity to sensor noise at the cost of reducing its overall accuracy. In order to maximise the accuracy of the algorithm it is essential to maximise the signal-to-noise ratio of the sensors, allowing θ to be set as close to 1 as possible. Perfect estimation of the travelling wave is not possible in practice, as that would require θ to equal 1 which causes instability in the estimator.

We decided to use an optical transmission-based sensor due to its high potential for linearity, but after modelling its behaviour we identified two major sources of nonlinearity with the potential to induce harmonic distortion and cause instability in the travelling wave control system.

The first source of nonlinearity is out-of-plane or elliptical motion of the string. When using a simple LED as a light source the geometric gain of the sensor varies with the horizontal distance between the string and the sensor surface. After modelling a simplified scenario in which the string vibrates in a static elliptical motion we identified that this nonlinearity has the potential to cause instability and significant harmonic distortion. By using a lens to collimate the light from the LED, the effect of this nonlinearity is effectively eliminated.

The second source of nonlinearity is the non-uniform distribution of light hitting the surface of the sensor due to the radiation pattern of the LED light source. By modelling the light distribution as a gaussian function we showed that when using a narrow-angled LED located close to the sensor the performance of the system was severely degraded, resulting in increased damping time, severe harmonic distortion and instability. By using a wide-angled LED with a half-angle of at least 67.5° and locating it over 4cm from our 1cm square photodiode, the effect of this nonlinearity was minimised.

Finally, we designed a circuit to correctly bias the photodiodes in our sensors, and to convert their output to a voltage of the correct range with the highest signal-to-noise ratio possible. We limited the bandwidth of the sensor circuit to reduce the impact of broadband noise in the signal from the photodiode, and analysed the contribution to the voltage noise at the output of the various sources in the circuit. We showed that the greatest contribution was made by the op-amp voltage noise, so we selected an op-amp optimised for low voltage noise. The next-greatest contribution was from the feedback resistor in the first stage transconductance

pre-amplifier circuit. We demonstrated that the signal-to-noise ratio is optimised by making this resistor as large as possible without causing clipping at the output of the first stage due to the constant current produced by the constantly-illuminated photodiode.

Chapter 5

Termination Based Actuation

The purpose of the actuator in a travelling wave control system is to displace the termination point by an amount proportional to the travelling wave incident upon it, absorbing some of the energy from the wave and preventing it from being reflected back into the string. The actuator must have high enough bandwidth to be able to absorb energy in the higher modal frequencies of the string, and must also be highly linear as any nonlinearity can degrade the performance of the control system (see Section 3.5). Stiffness is also an important parameter in this context; if it is too low the internal forces from the string being plucked could be sufficient to cause the actuator to move, requiring the use of feedback to accurately control the displacement. An actuator with higher stiffness therefore reduces the complexity of the control problem by eliminating the need for feedback to compensate for this.

5.1 Why Actuate the Termination?

Existing literature on actuating strings has not specifically examined termination-based actuation, focusing rather on actuating a point along the continuous portion of the string [6]. This adds complexity to the string's motion as a pair of travelling waves are generated moving in opposite directions away from the actuator. In contrast a force applied at the termination only generates a single travelling wave moving away from the actuator, significantly simplifying the resulting motion. This is illustrated in Figure 5.1.

Mechanically coupling an actuator to the continuous portion of a string is not practically possible as it would introduce an impedance boundary, causing waves to be reflected and undesirably interfering with the string's motion. As such most actuators in the literature rely

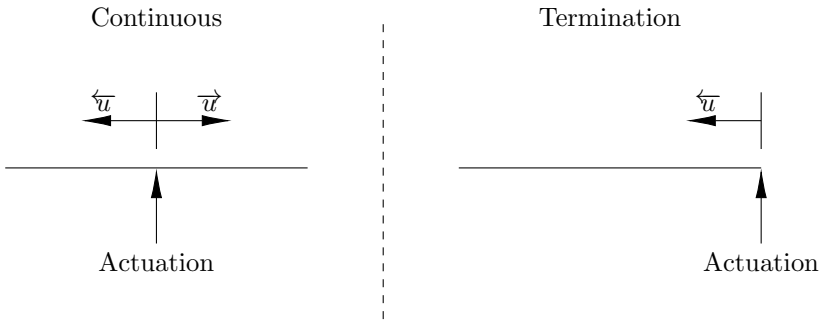

Figure 5.1: Actuation applied to a point along the continuous length of the string generates waves travelling in two directions (left) while actuation applied to the termination only creates one (right).

on electromagnetic forces, either directly by placing an electromagnet close to a ferromagnetic string [67], or through the Lorentz force by running an alternating current through an electrically conductive string located close to a strong permanent magnet [66]. When compared to the forces internal to the string when it is vibrating, the forces which can be exerted by these electromagnetic actuators are weak, and though they can be used to coax a string into resonant vibration or to gradually damp a string over several periods of vibration, when attempting to implement some form of travelling wave control they require impractically high control gains and suffer from problems with linearity [6].

At the termination point of the string there is already an impedance boundary so it is possible to mechanically couple an actuator to the string without causing any unwanted interference. This allows for the design of mechanically-coupled electromagnetic actuators and also allows consideration of alternative technologies such as piezoelectric actuation, both of which allow much higher forces to be exerted.

5.2 Actuation Technology

5.2.1 Electromagnetic

In Appendix F.5 of his thesis [6] Berdahl suggested a design for a termination-based electromagnetic actuator which involved terminating a string over a strong neodymium magnet which is mounted on a pair of steel springs to allow it to move vertically. An electromagnet is mounted above the termination and is able to exert a force on the permanent magnet

and through it the termination. We built an actuator based on this design, a thorough description of which can be found in Appendix B, however we encountered a number of problems which made it unsuitable for use in a travelling wave control system [25].

The relatively low force which the actuator was able to exert, coupled with the relatively low stiffness of the spring-based mounting, meant that even with the aid of a closed-loop feedback system it was impossible to prevent the vibrating string from causing the termination point to displace significantly. As such the termination could not be modelled as rigid in the absence of control which significantly complicates the implementation of a travelling wave control system. The actuator was also very lightly damped and therefore highly resonant with a low natural frequency of around 400Hz, well within the range of the dominant modes of a typical musical string. We successfully used posicast, an input shaping active control technique [99], to eliminate the resonance, however the bandwidth of the sensor was still too low. Although these problems could theoretically be countered with mechanical solutions such as using larger and more powerful magnets or stiffer springs, the relationship between the force exerted on the termination and the distance between the stationary electromagnet and the vibrating permanent magnet is inherently nonlinear, ultimately making this design of electromagnetic actuator unsuitable for use in travelling wave control.

5.2.2 Piezoelectric

Piezoelectric stack actuators are formed by stacking a large number of piezoelectric elements on top of each other [106]. They are capable of exerting large forces over wide bandwidths, and have high stiffnesses comparable to aluminium. Although they can exhibit hysteresis in response to static loads, when loaded dynamically as they would be in this application they exhibit a highly linear relationship between voltage and displacement, making them very well suited to travelling wave control.

The downside of using piezo stacks is that they are only capable of displacing with very low amplitudes, typically measured in micrometers, and require high voltages and currents. The actuator we used in our experiments was the AE0505D16F from Thorlabs, which has a rated maximum displacement of 11.6µm when driven at 100V. It has an unloaded resonant frequency of 69kHz, a stiffness of $4.4\text{x}10^{10}\text{N/m}^2$, and can exert a force of up to 850N.

5.3 Dealing with Limited Actuator Amplitude

The string sensors described in Chapter 4 are capable of detecting a string vibrating with a maximum amplitude of 5mm and the travelling waves have a maximum amplitude of half of that, 2.5mm. The range of the piezo stack actuator we are using is 11.6µm and its maximum amplitude is half of that, 5.8µm, over 400 times smaller than the maximum measurable travelling waves.

The most obvious way of implementing travelling wave control when the amplitude of the actuator is smaller than that of the travelling waves is to apply a linear gain K to the wave estimate which is small enough to ensure that the displacement is within the linear range of the actuator. In Section 3.3.1 we saw that this technique induces no additional harmonic distortion in the string's vibration, but comes at the cost of significantly increased damping times (see Figure 5.2).

There is an inherent inefficiency in the linear technique, which is that the gain K must be set to a value K_L which is equal to the ratio between the initial amplitude of the travelling wave $\overleftarrow{u}_0$ and the maximum actuator amplitude $u(0,t)_{max}$:

$$K_L = \frac{u(0,t)_{max}}{\overleftarrow{u}_0} \tag{5.1}$$

As time goes by the amplitude of the wave $\overleftarrow{u}$ decreases as the string is damped by the control action, but the value of K remains constant, so the actuator amplitude correspondingly decreases below its maximum even when the amplitude of the wave is still greater than the maximum of the actuator. This results in the exponential decay of the amplitude and an asymptotic approach to 0, but the actuator is not using its full range and so damping occurs slower than is necessary.

In this section we examine two techniques for reducing the damping time behind what is possible with linear travelling wave control in the face of limited actuator amplitude.

5.3.1 Clipping

One possible technique is to raise the gain K above the linear limit of the actuator and clip the waveform at the limit, or allow the actuator or drive circuitry to perform the clipping naturally. This has an advantage over the linear form of control in that it uses the full range of the actuator for longer during the damping period, but it introduces a nonlinearity into

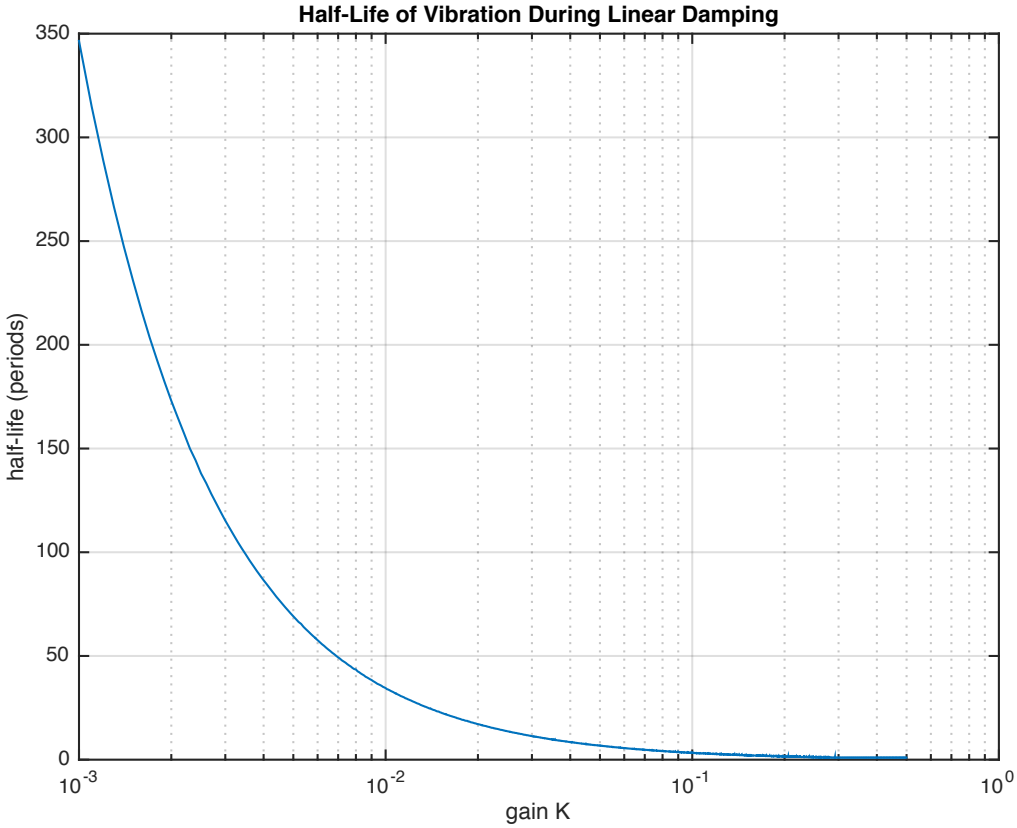

Figure 5.2: The half-life of vibration during damping with linear travelling wave control with gain K.

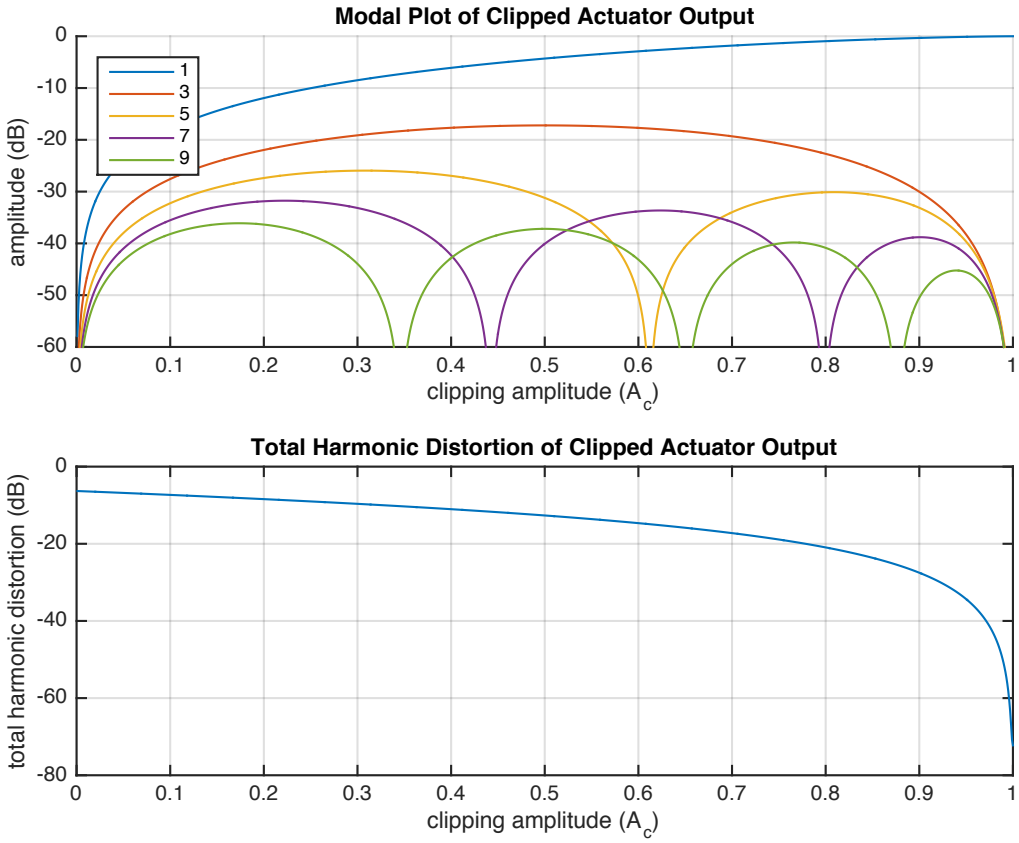

Figure 5.3: Modal plot and total harmonic distortion of a symmetrically clipped sinusoid. Clipping amplitude $A_c = 1$ means no clipping, while $A_c = 0$ means full clipping and therefore no output.

the control system which has the potential to introduce harmonic distortion into the string's vibration.

The effect of symmetrically clipping a simple sinusoid on the modal amplitudes and total harmonic distortion in the signal is shown in Figure 5.3. The process creates significant harmonic distortion, however only the odd-order modes are present and they are all positive. This is similar to the effect produced by adding a positive cubic nonlinearity to the output, which has a tendency to stabilise the system and reduce damping time in combination with low gains (Section 3.5).

To demonstrate the effect of clipping we will compare three scenarios which are illustrated in Figure 5.4. In two of the scenarios the actuator output is linear, one having a gain of

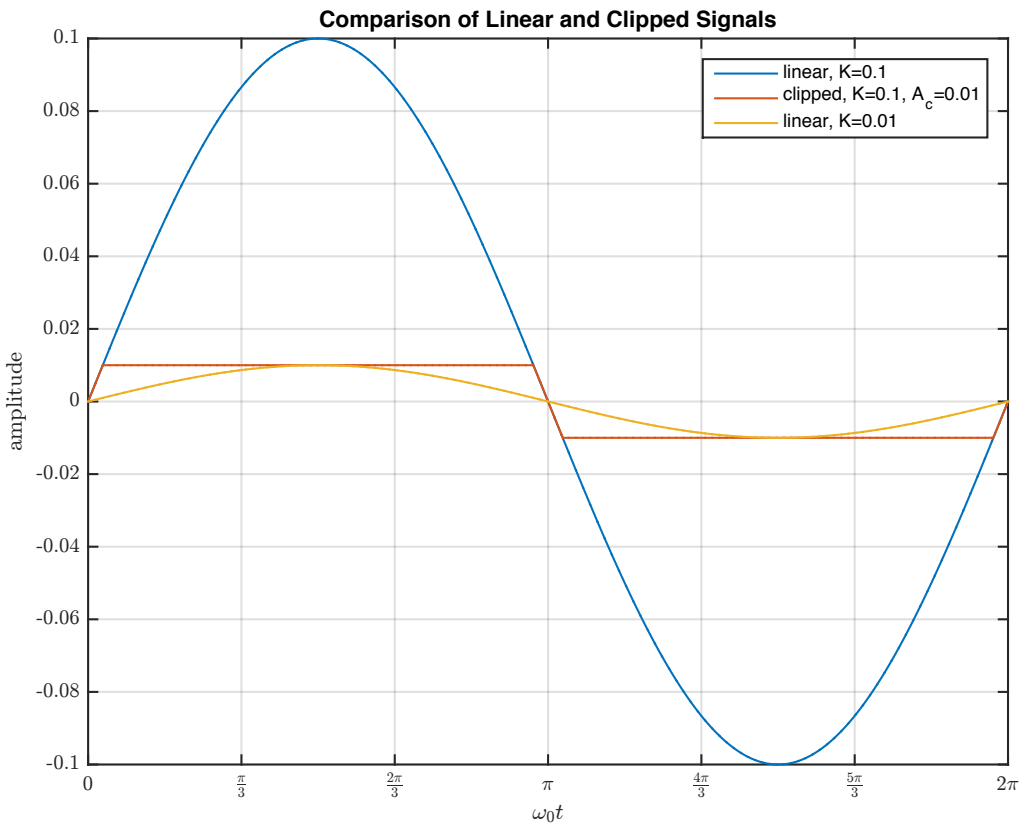

Figure 5.4: The output of the actuator during the first period of damping for a linear output with gain $K = 0.1$, a clipped output with $K = 0.1$ clipped at $A_c = 0.01$, and another linear output with $K = 0.01$.

0.1 and one with a gain ten times smaller, of 0.01. In the third scenario the output has a linear gain of 0.1 applied to it, but it is clipped at an amplitude of 0.01. The output of the actuator during the first period of a vibration with the initial state of the travelling wave being a simple sinusoid of amplitude 1 is plotted in Figure 5.4. The peak amplitude of the clipped output is equal to that of the linear scenario with the lower gain.

A comparison of the energy in the string during simulated damping in the three scenarios is shown in Figure 5.5.

The clipped output begins to decay at the same rate as the slower linear output, but as time goes on and the amplitude of the string and the linear output decrease, the rate of decay of the clipped output increases. After 90 periods the amplitude of the travelling waves has decayed to below the clipping threshold $A_c = 0.01$, the clipped output is no longer clipping

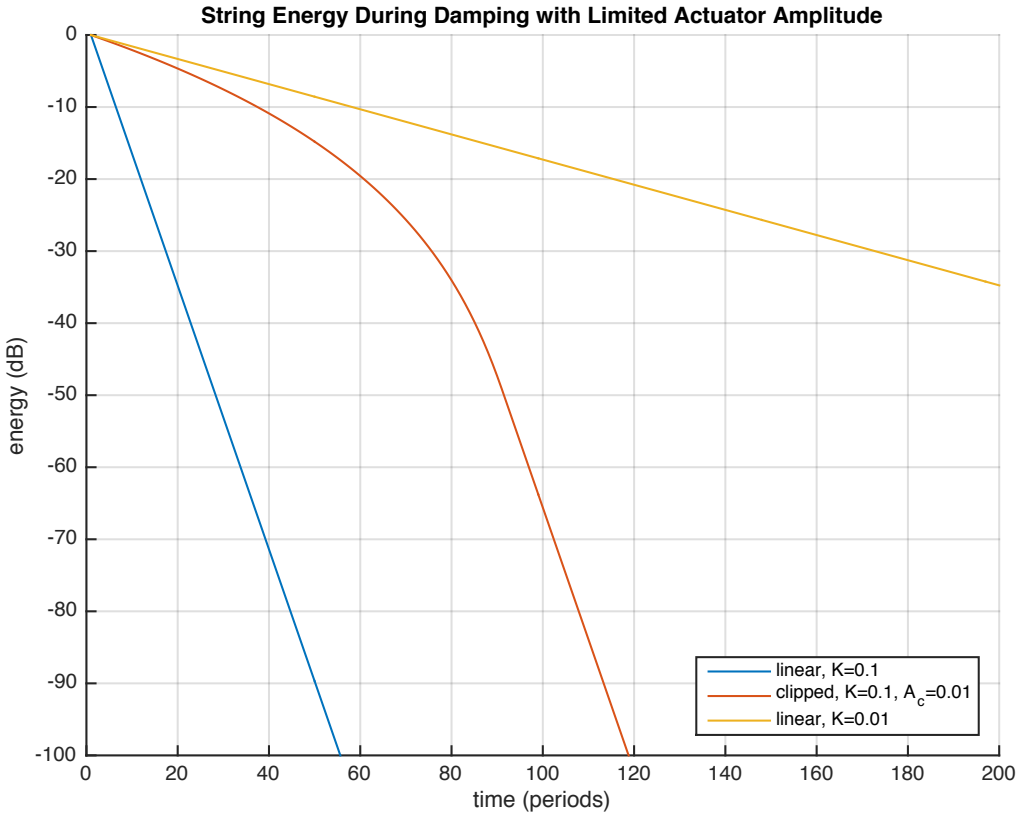

Figure 5.5: The simulated energy in the string during damping relative to the starting energy with a linear output with gain $K = 0.1$, a clipped output with $K = 0.1$ clipped at $A_c = 0.01$, and another linear output with $K = 0.01$.

and the rate of decay is equal to the faster linear output.

The mean half-life of the vibration before the wave has decayed to −80dB in the fast linear case with $K = 0.1$ is 3.3 periods, while in the slow linear case with $K = 0.01$ it is 33.7 periods. The mean half-life in the case of the clipped output is 5.4 periods, much closer to that of the fast linear case which requires ten times the actuator displacement.

Figure 5.6 demonstrates that clipping the output can produce much faster damping than a linear output with limited actuator amplitude. The plot shows how the mean half-life of the vibration, given by the number of periods taken for the energy in the string to reduce by half averaged over the damping period, varies when the maximum actuator amplitude A_{max} varies from 0.1 to 0. In the linear case, linear travelling wave control is simulated with the gain K equal to the maximum actuator amplitude A_{max}. In the clipped case, the gain K is set to 0.1, but the output is clipped at A_{max}, so that the peak actuator amplitude is equal to the linear case. The clipped output is capable of damping the string significantly faster than the linear output, particularly when the amplitude is severely limited.

The cost of clipping is also highlighted in Figure 5.6 which displays the peak total harmonic distortion of the string's vibration during damping. In the linear case there is no harmonic distortion, but when clipping is introduced the distortion becomes significant, showing the trade-off between the two methods for dealing with limited amplitude. One interesting thing to note is that clipping does not cause instability.

5.3.2 Adaptive Gain Theory

Clipping the output damps the string more quickly because it uses the full range of the actuator to absorb the wave for longer during the damping period. It does this by applying a constant high gain to the output and limiting the maximum amplitude, which introduces nonlinearity and harmonic distortion.

The adaptive gain algorithm also attempts to use the full range of the actuator but in a more sophisticated way without introducing significant nonlinearity. It does this by dynamically scaling the gain in order to match the amplitude of the output to the maximum amplitude of the actuator. In this way the shape and frequency content of the output is preserved, very little harmonic distortion is introduced and the full range of the actuator is used until the string is fully damped.

The adaptive gain algorithm can be applied to a signal in real-time by measuring the peak amplitude of the output during the previous period and setting the gain for the next period to be the inverse of this, leaving a small amount of headroom to ensure no clipping.

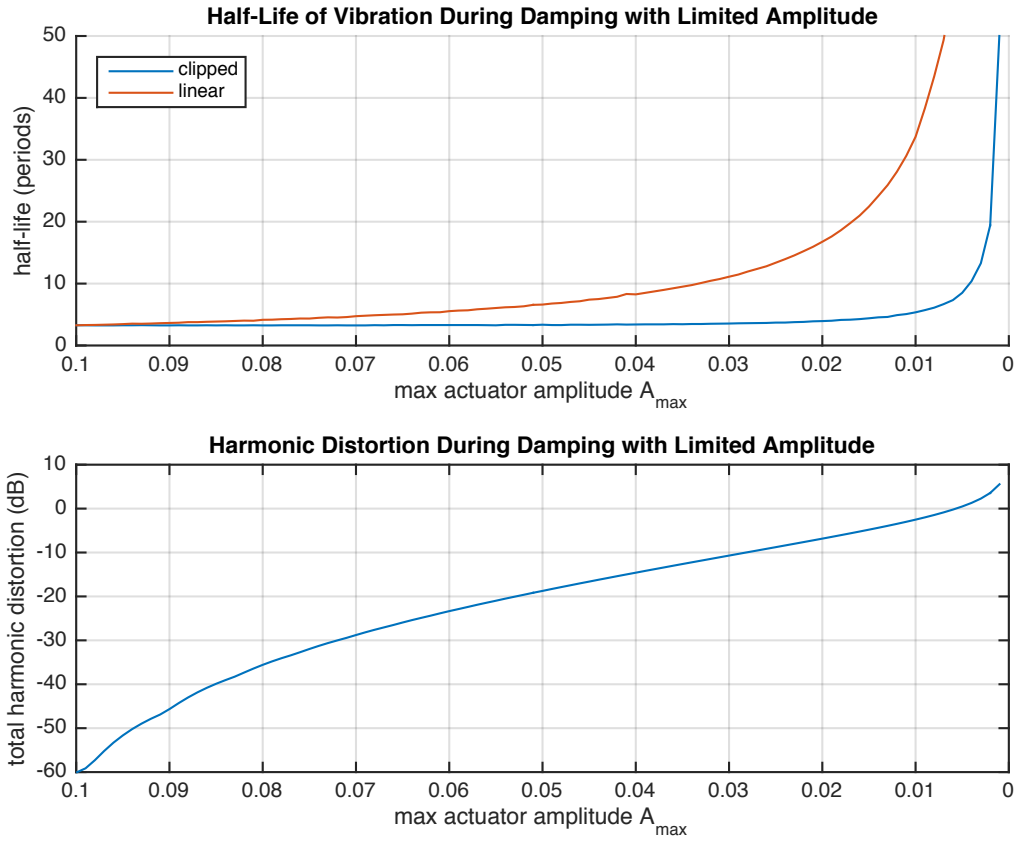

Figure 5.6: Plots of the half-life and harmonic distortion of the string's vibration with limited actuator amplitude. The plots are created by simulating a travelling wave control system. In the linear case the gain K is equal to the maximum actuator amplitude A_{max}, while in the clipped case the gain $K = 0.1$ and the output is clipped at A_{max}.

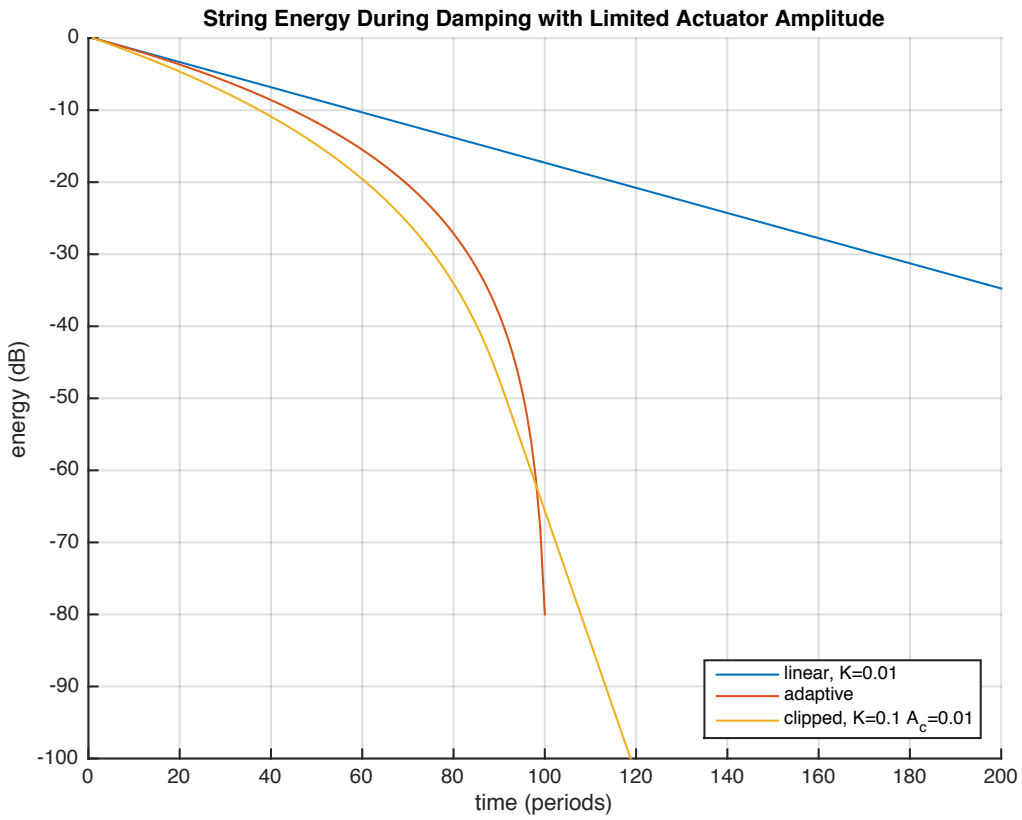

Figure 5.7: The energy in the string during damping with the maximum actuator amplitude set to 0.01.

A comparison of the energy in the string during damping with the maximum actuator amplitude limited to 0.1 for the three cases of linear, clipped and adaptive gain is given in Figure 5.7. While the adaptive gain does damp the string much more quickly than the linear gain, during the early part of the damping period when the amplitude of the string is large the clipped output performs better, reducing the energy to -60dB more quickly than the adaptive gain. The reason for this discrepancy is not clear, but one possibility is that the higher peak velocity of the clipped output more closely matches that of the travelling wave which allows it to be absorbed more quickly.

The mean half-life of the linear case in Figure 5.7 is 34.5 periods, the clipped case is 7.9 periods and the adaptive case is 8.2 periods. The maximum total harmonic distortion in both the linear and the adaptive case is zero, while for the clipped case it is -2.5dB which is indicative of severe distortion.

Which technique is better depends on the desired goals; if the fastest damping is required and the effect on harmonic distortion and timbre is not important, clipping the output will produce a better result, but if fast damping with minimal distortion is required the adaptive gain algorithm will perform better.

5.4 Actuator Drive Circuitry

The AE0505D16F piezo stack actuator can be modelled as a purely capacitative load with a rated capacitance of 1.4µF and a rated voltage of 100V. This presents a challenge for the driving amplifier which must provide large currents at high voltages and avoid instability caused by the capacitative load.

The relationship between the capacitance of the piezo C, the maximum output current of the driving amplifier I_{max} and the maximum slew rate of the circuit $\frac{dV}{dt}$ is:

$$\frac{dV}{dt} = \frac{I_{max}}{C} \tag{5.2}$$

We will be using the OPA541 power op-amp with a 50V power supply. To drive the actuator at this voltage over a bandwidth of 16kHz the required slew rate is 2.5V/µs, and the required peak current is approximately 3.5A which is just within the capabilities of the OPA541 with a large heatsink.

The amplifier is arranged in a first-order bandpass configuration as with the second stage of the photodiode preamplifier in Section 4.4 (see Figure 5.8). The component values used are:

$$\begin{aligned} R_1 &= 10\text{k}\Omega \\ c_1 &= 1\mu\text{F} \\ R_2 &= 100\text{k}\Omega \\ c_2 &= 100\text{pF} \end{aligned} \tag{5.3}$$

This gives a gain of 10 in the passband which maps the input range of 0-5V to the amplifier's range of 0-50V, a low corner frequency of 16Hz and a high corner frequency of 16kHz. Driving such a large capacitative load has the potential to cause instability in the amplifier, a risk which is mitigated by the relatively high gain used and the presence of the feedback capacitor c_2. To limit damage to the amplifier and actuator in the event of instability the built-in current limiting capability of the OPA541 can be engaged.

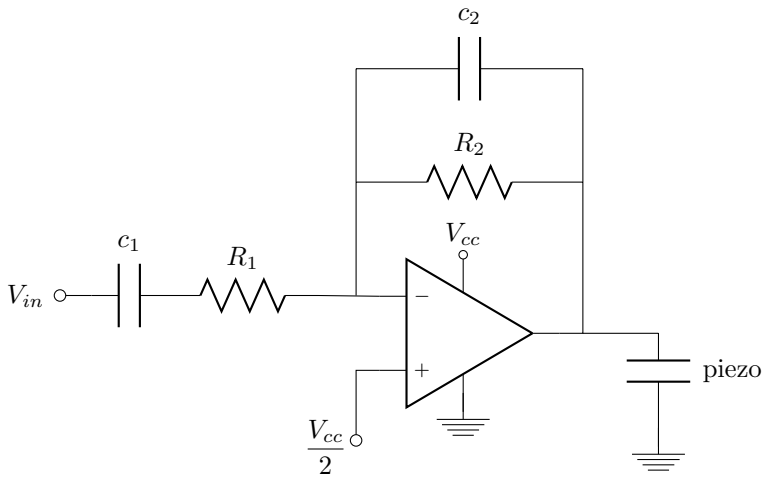

Figure 5.8: Schematic diagram of the amplifier circuit used to drive the piezo-stack actuator.

5.5 Summary

In this chapter we discussed the advantages of termination-based actuation over actuating a point along the continuous portion of the string for travelling wave control. Actuating the termination only creates a single travelling wave which simplifies analysis of the control system, and it allows the use of a mechanically-coupled piezo stack actuator with high linearity, bandwidth and stiffness compared to electromagnetic actuators. For these reasons we decided to actuate the termination point of the string with a piezo stack actuator, and developed the necessary amplifier circuitry to do so.

Because the maximum displacement of piezo stack actuators is significantly smaller than the typical amplitude of waves travelling on a string, we reviewed the effect of limited actuator amplitude on the ability of the system to damp the string, and examined two techniques to maximise it.

We showed that driving the actuator with high gains but clipping the output produces faster damping times than driving the actuator at the maximum possible linear gain without clipping, but comes at the cost of inducing harmonic distortion into the string's motion and affecting its timbre.

We also introduced an adaptive algorithm which dynamically scales the system's gain to maximise the amplitude of the actuator but keep it within its linear region throughout the damping process. We showed that this algorithm can damp the string more quickly than

the linear system without inducing significant harmonic distortion in the string's motion, though not as quickly as clipping the output.

We therefore conclude that if the goal of the control action is to damp the string as quickly as possible the best strategy is to drive the actuator with high gains and clip the output. If minimising the amount of harmonic distortion induced in the string is important however, as it is when attempting to control the timbre of the string, the adaptive gain algorithm can damp the string more quickly than linear control without significantly modifying the timbre.

Chapter 6

Experimental Results

In this chapter the theory discussed in the previous chapters is applied to build a travelling wave control system which is capable of damping the vibrations of a musical string. We describe the experimental setup we used and analyse the linearity of our custom sensors and the performance of the travelling wave decomposition algorithm. We investigate the sensitivity of the control system to a number of key parameters and demonstrate that the structural nonlinearity in the system is low.

We conclude by analysing the effect of deliberately adding nonlinearity into the system on the evolution of the modal amplitudes of the string.

6.1 Experimental Setup

A schematic overview of the system is shown in Figure 6.1, and photographs of the setup can be found in Appendix C. The string used in the experiment is a plain steel electric guitar string of gauge 0.017in manufactured by Ernie Ball, 50cm in length and tuned to 220Hz. The string is terminated at both ends over identical piezo stack actuators, though only the actuator at $x = 0$ is used to create an active termination, while the actuator at $x = L$ is held rigid. The actuators are mounted on a simple softwood baseboard, dimensions approximately 70cm x 20cm x 2.54cm.

The specific piezo stack actuator used is the AE0505D16F from Thorlabs. It has a rated maximum displacement of 11.6µm at 100V and a rated bandwidth of 69kHz. It was being driven with a maximum voltage of 50V, producing a maximum displacement amplitude of 2.9µm.

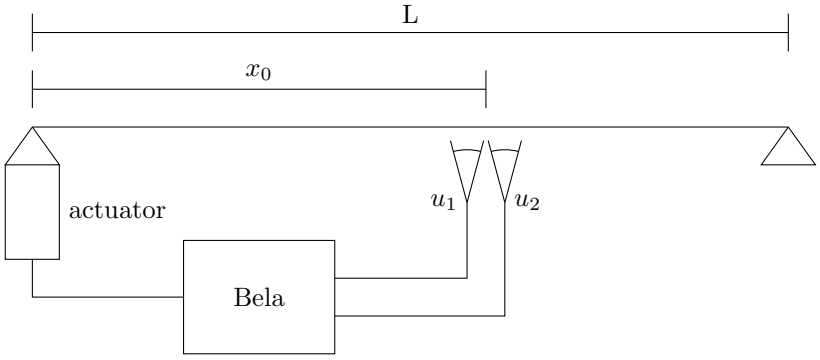

Figure 6.1: Schematic of the system.

A pair of custom sensors, u_1 and u_2, are located at x_0, 60% of the length or 30cm along the string from the left-hand termination at $x = 0$. A schematic cross-section of the sensor design is shown in Figure 6.2. It features a spherical N-BK7 plano-convex lens with an infra-red coating, a diameter of 25.4mm and a focal length of 56.7mm to collimate the light coming from an infra-red LED with a half-angle $\theta_{\frac{1}{2}} = 67.5°$ located at the focal point of the lens. This arrangement is designed to minimise nonlinearities arising from out-of-plane motion of the string and uneven distribution of light on the surface of the photodiode. The photodiode used is a square planar photodiode 10mm by 10mm in size, masked with a 3D-printed bracket to present a triangular sensitive surface. The sensors are centred around the point of the string 30cm from the termination at $x = 0$ and are separated by a distance of 3cm.

The output of the sensors is processed by the circuit described in Section 5.4 and is then connected to Bela, an embedded computer designed for ultra-low latency digital signal processing [71]. I was heavily involved in the development of Bela while writing this thesis [26], and a number of its features were directly inspired by the requirements of the experiment presented in this chapter. Bela samples the signals at 88.2kHz using a block size of 8 samples and uses the analog inputs and outputs rather than the sigma-delta audio converters for extremely low latency, performing the estimation of the wave $\overleftarrow{u}$ travelling to the left in the direction of the actuated termination at $x = 0$. The filtering described in Section 6.3 is performed digitally, and the output signal is delayed by Bela before being sent to the piezo stack actuator.

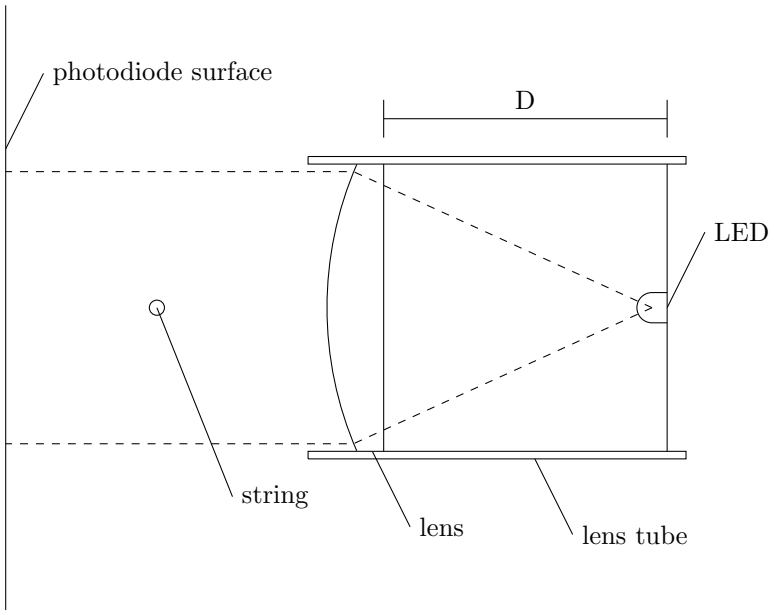

Figure 6.2: Schematic cross-section of the sensor design.

6.1.1 Stimuli

During the experiments the string is induced into vibration with two different methods. To simulate a realistic stimulation in a musical context the string is first plucked by hand using a small flexible piece of metal at a location 40% of the length of the string or 20cm from the active termination at $x = 0$. A reasonable attempt to maintain the same plucking amplitude and force for each measurement was made, however there was inevitably significant variation in both the amplitude and the spectral content of the resulting motion of the string. While it is useful to use the results of the plucked motion to demonstrate that the control system is robust to variations of this form as it would need to be in a musical context, the lack of precision makes direct comparison between individual plucks difficult.

To counter this the string was also induced into vibrating with a standing wave of increasing amplitude by displacing the actuator with a simple sinusoid at the fundamental frequency of the string. When the amplitude of the string reached a threshold of 0.8mm, corresponding to the travelling waves having amplitude of 0.4mm, the stimulation was removed and the travelling wave control system was switched on to begin the damping action. This produced a vibration with a much more repeatable and controlled set of initial conditions.

The mean of ten measurements of the total harmonic distortion present in the string during the first period of vibration without the control active was found to be -17.4dB with a pluck and -24.6dB with a standing wave. For plots of the evolution of the modal amplitudes of the string during uncontrolled decay in response to both stimuli, see Figure 6.9.

6.1.2 Quantifying the Results

The performance of the system is judged on two criteria: firstly the half-life of the energy of the vibrating string, defined as the time taken for the total energy in the string to fall by half and representing the ability of the control system to remove energy from the string; and secondly the harmonic energy, defined as the peak energy present in modal frequencies other than the fundamental, representing the harmonic distortion caused by nonlinearities present in the system.

To measure these two quantities, the displacement of the string during the controlled damping (taken as the mean of the two sensor readings) is split into individual periods of vibration using a robust zero-crossing detection algorithm. The algorithm exploits the fact that the period of the vibration is known to be 220Hz, searching 400 ± 25 samples (corresponding to one period) ahead of the previous zero-crossing and taking the mean of the zero crossings in that range to be the boundary of the period.

A digital Fourier transform (DFT) is then taken of each period of vibration. The first bin of the DFT's output representing the DC amplitude is discarded, and the remaining bins are taken to represent the amplitudes of the modal frequencies, or the coefficients C_n of the complex Fourier series of the string's motion:

$$u(x_0, t) = \sum_{n=1}^{N} C_n e^{jn\omega_0 t} \tag{6.1}$$

In this way the evolution of the string's modal frequencies can be measured over time. A measure proportional to the total energy of the string E is equal to the sum of the squares of the modal amplitudes:

$$E = \sum_{n=1}^{N} C_n^2 \tag{6.2}$$

The half-life of the vibration $t_{\frac{1}{2}}$ is defined as the number of periods taken for the energy to fall to half of its original value. Because the energy does not always decay in a perfectly logarithmic way, sometimes decaying at a slightly different rate toward the end of the

vibration compared to at the beginning, a number of different measurements of the half-life are taken during the controlled damping and the mean of these is presented as the half-life.

The harmonic energy E_h is defined as the energy in modes other than the fundamental:

$$E_h = \sum_{n=2}^{N} C_n^2 \tag{6.3}$$

It was found to be a more robust measurement in an experimental setting than the total harmonic distortion which is sensitive to variations in the amplitude of the fundamental mode. The value presented in the following results is the peak value of E_h over the course of the damped vibration which was found to be sensitive to variations in the initial conditions when the string was plucked due to the unpredictable amount of energy this stimulus induced in the higher modes. As such the quantity is only presented when the string is stimulated with a standing wave, which results in more controllable and repeatable initial conditions.

6.2 Sensor Nonlinearity

To estimate the nonlinearity of the sensors the string is induced into a standing-wave vibration as described in Section 6.1.1 and the total harmonic distortion of the sensor output is recorded. There are a number of sources of nonlinearity which contribute to the distortion in the sensor output, including the actuator driving the string and nonlinear vibration of the string itself. With no clear way of separating these sources or ensuring that the string is vibrating in a perfectly sinusoidal manner, these measurements can only serve as an upper bound to the sensor nonlinearity.

The string was induced into a steady-state vibration at four different amplitudes before measuring the THD, which is plotted in Figure 6.3. The minimum THD measured was -23.1dB at an amplitude of 1.3mm. The distortion increases significantly as the amplitude increases which is expected as the nonlinearity originating from both the string and the sensor is likely to increase with amplitude.

While the THD measured is relatively high, there are signs that a significant proportion of it originates from nonlinear vibration of the string. Figure 6.4 shows how the total harmonic distortion evolves during the decay of the string in response to a standing wave stimulus but without any control action applied. The sharp increase in distortion from the initial value of -24.6dB to -16.3dB is indicative of energy being transferred into the higher modes of the

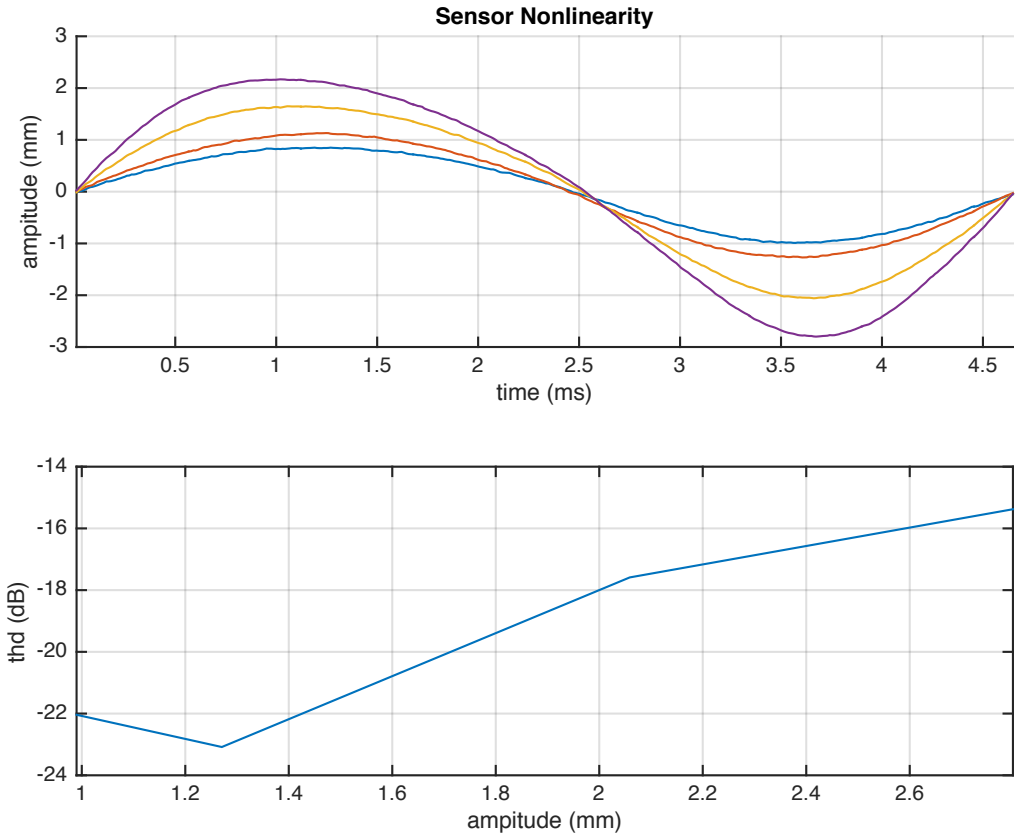

Figure 6.3: Top: A single period of vibration captured by the sensors during constant standing-wave vibration of the string at different amplitudes. Bottom: The total harmonic distortion of the four vibration periods plotted against the amplitude.

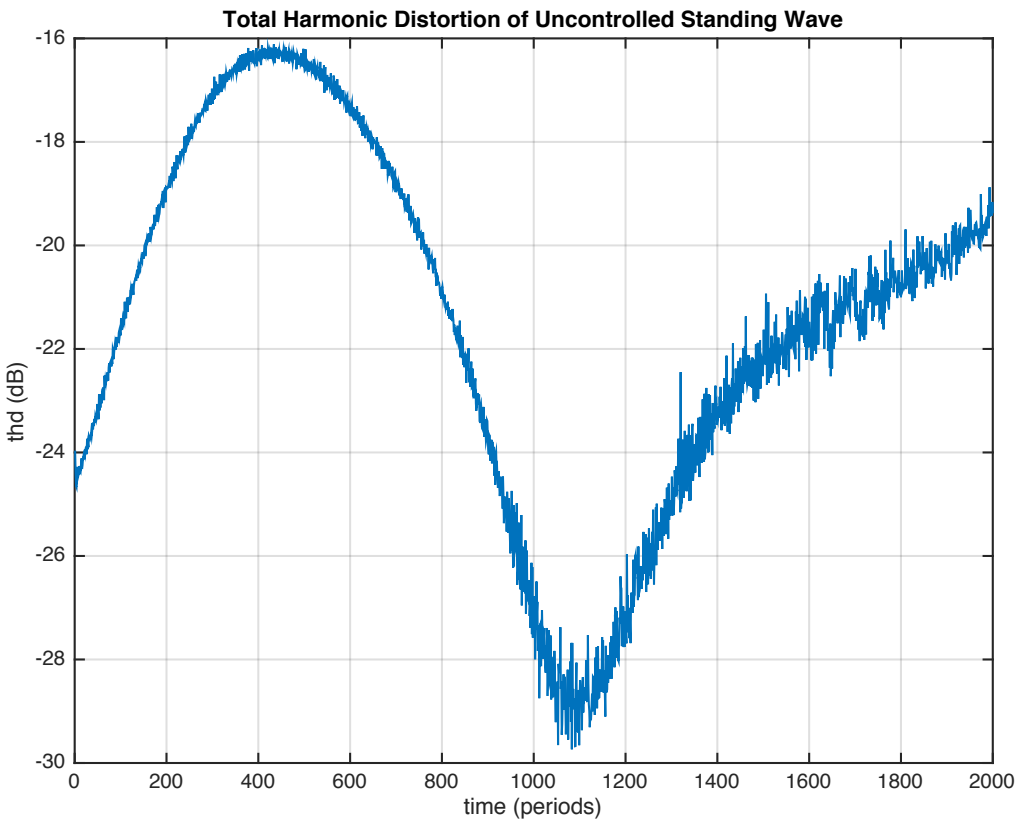

Figure 6.4: The variation in total harmonic distortion during the natural decay of the string without control in response to a standing wave stimulus.

string without any influence from the control system and is therefore likely to be a result of nonlinear string vibration.

6.3 Travelling Wave Estimator

As seen in Section 4.1 the purpose of the estimator is to decompose the two sensor readings u_1 and u_2 into estimates of the travelling waves, $\overleftarrow{\hat{u}}$ and $\overrightarrow{\hat{u}}$, using the following formulae:

$$\begin{aligned} \overleftarrow{\hat{u}} &= \frac{u_1 z^{-\tau} - u_2 z^{-3\tau}}{1 - \theta z^{-4\tau}} \\ \overrightarrow{\hat{u}} &= \frac{u_2 z^{-\tau} - u_1 z^{-3\tau}}{1 - \theta z^{-4\tau}} \end{aligned} \tag{6.4}$$

The key to achieving good performance from the estimator is to tune the parameter θ to minimise the estimator error ϵ which is defined as the difference between the mean value of the two sensors and the sum of the estimated travelling waves:

$$\epsilon = \frac{u_1 + u_2}{2} - \left(\overleftarrow{\hat{u}} + \overrightarrow{\hat{u}}\right) \tag{6.5}$$

The time domain response of the estimator and its error is shown for two periods of the string's motion during a pluck in Figure 6.5 for three different values of θ. The frequency spectrum of the error ϵ over the course of an entire pluck is shown in Figure 6.6 for the same values of θ. When θ is small the error is large and is dominated by the modal frequencies of the string, signifying that the estimates are badly misrepresenting the shape of the travelling waves in the key frequency range of interest. As θ is increased the amplitude of the error at the modal frequencies reduces but high-frequency noise is introduced by sharp peaks which appear in the upper range of the error spectrum. As θ approaches 1 the error at the modal frequencies is reduced significantly demonstrating that the shape of the estimated travelling waves is close to reality, however the error and the estimates themselves are dominated by high-frequency noise.

Integrating the estimator error spectrum over the frequency range in which the modal frequencies are dominant gives 0.022 when $\theta = 0.5$ and 0.0033 when $\theta = 0.99$, demonstrating that the error is higher in this range for lower values of θ. Integrating over higher frequencies in which noise is dominant gives 0.061 for $\theta = 0.5$ and 0.102 for $\theta = 0.99$, demonstrating that the error is higher in this range for higher values of θ.

With such a large portion of the noise present in the estimator error lying in a frequency range which is above the range in which the string's dominant modal frequencies lie, applying a low-pass filter to the estimates can significantly attenuate much of the noise without adversely affecting the important frequency ranges of the signals. For this application we chose a fourth-order butterworth filter with a cutoff frequency of 7.4kHz.

The lowest-frequency spike in the estimator error spectrum lies at 3.7kHz which presents a problem as it is too close to the modal frequency range to be attenuated sufficiently by the low-pass filter. A notch filter $N(s)$ was therefore applied to directly target the peak, with transfer function:

$$N(s) = \frac{s^2 + 2s\frac{\omega_0}{Q} + \omega_0^2}{s^2 + 2s\omega_0 + \omega_0^2} \tag{6.6}$$

The centre frequency was chosen to be precisely 3.7kHz and the quality factor Q was chosen to be 100 to attenuate the peak. In Figure 6.7 the error spectrum is plotted before and after

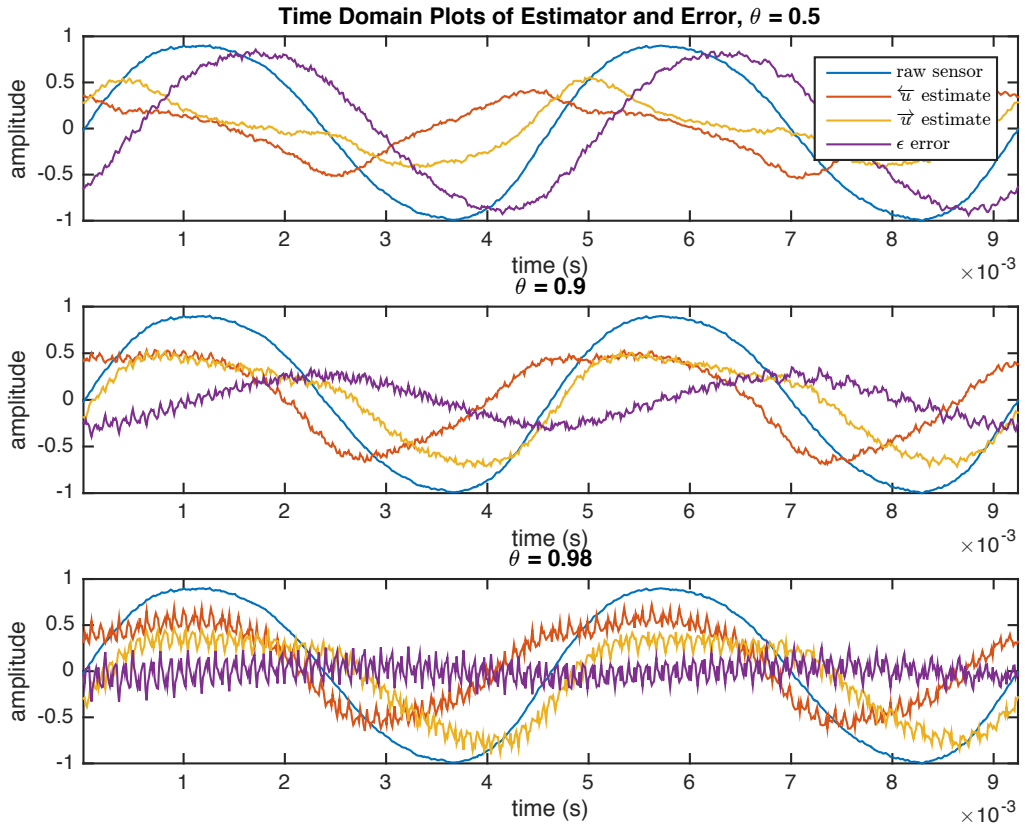

Figure 6.5: Time domain plots of the estimated travelling waves and the corresponding error for different values of θ during two periods of a pluck. The trace labelled 'raw sensor' is the mean of the two sensor readings.

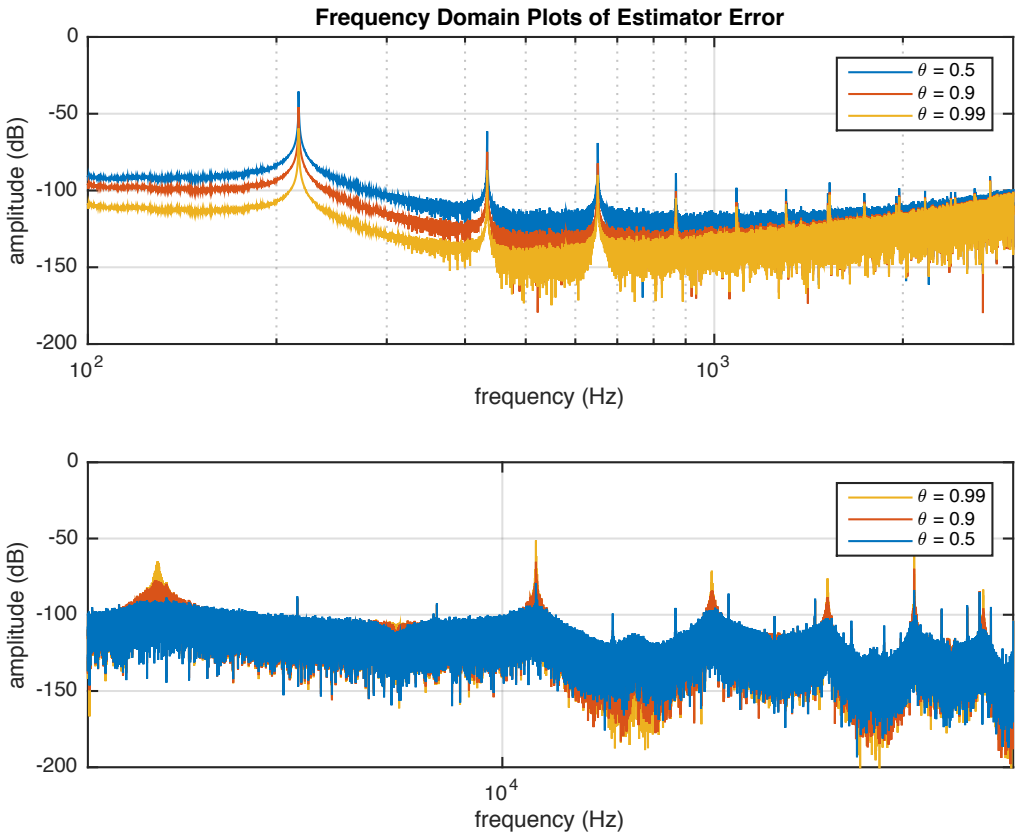

Figure 6.6: Frequency domain plots of the estimator error for different values of θ over the course of an entire pluck. The top plot shows frequencies between 100Hz and 3kHz, i.e the range in which the modal frequencies lie, while the bottom plot shows frequencies between 3kHz and 44.1kHz which is predominantly noise.

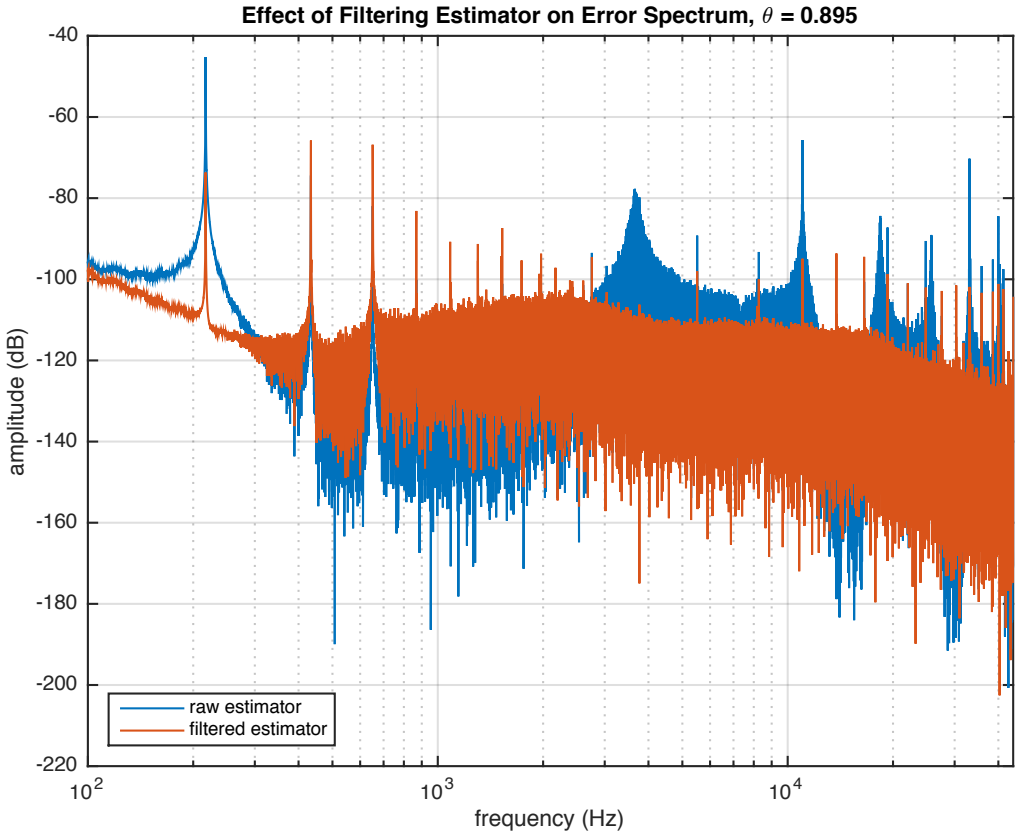

Figure 6.7: Frequency domain plots of the estimator error over the course of an entire pluck when using a raw estimator and when filtering the estimators with a notch filter at 3.7kHz with $Q = 100$, and with a fourth-order butterworth low-pass filter at 7.4kHz.

applying both filters to both estimates with $\theta = 0.895$. The filtering attenuates the noise peak at 3.7kHz by 31dB, and the next noise peak at 11kHz by 45dB. The filtering reduces the integral of the spectrum over the modal frequency range from 0.0084 with the raw estimator to 0.0072 when filtered. Over the higher frequency range the integral is reduced from 0.0776 to 0.0201.

The energy of the estimator error over a certain time period is defined as the integral over that period of the error squared:

$$E = \int_{t_1}^{t_2} \epsilon(t)^2 dt \tag{6.7}$$

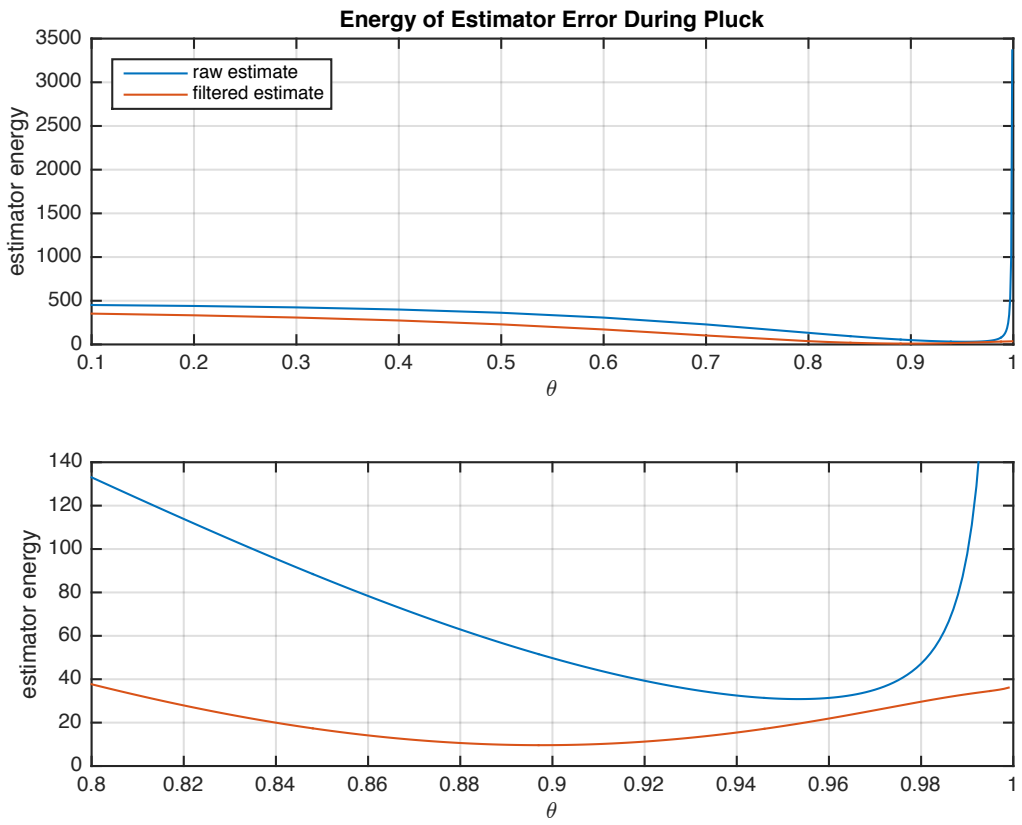

Figure 6.8: The energy of the estimator error ϵ over the course of a single pluck plotted against the parameter θ in the case of raw and filtered estimators. This graph is extrapolated from a single data point.

In Figure 6.8 a single pluck of the string with the control system inactive is decomposed into travelling waves using a range of different values of θ, and the energy of the error is plotted against θ for both the raw and filtered estimate. The error energy of the raw estimator is at a minimum at $\theta \approx 0.95$ and increases drastically as θ approaches 1. The optimal value of θ for the filtered estimator is lower, at approximately 0.89, and the error energy at the minimum is lower than it is for the raw estimator.

The effect of the parameter θ on the behaviour of the travelling wave control system is examined in Section 6.4.4.

6.4 Damping Vibrations

In this section we examine the effect of linear travelling wave control on the half-life and harmonic energy of the string's motion. We also examine the effect of changing three key parameters of the travelling wave control system, specifically the delay and gain applied to the travelling wave estimate before it is sent to the actuator and the estimator parameter θ, on the ability of the system to damp the vibration of the string.

6.4.1 Uncontrolled Decay

As a point of reference the response of the string to both a pluck and a standing wave stimulus without the control system engaged is presented first.

A comparison of the evolution of the modal amplitudes in response to a pluck and a standing wave is plotted in Figure 6.9, while a comparison of the harmonic energy E_h in both cases is plotted in Figure 6.10. The pluck clearly begins with more harmonic distortion having significant energy in all of the modes up to the sixth, while the standing wave only has significant energy in the second mode. Both stimulus methods see a modest increase in the relative energy between the second and fundamental mode near the beginning of the time period which is indicative of energy being injected into the second mode by nonlinear processes. There is also noticeable fluctuation of energy present in the higher modes during the pluck, which may be an indication of out-of-plane motion of the string caused by the action of the pluck not being perfectly aligned in the vertical plane.

The mean half-life of ten uncontrolled plucks was 224 periods, while that of standing waves was 231 periods. This decay with the control system not active is due to the string naturally losing energy to the environment. Hypothetically, if the string were ideal and the only source of energy loss was a linear travelling wave control system with termination displacement function

$$f(\overleftarrow{u}) = K\overleftarrow{u} \tag{6.8}$$

then the value of the gain K required to replicate the natural energy loss, calculated from Figure 5.2, would be approximately 0.0015.

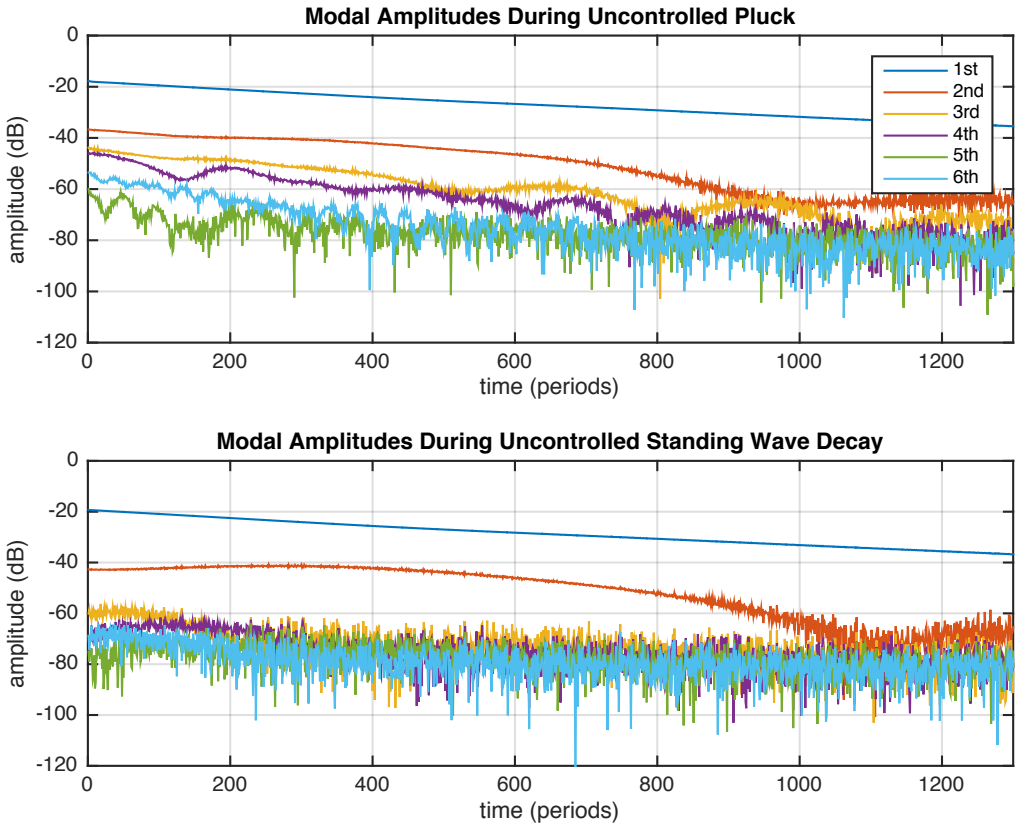

Figure 6.9: Comparison of the evolution of the modal amplitudes in response to an uncontrolled pluck and standing wave stimulus

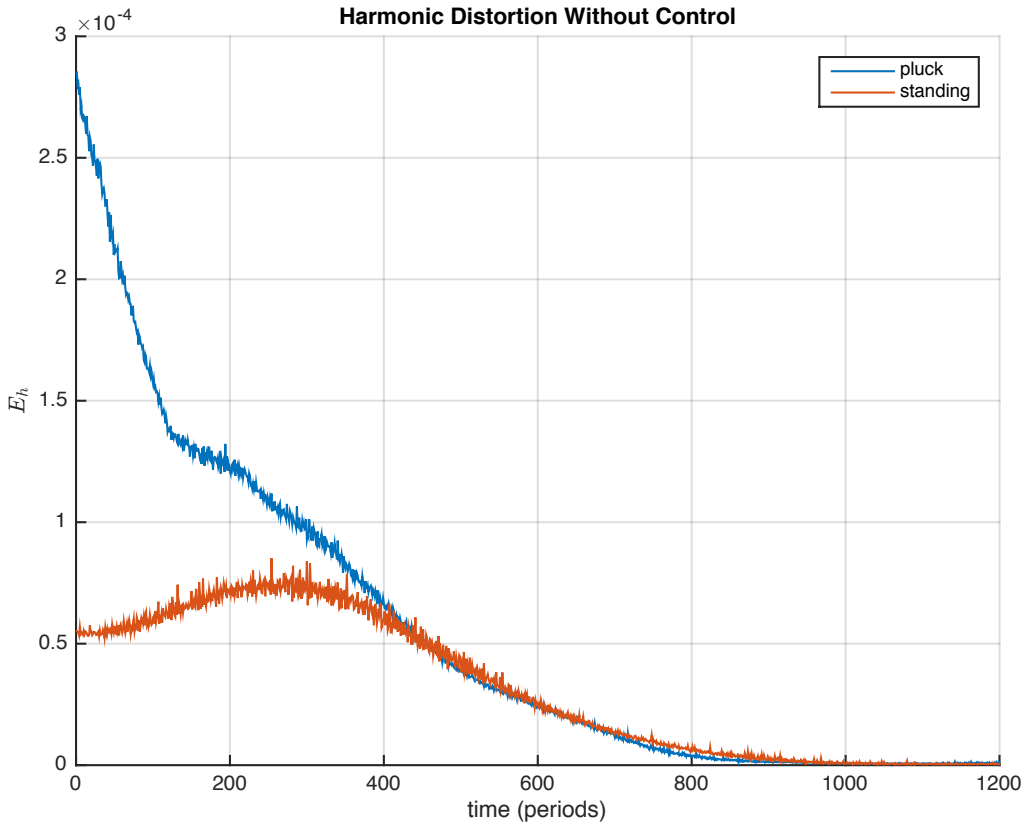

Figure 6.10: Comparison of the evolution of the harmonic energy of the string E_h in response to an uncontrolled pluck and standing wave stimulus

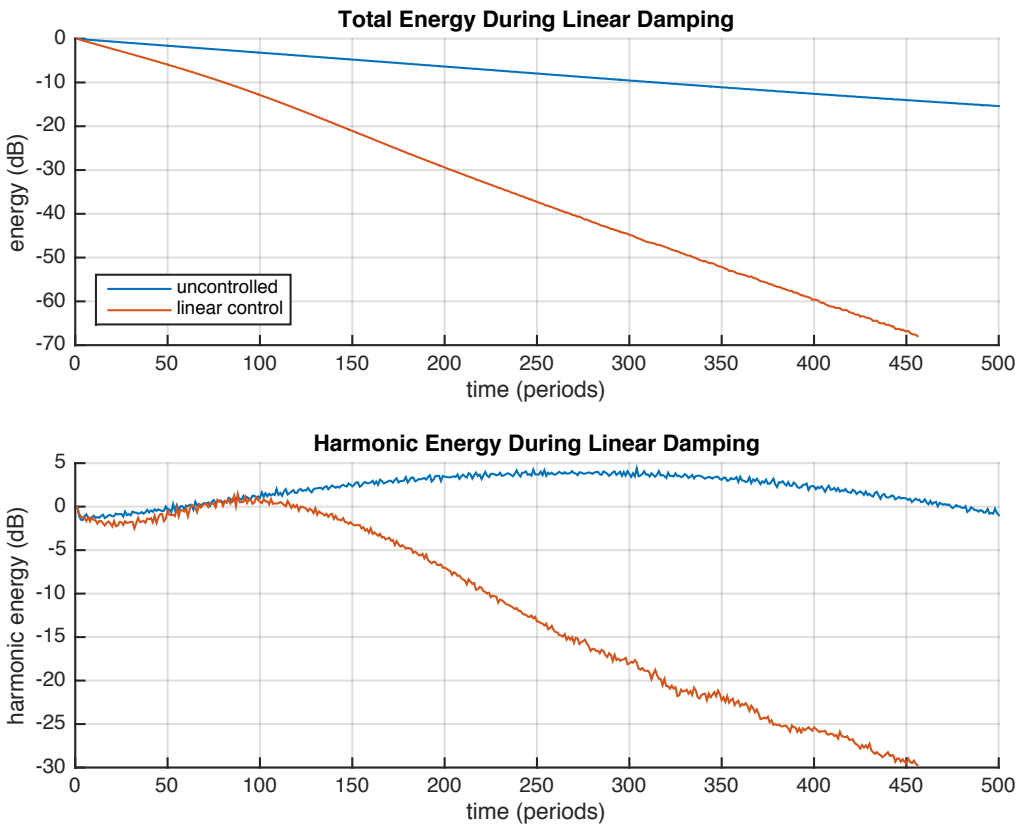

Figure 6.11: The total and harmonic energy in the string in the case of no control compared to linear travelling wave control with $K \approx 0.00725$ in response to a standing wave stimulus.

6.4.2 Linear Control

To achieve linear control the estimate of the travelling wave is multiplied by the largest value K which produces no clipping in the actuator. The initial amplitude of the travelling wave when using a standing wave stimulus is 0.4mm while the maximum displacement of the piezo is approximately 2.9µm, meaning that the maximum achievable gain is in theory approximately 0.00725.

In Figure 6.11 the total energy in the string during damping is plotted both with and without the maximum possible linear travelling wave control active. With the control active the half-life of vibration is 38.6 periods, six times smaller than the uncontrolled half-life of 231. In theory, the gain K required to achieve this half-life is 0.0089 (calculated from Figure 5.2) which is very close to the expected gain of 0.00725 summed with the equivalent gain of the

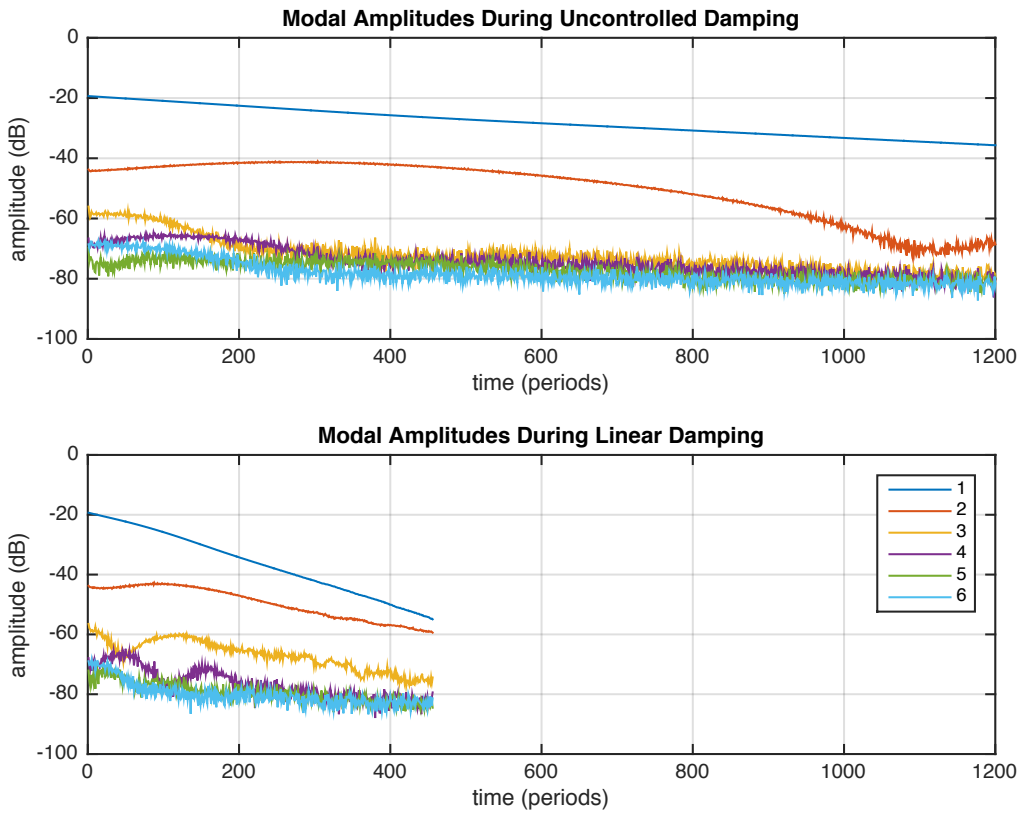

Figure 6.12: The evolution in the modal amplitudes in the case of no control compared to linear travelling wave control with $K \approx 0.00725$ in response to a standing wave stimulus.

uncontrolled system 0.0015.

Figure 6.11 also shows that the harmonic energy in the string during linear damping is at all times less than or equal to that of the uncontrolled case. This strongly suggests than the nonlinearity in the control system is low, both in absolute terms and when compared to the natural nonlinearity of the string's vibration.

Figure 6.12 compares the evolution of the modal amplitudes with and without linear damping. The control action damps both the first and second modes much more quickly than in the uncontrolled case, however the third mode is damped less quickly, remaining above the noise floor for longer when control is applied. This would imply that a small amount of nonlinearity in the control system is transferring energy into the third mode of the string, though the effect is minimal and its amplitude remains at least 20dB below that of the second mode throughout the damping period.

6.4.3 Delay

Before sending the estimated travelling wave to the actuator it must be delayed in software by the amount of time it takes for the wave to travel along the string from the sensor to the actuator, less the delay added by the latency of the digital system and the group delay of the various filters involved.

With the fundamental frequency of the string tuned to 220Hz and the length of the string fixed at 50cm the speed at which waves travel along the string is $220ms^{-1}$. With the travelling wave sensor located 30cm from the actuated termination the time taken for the wave to travel between them is approximately 1.36ms or 120 samples at a sample rate of 88.2kHz. The delay added by the digital system and filter group delay was measured to be 300µs or approximately 27 samples, so the expected optimal number of samples of delay which need to be added in software is approximately 93, or 1.05ms.

The effect of varying the delay on the half-life of a pluck under linear travelling wave control is plotted in Figure 6.13, and the effect on the half-life and harmonic energy of a standing wave is plotted in Figure 6.14. In both cases the gain was set to 0.00725 which is the highest possible linear gain which avoids clipping, and θ was set to 0.98.

The optimal delay in the case of a pluck was found to be 80 samples while for a standing wave it was 90. The reason for the discrepancy between the optimal delay for pluck and standing wave is not clear. When applying a shorter delay than the optimal 80 or 90 samples the system is surprisingly forgiving, with a delay of 30 samples less than optimal only increasing the half-life by approximately ten periods and creating no significant harmonic distortion.

When applying a longer delay than optimal there is a sharper uptick in half-life and harmonic distortion, and when applying a delay longer than approximately 120 samples the system is no longer able to damp the string, instead allowing it to settle into a non-zero steady-state vibration. For an example of this, see Figure 6.15 which plots the evolution of the string's modes in response to a standing wave with an applied delay of 150 samples. Although the fundamental mode is damped fairly rapidly, significant energy is injected into the third and fourth modes which remain active indefinitely, until the control action is removed. The reason this happens with a longer delay but not with a shorter one is not clear, but it is clear that a longer delay can result in a failure of the control system, reinforcing the need to use a low-latency digital processor to perform the travelling wave estimate.

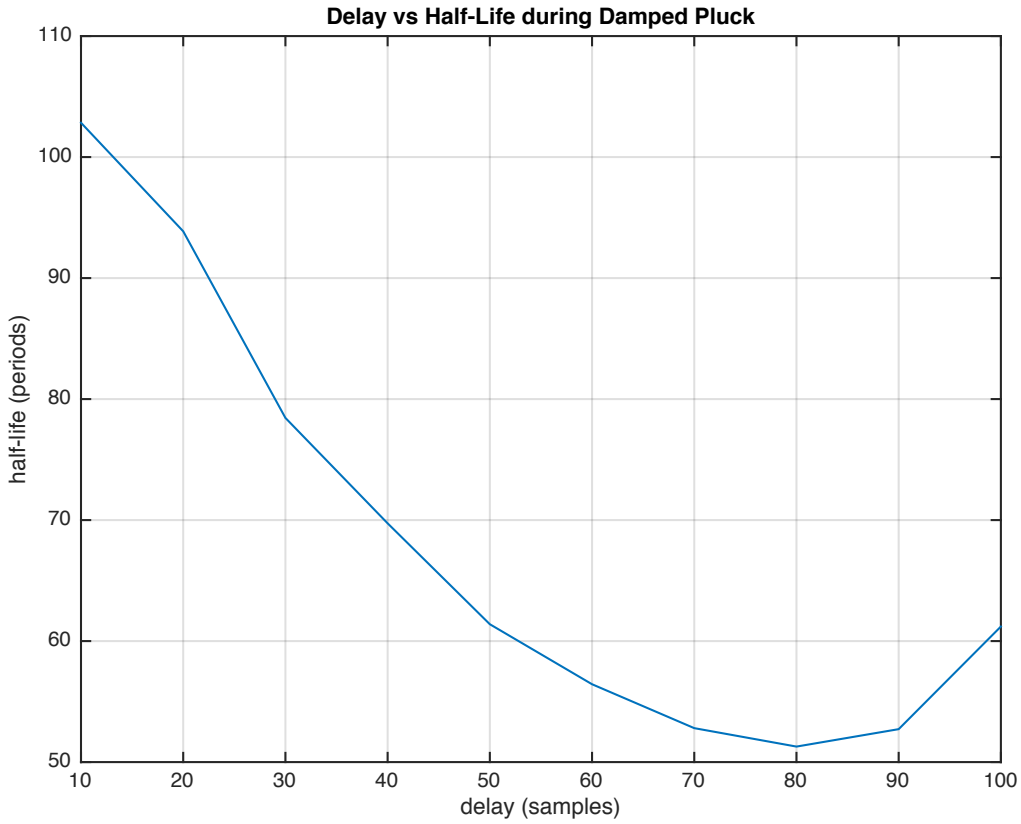

Figure 6.13: The half-life of vibration during a damped pluck plotted against the delay imposed on the travelling wave estimate. The damping is performed by linear travelling wave control with a gain of $K = 0.00725$. An uncontrolled pluck has a half-life of 224 periods.

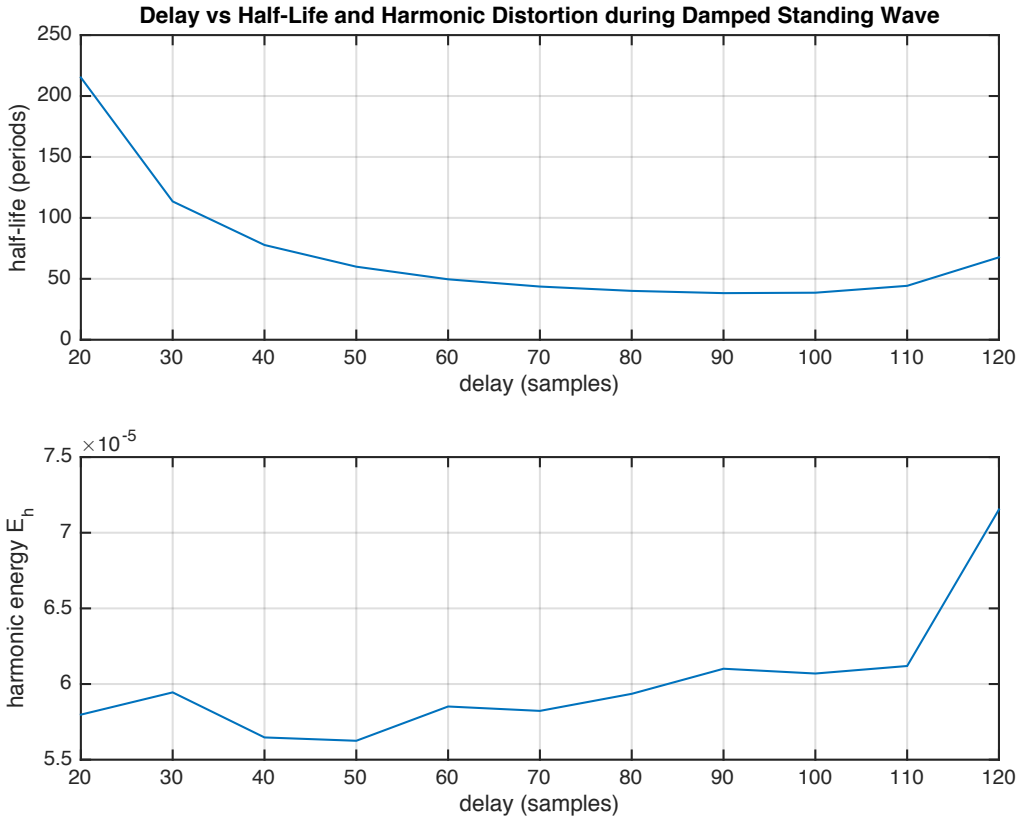

Figure 6.14: The half-life and peak harmonic energy of vibration during a damped standing wave plotted against the delay imposed on the travelling wave estimate. The damping is performed by linear travelling wave control with a gain of $K = 0.00725$. Without control the half-life is 231 periods and the peak harmonic energy is 8.02x10^{-5}

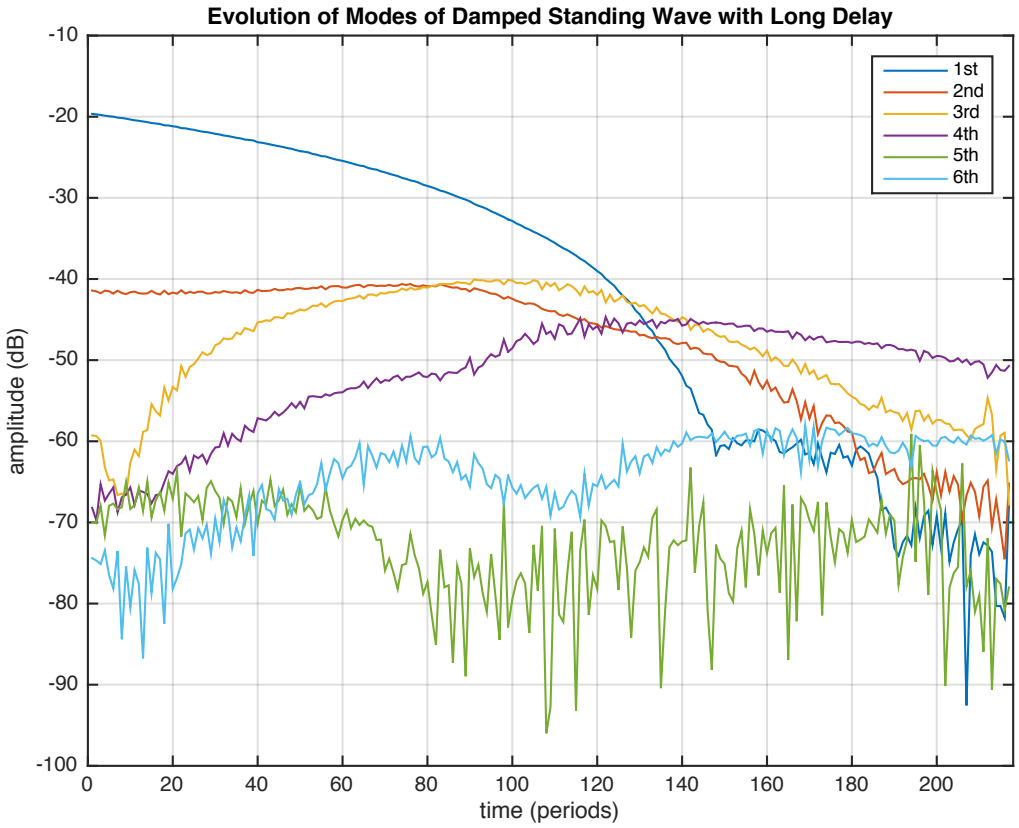

Figure 6.15: The evolution of the modal amplitudes after a standing wave stimulus with a long applied delay of 150 samples

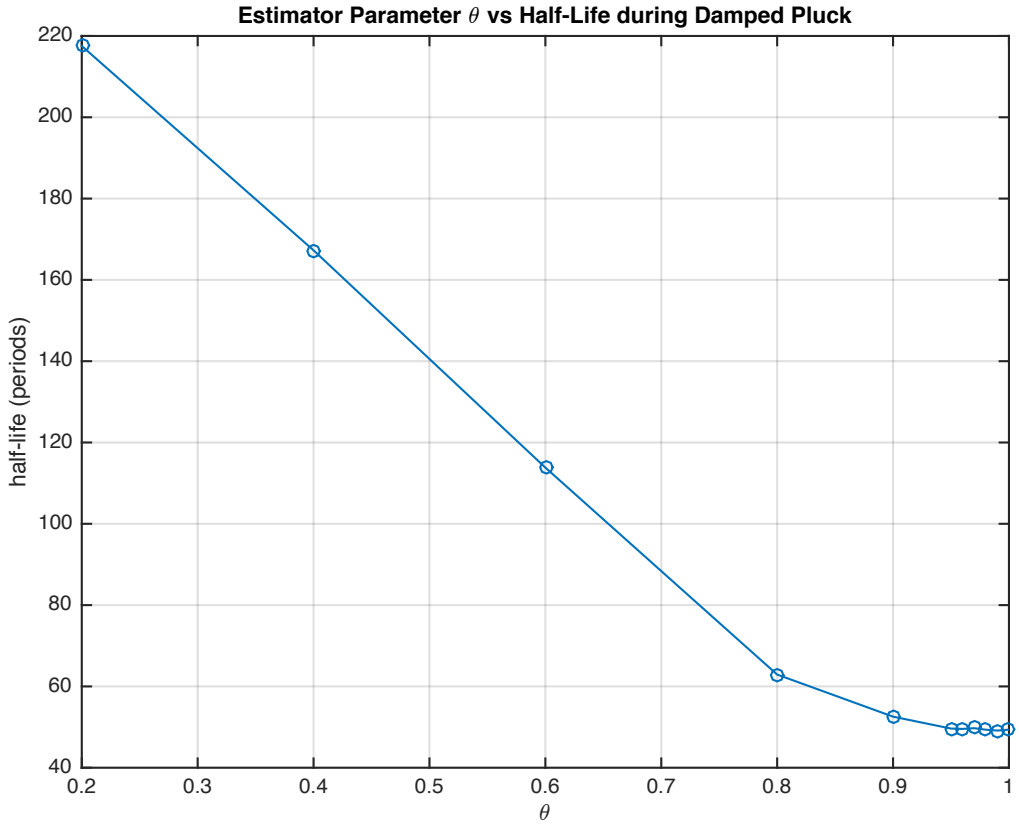

Figure 6.16: The half-life of vibration during a damped pluck plotted against the estimator parameter θ.

6.4.4 Estimator Parameter Theta

The variation in half-life and harmonic distortion for both stimuli in response to modifying the travelling wave estimator parameter θ is plotted in Figure 6.16 and Figure 6.17. In both cases the linear travelling wave control gain K is set to 0.00725 and the applied delay is 80 samples.

Despite the results in Figure 6.8 which showed that the minimum error energy of the estimator occurs when $\theta \approx 0.89$, the travelling wave control system performs best when θ is as close to 1 as possible.

Varying θ between 0.8 and 0.99 causes negligible changes in the harmonic distortion. It is important that θ is kept below 1 however, as when it is equal to 1 it is unstable as predicted by theory.

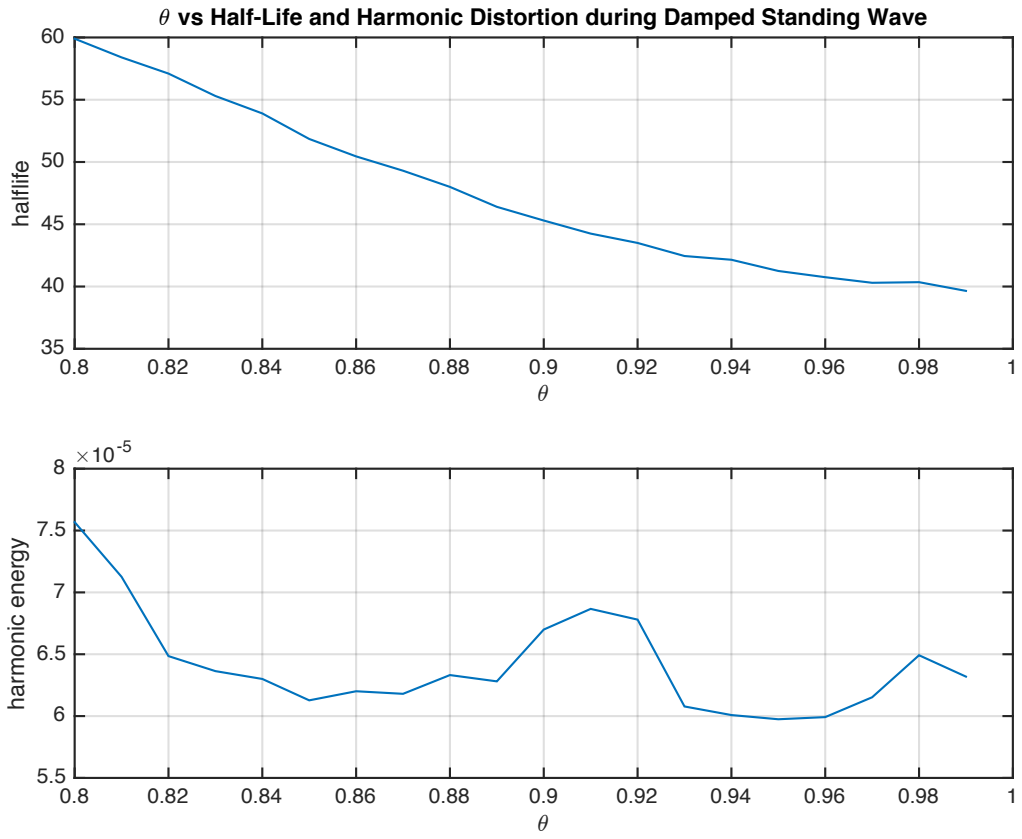

Figure 6.17: The half-life and peak harmonic energy of vibration during a damped standing wave plotted against the estimator parameter θ.

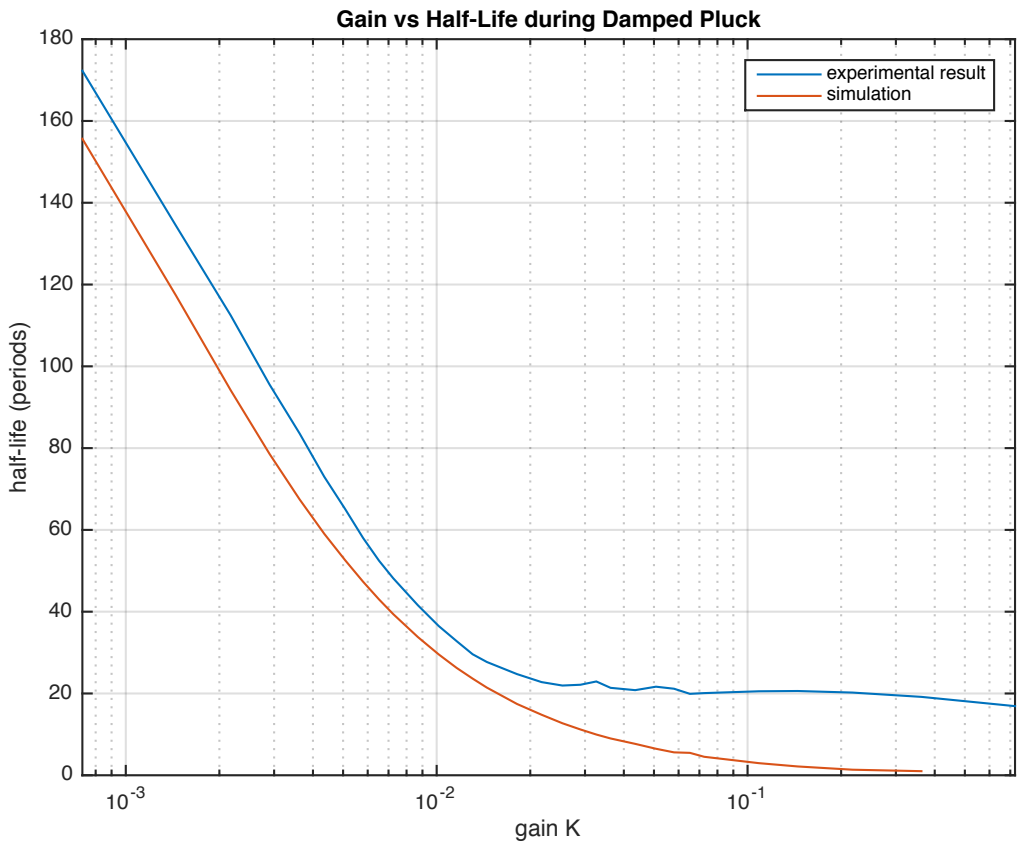

Figure 6.18: The half-life of vibration during a damped pluck plotted against the gain K of the linear travelling wave control system, for both simulated and experimental results. In the simulated case 0.0015 is added to the gain to account for natural energy loss.

6.4.5 Gain

Having found the optimal values for delay and θ we now investigate the effect of modifying the gain on the half-life and harmonic energy, which is plotted in Figure 6.18 and Figure 6.19.

The plots compare the experimentally recorded half-lives with the same simulation used to generate Figure 5.2, but with 0.0015 added to the gain in order to simulate the natural energy lost during uncontrolled decay of the string. The behaviour can be clearly divided into two regions with the boundary at the maximum linear gain of 0.00725. Below this threshold there is no clipping of the output so the control system is as close to linear as possible, and the relationship between the half-life and the gain is very similar to the simulation, particularly in response to a standing wave. The extra time taken for the pluck to decay is

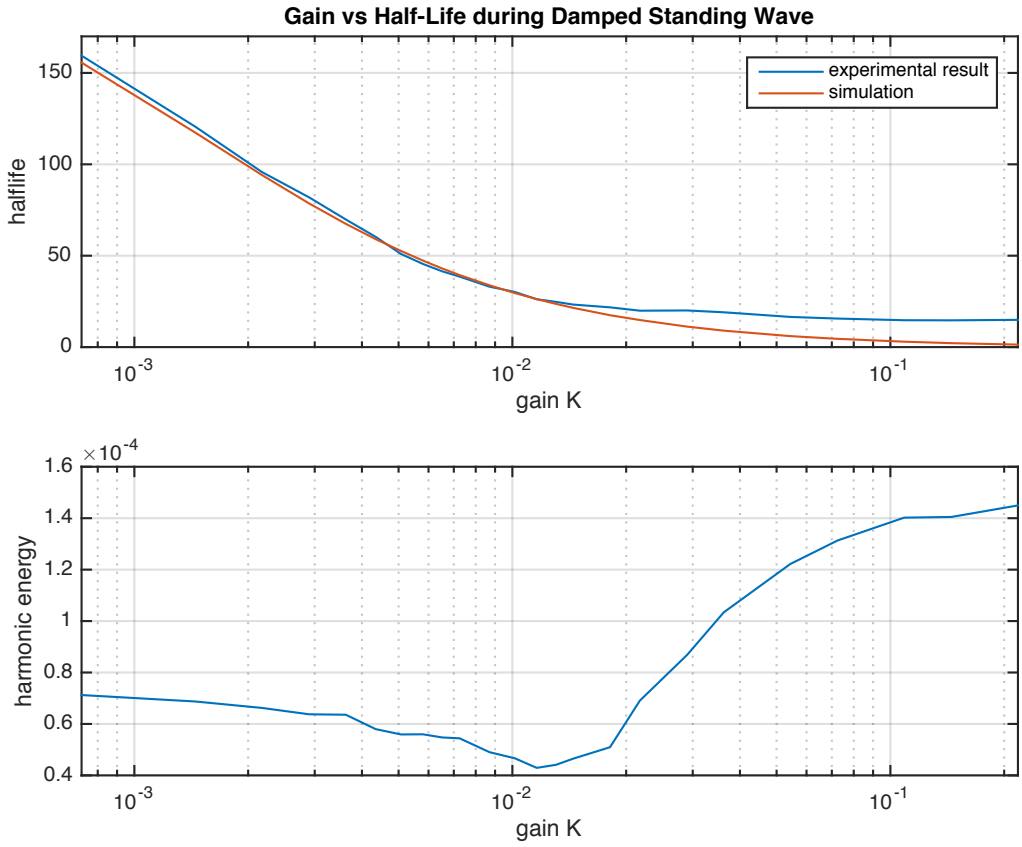

Figure 6.19: The half-life and peak harmonic energy of vibration during a damped standing wave plotted against the gain K of the linear travelling wave control system, for both simulated and experimental results. In the simulated case 0.0015 is added to the gain to account for natural energy loss.

likely to be because of the extra energy transferred into the string by that stimulus method, and by out-of-plane motion of the string.

At gains greater than 0.00725 clipping is introduced into the actuator's output, and the behaviour changes. Between gains of 0.00725 and 0.012 the half-life continues to decrease (though at an increasingly lower rate) and the harmonic energy remains lower than during uncontrolled vibration, which suggests that small amounts of clipping do not have a seriously negative effect on the control system. As the gain and the amount of clipping increases however, the half-life stops decreasing and reaches a floor of approximately 20 periods, while the harmonic energy climbs rapidly as the nonlinearity from the clipping introduces energy into the higher modes of the string. The experimental results diverge from the simulation in this region as the clipping is not simulated.

The evolution of the modal amplitudes during a damped standing wave are plotted in Figure 6.20 for the case of a linear gain of 0.00725 with no clipping and for the case of a gain of 0.145 with harsh clipping. In the former case only a little more energy is introduced into the higher modes when compared with the uncontrolled case plotted in Figure 6.9 and modes above the second contribute little to the response of the string. In the latter case however, while the fundamental mode is damped rapidly, a significant amount of energy is introduced into the third, fourth and fifth modes with the third mode becoming dominant towards the end of the damping period.

6.4.6 Adaptive Gain Results

The adaptive gain algorithm described in Section 5.3.2 dynamically matches the amplitude of the output to the full-scale range of the actuator in an attempt to achieve damping times comparable to the harshly clipped output seen above without the harmonic distortion induced by the saturating nonlinearity.

Plots of the total energy in the string during the damping period for both stimuli are shown in Figure 6.21 for the case of uncontrolled damping, linear damping (with a gain of 0.00725), harshly clipped damping (with a gain of 0.145) and the adaptive gain. For both stimuli the energy decays much more rapidly in the linear case compared to the uncontrolled case, and the fastest damping is achieved with harsh clipping. For the harshly clipped standing wave it is possible to see the transition or corner where the amplitude of the standing wave becomes low enough that clipping is no longer occurring, and the damping becomes linear and faster.

In response to a standing wave the adaptive gain damps the string more quickly than the linear case but not as quickly as the clipped case, which is as predicted in theory. The energy

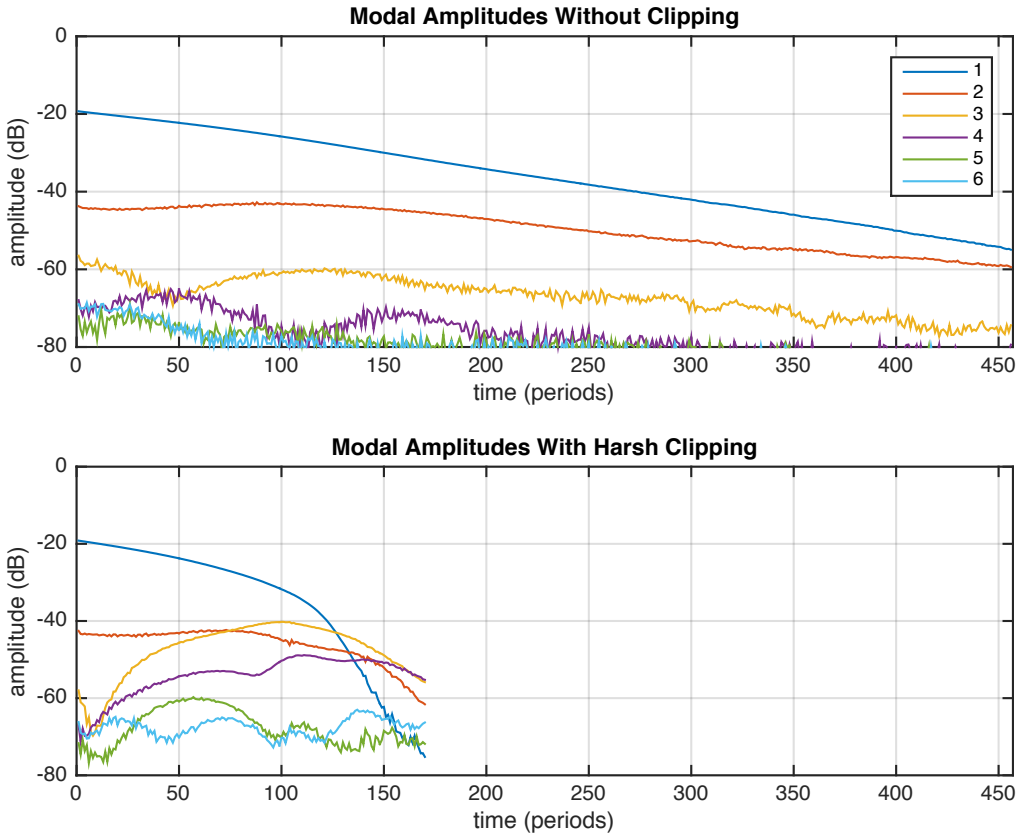

Figure 6.20: Comparison of the evolution of the modal amplitudes during damping of a standing wave with a linear gain of 0.00725 resulting in no clipping (top) and a gain of 0.145 resulting in harsh clipping (bottom).

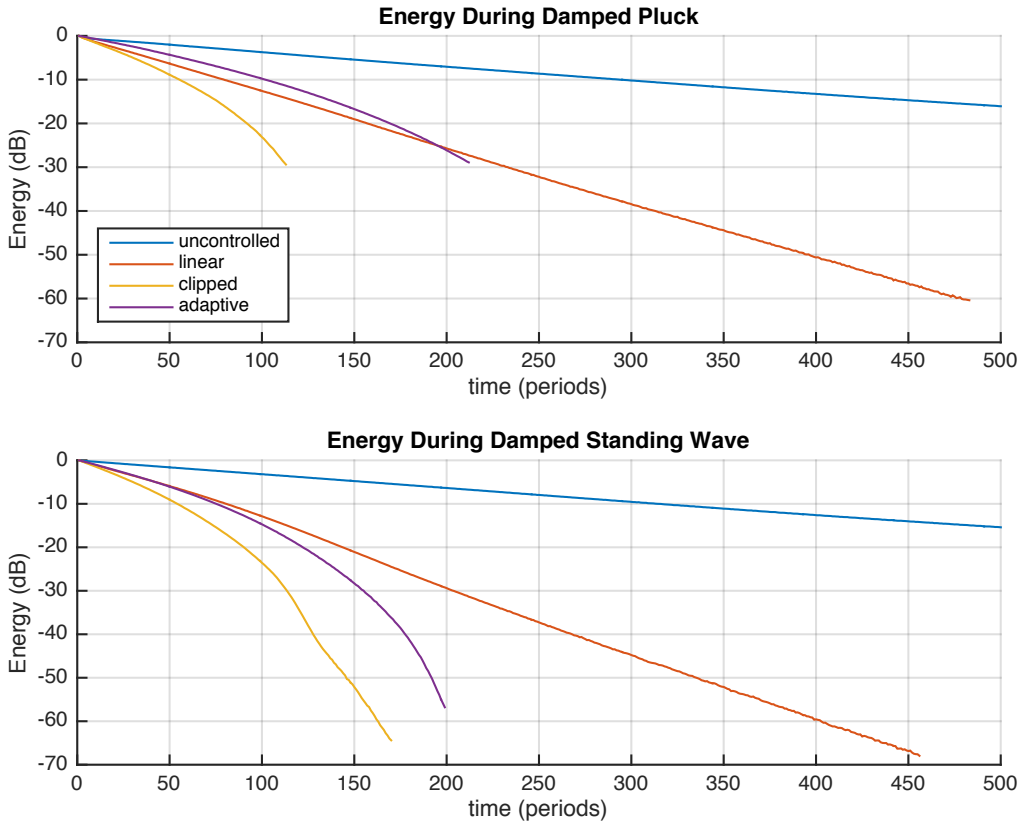

Figure 6.21: The total energy in the string during damping for the uncontrolled case (with the control system inactive), the linear case (with an applied gain of 0.00725), the clipped case (with an applied gain of 0.145), and the adaptive case which implements the adaptive gain algorithm.

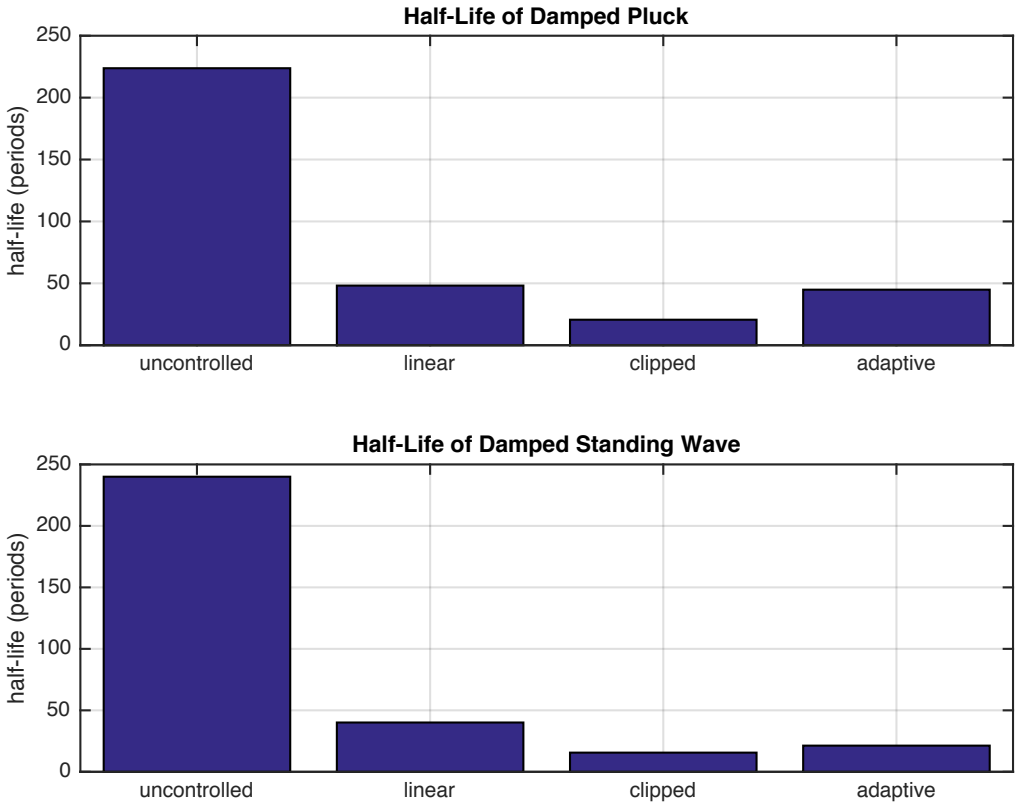

Figure 6.22: The half-life of vibration during damping for the uncontrolled case (with the control system inactive), the linear case (with an applied gain of 0.00725), the clipped case (with an applied gain of 0.145), and the adaptive case which implements the adaptive gain algorithm.

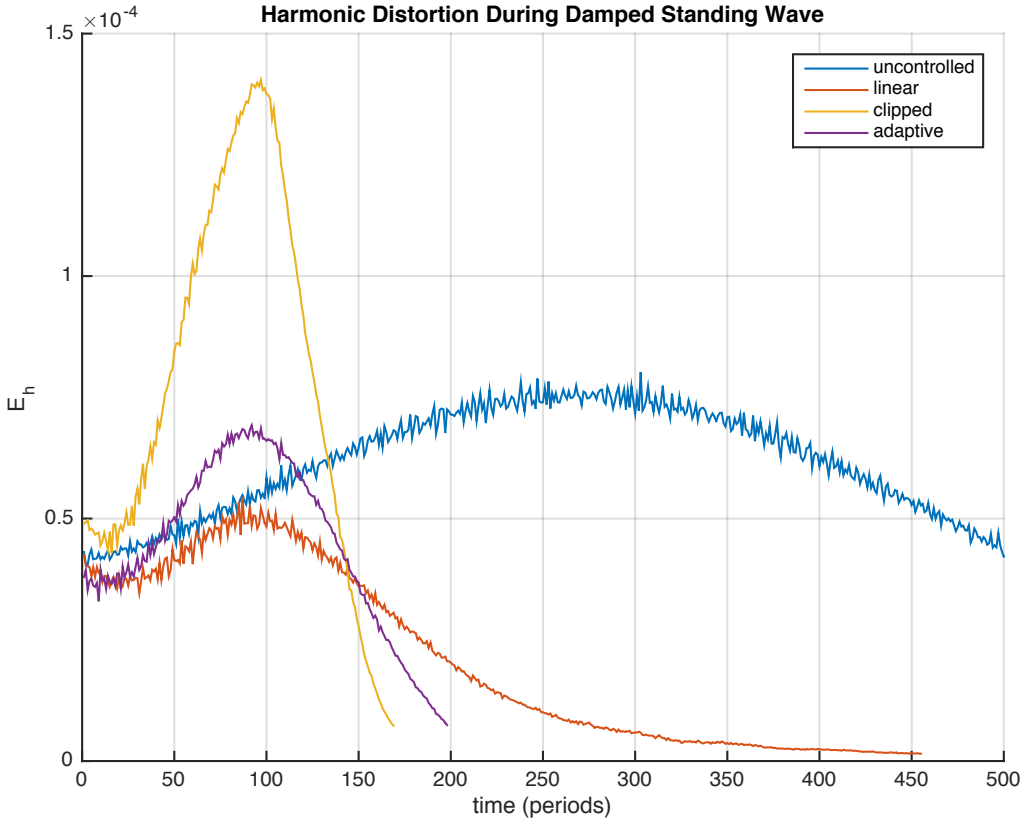

Figure 6.23: The harmonic distortion in the string's motion while damping a standing wave for the uncontrolled case (with the control system inactive), the linear case (with an applied gain of 0.00725), the clipped case (with an applied gain of 0.145), and the adaptive case which implements the adaptive gain algorithm.

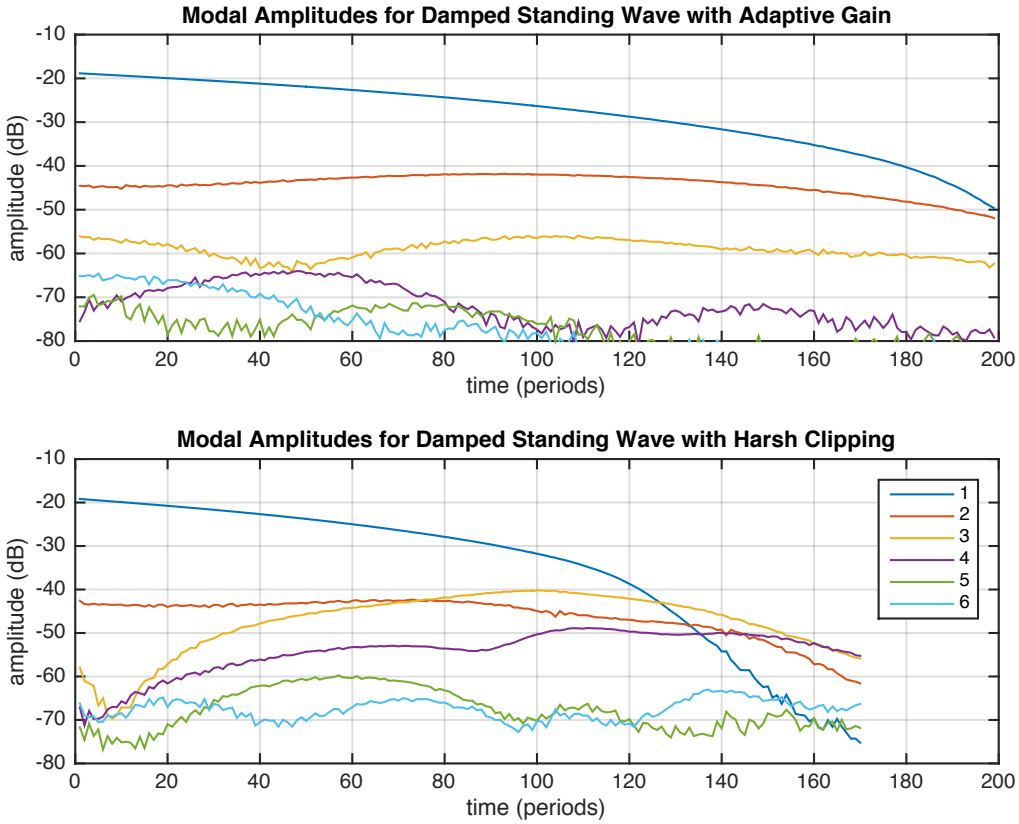

Figure 6.24: A comparison of the evolution of the modal amplitudes during damping of a standing wave with the adaptive gain algorithm and the case of harsh clipping with an applied gain of 0.145.

transferred into the higher modes is much less with the adaptive gain than with clipping as is shown in Figure 6.23, meaning that the adaptive gain does damp the string more quickly than the linear case without inducing as much harmonic distortion as when clipping the output. This is supported by Figure 6.24 which shows how the third and fourth modes in particular are strongly stimulated when clipping the output, whereas with the adaptive gain much less energy is introduced into them.

In response to a pluck the adaptive gain performs worse than the linear gain in terms of damping speed. This is unexpected and is contrary to what the theory predicts and the system shows in practice in response to a standing wave stimulus. A likely explanation is that the implementation of the adaptive gain algorithm is not sufficiently robust in this case to handle the additional harmonic distortion and out-of-plane motion induced in the string by a pluck.

6.5 Nonlinear Timbre

In this section we examine the effect of deliberately introducing nonlinearity into the travelling control system on the behaviour of the string. We do this by adding quadratic and cubic terms into the termination displacement function as described in Section 3.2.2, so it becomes:

$$f(\overleftarrow{u}) = K(\overleftarrow{u} + b\overleftarrow{u}^2 + c\overleftarrow{u}^3) \tag{6.9}$$

We set the gain K to 0.000725, i.e. one tenth of the maximum linear gain, in order to damp the string relatively slowly to allow the effect of the nonlinearity time to become apparent, and to leave some headroom in the actuator to allow large amounts of nonlinearity to be added without causing clipping. We then vary the coefficient b to add quadratic nonlinearity, and the coefficient c to add cubic nonlinearity. All experiments in this section use a standing wave stimulus to allow easier comparison.

6.5.1 Damping and Stability

The half-life of the vibration with purely quadratic nonlinearity (i.e. where $c = 0$ and b is varied) and purely cubic nonlinearity (where $b = 0$ and c is varied) is plotted in Figure 6.25.

In Section 3.3 we predicted from theory that the stability criterion for purely quadratic nonlinearity would be:

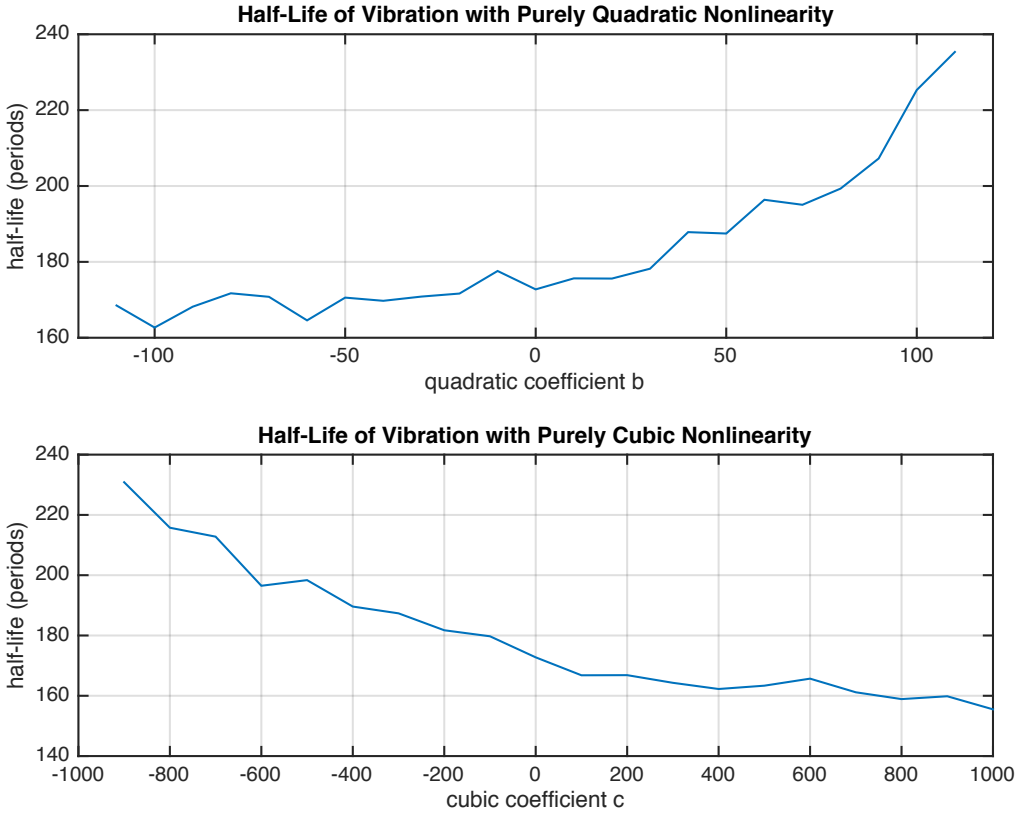

Figure 6.25: Vibration half-life with pure quadratic (top) and cubic (bottom) nonlinearity. The system is stable for all plotted values and unstable beyond the axes limits except for values of c greater than 1000.

$$-1 \leq b \leq 1 \tag{6.10}$$

In practice we found that stable values of b lie with the range:

$$-110 \leq b \leq 110 \tag{6.11}$$

Clearly there is a large discrepancy in the magnitude of the limits on b between theory and practice, and the experimental system is two orders of magnitude less sensitive to instability under quadratic nonlinearity than predicted. It is notable however that the predicted symmetry of the stability criterion, i.e. the fact that the sign of b is irrelevant and only its magnitude is important for determining the stability of the system, is correct. The predicted stability criterion for cubic nonlinearity was:

$$-1 \leq c \leq \frac{2}{K} - 1 \tag{6.12}$$

In practice we found that the boundary of stability for negative c was -900, almost three orders of magnitude greater than predicted. For positive c with $K = 0.000725$ the theory predicts that the limit of stability should be approximately 2760. We were unable to confirm this in practice, as for $c > 1000$ the response is dominated by clipping. It is notable again that while the experimental system is orders of magnitude less sensitive to instability than predicted, the qualitative predictions of the cubic stability criterion, i.e. that the boundary of stability for negative c is significantly smaller in magnitude than the boundary for positive c, is correct.

The theoretical stability criteria were derived using an idealised model of the string which did not take into account effects such as inharmonicity. All real strings are inharmonic to some extent due to their non-zero stiffness and coupling with the surrounding system, which means that the modal frequencies of the string do not occur at perfect integer multiples of the fundamental. The nonlinear control does generate energy at perfectly harmonic intervals however, and the mismatch between those frequencies and the modal frequencies of the real string could explain the large difference in the magnitude of the stability boundary between the simulated and measured responses of the string, and warrants further investigation.

We also made an implicit assumption that the bandwidth of the control system was unlimited, and that all of the string's modes could be activated without prejudice. In practice we are limiting the bandwidth of the control system by digitally filtering the travelling wave estimate (Section 6.3) and by applying filtering in the analog domain in the sensor circuitry

(Section 4.4) and the actuator circuitry (Section 5.4) to reduce the effects of noise. The bandwidth of a real, non-ideal string is also limited itself.

The mechanism by which nonlinearity causes instability involves energy being injected into the string's modes by the control system at a faster rate than it can be removed. The limited bandwidth of the real system causes energy in the higher modes to be attenuated more quickly than in an ideal system, which would have the effect of stabilising the system and may go some way towards explaining the discrepancy between the theoretical stability criteria and the behaviour of the real system.

We also predicted in theory that the damping time of the string would be independent of the sign of the quadratic coefficient b, while our experimental results in Figure 6.25 show that negative quadratic nonlinearity has little effect on the half-life while positive quadratic nonlinearity causes a significant increase in the half-life. For cubic nonlinearity we predicted that negative values of c would cause a significant increase in the damping time as the system approaches instability, while positive values of c would actually have the effect of decreasing the damping time. The results in Figure 6.25 agree with this prediction.

6.5.2 Harmonic Distortion

In contrast to previous sections of this chapter where we were investigating the negative effect of structural nonlinearities in the control system on its ability to damp the string, in this section we are investigating the positive effects of deliberately adding nonlinearity to the system on the timbre of the string. As such, instead of using the peak harmonic energy to judge the amount of harmonic distortion caused by nonlinearities in the system as before, here we will use the integral of the harmonic energy over the full period of damping. We suggest that this measure captures more accurately the magnitude of the audible effect of the nonlinearity on the sound produced by the string.

In Figure 6.26 the integrated harmonic energy of the string is plotted for stable values of pure quadratic nonlinearity, and for stable values of pure cubic nonlinearity for $c \leq 1000$. We find that negative cubic nonlinearity results in increasing amounts of audible harmonic distortion as the system approaches instability, whereas positive cubic nonlinearity has little effect on the harmonic distortion. Quadratic nonlinearity also produces significant amounts of audible harmonic distortion as the system approaches instability, and although the effect is nearly symmetrical as theory would predict, small amounts of positive quadratic nonlinearity where $b < 50$ have less of an effect than negative values.

Figure 6.27 plots the integrated harmonic energy over the $b-c$ plane. For negative c, missing

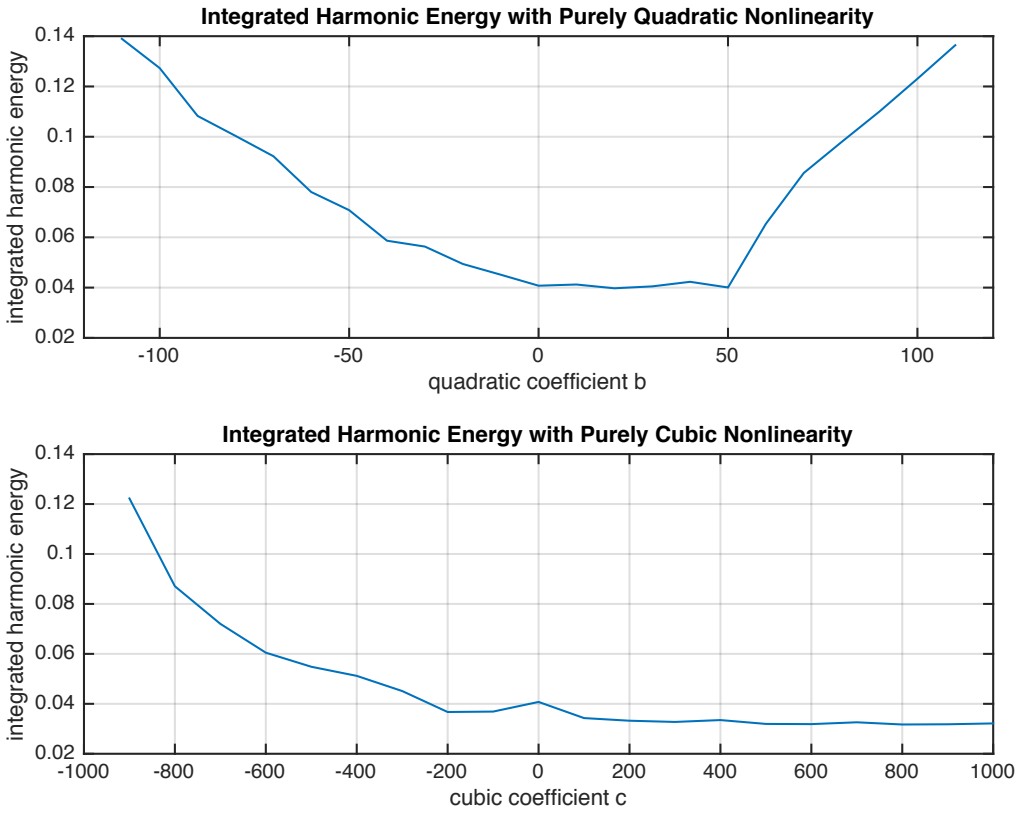

Figure 6.26: Integrated harmonic energy with pure quadratic (top) and cubic (bottom) nonlinearity

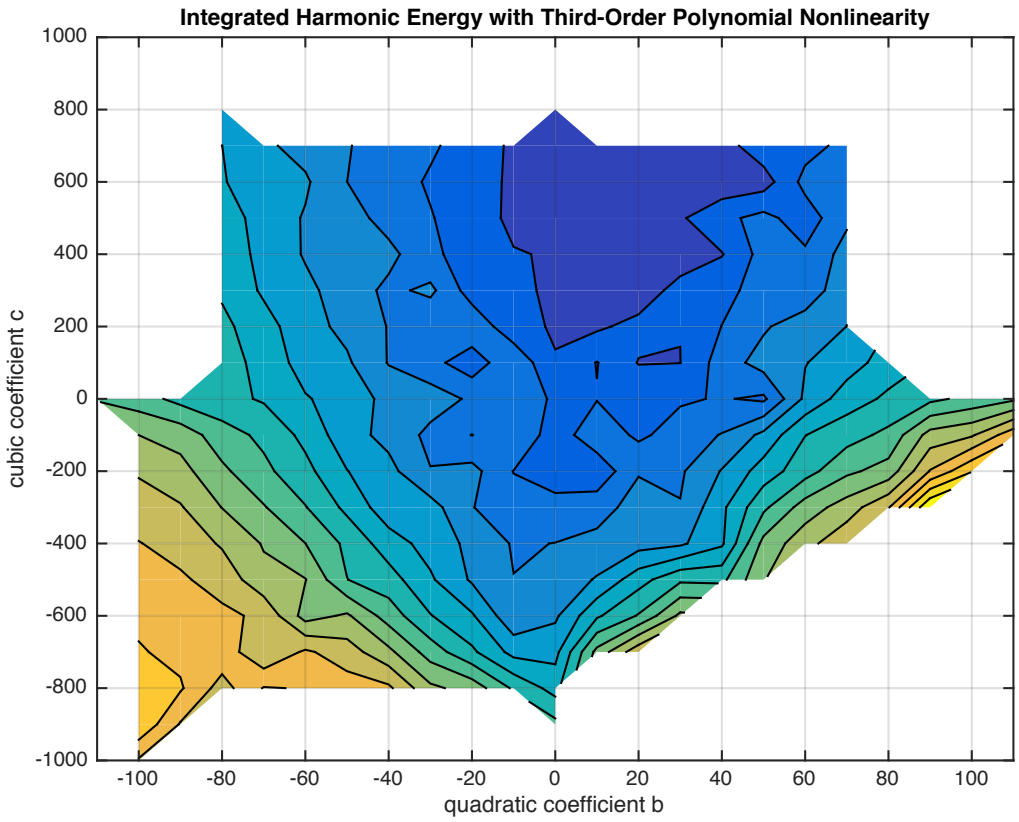

Figure 6.27: Integrated harmonic energy with third-order polynomial nonlinearity. Warmer colours correspond to higher values

data indicates the system is unstable with those values, while for positive c missing data indicates the response was dominated by clipping.

The plot shows that there is a stability boundary following an approximately straight line between the point at $b = 0$, $c = -800$ and the point at $b = 110$, $c = 0$. This is predicted by the theory in Section 3.3.1 and visible in Figure 3.3, adjusting for the different magnitudes of the coefficients. There is no corresponding stability boundary between the point at $b = 0$, $c = -800$ and the point at $b = -110$, $c = 0$, however. Instead, in this region the system remains stable and generates the largest amount of audible harmonic distortion over the whole plane. Though not identical, the plot in Figure 6.27 shows a definite similarity to the simulated total harmonic distortion plotted in Figure 3.9.

6.5.3 Modal Dominance

While the integrated harmonic energy presented above gives a useful insight into the magnitude of the audible harmonic distortion, it does not demonstrate the difference in the prominence of different modes during the vibration. To do that we define the *modal dominance* of the nth mode D_n to be the integral of the ratio between the amplitude of that mode c_n and the amplitude of the fundamental mode c_1 over the damping period:

$$D_n = \int \frac{c_n}{c_1} dt \tag{6.13}$$

The modal dominance of the second to the fifth modes under pure quadratic and pure cubic nonlinearity is plotted in Figure 6.28.

It shows that cubic nonlinearity (and particularly negative cubic nonlinearity) does not strongly emphasise the second mode in comparison to quadratic nonlinearity, which is predicted by theory (Section 3.4.3).

The dominance of the second mode over the b-c plane is plotted in Figure 6.29, and the dominance of the third mode is plotted in Figure 6.30. The plots show that different amounts and forms of nonlinearity affect which modes are most prominent during the decay of the string's vibration, and therefore demonstrate that nonlinearity can be used to affect the timbre of the string.

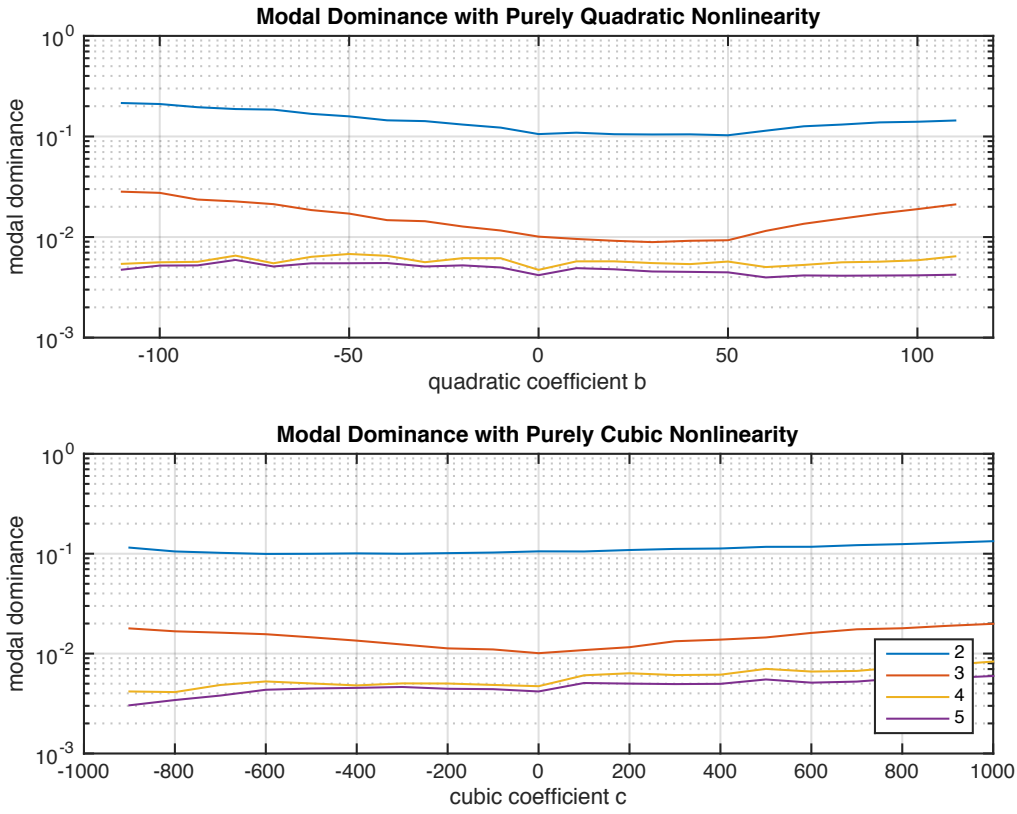

Figure 6.28: Modal Dominance with pure quadratic (top) and cubic (bottom) nonlinearity

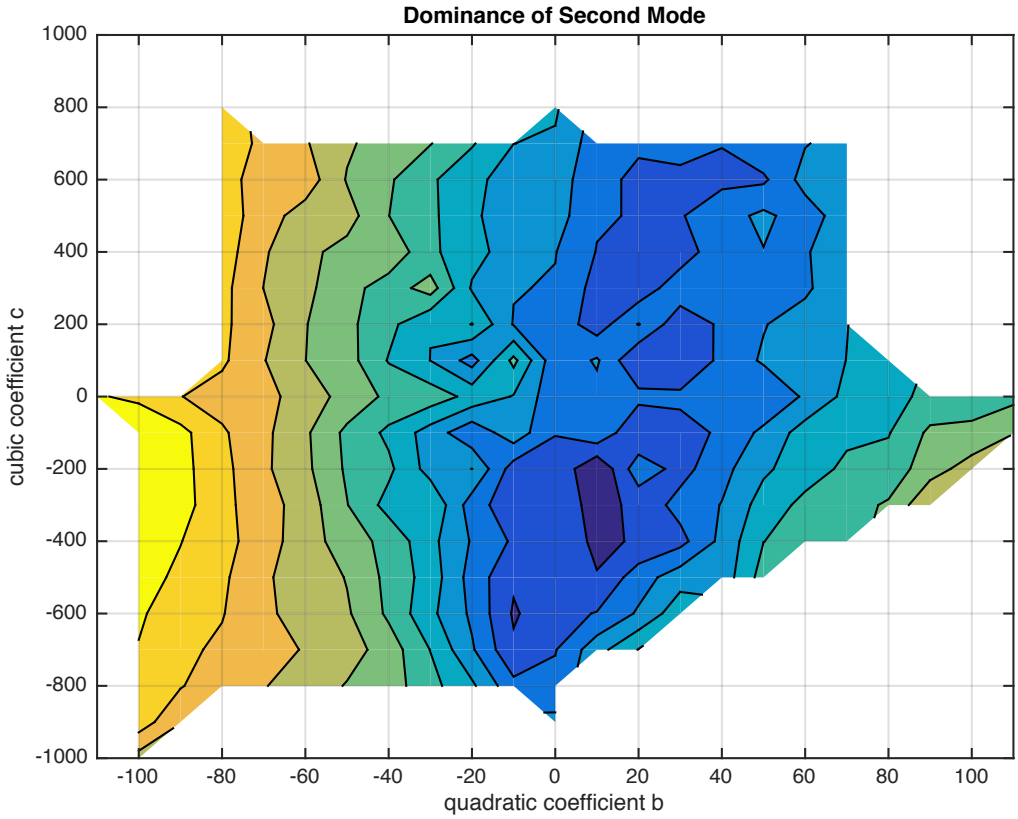

Figure 6.29: Dominance of second mode with third-order polynomial nonlinearity

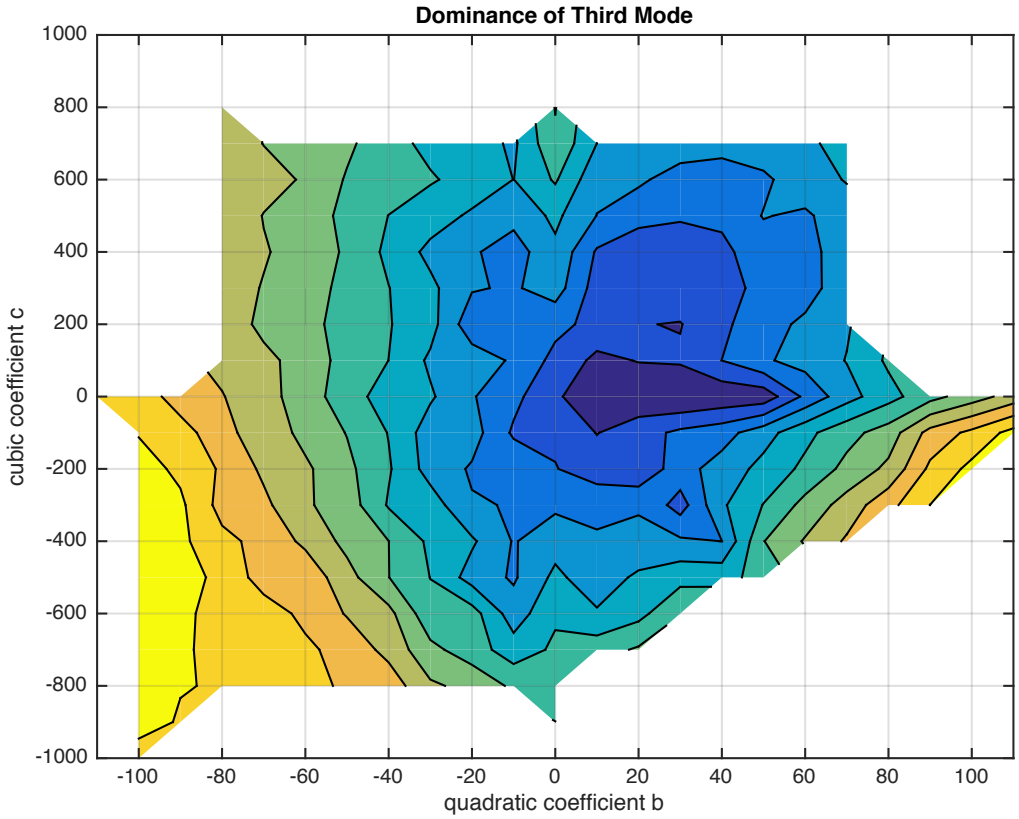

Figure 6.30: Dominance of third mode with third-order polynomial nonlinearity

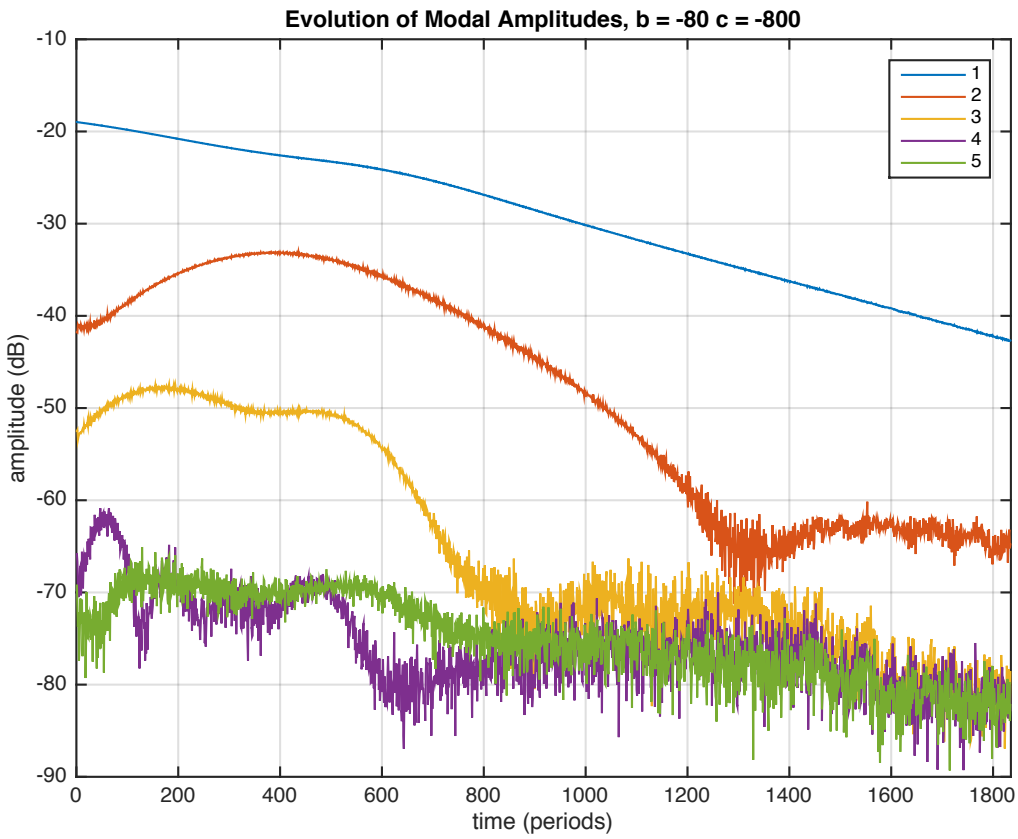

Figure 6.31: Evolution of modal amplitudes with $b = -80$, $c = -800$

6.5.4 Modal Amplitudes

We conclude by plotting the evolution of the modal amplitudes of four different damping periods taken from the corners of the b-c plane in Figure 6.31 to Figure 6.34. They demonstrate a range of different behaviours and timbres achievable with the addition of third-order polynomial nonlinearity to a travelling wave control system.

6.6 Summary

In this chapter we have presented an experimental setup for performing travelling wave control on a real string consisting of a pair of custom optical displacement sensors, an algorithm to estimate the travelling wave components, and a termination-based piezo stack

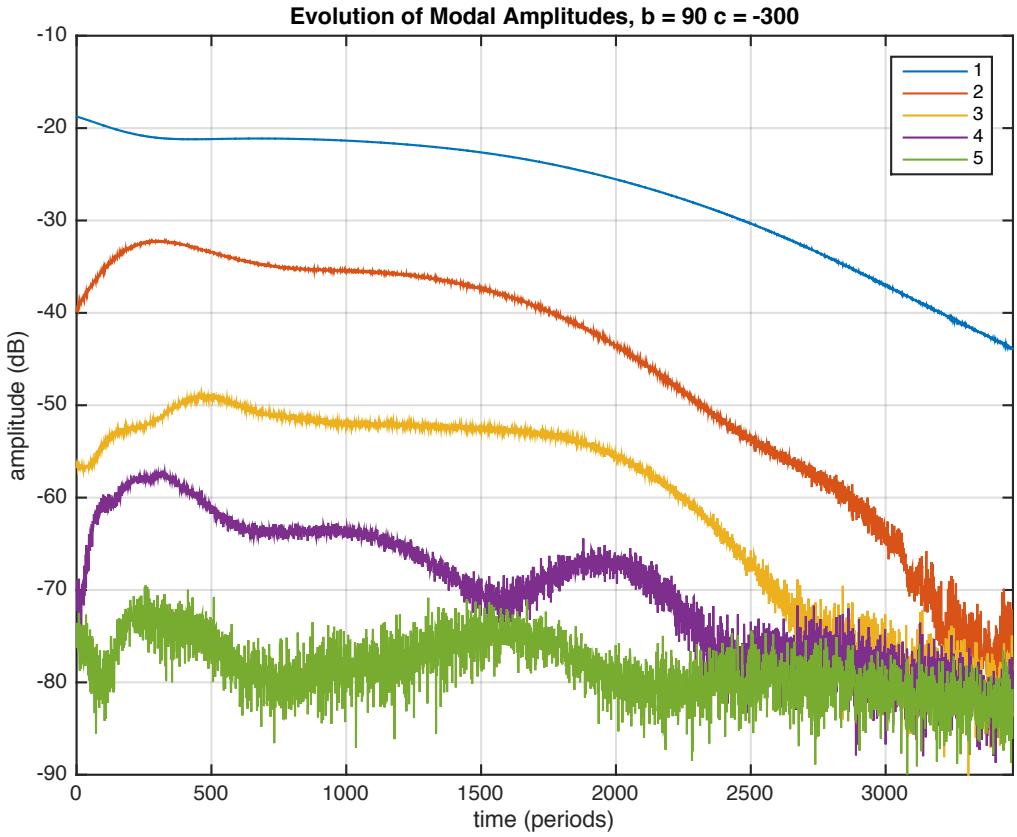

Figure 6.32: Evolution of modal amplitudes with $b = 90$, $c = -300$

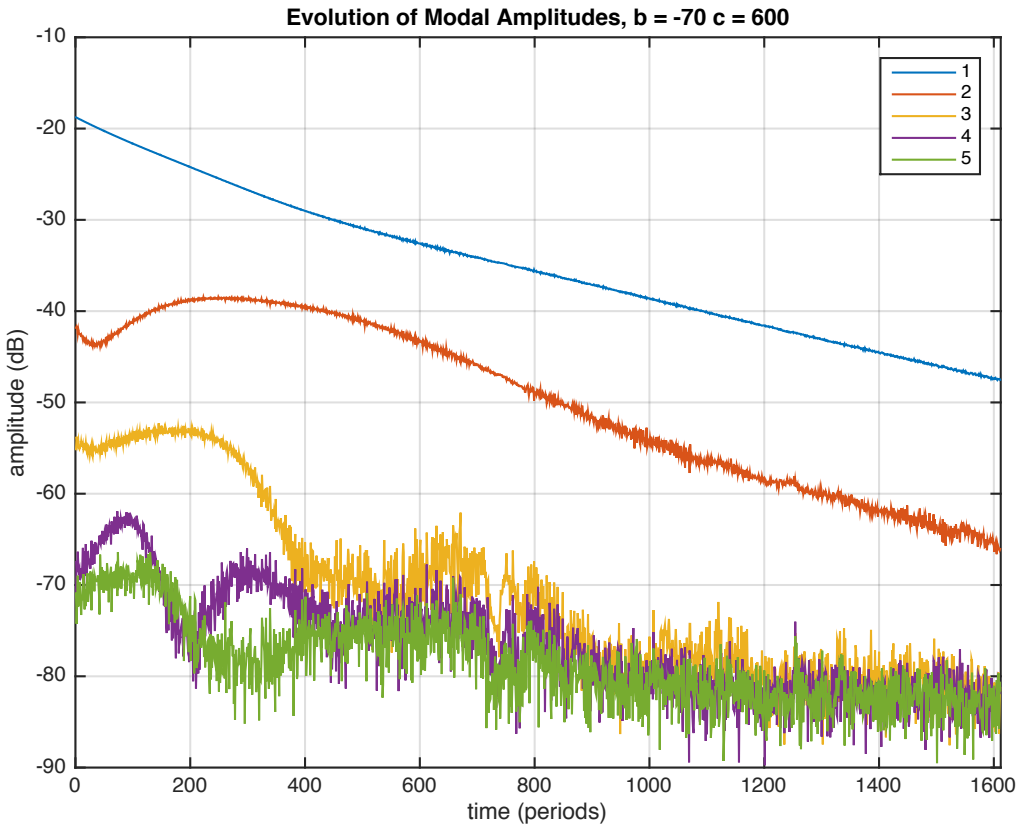

Figure 6.33: Evolution of modal amplitudes with $b = -70$, $c = 600$

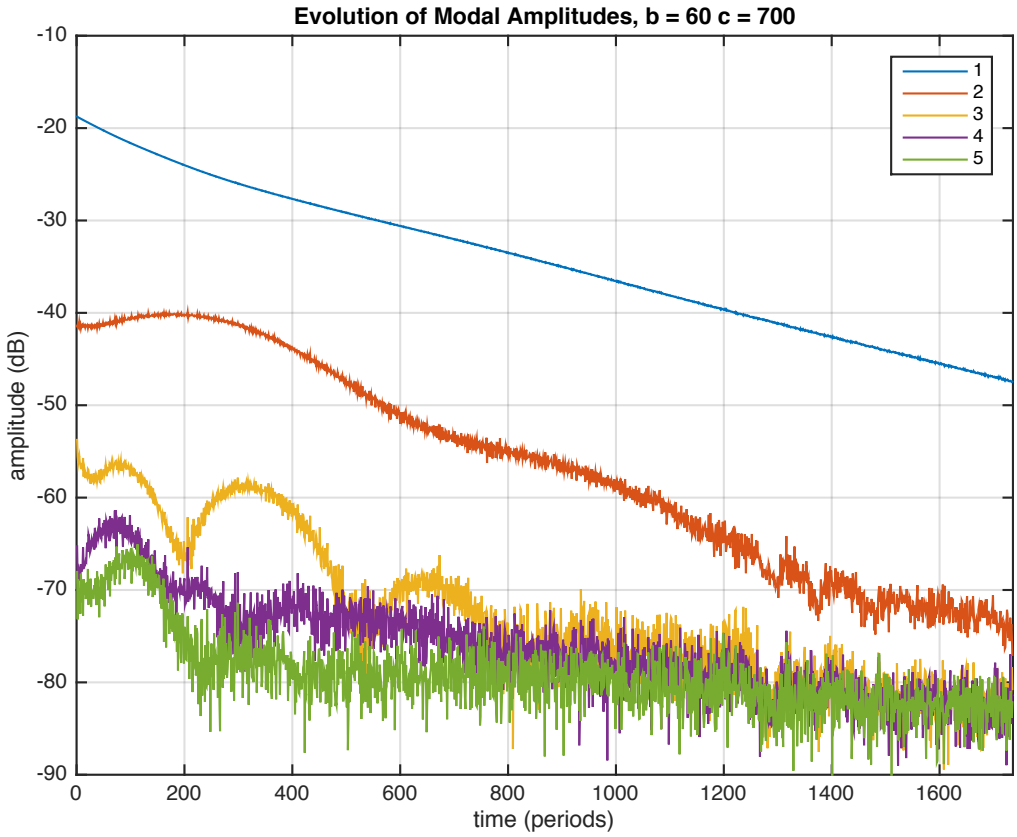

Figure 6.34: Evolution of modal amplitudes with $b = 60$, $c = 700$

actuator.

We analysed the linearity of the sensors by using the actuator to vibrate the string at its fundamental frequency and measuring the total harmonic distortion of the sensor output.

We evaluated the performance of the travelling wave estimation algorithm by examining the energy present in the error signal over different frequency ranges. We identified a pair of filters which were able to reduce the noise present in the estimation without significantly degrading the performance of the estimator in the modal frequency range of the string.

We then demonstrated that the travelling wave control system is capable of damping a plucked string without inducing significant amounts of harmonic distortion in its motion at a rate approximately six times faster than without control.

We showed that system was relatively tolerant to small errors in the time delay between estimating the travelling wave and displacing the actuator, but that if the delay was approximately 300µs too long the string was induced into a self-sustaining oscillation, reinforcing the need to use an ultra-low latency digital signal processor to perform the estimation.

We showed that in the linear region of the actuator, the performance of the system in response to varying linear gains matched our theoretical predictions closely, suggesting that the structural nonlinearities in the control system are low. We found that applying high gains and clipping the actuator resulted in faster damping at the cost of inducing harmonic distortion, and we demonstrated that an adaptive gain algorithm was capable of damping standing waves more quickly than linear control.

Finally, we demonstrated that deliberately adding nonlinearity into the control system allowed us to modify the timbre of the string by emphasising different modes by different amounts depending on the amount and type of nonlinearity we introduced.

Chapter 7

Conclusions

In this thesis we have demonstrated the feasibility of using travelling wave control to affect the vibration of a musical string. We showed that an ideal form of travelling wave control is capable of damping a vibrating string within one period of vibration, but that realistic non-idealities such as limited actuator amplitude and sensor nonlinearity degrade this capability. We derived a stability criterion for general forms of travelling wave control and applied it to show that certain forms of nonlinearity can cause instability independent of the controller gain. We demonstrated that nonlinearity has the effect of progressively shifting energy up into the higher modes thereby modifying the timbre of the string, and that different forms of nonlinearity do this at different rates and with different characteristics.

We designed, built and evaluated a pair of custom optical string displacement sensors with very high linearity and signal-to-noise ratio, identifying and eliminating or minimising major sources of nonlinearity such as out-of-plane string motion and uneven light distribution. We used the sensors in combination with an algorithm taken from the domain of industrial vibration control [79] to build a travelling wave sensor, capable of decomposing the components of the waves travelling along the string in the presence of sensor noise.

We used a piezo stack actuator to displace the termination point of the string and progressively absorb energy from the waves travelling along the string. We discussed how the high linearity and stiffness of piezo stack actuators make them better suited to this task than electromagnetic actuators, and described an adaptive gain algorithm to compensate for their limited amplitude.

We demonstrated the ability of the travelling wave control system to damp the vibrations of a plucked string in an experimental setting, showing that it was able to remove energy

from the string up to 100 times faster than without control. We demonstrated the possibility of building a highly linear travelling wave control system capable of damping the string without shifting significant amounts of energy into the higher modes and modifying the string's timbre, and analysed the sensitivity of the system to a number of key parameters. Finally we showed that with the deliberate addition of varying amounts of quadratic and cubic nonlinearity to the system, we were able to control the flow of energy into the higher modes of the string and modify its timbre in a subtle, natural and controlled way.

7.1 Advantages Over Modal Control

The advantages of ideal travelling wave control over modal control in terms of its ability to damp the vibrations of a string are well known; travelling wave control is theoretically capable of full damping within a single period of vibration, while modal control can only asymptotically reduce the modal amplitudes and requires a separate feedback loop for independent control over each dominant mode. In fact, the limited amplitude of the piezo stack actuators used in this work mean that the ability of this form of travelling wave control to damp a string's vibrations is likely to be less than that of the form of modal control advocated by Berdahl [6], where collocated sensors and actuators and positive-real feedback control laws allow the loop gains to be made very high and the damping to be made fast.

The sensitivity of travelling wave control to nonlinearity has been considered previously as a major disadvantage when compared with modal control, however we have shown here that by explicitly modelling the sources of nonlinearity in the sensor and actuator systems and working to minimise or eliminate them, it is possible to construct a highly linear travelling wave control system which is capable of damping string vibrations without inducing significant harmonic distortion in the string's motion. From there we've shown that by deliberately adding nonlinearity into the system we can modify the timbre of the string by affecting the evolution of its modal amplitudes. The sensitivity of travelling wave control to nonlinearity then becomes an advantage, unlocking a huge new space of creative possibilities which we have only barely begun to explore with our investigation of simple third-order polynomial nonlinearity. Other forms of nonlinearity have the potential to produce other distinct timbres, and deeper investigation into the effect of nonlinearity on the system has the potential to reveal more exotic nonlinear behaviours including bifurcations and chaotic motion [21], with as yet unexplored musical implications.

7.2 Limitations of Travelling Wave Control

Travelling wave control has a number of limitations in comparison to modal control, both theoretical and practical. On the theoretical side, travelling wave control is relatively more sensitive to parameter mismatch than modal control. In particular, the wave speed and hence the tuning of the string must be known. Our results show that small mismatches in delay don't cause instability, and in the case of a practical instrument, fingering the string (hence changing its length) would not change the wave speed, so this is not an insurmountable limitation. Nonetheless, for optimum performance some degree of dynamic pitch detection might be needed. Both theory and experiments also show that travelling wave control is sensitive to nonlinearity in a way that modal control is typically not. All of these limitations stem from the fact that travelling wave control involves a certain degree of feedforward control, detecting an incident wave before it arrives at the termination and displacing the termination point to coincide with its arrival.

The most significant practical limitation of the form of travelling wave control presented here is its dependance on piezo stack actuators with limited amplitude, and the correspondingly reduced impact of the control on damping time when compared with an ideal form of the control strategy. While we have presented here a number of methods to deal with this limitation and demonstrated that significant damping and timbre modification is possible even with the severely limited amplitudes we have been working with, the most obvious way of improving the control strategy is to increase the amplitude of the actuation. Piezo stack actuators are a relatively new technology and there is definitely the possibility as the technology becomes more mature that actuators with larger amplitudes and comparable linearity, stiffness and bandwidth will become available. Alternatively, a more mechanically stiff electromagnetic bridge with a more stringent minor-loop feedback control system along the lines of Appendix B might provide a sufficient combination of displacement, stiffness and linearity.

The practical limitations of the control strategy within a musical instrument context are also considerable. The sensors we have designed are bulky and fragile and would need to be miniaturised. The piezo stack actuators we are using require high voltage and current supplies and amplifiers with large heatsinks. Installing the control system on an existing instrument would be a challenge because the actuators would need to replace the existing string terminations, requiring heavy modification of the instrument.

7.3 Next Steps

This thesis has explored the theoretical and practical viability of travelling wave control as a resource for the actuation of musical strings. In the musical instrument literature, travelling wave control previously appears mainly as a speculative endnote in Edgar Berdahl's thesis [6]. By developing theory from industrial control, particularly the travelling wave decomposition method of Nauclér and Söderström [79], and extending the analysis into the behaviour under nonlinearity, we show that travelling wave control is indeed practical for manipulating strings.

Having demonstrated the feasibility and performance of the damping application and explored certain nonlinearities, other researchers could next develop this work in several directions. One would be a theoretical direction, further exploring the behaviour under nonlinearity and parameter mismatch, even including the potential for chaotic behaviour [21]. This theory could be used either to better avoid instability and unpredictable behaviour, or to deliberately exploit it as a creative resource. In fact, in electronic music it has long been noted that the failure modes of technology have aesthetically interesting properties [20], and in previous actuated instruments, initially unanticipated behaviours sometimes produced results that were as artistically compelling as the original intended outputs [69].

A second line of further development would extend the practical engineering of travelling wave control systems, with a particular focus on addressing the problem of limited displacement. The theory of travelling wave control shows that termination-based actuation is superior to actuation along the continuous length of the string. Future termination-based actuation might be addressed through higher-voltage piezo stack drivers, piezo stacks with mechanical lever loading to increase their displacement, feedback-stiffened electromagnetic solutions, or even simply using thicker, higher-tension strings which require less displacement to product significant sound. In the latter case, the dominant constraint would then become sensor noise floor for measuring small displacements.

A third line of development, even more practical in nature, would consist of the integration of travelling wave control into complete actuated acoustic instruments. Here, the control would have to coexist with the actions of the performer, which could impose more varied and less predictable conditions on the control system. Durability of components would also need to be considered.

Finally, and perhaps most interestingly, future research could investigate the complex relationship between travelling wave control under nonlinearity and musical timbre, i.e. the temporal evolution of the relative amplitudes of the modal frequencies of the strings. This work could productively involve perceptual and psychoacoustic models of timbre as well as

engineering approaches to the subject. Although this thesis primarily focuses on establishing the foundational principles of travelling wave control, timbre manipulation remains an intriguing opportunity ripe for future exploration.

Bibliography

[1] Y. Achkire and A. Preumont. Optical measurement of cable and string vibration. *Shock and vibration*, 5(3):171–179, 1998.

[2] S. Benacchio, B. Chomette, A. Mamou-Mani, and V. Finel. Mode tuning of a simplified string instrument using time-dimensionless state-derivative control. *Journal of sound and vibration*, 334:178–189, 2015.

[3] S. Benacchio, A. Mamou-Mani, B. Chomette, and F. Ollivier. Combined state and state derivative control applied to musical string instruments. In *Proceedings of meetings on acoustics*. Vol. 19. Acoustical Society of America, 2013.

[4] S. Benacchio, R. Piéchaud, A. Mamou-Mani, B. Chomette, and V. Finel. Active control of string instruments using xenomai. In *Proceedings of the 15th real time linux workshop*, 2013, 1–8.

[5] E. J. Berdahl and A. Freed. Active damping of a vibrating string. In *Proc. active*, 2006.

[6] E. J. Berdahl. Applications of feedback control to musical instrument design. PhD thesis. Stanford University, 2010.

[7] E. Berdahl, S. Backer, and J. Smith. If i had a hammer: design and theory of an electromagnetically-prepared piano. In *Proceedings of the international computer music conference*, 2005, 81–84.

[8] E. Berdahl, G. Niemeyer, and J. O. Smith. Using haptics to assist performers in making gestures to a musical instrument. In *Proc. New Interfaces for Musical Expression*, 2009, 177–182.

[9] E. Berdahl, J. O. Smith III, and G. Niemeyer. Feedback control of acoustic musical instruments: collocated control using physical analogs. *The journal of the acoustical society of america*, 131(1):963–973, 2012.

[10] E. Berdahl and J. Smith. Estimating the state of a one-dimensional waveguide. *Journal of the acoustical society of america*, 121(5):3049, 2007.

[11] P. Bloland. The electromagnetically-prepared piano and its compositional implications. In *Proc. International Computer Music Conference*, 2007.

[12] M. Bodson. An adaptive algorithm for the tuning of two input shaping methods. *Automatica*, 34(6):771–776, 1998.

[13] H. Boutin and C. Besnainou. A modal method adapted to the active control of a xylophone bar. In *Proc. acoustics*, 2012.

[14] H. Boutin and C. Besnainou. Physical parameters of an oscillator changed by active control: application to a xylophone bar. In *Proc. digital audio effects*, 2008.

[15] H. Boutin and C. Besnainou. Physical parameters of the violin bridge changed by active control. *Journal of the acoustical society of america*, 123(5):3656, 2008.

[16] N. C. Britt, J. Snyder, and A. McPherson. The EMvibe: an electromagnetically actuated vibraphone. In *Proc. new interfaces for musical expression*, 2012.

[17] R. Burridge, J. Kappraff, and C. Morshedi. The sitar string, a vibrating string with a One-Sided inelastic constraint. *SIAM journal on applied mathematics*:1231–1251, 1982.

[18] K. Buys, D. Sharp, and R. Laney. Developing and evaluating a hybrid wind instrument. *Acta acustica united with acustica*, 103(5):830–846, 2017.

[19] K. Buys, D. Sharp, and R. Laney. Development of a hybrid wind instrument—Some key findings. *The journal of the acoustical society of america*, 141(5):3620–3620, 2017.

[20] K. Cascone. The aesthetics of failure:"post-digital" tendencies in contemporary computer music. *Computer music journal*, 24(4):12–18, 2000.

[21] G. Chen, S. Hsu, and J. Zhou. Chaotic vibrations of the one-dimensional wave equation due to a self-excitation boundary condition. III. natural hysteresis memory effects. *International journal of bifurcation and chaos*, 8(03):447–470, 1998.

[22] G. Chen, S. Hsu, J. Zhou, G. Chen, and G. Crosta. Chaotic vibrations of the one-dimensional wave equation due to a self-excitation boundary condition. part i: controlled hysteresis. *Transactions of the american mathematical society*, 350(11):4265–4311, 1998.

[23] G. Chen. *Controlling chaos and bifurcations in engineering systems*. CRC press, 1999.

[24] P. R. Cook. Physically informed sonic modeling (phism): synthesis of percussive sounds. *Computer music journal*:38–49, 1997.

[25] L. B. Donovan and A. McPherson. Active control of a string instrument bridge using the posicast technique. In *Audio engineering society convention 138*. Audio Engineering Society, 2015.

[26] L. Donovan, S. Bin, J. Armitage, and A. P. McPherson. Building an IDE for an embedded system using web technologies. In *Proc. web audio conference*, 2017.

[27] A. Eldridge and C. Kiefer. The self-resonating feedback cello: interfacing gestural and generative processes in improvised performance. *Proceedings of new interfaces for music expression*:25–29, 2017.

[28] S. J. Elliott and L. Billet. Adaptive control of flexural waves propagating in a beam. *Journal of sound and vibration*, 163(2):295–310, 1993.

[29] M. L. Facchinetti, X. Boutillon, and A. Constantinescu. Numerical and experimental modal analysis of the reed and pipe of a clarinet. *The journal of the acoustical society of america*, 113(5):2874–2883, 2003.

[30] H. Fletcher. Normal vibration frequencies of a stiff piano string. *The journal of the acoustical society of america*, 36(1):203–209, 1964.

[31] N. H. Fletcher and T. Rossing. *The physics of musical instruments*. Springer Science & Business Media, 2012.

[32] A. Freed and O. Isvan. Musical applications of new, multi-axis guitar string sensors. In *Proc. ICMC*, 2000.

[33] C. Gough. The nonlinear free vibration of a damped elastic string. *The journal of the acoustical society of america*, 75(6):1770–1776, 1984.

[34] P. Gren, K. Tatar, J. Granström, N. E. Molin, and E. V. Jansson. Laser vibrometry measurements of vibration and sound fields of a bowed violin. *Measurement science and technology*, 17(4):635, 2006.

[35] J. M. Grey. An exploration of musical timbre. PhD thesis. Stanford University, 1975.

[36] J. M. Grey. Multidimensional perceptual scaling of musical timbres. *The journal of the acoustical society of america*, 61(5):1270–1277, 1977.

[37] J. M. Grey. Timbre discrimination in musical patterns. *The journal of the acoustical society of america*, 64(2):467–472, 1978.

[38] S. Hanagud and S. Griffin. Active structural control for a smart guitar. In *Fourth european conference on smart structures and materials*, 1998, pp. 169–175.

[39] J. Harriman. Feedback lapsteel: exploring tactile transducers as string actuators. In *Proc. new interfaces for musical expression*, 2015.

[40] G. S. Heet. *String instrument vibration initiator and sustainer*, Feb. 1978. US Patent 4,075,921.

[41] A. Hoover and G. Osborne. *Basic sustainer components*. Google Patents, Dec. 2000. US Patent App. 09/819,047.

[42] J. Y. Hung. Feedback control with posicast. *Industrial electronics, IEEE transactions on*, 50(1):94–99, 2003.

[43] A. Hunt, M. M. Wanderley, and M. Paradis. The importance of parameter mapping in electronic instrument design. *Journal of new music research*, 32(4):429–440, 2003.

[44] HyVibe. The hyvibe guitar. 2018. URL: http://hyvibe.audio.

[45] S. Jordà. Instruments and players: some thoughts on digital lutherie. *Journal of new music research*, 33(3):321–341, 2004.

[46] R. E. Kalman and J. E. Bertram. Control system analysis and design via the "second method" of lyapunov: I—Continuous-time systems. *Journal of basic engineering*, 82(2):371–393, 1960.

[47] A. Kapur. A history of robotic musical instruments. In *Proc. international computer music conference*, 2005, 21–28.

[48] M. Karjalainen, V. Välimäki, and T. Tolonen. Plucked-string models: from the Karplus-Strong algorithm to digital waveguides and beyond. *Computer music journal*, 22(3):17–32, 1998.

[49] D. H. Keefe. Physical modeling of wind instruments. *Computer music journal*, 16(4):57–73, 1992.

[50] E. Kreuzer and M. Steidl. Controlling torsional vibrations of drill strings via decomposition of traveling waves. *Archive of applied mechanics*, 82(4):515–531, 2012.

[51] E. Kreuzer, L. Krumm, M. Pick, E. Solowjow, and M. Steidl. Active vibration isolation via decomposition of travelling waves, 2013.

[52] C. L. Krumhansl. Why is musical timbre so hard to understand. *Structure and perception of electroacoustic sound and music*, 9:43–53, 1989.

[53] O. Lähdeoja. Active acoustic instruments for electronic chamber music. In *Proceedings of the international conference on new interfaces for musical expression (2220-4806)*. Vol. 16, 2016.

[54] S. Lakatos. A common perceptual space for harmonic and percussive timbres. *Perception & psychophysics*, 62(7):1426–1439, 2000.

[55] C. Lee and F. C. Moon. Modal sensors/actuators. *Journal of applied mechanics*, 57(2):434–441, 1990.

[56] N. Leroy, E. Fléty, and F. Bevilacqua. Reflective optical pickup for violin. In *Proceedings of the 2006 conference on new interfaces for musical expression*. IRCAM—Centre Pompidou, 2006, 204–207.

[57] LightWave. Lightwave optical pickup system. URL: https://www.willcoxguitars.com/lightwave-optical-pickup-system/.

[58] C. Maganza, R. Caussé, and F. Laloë. Bifurcations, period doublings and chaos in clarinetlike systems. *EPL (Europhysics letters)*, 1(6):295, 1986.

[59] T. Magnusson. Designing constraints: composing and performing with digital musical systems. *Computer music journal*, 34(4):62–73, 2010.

[60] T. Magnusson and E. H. Mendieta. The acoustic, the digital and the body: a survey on musical instruments. In *Proc. new interfaces for musical expression*, 2007, 94–99.

[61] D. C. Massie. Wavetable sampling synthesis. In, *Applications of digital signal processing to audio and acoustics*, 311–341. Springer, 2002.

[62] M. Mathews and B. Verplank. Scanned synthesis. In *Proc. international computer music conference*, 2000, pp. 368–371.

[63] S. McAdams, S. Winsberg, S. Donnadieu, G. De Soete, and J. Krimphoff. Perceptual scaling of synthesized musical timbres: common dimensions, specificities, and latent subject classes. *Psychological research*, 58(3):177–192, 1995.

[64] M. E. McIntyre, R. T. Schumacher, and J. Woodhouse. On the oscillations of musical instruments. *The journal of the acoustical society of america*, 74(5):1325–1345, 1983.

[65] A. McPherson. Portable measurement and mapping of continuous piano gesture. In *Proc. new interfaces for musical expression*, 2013.

[66] A. McPherson. Techniques and circuits for electromagnetic instrument actuation. In *Proceedings of the twelfth international conference on new interfaces for musical expression*, 2012.

[67] A. McPherson. The magnetic resonator piano: electronic augmentation of an acoustic grand piano. *Journal of new music research*, 39(3):189–202, 2010.

[68] A. McPherson. TouchKeys: capacitive multi-touch sensing on a physical keyboard. In *Proc. NIME*, 2012.

[69] A. P. McPherson and Y. E. Kim. The problem of the second performer: building a community around an augmented piano. *Computer music journal*, 36(4):10–27, 2012.

[70] A. McPherson and Y. Kim. Augmenting the acoustic piano with electromagnetic string actuation and continuous key position sensing. In *Proc. new interfaces for musical expression*, 2010.

[71] A. McPherson and V. Zappi. An environment for Submillisecond-Latency audio and sensor processing on BeagleBone black. In *Audio engineering society convention 138*. Audio Engineering Society, 2015.

[72] C. B. Medeiros and M. M. Wanderley. A comprehensive review of sensors and instrumentation methods in devices for musical expression. *Sensors*, 14(8):13556–13591, 2014.

[73] L. Meirovitch and H. Baruh. The implementation of modal filters for control of structures. *Journal of guidance, control, and dynamics*, 8(6):707–716, 1985.

[74] L. Meirovitch and S. Thangjitham. Active control of sound radiation pressure. *ASME, transactions, journal of vibration and acoustics*, 112:237–244, 1990.

[75] T. Meurisse, A. Mamou-Mani, R. E. Caussé, and D. Sharp. Active control applied to simplified wind musical instrument. In *Proceedings of meetings on acoustics*. Vol. 19. Acoustical Society of America, 2013, p. 030057.

[76] T. Meurisse, A. Mamou-Mani, R. Causse, B. Chomette, and D. B. Sharp. Simulations of modal active control applied to the self-sustained oscillations of the clarinet. *Acta acustica united with acustica*, 100(6):1149–1161, 2014.

[77] E. R. Miranda and M. M. Wanderley. *New digital musical instruments: control and interaction beyond the keyboard*. Vol. 21. AR Editions, Inc., 2006.

[78] I. Moreno, C. Tsai, D. Bermúdez, and C. Sun. Simple function for intensity distribution from LEDs. In *Proc. SPIE*. Vol. 6670, 2007.

[79] P. Nauclér and T. Söderström. Separation of waves governed by the one-dimensional wave equation—a stochastic systems approach. *Mechanical systems and signal processing*, 23(3):823–844, 2009.

[80] D. Overholt. The overtone violin: a new computer music instrument. In *Proc. international computer music conference*, 2005, 604–607.

[81] D. Overholt, E. Berdahl, and R. Hamilton. Advancements in actuated musical instruments. *Organised sound*, 16(02):154–165, 2011.

[82] D. Overholt. The overtone fiddle: an actuated acoustic instrument. In *Proc. new interfaces for musical expression*, 2011.

[83] R. C. Paiva, J. Pakarinen, and V. Välimäki. Acoustics and modeling of pickups. *Journal of the audio engineering society*, 60(10):768–782, 2012.

[84] L. S. Pardue. Violin augmentation techniques for learning assistance. PhD Thesis. Queen Mary University of London, 2017.

[85] L. S. Pardue and A. P. McPherson. Near-field optical reflective sensing for bow tracking. In *Proc. new interfaces for musical expression*, 2013.

[86] A. Piepenbrink and M. Wright. The bistable resonator cymbal: an actuated acoustic instrument displaying physical audio effects. In *Proc. new interfaces for musical expression*, 2015.

[87] J. Pressing. Cybernetic issues in interactive performance systems. *Computer music journal*, 14(1):12–25, 1990.

[88] C. V. Raman. On some indian stringed instruments. *Proceedings of the indian association for the cultivation of science*, 7:29–33, 1921.

[89] D. Rector and S. Topel. EMdrum: an electromagnetically actuated drum. *Proc. new interfaces for musical expression*, 2014.

[90] J. Risset and D. L. Wessel. Exploration of timbre by analysis and synthesis. *The psychology of music*, 2:151, 1999.

[91] T. Rossing, ed. Springer handbook of acoustics. Springer, 2015.

[92] D. Schwarz. Data-driven concatenative sound synthesis. In *Proc. digital audio effects*, 2000.

[93] S. Serafin. The sound of friction: real time models, playability and musical applications. PhD thesis. Stanford University, 2004.

[94] G. Shear. The electromagnetically sustained Rhodes piano. In *Proc. new interfaces for musical expression*, 2011.

[95] S. Siddiq. A physical model of the nonlinear sitar string. *Archives of acoustics*, 37(1):73–79, 2012.

[96] J. O. Smith. Physical modeling using digital waveguides. *Computer music journal*, 16(4):74–91, 1992.

[97] J. O. Smith. Principles of digital waveguide models of musical instruments. In, *Applications of digital signal processing to audio and acoustics*, 417–466. Springer, 2002.

[98] J. O. Smith. Virtual acoustic musical instruments: review and update. *Journal of new music research*, 33(3):283–304, 2004.

[99] O. J. Smith. Posicast control of damped oscillatory systems. *Proceedings of the ire*, 45(9):1249–1255, 1957.

[100] P. Taillard, J. Kergomard, and F. Laloë. Iterated maps for clarinet-like systems. *Nonlinear dynamics*, 62(1):253–271, 2010.

[101] N. Tanaka and Y. Kikushima. Active wave control of a flexible beam: fundamental characteristics of an active-sink system and its verification. *JSME international journal. ser. 3: vibration, control engineering, engineering for industry*, 34(2):159–167, 1991.

[102] N. Tanaka and Y. Kikushima. Active wave control of a flexible beam. fundamental characteristics of an Active-Sink system and its verification. *JSME international journal. ser. 3, vibration, control engineering, engineering for industry*, 35(2):236–244, 1992.

[103] S. C. Thompson. The effect of the reed resonance on woodwind tone production. *The journal of the acoustical society of america*, 66(5):1299–1307, 1979.

[104] Thorlabs. Thorlabs lens tutorial. 2018. URL: https://www.thorlabs.com/tutorials.cfm?tabID=4BD528B8-11B1-4D32-BE81-CB0C6EBF020C.

[105] Thorlabs. Thorlabs photodiode tutorial. 2018. URL: https://www.thorlabs.com/tutorials.cfm?tabID=31760.

[106] Thorlabs. Thorlabs piezoelectric tutorial. URL: https://www.thorlabs.com/newgrouppage9.cfm?objectgroup_id=5030.

[107] H. Úlfarrson. About halldorophones. 2004. URL: http://www.halldorulfarsson.info/halldorophone5/about_halldorophones/index.html.

[108] V. Välimäki, J. Huopaniemi, M. Karjalainen, and Z. Jánosy. Physical modeling of plucked string instruments with application to real-time sound synthesis. In *Audio engineering society convention 98*. Audio Engineering Society, 1995.

[109] V. Välimäki, J. Pakarinen, C. Erkut, and M. Karjalainen. Discrete-time modelling of musical instruments. *Reports on progress in physics*, 69(1):1, 2005.

[110] V. Verfaille, M. M. Wanderley, and P. Depalle. Mapping strategies for gestural and adaptive control of digital audio effects. *Journal of new music research*, 35(1):71–93, 2006.

[111] P. Vo. The Wond II project. 2018. URL: http://voinventions.com/wond-ii-project/.

[112] P. Vo. Vo-96. 2012. URL: http://voinventions.com/vo-96/.

[113] A. H. Von Flotow. Traveling wave control for large spacecraft structures. *Journal of guidance, control, and dynamics*, 9(4):462–468, 1986.

[114] A. H. Von Flotow and B. Schäfer. Wave-absorbing controllers for a flexible beam. *Journal of guidance, control, and dynamics*, 9(6):673–680, 1986.

[115] M. M. Wanderley and P. Depalle. Gestural control of sound synthesis. *Proceedings of the IEEE*, 92(4):632–644, 2004.

[116] L. M. Wang and C. B. Burroughs. Acoustic radiation from bowed violins. *The journal of the acoustical society of america*, 110(1):543–555, 2001.

[117] G. Weinreich. Coupled piano strings. *The journal of the acoustical society of america*, 62(6):1474–1484, 1977.

[118] G. Weinreich and R. Caussé. Digital and analog bows: hybrid mechanical-electrical systems. In *Proc. ieee international conference on acoustics, speech, and signal processing*. IEEE, 1986, 1297–1299.

[119] D. L. Wessel. Timbre space as a musical control structure. *Computer music journal*:45–52, 1979.

[120] D. Wessel and M. Wright. Problems and prospects for intimate musical control of computers. *Computer music journal*, 26(3):11–22, 2002.

[121] J. Woodhouse. Plucked guitar transients: comparison of measurements and synthesis. *Acta acustica united with acustica*, 90(5):945–965, 2004.

[122] G. Q. Xu, S. P. Yung, and L. K. Li. Stabilization of wave systems with input delay in the boundary control. *ESAIM: control, optimisation and calculus of variations*, 12(4):770–785, 2006.

Appendices

Appendix A

Termination-Point Impedance

In order to understand how travelling wave control works it is necessary to understand the concept of a string's impedance. For a uniform string under constant tension, impedance is a constant physical property defined as:

$$Z = \frac{T}{c} = \sqrt{T\mu} \tag{A.1}$$

where T is the tension, μ is the linear density and c is the wave velocity along the string. It is independent of the string's motion and constant along its full continuous length.

It also describes the relationship between the transverse velocity of any point along the string $u_t(x,t)$ and the transverse force exerted by that point on its neighbour, $F_y(x,t)$:

$$Z = \frac{F_y(x,t)}{u_t(x,t)} \tag{A.2}$$

When a wave travelling along a string encounters an impedance boundary (an abrupt change in μ for example, or a termination point) a certain proportion of its energy is reflected and the rest is transmitted past the boundary. When the two impedances are given by Z_1 and Z_2, the proportion reflected is given by the reflection coefficient R:

$$R = \frac{Z_1 - Z_2}{Z_1 + Z_2} \tag{A.3}$$

The corresponding transmission coefficient T is given by:

$$T = \frac{2Z_1}{Z_1 + Z_2} \tag{A.4}$$

In order to satisfy the conservation of energy, these must sum to 1:

$$|T + R| = 1 \tag{A.5}$$

The defining property of a termination point is that it is completely restricted from moving, and therefore has a transverse velocity $u_t(x,t)$ of 0. From Equation A.2 the impedance of the termination point is therefore infinite, giving a transmission coefficient of 0 and a reflection coefficient of -1, causing the incident wave to be inverted and perfectly reflected. Conversely, the defining property of an active sink is that it absorbs any wave incident upon it and prevents any reflections, resulting in a reflection coefficient of 0. From Equation A.3 this is achieved when the impedance of the termination point matches the impedance of the string, i.e. $Z_1 = Z_2$.

In theory, such a matched impedance boundary could be created by coupling the string to another of identical impedance, and extending it off to infinity. This hypothetical case would produce a transmission coefficient of 1, causing all waves to move past the termination and disappear, never to be reflected back into the original string. In practice of course such an infinitely long string is impossible; instead the wave must be fooled into thinking it exists by manipulating the termination point impedance with an actuator to match it to that of the string.

Equation A.2 suggests that if the termination point is displaced by an actuator such that the transverse force $F_y(x,t)$ and velocity $u\_t(x,t)$ is equal to what it would be on the hypothetical infinite string, the termination point impedance would be matched to the string, and the wave is not be reflected.

Figure A.1a shows what happens to a point P_n on a string as a wave approaches from the right. As the point immediately to the right P_{n+1} is lifted by the wave, P_n feels a transverse force $F_y = T\sin(\theta)$ from the tension in the string, causing it to accelerate upwards. This exerts a similar force on the point to the left P_{n-1} and causes the wave to propagate. Figure Figure A.1b shows what happens when the wave reaches the termination. The point to the right P_1 lifts, exerting the same force $T\sin(\theta)$ from the string's tension, but rather than accelerating upwards P_0 feels an equal opposing force F_{term} from the rigid termination such that the resulting transverse force is 0:

$$F_y = T\sin(\theta) - F_{term} = 0 \tag{A.6}$$

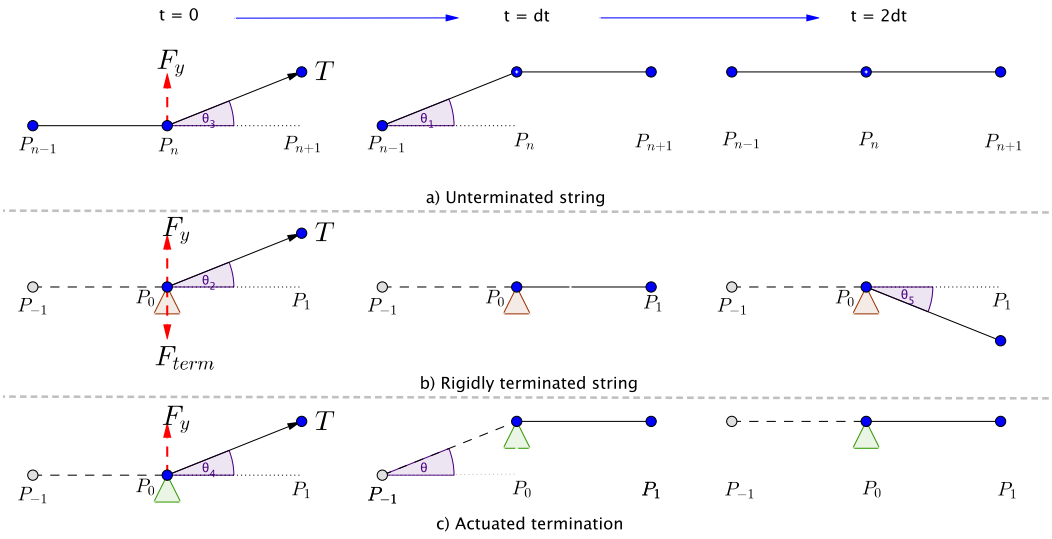

Figure A.1: Schematic diagram of the termination point of a vibrating string in the case of a) no termination (top) b) a rigid termination (centre) and c) an actuated impedance-matched termination. Three discrete time steps are shown from left to right. In b) and c) the dashed line represents the behaviour of a hypothetical continuation of the string past the termination.

The termination point therefore does not move and the additional force F_{term} pulls down on P_1 causing the wave to be inverted and reflected. If another hypothetical string of the same impedance were to be attached to the left of the termination, the first point along, P_{-1}, would not experience any force and would remain still.

Figure A.1c shows what happens when P_0 is displaced by an actuator the same amount as if it were just a normal point along the string. In this case the actuator is essentially cancelling the force from the termination F_{term}, allowing the point P_0 to feel the transverse force $F_y = T\sin(\theta)$ exactly like P_n above, accelerating upwards in the same way. In this case the wave would be transmitted into the hypothetical string to the left of the termination, and point P_{-1} would be displaced exactly as P_{n-1} is above. Notice how the three points in figure Figure A.1c have finished up in the same positions as Figure A.1a where the wave was transmitted straight through with no reflections, and in different positions to Figure A.1b where the wave was reflected at the termination.

In this case however we appear to be violating the conservation of energy, as there is no reflected wave (i.e. $R = 0$) and there is no real string for the wave to be transmitted into, so T is effectively 0 too. The only place left for the incident wave's energy to go is into the

actuator.

Consider the case when the string is fully at rest and we attempt to displace the termination point with an actuator. To do this the actuator must do work against its own internal inertial forces, and it must do more work to increase the potential energy of the string by displacing it. Now consider the case when the actuator is displaced by an identical amount to the displacement of a travelling wave incident upon it. It must still do work against its own inertial forces, but it is no longer exerting any force on the string, and is not doing any work to increase the string's potential energy, as the wave is doing that already. It has moved the same distance as in the first case but it has done less work because it has absorbed the energy from the travelling wave. Almost ironically, the string actually helps the actuator to absorb the energy in the wave.

The stroboscopic plot Figure A.2 visualises a string's response to a pluck and shows how ideal travelling wave control can be applied to create an active sink at the left-hand termination point and remove all the energy from the string in just over a single period.

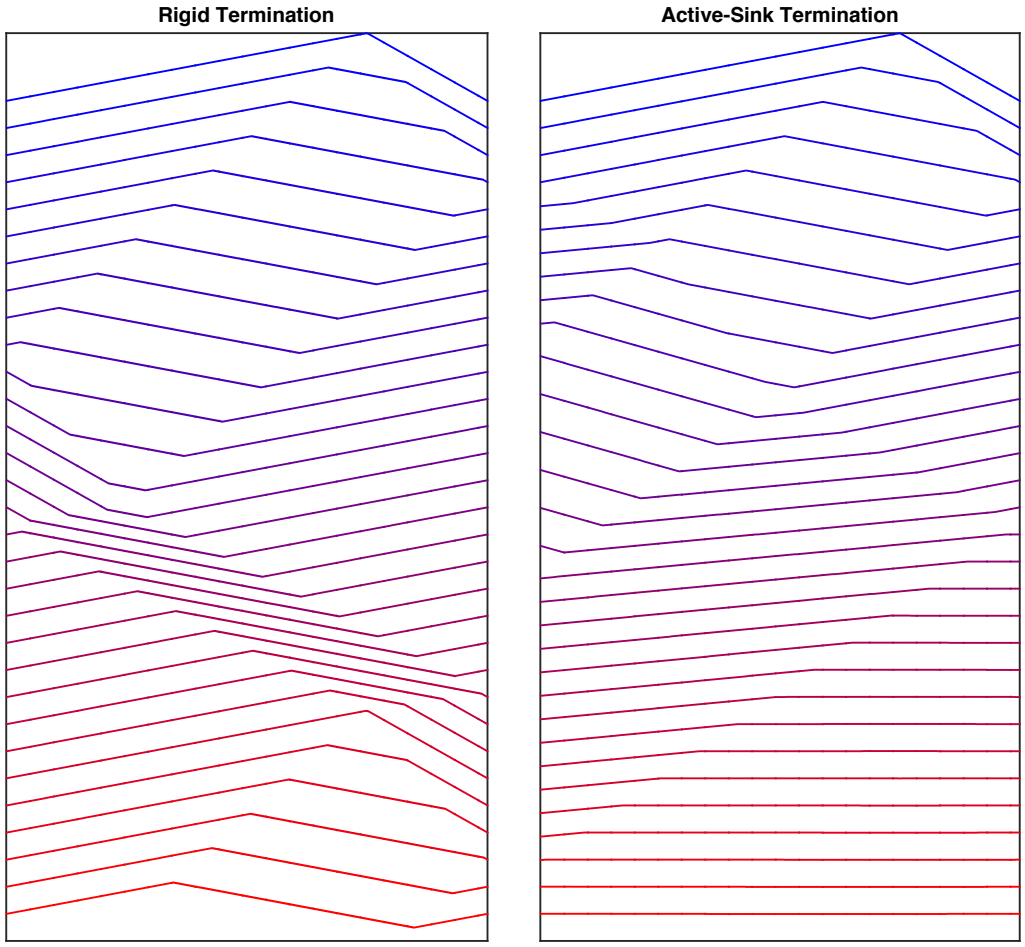

Figure A.2: Stroboscopic plot showing the string's displacement in response to a pluck with a rigid termination (left) and with travelling wave control applied to create an active-sink termination at the left-hand end of the string (right). The total time elapsed is 125% of the string's fundamental period.

Appendix B

Active Control of a String Instrument Bridge using the Posicast Technique

In this appendix we reproduce a paper submitted to the 138th Convention of the AES [25]. It is included here to provide context for the use of termination-based actuation in the travelling wave control system, though does not contribute directly to the work presented in the thesis.

B.1 Introduction

The goal of the research presented here is to affect the timbre of a vibrating string through active control of the string's termination at the bridge. Specifically, the work presented in this paper is concerned with the design of a mechanical system to allow manipulation of the bridge, and the design of a sensor, actuator and control system to provide precise and fast control over the dynamic response of the system. The benefits of *posicast* [99], a feedforward control technique used to damp the oscillations of high-Q second order systems, are presented and compared to typical PID feedback control.

The inspiration for this work came from study of the *javari* effect found in classical Indian instruments such as the sitar and tanbura. In these instruments the shape of the bridge is a shallow, flat curve rather than a sharp point as in western instruments, presenting a one-sided non-linear constraint on the movement of the string near the bridge [95]. This constraint is responsible for the characteristic and unique buzzing timbre created by these instruments [17], and the work presented in this paper is working towards the creation of a system which can replicate and extend this concept in order to create new timbres and sounds.

Control over the bridge is a compelling way of introducing vibrations in a string due to its privileged position at the termination point of the string. When applying a force at a point internal to the string a pair of travelling waves are generated moving in opposite directions; these waves reflect off the terminations and return to the actuation point, where the displacement is described by their sum in addition to the sum of other waves caused by disturbances of the string. At the bridge, however, an applied force generates a single travelling wave moving away from the bridge, and the force exerted on the bridge by the string is also only affected by the single incoming travelling wave, significantly simplifying the process of controlling the string.

B.2 Literature Review

Directly actuating strings through electromagnetic stimulation has been extensively explored. Berdahl has investigated embedding actuators into an electric guitar [82]. Commercial solutions to actuating guitar strings also exist in the Ebow [40], the Sustainiac [41] and the Vo-96 acoustic guitar synth. Actuated pianos have also been investigated by McPherson with the magnetic resonator piano [70] and Berdahl with the electromagnetically prepared piano [7].

Feedback control of strings has been explored by Berdahl, particularly in terms of using positive-real feedback controllers to affect fundamental frequency and damping [5]. In his thesis [6] he explored 'termination-based control' using a single sensor-actuator pair at an internal point in the string to attempt to specify the reflection transfer function at the termination, but ran into problems with sensor non-linearity and limits on possible loop-gain.

Boutin and Besnainou used active control to alter physical characteristics such as stiffness and foot-spacing of a violin bridge in order to alter the frequency response of the transmission between string vibration and radiated sound [15]. Similar work has also been done by Hanagud and Griffin by using active control of the structure of a guitar to influence its spectral characteristics and make it sound more expensive [38]. Many active bridge control systems use *piezo stack* actuators, which provide high force and wide bandwidth. However, they are limited by low displacements, high cost, and the need for specialised amplifiers driving hundreds of volts into a capacitive load. We therefore sought to create an electromagnetic solution suitable for integration into a playable instrument.

B.3 System Description

B.3.1 Setup

In order to allow for vertical movement of the bridge the string termination was mounted on a pair of steel springs. Actuation was achieved by attaching a strong neodymium magnet to the bridge and applying force with an electromagnet and corresponding transconductance amplifier, both of which are identical to those used in the magnetic resonator piano [68]. The use of the transconductance amplifier served to remove a low frequency first-order pole caused by the inductance of the electromagnet, resulting in a faster and lower-order response. A diagram and photograph showing the mechanical setup can be seen in Figures B.1 and

B.2.

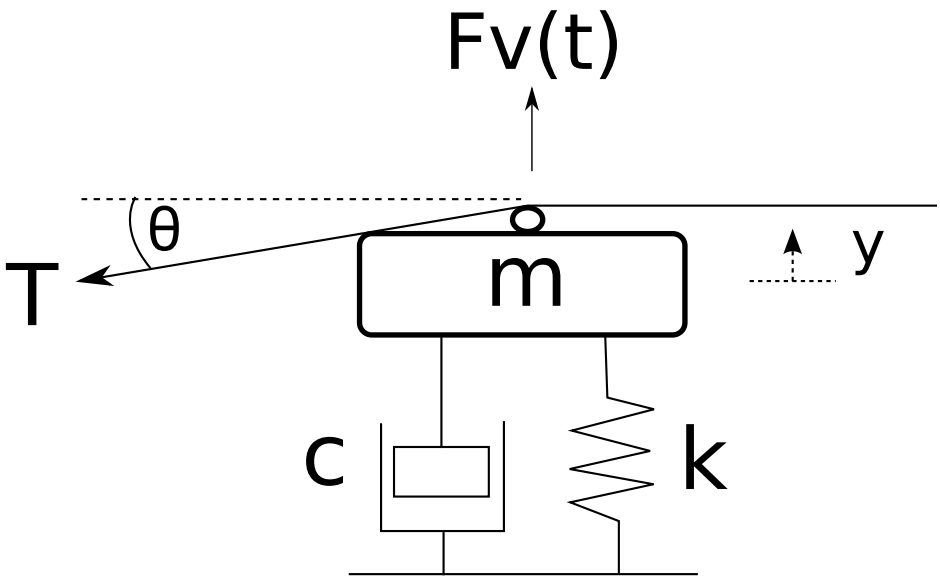

Figure B.1: Schematic diagram of the system

The bridge height was sensed using a QRE1113 optical reflectance sensor mounted under the bridge. This was found preferable to a Hall-effect sensor measuring proximity to the magnets on the bridge due to a lower signal-to-noise ratio, and because it was difficult to completely magnetically de-couple the actuator and Hall-effect sensor.

The posicast and feedback controllers were implemented using a Beaglebone Black with the BeagleRT environment and audio cape. This allowed a 22kHz sampling rate and a measured $100\mu s$ latency.

B.3.2 Modelling

The system was modelled as a simple mass-spring-damper with a pair of complex poles, along with another first order pole to approximate the losses in the electromagnet at high frequencies. The string affects the system in two ways: firstly by altering the effective stiffness of the springs by resisting the vertical movement of the bridge, and secondly by resonating at harmonics of its fundamental frequency. Fortunately, due to the high Q-factor of the string's modes, the second of these effects is limited to extremely narrow frequency ranges. The first of the effects was mitigated by minimising the angle at which the string was bent over the bridge (θ in Figure B.1) while still ensuring the string was adequately

Figure B.2: Photograph of the system

terminated. Despite these attempts, experiments still showed that a 10% change in string tension resulted in an approximately 5% change in the natural frequency of the bridge, so in the future more work needs to go on designing the string termination to be independent of tension.

Because both of the effects caused by the string are dependant upon its tension, material and other properties, they were not modelled explicitly and instead treated as a disturbance on the bridge in order to allow the bridge to be controlled independently of the properties of the string.

The transfer function between vertical displacement $y(t)$ and input voltage $v(t)$ was modelled in the laplace domain as:

$$G(s) = \frac{Y(s)}{V(s)} = \frac{k}{s^2 + 2s\zeta\omega + \omega^2} \cdot \frac{1}{s\frac{1}{w_a} + 1} \tag{B.1}$$

The parameters of the model were estimated by measuring the frequency response of the bridge experimentally and comparing the results to the model. A comparison of the nyquist and bode plots of the real system and the model can be seen in figures B.3 and B.4.

The parameters were estimated as follows:

$$k = 1.934 \cdot 10^5 \tag{B.2}$$

$$\zeta = 0.007 \tag{B.3}$$

$$f = \frac{\omega}{2\pi} = 350Hz \tag{B.4}$$

$$f_a = \frac{\omega_a}{2\pi} = 380Hz \tag{B.5}$$

The frequency of the second-order poles f was intentionally increased by using stiffer springs until it approached the frequency of the first order pole f_a caused by losses in the electromagnet. This allowed the bandwidth to be maximised at the cost of lower gain k, and thus lower displacement to a given input. Increasing the stiffness of the springs to push f above f_a would simply reduce k without usefully increasing bandwidth.

When attempting to control the system described in Equation B.1 there are two main problems which can be identified from the system model: firstly the nyquist plot of the system encircles the -1 point meaning the system will be unstable under unity feedback, and secondly the system is highly under-damped with a damping factor of 0.007 (a Q-factor of over 70) leading to high amplitudes at resonance and very large overshoot and settling time in response to a step input.

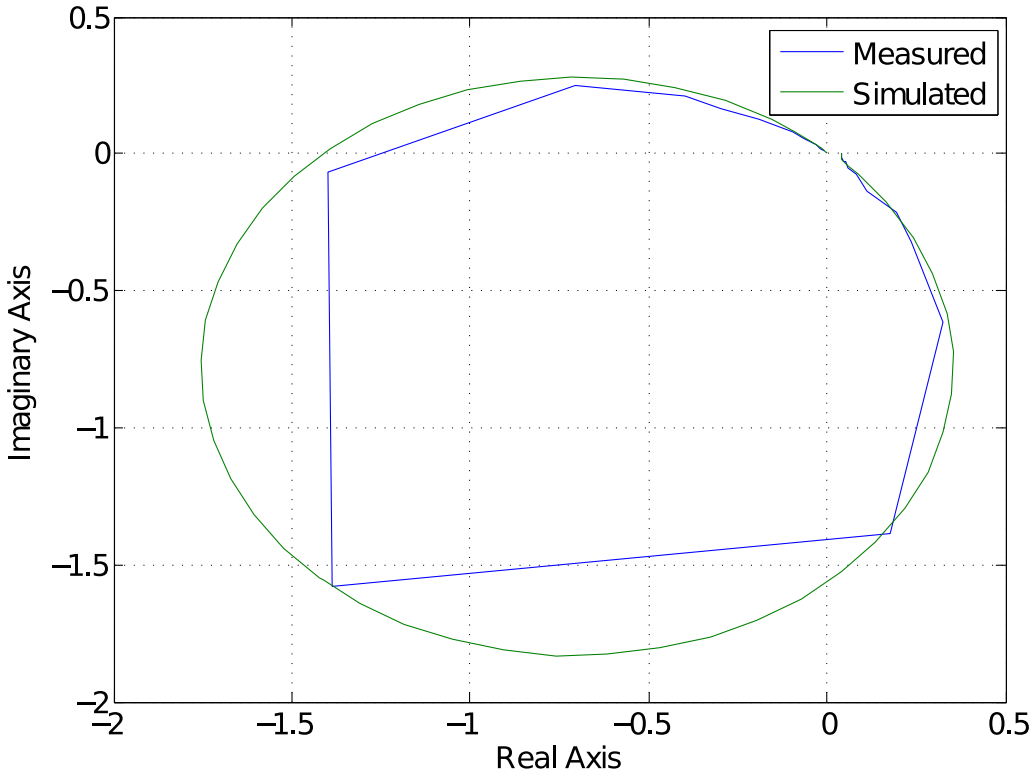

Figure B.3: Comparison of nyquist diagrams of modelled and measured systems

B.4 Lead Compensator

The main objective of the controller was to get a grip over the dynamic response of the system and eliminate the ringing in the step response by introducing damping, without reducing bandwidth. The first attempt at doing this used a lead compensator, a pole-zero pair located around the cross-over frequency of the system which serves to inject phase, increasing the phase margin and thereby the damping factor of the closed-loop system. The compensator used was of the following form:

$$G_c(s) = \frac{\frac{\alpha}{\omega_c\sqrt{\alpha}}s + 1}{\frac{1}{\omega_c\sqrt{\alpha}}s + 1} \cdot \frac{1}{\frac{1}{100\omega_c}s + 1} \tag{B.6}$$

A block-diagram of the compensated system can be seen in Figure B.5. One of the drawbacks of using lead compensation is that it involves derivative action and is therefore inherently sensitive to noise, which is why a high frequency pole was added to the controller to reduce the

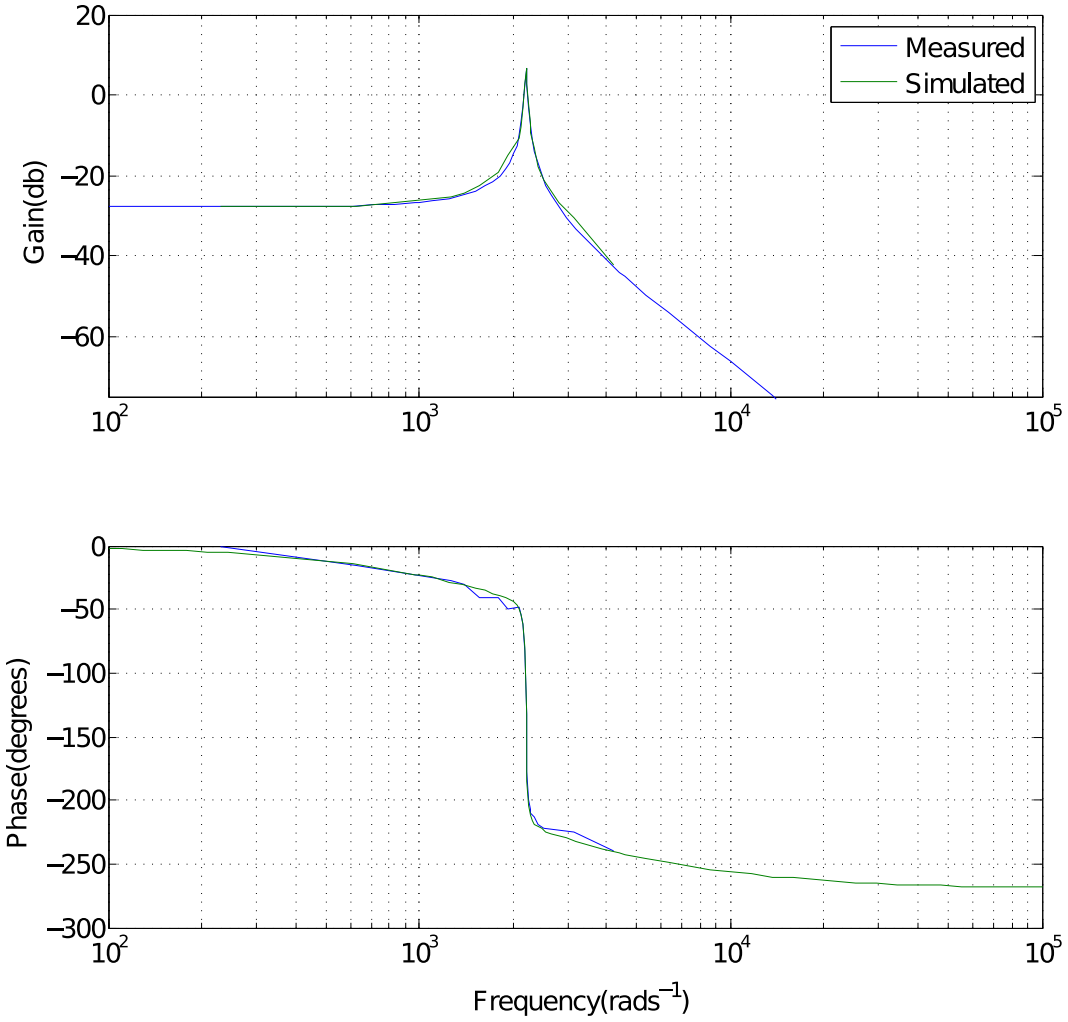

Figure B.4: Comparison of bode plots of modelled and measured systems

gain at high frequencies. By setting ω_c equal to the crossover frequency of the uncompensated system ω, the maximum amount of phase lead was added at the crossover frequency. Varying the parameter α then increases the amount of phase lead added. It was found that the maximum value of α before noise became intolerable was approximately 10, leading to an open-loop phase margin of approximately 20° (Figure B.6).

Figure B.7 shows the step response. Although a significant improvement can be seen using the lead controller (Figure B.7b) versus the open loop system (Figure B.7a), it was not able to damp the system to acceptable levels.

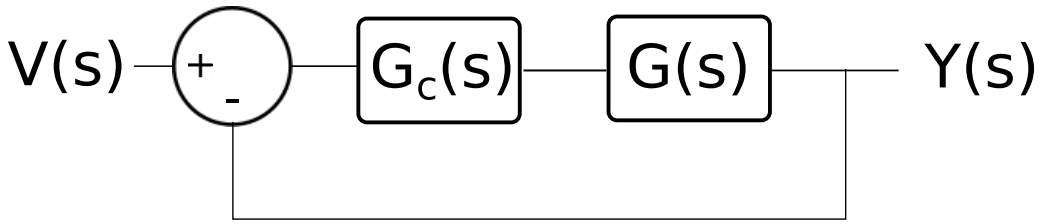

Figure B.5: Block diagram of lead compensator

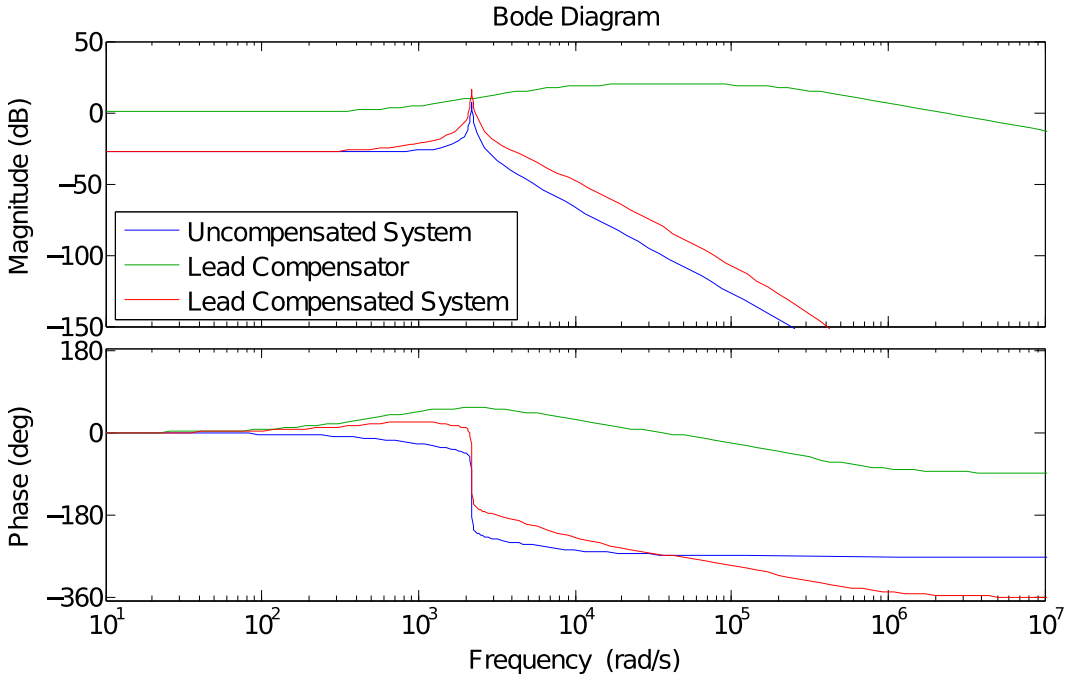

Figure B.6: Bode plots of the lead controller and resulting open-loop compensated system $G_c(s)G(s)$

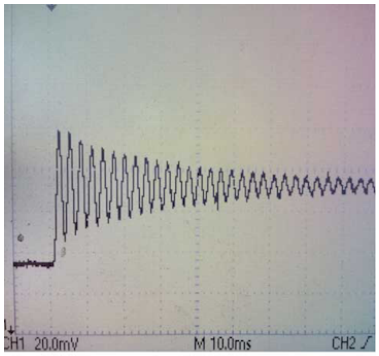

a) Open–Loop

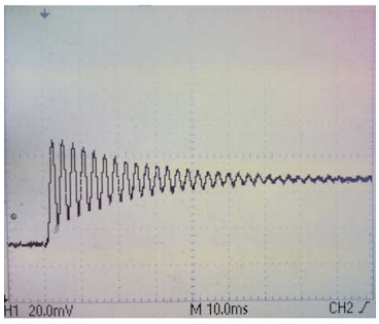

b) Lead Controller

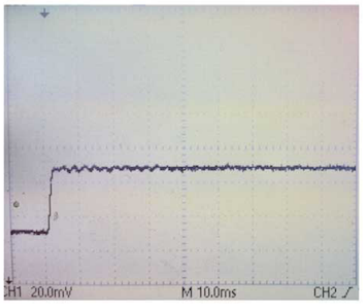

c) Posicast Controller

Figure B.7: Comparison of responses of the open-loop system and two controlled systems to a 1V step input. Y-axis units are mV of output from the height sensor, large divisions are 20mV. X-axis units are ms, large divisions are 10ms.

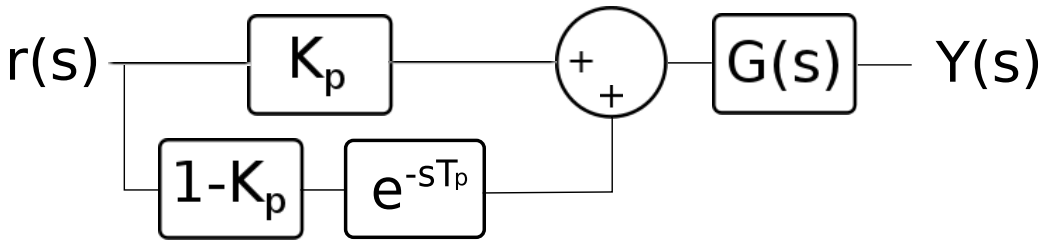

Figure B.8: Block diagram of posicast controller

B.5 Posicast

Posicast control is a term coined by Otto Smith in 1957 and is a form of feedforward control based on input-shaping techniques which is designed to produce a deadbeat response (i.e zero overshoot to a step input) in under-damped second-order systems [99]. It fell out of academic favour due to its reliance on precise knowledge of the system response and its inferiority in dealing with uncertainties and disturbances when compared with standard PID-based feedback control, although there has been significant interest in recent years towards incorporating posicast controllers into feedback loops [42]. When dealing with a system like this where audio frequencies and therefore the transient response of the system is the most important factor, it excels even in its original feedforward configuration.

Half-cycle posicast, which was implemented here, consists of taking a delayed and scaled version of the input and then adding it back to itself, converting a step into a staggered pair of steps, and is described in the frequency domain by:

$$G_p(s) = K_p + (1 - K_p)e^{-sT_p} \tag{B.7}$$

A block diagram of the controller is shown in figure B.8. The length of the delay is equal to half the period of the resonant frequency of the system (with a resonant frequency of 350Hz the delay is 1.4ms) and the scaling factor is determined by the amount of overshoot in the system response (in this case, approximately 0.5).

The frequency response of the posicast controller is effectively a comb filter with an infinite number of sharp notches in its magnitude response and a phase response which oscillates around zero, never adding or subtracting more than 90° of phase even at high frequencies. In Figure B.9 it can be seen how in a correctly tuned posicast controller, the first notch in its frequency response perfectly cancels the resonant peak of the system.

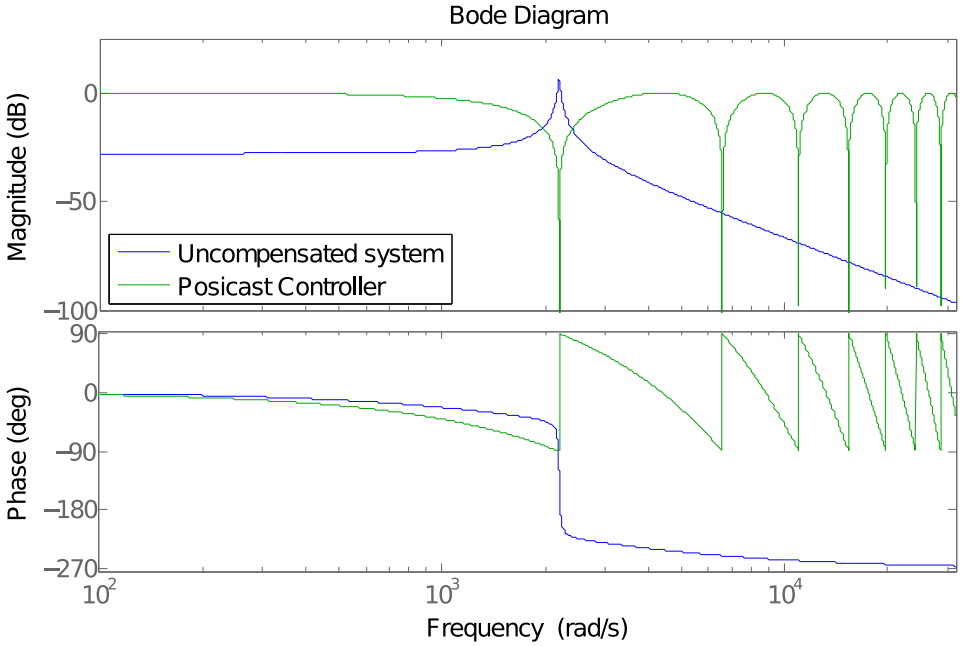

Figure B.9: Bode plots of the open-loop system and the tuned posicast controller

Figure B.7 is a comparison of the step responses of the uncompensated system, the lead-compensated system, and the system with a half-cycle posicast controller. Figure B.10 shows a close-up of the posicast response along with the output of the posicast controller. The benefits of the posicast controller are clear - with a settling time of under 2ms and virtually zero overshoot, the system exhibits a dynamic response well within the specifications for its purpose.

B.5.1 Parameter Sensitivity

One of the main problems with posicast is that it is a feedforward technique and relies on cancelling the second-order poles of the system through precise knowledge of their locations. Table B.1 shows how the dynamic response changes as the two posicast parameters, gain (K_p) and delay time (T_p), are varied away from their optimal values. One impressive result is that it requires a parameter error of over 50% to degrade the dynamic response to the levels of the lead compensated system. It can be seen that the system is generally more sensitive to variations in the delay time as opposed to the gain, and that even small errors result in significant increases in settling time. This sensitivity can be remedied by using an adaptive posicast algorithm [12], which will be the subject of future work.

Controller Type	Parameter	Error (%)	Settling Time (ms)	Overshoot
None	-	-	100 +	0.625
Lead	-	-	80	0.56
Posicast	-	-	2	0
Posicast	Gain (K_p)	±5	15	0.05
		±10	30	0.0875
		±15	40	0.125
		±20	50	0.15
		±50	55	0.3
Posicast	Delay (T_p)	±5	15	0.05
		±10	45	0.15
		±15	55	0.2
		±20	60	0.225
		±50	85	0.5

Table B.1: A table showing the sensitivity of the posicast controller to parameter variations. Settling time is defined as the time taken for the oscillations in the response to decay to less than 1% of the steady-state level. Overshoot is defined as the ratio between the peak voltage above the steady-state level to the steady-state level.

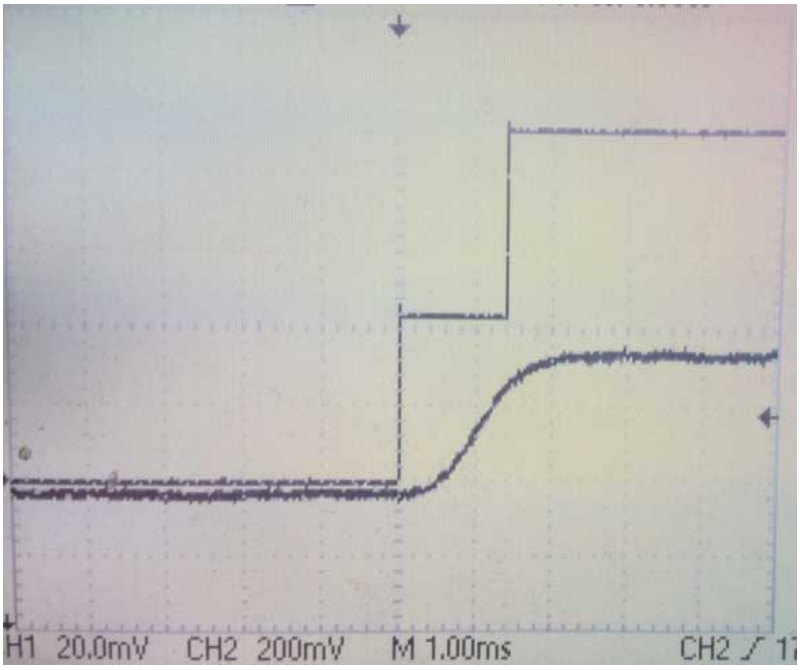

Figure B.10: Close-up of step response of posicast system, also showing the input voltage after the posicast controller. Y-axis is 200mV/division for the input signal, 20mV/division for the height sensor output. The X axis is 1ms/division.

B.6 Conclusion

An active bridge for affecting the timbre of string vibrations was developed, using electromagnetic actuation to manipulate its vertical position. Upon analysis the system was found to be severely under-damped, exhibiting unacceptable levels of ringing in response to input commands. A feedback-based lead controller was developed but was insufficient to damp the system acceptably without becoming susceptible to noise. Instead a feedforward posicast controller was developed which, when properly tuned, was able to almost completely eliminate ringing from the response of the system.

B.7 Acknowledgements

This work was supported by the EPSRC Centre for Doctoral Training in Media and Arts Technology, Queen Mary University of London.

Appendix C

Photographs

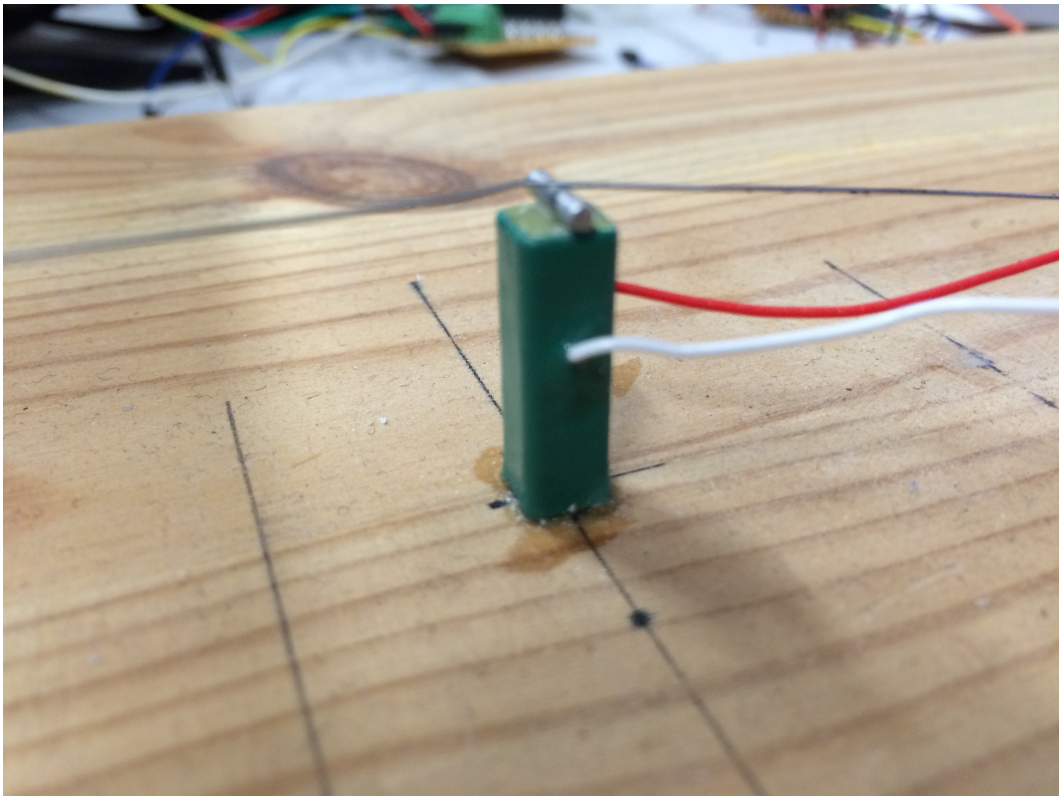

Figure C.1: Termination-based piezo stack actuator

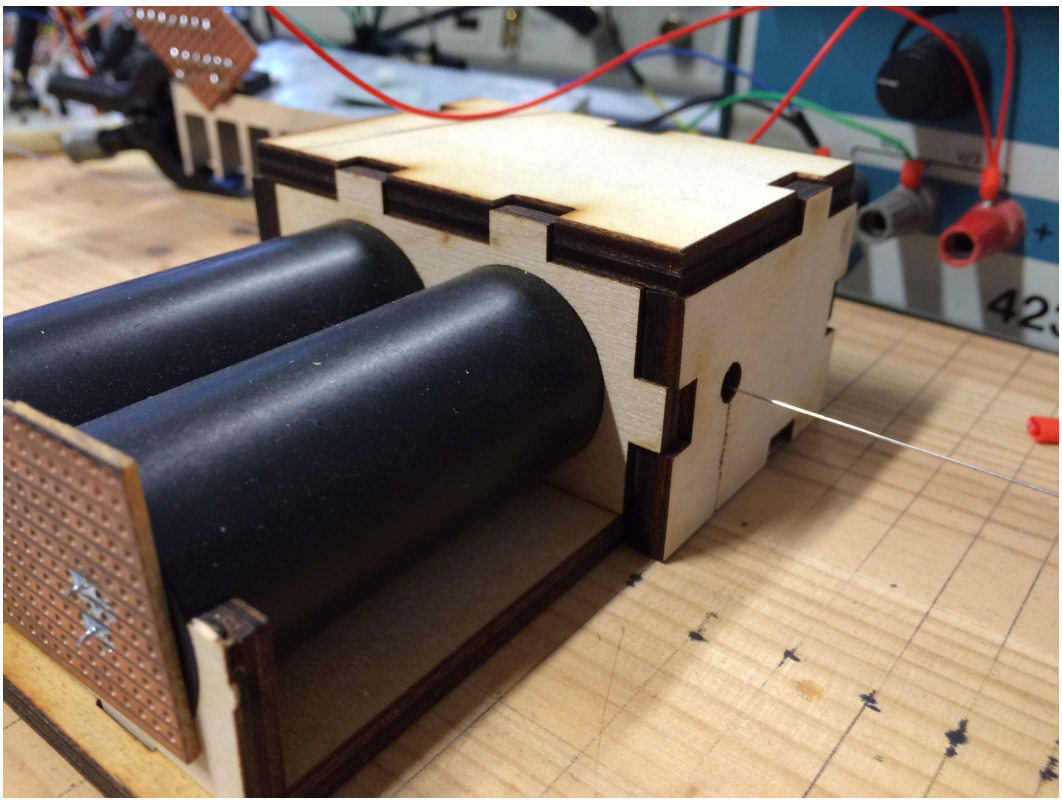

Figure C.2: Travelling wave sensor assembly

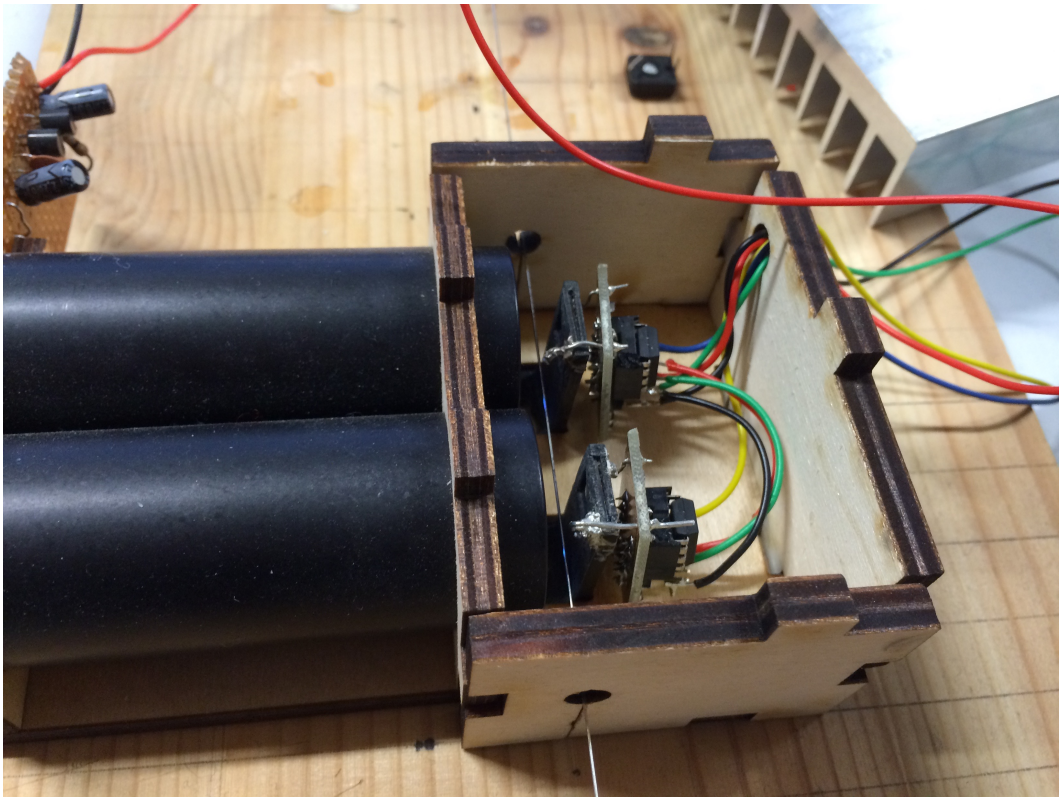

Figure C.3: Inside the travelling wave sensor assembly, showing the pair of lens tubes and the two masked planar photodiodes with preamplifier circuits attached

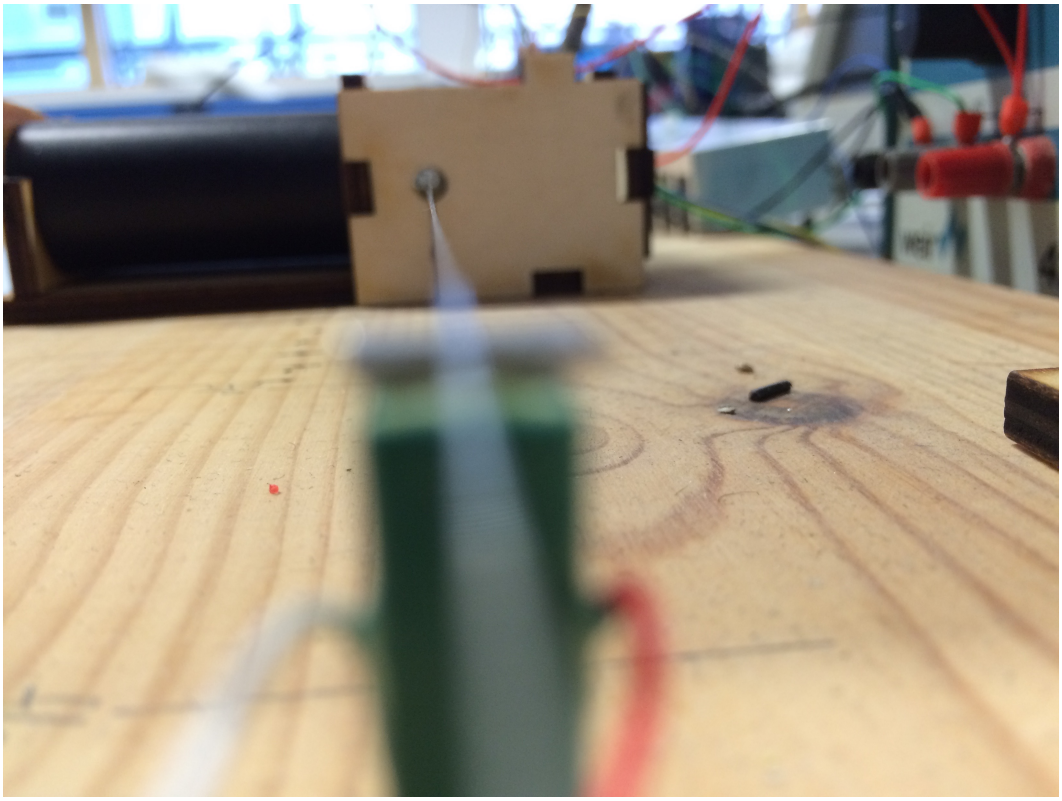

Figure C.4: View down the string from the piezo stack actuator looking towards the sensor assembly

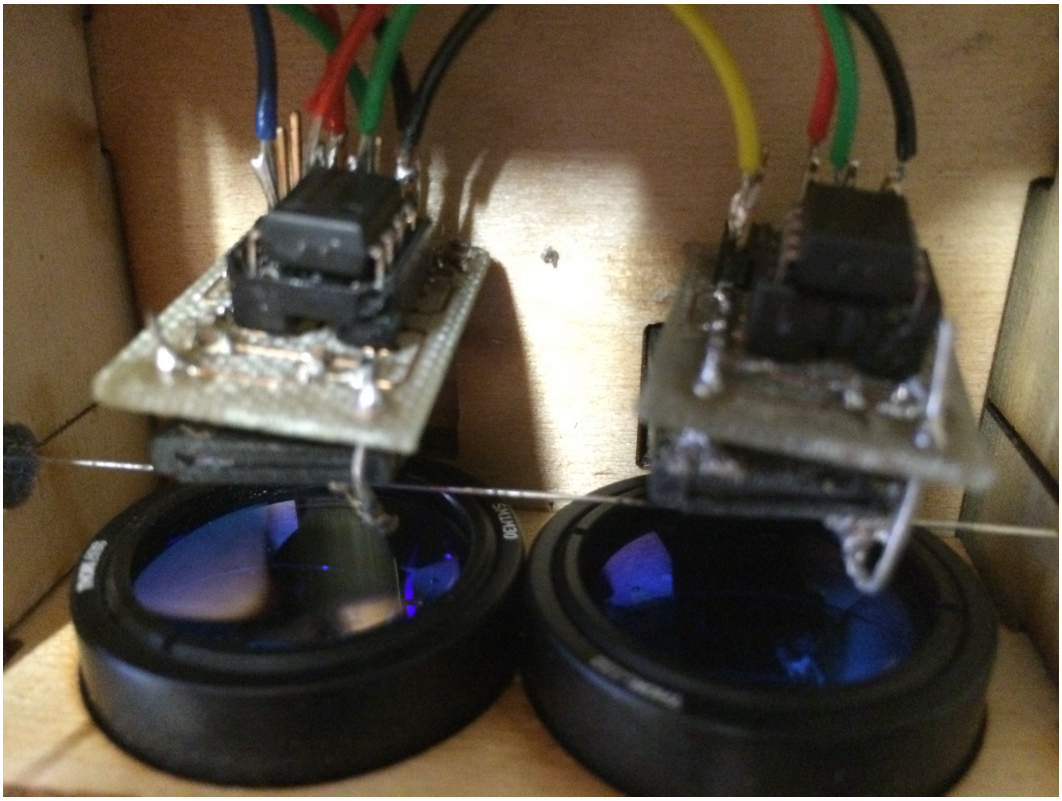

Figure C.5: Internal closeup of the sensor, showing the collimating lenses and the photodiode preamplifier circuits

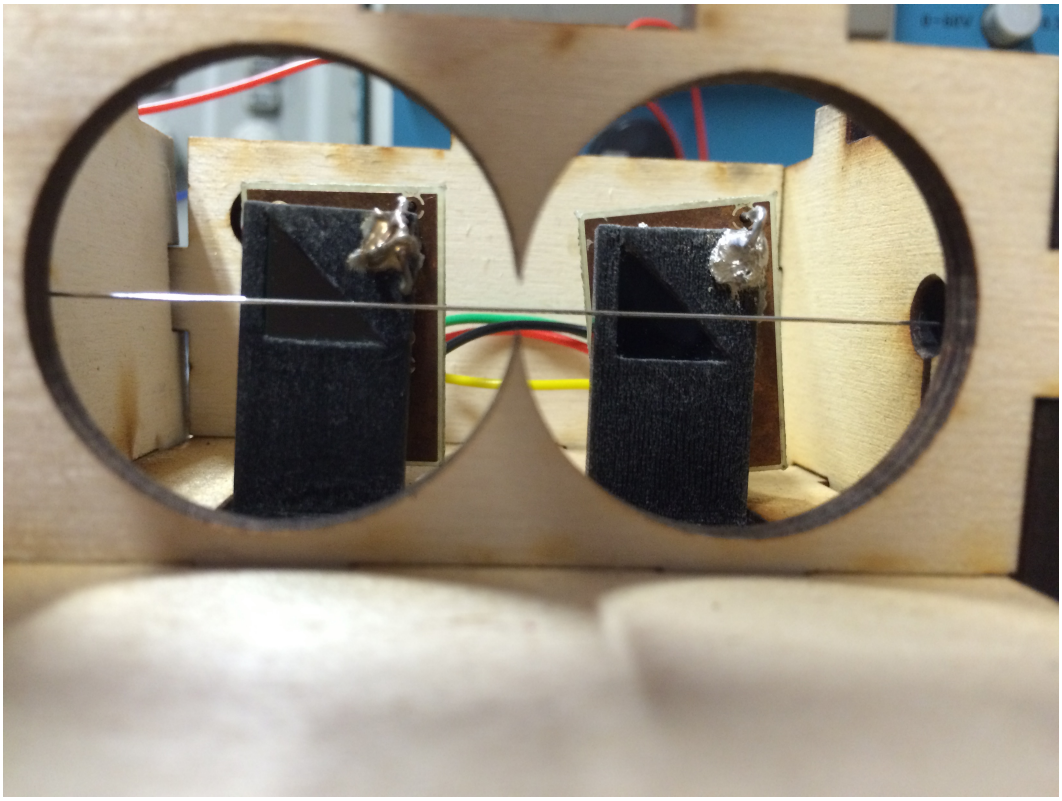

Figure C.6: View of the photodiode sensors with the lenses removed, showing the triangular mask